JAN 24 '72
Chem.

SECTION **A**

A UNITED STATES DEPARTMENT OF COMMERCE PUBLICATION

JOURNAL OF RESEARCH

of the NATIONAL BUREAU OF STANDARDS

Volume 75A, Number 6 November-December 1971

Physics and Chemistry

JAN 17 1972

MIAMI UNIVERSITY LIBRARY

U.S. DEPARTMENT OF COMMERCE
National Bureau of Standards

Journal of Research

of the

National Bureau of Standards

A. Physics and Chemistry

Nov.–Dec. • 1971

VOLUME • 75A

NUMBER • 6

Editor: C. W. Beckett

Associate Editor: D. D. Wagman

Publication dates:
Feb. 1, Apr. 1, June 1, Aug. 1, Oct. 1, Dec. 1, 1971

J. Res. Nat. Bur. Stand. (U.S.), A
CODEN: JNBAA 75A (6) 535–627 (1971)

JOURNAL OF RESEARCH

The National Bureau of Standards Journal of Research reports research and development in the fields of activity shown at right. Also included from time to time are survey articles on topics closely related to the Bureau's scientific and technical program.

The Journal is published in three separate sections as follows:

A. Physics and Chemistry

Contains papers of interest primarily to scientists working in these fields. Issued six times a year. Annual subscription: domestic, $9.50; foreign $11.75. Single copy, varies.

B. Mathematical Sciences

Presents studies and compilations designed mainly for the mathematician and the theoretical physicist. Issued quarterly. Annual subscription: domestic, $5.00; foreign, $6.25. Single copy, $1.25.

C. Engineering and Instrumentation

Reports research and development results of interest chiefly to the engineer and the applied scientist. Issued quarterly. Annual subscription: domestic, $5.00; foreign, $6.25. Single copy, $1.25.

U.S. DEPARTMENT OF COMMERCE
Maurice H. Stans, Secretary
NATIONAL BUREAU OF STANDARDS
Lewis M. Branscomb, Director

The National Bureau of Standards[1] was established by an act of Congress March 3, 1901. The Bureau's overall goal is to strengthen and advance the Nation's science and technology and facilitate their effective application for public benefit. To this end, the Bureau conducts research and provides: (1) a basis for the Nation's physical measurement system, (2) scientific and technological services for industry and government, (3) a technical basis for equity in trade, and (4) technical services to promote public safety. The Bureau consists of the Institute for Basic Standards, the Institute for Materials Research, the Institute for Applied Technology, the Center for Computer Sciences and Technology, and the Office for Information Programs.

THE INSTITUTE FOR BASIC STANDARDS provides the central basis within the United States of a complete and consistent system of physical measurement; coordinates that system with measurement systems of other nations; and furnishes essential services leading to accurate and uniform physical measurements throughout the Nation's scientific community, industry, and commerce. The Institute consists of a Center for Radiation Research, an Office of Measurement Services and the following divisions:

Applied Mathematics—Electricity—Heat—Mechanics—Optical Physics—Linac Radiation[2]—Nuclear Radiation[2]—Applied Radiation[2]—Quantum Electronics[3]—Electromagnetics[3]—Time and Frequency[3]—Laboratory Astrophysics[3]—Cryogenics[3].

THE INSTITUTE FOR MATERIALS RESEARCH conducts materials research leading to improved methods of measurement, standards, and data on the properties of well-characterized materials needed by industry, commerce, educational institutions, and Government; provides advisory and research services to other Government agencies; and develops, produces, and distributes standard reference materials. The Institute consists of the Office of Standard Reference Materials and the following divisions:

Analytical Chemistry—Polymers—Metallurgy—Inorganic Materials—Reactor Radiation—Physical Chemistry.

THE INSTITUTE FOR APPLIED TECHNOLOGY provides technical services to promote the use of available technology and to facilitate technological innovation in industry and Government; cooperates with public and private organizations leading to the development of technological standards (including mandatory safety standards), codes and methods of test; and provides technical advice and services to Government agencies upon request. The Institute also monitors NBS engineering standards activities and provides liaison between NBS and national and international engineering standards bodies. The Institute consists of the following technical divisions and offices:

Engineering Standards Services—Weights and Measures—Flammable Fabrics—Invention and Innovation—Vehicle Systems Research—Product Evaluation Technology—Building Research—Electronic Technology—Technical Analysis—Measurement Engineering.

THE CENTER FOR COMPUTER SCIENCES AND TECHNOLOGY conducts research and provides technical services designed to aid Government agencies in improving cost effectiveness in the conduct of their programs through the selection, acquisition, and effective utilization of automatic data processing equipment; and serves as the principal focus within the executive branch for the development of Federal standards for automatic data processing equipment, techniques, and computer languages. The Center consists of the following offices and divisions:

Information Processing Standards—Computer Information—Computer Services—Systems Development—Information Processing Technology.

THE OFFICE FOR INFORMATION PROGRAMS promotes optimum dissemination and accessibility of scientific information generated within NBS and other agencies of the Federal Government; promotes the development of the National Standard Reference Data System and a system of information analysis centers dealing with the broader aspects of the National Measurement System; provides appropriate services to ensure that the NBS staff has optimum accessibility to the scientific information of the world, and directs the public information activities of the Bureau. The Office consists of the following organizational units:

Office of Standard Reference Data—Office of Technical Information and Publications—Library—Office of Public Information—Office of International Relations.

[1] Headquarters and Laboratories at Gaithersburg, Maryland, unless otherwise noted; mailing address Washington, D.C. 20234.
[2] Part of the Center for Radiation Research.
[3] Located at Boulder, Colorado 80302.

Order all publications from the Superintendent of Documents
U.S. Government Printing Office, Washington, D.C. 20402

Use of funds for printing this publication approved by the Director of the Bureau of the Budget (June 22, 1966).

JOURNAL OF RESEARCH of the National Bureau of Standards—A. Physics and Chemistry
Vol. 75A, No. 6, November–December 1971

The Accuracy of Measurements of Viscosity of Liquids

Robert S. Marvin

Institute for Basic Standards, National Bureau of Standards, Washington, D.C. 20234

(July 28, 1971)

Most absolute measurements of viscosity have utilized capillary flow, and required semiempirical corrections amounting to several times their precision and estimated accuracy. The range of values found from these measurements and the possibility of unrecognized systematic errors make it impossible to base a realistic estimate of accuracy on the results of only one type of measurement. The results of two independent absolute measurements involving different types of flow, reported in the two accompanying papers, are summarized here. The estimated accuracy in each case is about 0.1 percent. The two results differ by 0.5 percent. It is suggested that we continue to base the calibration of relative viscometers on the value of 1.002 centipoise (cP) for the viscosity of water at 20 °C and one atmosphere. This provides a generally accepted base which limits comparability only by the precision of the measurements. However, whenever the true values of viscosity are required the limits of uncertainty including an estimate of systematic error should be taken as no better than ±0.25 percent.

Key words: Absolute measurement of viscosity; accuracy of viscosity measurement; calibration of viscometers; viscosity; uncertainty of viscosity measurements.

1. Introduction

The viscosity (shear viscosity) of a Newtonian liquid is normally measured by a relative technique in an instrument calibrated using a liquid of known viscosity. The common practice is to calibrate viscometers by a step-up technique, using a series of instruments and test fluids, based on the viscosity of water.

For viscosities above 1000 poise (P) or so, the accuracy of such measurements is generally limited by their variability. Such liquids normally have a very high temperature coefficient of viscosity, and problems of adequate temperature control alone make it difficult to attain better than one percent agreement. The agreement between measurements using various standard and accepted types of viscometers [1, 2, 3], [1] gives us sound grounds for believing that systematic errors can be kept below this one percent level.

It is quite common and relatively simple to make measurements to within 0.1 percent on ordinary liquids with viscosities below 1 P. It is often assumed that this precision also represents the accuracy of such measurements. It appears that any systematic errors associated with the step-up procedure are less than 0.1 percent at least up to viscosities of 1 P, although most of the evidence on which this conclusion is based has been obtained with capillary viscometers, leaving a possibility of some unrecognized bias. There remains a question of the accuracy of the value used for the viscosity of the initial calibrating liquid, that is of our absolute measurements of viscosity. This question is the subject of this and the two accompanying papers [4, 5].

2. Systematic Errors in Absolute Measurements

Nearly all absolute measurements of viscosity have been based on capillary flow because of the high precision attainable. The analysis of capillary measurements is based on the Poiseuille equation,

$$P_z/Q = 8\eta/(\pi r^4), \tag{1}$$

where P_z is the pressure gradient along the capillary in the region where steady flow exists, Q the rate of flow (volume/time), η the viscosity, and r the radius of the (circular) capillary tube. In the usual case P_z is approximated by P/l, where P is the total pressure drop between reservoirs connected by a capillary of length l. Two small corrections are normally introduced to correct this approximation. One, the kinetic energy correction, accounts for the pressure increment, proportional to Q^2, required to accelerate the liquid to the steady (parabolic) velocity profile consistent with eq (1). The other, the Couette correction, accounts for the pressure increment, proportional to Q, required to overcome viscous flow resistance in the reservoirs. This can be expressed as a small addition to the length and is normally taken as proportional to the radius of the capillary. The inclusion of these two corrections in (1) yields:

$$P/Q = 8\eta(l+nr)/(\pi r^4) + m\rho Q/(\pi^2 r^4) \tag{2}$$

[1] Figures in brackets indicate the literature references at the end of this paper.

where ρ is the density and m and n are presumed to be constants for a particular instrument.

The many attempts to derive eq (2), going back to the nineteenth century, are based on assumed flow patterns not exactly realized in practice [6, 7, 8, 9]. Different calculations have yielded various values for the "constants" m and n, and experimental tests suggest that they differ appreciably for differing velocities of flow, capillary dimensions, and entrance and exit shapes. For square-cut ends, P/Q appears to be independent of Q at low flow rates and linear in Q at higher rates [10]. Trumpet shaped entrances diminish the magnitude of this kinetic energy effect and appear to create flow conditions more compatible with the most convincing theoretical derivations. But even in this case the effective value of m is a pronounced function of Reynolds number, varying from less than 0.1 to 1.0 according to one study [11]. As a rule absolute measurements have been made with square-cut ends on the ground that this configuration permits a more precise determination of l, or of Δl if two capillaries are employed, than would a more complicated shape.

Pressure drops between taps through a capillary or pipe wall have sometimes been used to eliminate the need for these corrections, but generally in work at high Reynolds numbers rather than in measurements intended for the most accurate determinations of viscosity. Many measurements have taken m and n as empirical constants to be evaluated by varying Q and l. The magnitude of these two correction terms varies widely in different measurements; one or both ordinarily influence the final result by several tenths of one percent, and in some cases by several percent. One can certainly question whether corrections of this magnitude with a somewhat nebulous theoretical basis can justify an assumption that any associated systematic error is below 0.1 percent.

Other possible sources of systematic error, which may be even more significant in some cases, have influenced various absolute measurements in capillary instruments. One arises from the normal use of capillaries with diameters of a millimeter or less, and the problem of obtaining capillaries of this size with uniform bores. The average radius of such capillaries can be measured with adequate accuracy, and a reasonable correction for any small average ellipticity or for a small uniform taper made. However, any irregular variation in radius along the length would seem bound to result in radial flow whose influence cannot be calculated. The information available on this type of variation in the tubes used in earlier determinations, quite limited in many cases, indicates that irregular variations in radius of at least 1 percent are common.

Other methods of absolute measurement are subject to difficulties analogous to those above. In nearly all cases some type of end effect or wall effect which cannot be calculated exactly is present. Some variation in the assumed geometrical shape is present, causing some variation from the flow assumed and hence a possible systematic error in the results. With many methods it is difficult to attain the precision required for an overall uncertainty of 0.1 percent.

3. Survey of Previous Measurements

Most absolute measurements of viscosity which have aimed at an accuracy of better than 1 percent have been made on water. Most of the early measurements employed capillary flow. Bingham and Jackson [12] arrived at a value of 1.005 cP for the viscosity of water at 20 °C, based on their evaluation of all the available measurements (at several temperatures) they considered justified in including as valid absolute measurements. These ranged from the work of Poiseuille in 1840–46 to that of Washburn and Williams in 1913. Dorsey, considering the same set of values, arrived at a value of 1.009 on which he based his tabulations for the International Critical Tables [13]. In an attempt to resolve this discrepancy, Bingham [14] presented the conclusions of a group which had reexamined the same measurements, stating: "No research has been sufficiently complete so that all of the needed corrections can be estimated with sufficient accuracy."

The value for the viscosity of water now generally accepted, 1.002 cP at 20 °C and 1 atm, was reported by Swindells, Coe, and Godfrey (SCG) [15] in 1952 based on work which extended over a period of some twenty years. They used four capillaries with square-cut ends, two with lengths differing by approximately a factor of two for each of two radii differing by about 20 percent.

In this work the Couette correction was negligible, but the kinetic energy correction for individual measurements varied from 0.3 to 5 percent as Q was varied to give Reynolds numbers ranging from 100 to 650. Their capillaries were more uniform than most used in earlier work, with a maximum variation in diameter of about ± 0.5 percent and about half that variation in the mean diameters at various positions along the tubes. They established a mean Q with a piston driven by a synchronous motor through a gear train, and measured the pressure in input and output reservoirs with mercury manometers. Later attempts to use this same injector with a pressure measuring device having a much shorter response time disclosed a high frequency fluctuation in Q, representing an additional deviation from the assumed flow.

The "accuracy" of ± 0.03 percent estimated by SCG represents the standard deviation of the mean of values calculated from the intercepts of linear relations between P/Q and Q for the four tubes, treated both individually and in pairs. Deviations of individual measurements from the calculated lines did not exceed 0.04 percent and appear random. Uncertainties in values of the average radii, lengths, mean rates of flow, and temperature were ignorable, but of course no allowance could be estimated for the type of possible systematic error discussed in the preceding section.

Only a few attempts at an absolute measurement have been made since the work of SCG. Roscoe and Bainbridge [16] measured the decrement of a glass sphere filled with water and suspended from a torsion wire. They reported a value of 1.0025 cP with a computed standard error of 0.0005 cP. This error was

estimated from the variability found in measuring the various quantities involved. The magnitude of several possible systematic errors cannot be estimated. The polar and equatorial diameters of their sphere differed by 0.3 percent, which could cause some deviation from the assumed flow. A three percent correction was required for the effect of air damping. This was a theoretical estimate with a correction based on the differences between measurements with air and with a rigid gel in the sphere and theoretical estimates for those two conditions.

G. A. Maliarov [17] reported a value of 1.0035 with an uncertainty of ± 0.1 percent. This was based on the differences between the pressure drops across two capillaries connected in series through a central reservoir. Unexplained variations in the reported replicate pressure measurements across each individual capillary were more than ten times the variations found for the differences between the pressure drops across the individual capillaries in series. For two of these pairs the rates of flow reported covered a range sufficient to make an estimate of the corrections required to calculate viscosity values from pressure drops across individual capillaries. This calculation yields values varying from 1.002 to 1.014, a difference which appears inconsistent with the estimated uncertainty of 0.1 percent.

Kawata, Kurase, and Yoshida [18] measured the viscosity of a 1.89 P hydrocarbon liquid using an absolute capillary technique essentially the same as that employed by SCG. Their Reynolds numbers were 0.14 and below and no kinetic energy correction was needed, but they did require a Couette correction ranging from 0.3 to 0.5 percent. This was determined empirically from measurements with two capillaries, yielding values of n in eq (2) which ranged from 0.79 to 0.88 for different flow rates. This measurement yielded values consistent with a viscosity of water at 20 °C of 1.0016 cP as determined by relative capillary measurements. These were equivalent to the relative measurements used in this work and discussed in section 5. Even if the measurement of viscosity ratios can be considered free of systematic error up to this range the magnitude and uncertain nature of the Couette correction required leave a question as to whether this agreement is enough to confirm the value of 1.002 cP to 0.1 percent. It should be noted that the authors did not present these results as a check of the viscosity of water, but rather of the adequacy of the customary step-up calibration procedure.

4. Objectives and Outline of This Study

We conclude that existing absolute measurements are inadequate for estimating the accuracy of our values of viscosity within limits comparable to their precision. The stated uncertainties of the best measurements are based on the precision attained. Some possible systematic errors associated with deviations from the assumed flow cannot be evaluated. Though there is good agreement of the Roscow and Bainbridge measurement with the SCG value, both involve indirect or empirical corrections uncomfortably large compared to the accuracy claimed.

In most cases where a comparison of viscosity measurements to 0.1 percent is sought, relative measures referred to a common base are sufficient. The "true" value of viscosity is seldom needed with an accuracy of better than 1 percent. However, we certainly cannot claim to understand our measurement process until we have established a reliable estimate of the limits of systematic errors.

The only way of arriving at such an estimate is by comparison of absolute measurements utilizing different types of flow. To reduce the uncertainty associated with the comparison of earlier measurements the geometry should be realized more closely than in previous work, and this realization should be confirmed by independent checks. Any corrections required should be based as nearly as possible on direct measurements. And of course the precision must be commensurate with the accuracy of the final comparison. Even though we might not be certain we had identified all possible systematic errors in either method, the difference found between measurements meeting these criteria should indicate the probable magnitude of any unrecognized systematic errors.

The first of the two methods we selected was based on a measurement of the period of oscillation of a sphere filled with liquid and supported by a torsion wire [4]. If the liquid is Newtonian, its viscosity may be determined from either the period or decrement. Since period can be measured with much greater accuracy, our instrument was designed to maximize the sensitivity of period, rather than decrement, in the design range. There are no end effects to disturb the flow of liquid within a sphere. The two basic problems we can identify in this method are producing a sphere with uniform internal diameter and the possibility of a secondary flow caused by inertial forces.

The second method used a modified capillary flow technique [5]. A much more uniform channel than any previously employed was obtained by forming it from two accurate cylinders and an optical flat, yielding a pipe with a triangular cross section with one side a straight line and the other two circular arcs. In order to eliminate end effects, pressure drops were measured at taps through the pipe wall. Four taps with varying spacing, and flows in both directions at several rates were employed in an attempt to detect any possible effect of a perturbation of flow at the taps.

Since this was planned as an experiment to assess systematic errors rather than as another measurement of the viscosity of water, we used di(2-ethylhexyl) sebacate as a test fluid. It has a viscosity about twenty times that of water, and a much lower vapor pressure and surface tension. We used a commercial grade purified by molecular distillation, Octoil S,[2] for the sphere measurements. For the channel meas-

[2] This material, as presently available, is apparently not reproducible enough to use in lieu of water in the calibration of viscometers. The viscosity of three batches, provided through the courtesy of Dr. B. B. Dayton of the Vacuum Division of the Bendix Corporation, yielded values varying by two percent.

urements, which required much larger quantities of fluid, we used Plexol 201, a less expensive grade of the same chemical. The correction for the small difference in viscosity of these two test fluids, based on relative measurements, did not introduce any significant uncertainty into our comparison of the two results as will be shown later.

For convenience in relating our results to other work, we have referred all measurements to the viscosity of water at 20 °C by comparing the values measured by the absolute techniques with those measured in a pair of Cannon Master intruments calibrated in the usual fashion in terms of water. It would be entirely equivalent, so far as the conclusions we shall draw, to express our results in terms of the viscosity at 25 °C of either of the samples of di(2-ethylhexyl) sebacate used.

5. Results and Discussion

Our measurements of viscosity in the oscillating sphere intrument gave values consistent with a viscosity of water at 20 °C of 1.006 cP. The sum of the magnitudes of all systematic errors that could be identified came to 0.07 percent. The major contributions to this figure came from an uncertainty in the radius of the sphere of 0.01 percent, and an uncertainty in the constant of the torsion wire of 0.015 percent. Some radial flow, expected at large amplitudes, was presumed to account for a slight dependence of the observed period on amplitude which could be seen only at amplitudes much larger than those used in these measurements.

The temperature of the sphere and liquid was known and constant to ± 0.005 °C; that of the torsion wire to ± 0.05 °C. Variations within these limits will cause undetected changes in the viscosity of the liquid and in the spring constant and hence a variability in the final measurements. Repeated measurements of the moment of inertia of the empty sphere showed a spread of ± 0.01 percent, apparently due to a slight variability in the condensed or adsorbed material on the sphere wall after cleaning and subjecting to a vacuum. These three factors can be combined to predict the variability in the measured values of viscosity either by summing the absolute values to yield 0.1 percent or by taking the square root of the sum of squares to yield 0.066 percent. Eighteen observations were included within limits of ± 0.069 percent about the average, with a coefficient of variation of 0.03 percent.

The channel flow measurements yielded a value compatible with a viscosity of water at 20 °C of 1.001 cP. Here the major contributions to the estimated systematic error were ± 0.04 percent from uncertainties in the geometry of the channel and ± 0.06 percent in the pressure measurements. The sum of the magnitudes of all contributions was 0.13 percent. The coefficient of variation of the pressure measurements was 0.02 percent; all measurements were included within the limits of ± 0.03 percent about the mean. As in other pipe flow measurements, no estimate of the effect of possible radial flow can be made. However, the deviations from the assumed shape here were much less than the variation in the internal radii of any of the capillaries used in previous measurements.

The sphere measurements were made on Octoil S both saturated with air and air-free and under various pressures from 1 atm down to less than 0.2 mm Hg. The simplest consistent presentation of all these results and their comparison with measurements on Plexol 201 in the channel is made by relating them all to the viscosity of water at 20 °C using conventional relative capillary viscometers. However, our final comparison of the results of these two measurements does not rely on the accuracy of the instrument constants of our relative instruments.

All the relative viscosity measurements were made in one pair of Cannon Master viscometers with constants of about 0.04 cSt/s. The viscosities of our Octoil S and Plexol 201 differed by slightly less than one percent. The kinetic energy correction was completely negligible, regardless of any reasonable value assigned m in eq (2). Our instruments were filled at 25 ± 1 °C, and the nominal 25° runs made at 25.000 ± 0.001 °C. The surface tensions of hydrocarbons of this type do not differ enough to require a correction when comparing flow times; a difference of ten percent would require a correction to the ratio of flow times of 0.01 percent.

Thus the true kinematic viscosities of these two liquids should be accurately proportional to the flow times. Any uncertainty in the value of the proportionality constant can be avoided, for the purpose of comparing our two absolute measurements, by comparing ratios of the two absolute viscosities as measured in the sphere and channel with the ratio of flow times for the same two liquids in one of the relative viscometers.

A number of measurements were made on each of our liquids in the two relative viscometers. Typical results are shown in table 1. The two samples of Octoil S were taken about two years apart, once near the beginning and once near the end of an extended series of measurements in the sphere. The samples of Plexol 201 were taken from the channel apparatus before each

TABLE 1. *Flow times for Octoil S and Plexol 201 in relative viscometers at 25 °C*

	Viscometer M–204		Viscometer M–205	
	Octoil S	Plexol 201	Octoil S	Plexol 201
1st Sample	481.13	485.80	486.24	490.70
	481.06	485.82	486.14	490.76
	481.01	485.76	486.11	490.61
Av.	481.067	485.793	486.163	490.690
2nd Sample	481.05	485.84	485.93	490.50
	481.04	485.73	486.05	490.50
	481.22	485.81	486.23	490.42
	481.03		486.21	
Av.	481.085	485.793	486.105	490.473
Av., 2 Samples	481.077	485.793	486.130	490.582
s	0.073	0.041	0.112	0.132
Ratio, Plexol/Octoil	1.0098		1.0092	
Av. Ratio	1.0095			

of two runs on successive days. The estimates of standard deviation of the inidividual flow measurements shown, corresponding to coefficients of variation of 0.027 percent or less, are consistent with those normally found with instruments of this type.

These flow times were measured at atmospheric pressure with air-saturated samples. The average ratio in the two instruments is 1.0095. The ratio of the viscosities of the two liquids, again both air-saturated and at atmospheric pressure, as measured in the channel and sphere instruments is 1.0043. This difference of 0.5 percent is ten times the coefficient of variation of any of the measurements involved and about five times our estimate of the maximum systematic error for either of the absolute measurements. It is apparent that some unrecognized systematic error is present in one or both of the absolute measurements.

The comparison of these with earlier measurements can be done only through our measurements of the ratios of the viscosities of our test liquids to that of water by use of our relative viscometers. This involves measurements of the ratios of flow times of water and one intermediate liquid in one set of instruments, of the first and a second intermediate liquid in a second set, and of the second intermediate and our samples in a third set. Thus three ratios of flow times are involved. The first, involving water, required a correction of 0.12 percent because of the large difference in surface tensions. The others involved corrections of about 0.01 percent. The kinetic energy corrections were 0.015 percent or less. The Reynolds numbers involved ranged from 0.3 to 22.

Since we have not identified the systematic errors in the absolute measurements, we cannot arbitrarily rule out the possibility of some unsuspected systematic error in our measurement of viscosity ratios. However, it is difficult to believe that any such error could exceed 0.1 percent, the maximum correction involved in obtaining the ratios between the viscosities of our test liquids and water. If we accept this conclusion we would say that our channel flow measurement corresponds to a value for the viscosity of water marginally lower than the SCG value, and the sphere measurement one significantly higher. Also our two measurements correspond to values which include most of the earlier measurements on water and all of those since the work of SCG.

6. Conclusion

From the results of our measurements and the indirect comparison of these with earlier measurements, we conclude that the best estimate of the contribution of systematic errors to the total uncertainty associated with values of the viscosity of liquids should be taken as ± 0.25 percent. This is 2.5 times the quantity now generally assumed.

These results do not suggest a change in the value of 1.002 cP now generally used as the viscosity of water at 20 °C in the calibration of relative viscometers. We have no grounds for believing either of our results is more likely to be correct than the other. And their average, which differs from either measurement by 2.5 times its expected uncertainty, is unlikely to be correct.

Most users who desire precise viscosity values require only agreement between measurements in different laboratories, achieved by referring their relative measurements to a common base. Such comparisons need not include the additional uncertainty associated with the absolute measurements and there is no present justification to change the accepted base. In cases where the true value of viscosity is important, a value based on 1.002 cP for the viscosity of water at 20 °C seems as good a choice as any, but we believe this value should be assigned an uncertainty of ± 0.25 percent.

This work extended over a number of years, and several individuals made contributions which we are pleased to acknowledge. James F. Swindells participated in many of our early discussions and his knowledge of earlier work (both his own and that of others) and of many far from obvious pitfalls and difficulties was most helpful. Herbert Goldstein, now with the Patent Office, carried out the early development work for the pipe flow measurement. His work uncovered fatal defects in several approaches we had all originally expected would be satisfactory. Theodore R. Young suggested the geometry of the pipe finally used and made a number of valuable suggestions about its assembly. Professor Joseph Kestin of Brown University and Dr. R. E. Manning of the Cannon Instrument Company have given us very helpful advise and suggestions concerning various aspects of the experimental work and interpretation of the results. Dr. Kawata provided us with some additional, unpublished, information about the absolute measurements in the Kawata, Kurase, and Yoshida work [18].

7. References

[1] Barr, G., A Monograph of Viscosity, (Oxford University Press, London, 1931).
[2] Merrington, A. C., Viscometry (Edward Arnold & Co., London, 1949).
[3] van Wazer, J. R., Lyons, J. W., Kim, K. Y., and Colwell, R. E., Viscosity and Flow Measurement, (Interscience, New York, 1963).
[4] White, H. S., and Kearsley, E. A., An absolute determination of viscosity using a torsional pendulum, J. Res. Nat. Bur. Stand. (U.S.), **75A** (Phys. and Chem.) No. 6, 541–551. (Nov.–Dec. 1971).
[5] Penn, R. W., and Kearsley, E. A., An absolute determination of viscosity using channel flow, J. Res. Nat. Bur. Stand. (U.S.), **75A** (Phys. and Chem.), No. 6, 553–560. (Nov.–Dec. 1971).
[6] Barr, G., loc. cit., pp. 12–35.
[7] Goldstein, S., Modern Developments in Fluid Dynamics, Vol. **1**, pp. 297–308, (Oxford University Press, London, 1938).

[8] Weissberg, H. L., End corrections for slow viscous flow through long tubes, Phys. Fluids **5,** No. 9, 1033–1036 (Sept. 1962).

[9] Christiansen, E. B., and Lemmon, H. E., Entrance region flow A.I.Ch.E. J. **11,** No. 6, 995–999, (Nov. 1965).

[10] Swindells, J. F., Hardy, R. C., and Cottington, R. L., Precise measurements with Bingham viscometers and Cannon Master viscometers, J. Res. Nat. Bur. Stand. (U.S.), **52,** No. 3, 105–120, (March 1954) RP 2479.

[11] Cannon, M. R., Manning, R. E., and Bell, J. D., Viscosity measurement, The kinetic energy correction and a new viscometer, Anal. Chem. **32,** No. 3, 355–358 (March 1960); Einfeldt, J., Zur Kapillarviskosimetrie verdünnter Lösungen, II. Bestimmung der Abhängigkeit der kinetischen Energiekorrektur von der Ausflusszeit, Rheologica Acta **9** (3), 429–434, (1970).

[12] Bingham, E. C., and Jackson, R. F., Standard substances for the calibration of viscometers, Nat. Bur. Stand. (U.S.) Bull. **14,** (1919), pp. 59–86.

[13] Dorsey, N. E., Viscosity of water, sulfuric acid, liquid carbon dioxide and certain organic liquids, Int. Crit. Tables **5,** Ed. E. W. Washburn, p. 10, (McGraw-Hill, New York, 1929); Properties of Ordinary Water Substance, pp. 182–184, (Reinhold Pub. Co., New York, 1940).

[14] Bingham, E. C., Notes on the fluidity of water at 20 °C, J. Rheology **2,** No. 4, pp. 403–423, (Oct. 1931).

[15] Swindells, J. F., Coe, J. R., Jr., and Godfrey, T. B., Absolute viscosity of water at 20 °C, J. Res. Nat. Bur. Stand. (U.S.), **48,** No. 1, pp. 1–31, (Jan. 1952) RP 2279.

[16] Roscoe, R. and Bainbridge, W., Viscosity determination by the oscillating vessel method, II. The viscosity of water at 20 °C. Proc. Physical Society **72,** Part 4, pp. 585–595, (Oct. 1958).

[17] Mailiarov, G. A., Absolute viscosity of water at a temperature of 20 °C, Trudy Vses. Nauchn-Issled, Inst. Metrl. (Proc. of the All-Union Sci. Res. Inst. of Metrology), No. 37(97), pp. 125–140 (1959). (In Russian.)

[18] Kawata, M., Kurase, K., and Yoshida, K., Realization of a viscosity standard, Proc. Fifth Int. Congress on Rheology, Vol. **1,** Ed. S. Onogi pp. 453–472 (Univ. of Tokyo Press, 1969).

(Paper 75A6–684)

JOURNAL OF RESEARCH of the National Bureau of Standards—A. Physics and Chemistry
Vol. 75A, No. 6, November–December 1971

An Absolute Determination of Viscosity Using a Torsional Pendulum

Hobart S. White* and Elliot A. Kearsley

Institute for Basic Standards, National Bureau of Standards, Washington, D.C. 20234

(July 28, 1971)

An absolute measurement of the viscosity of di(2-ethylhexyl) sebacate with a torsional pendulum viscometer. The apparatus and calibration procedures are discussed and a detailed study of errors is made. The systematic error was estimated to be less than ±0.07 percent and the variability was shown to be less than ±0.07 percent. There is an unexplained difference of 0.3 to 0.4 percent between these measurements and measurements with a capillary instrument.

Key words: Absolute measurement; calibration; standard; torsional pendulum; viscosity.

1. Introduction

In calculating the accuracy of any physical measurement, it is not possible to be sure that *all* systematic errors have been taken into account. Moreover, the more the precision is improved, the greater is the possibility that an overlooked error is significant. A comparison of measurements made by different methods, each of which insofar as possible gives rise to quite different errors, is the most direct evidence of the completeness of the error estimates. For this reason, some years ago we attempted a measurement of viscosity by an absolute method and with errors not exceeding 0.1 percent in order to compare with measurements of presumed equal accuracy made with a capillary viscometer.

We chose to make the measurement with a viscometer consisting of a spherical shell suspended from a torsion wire and filled with the fluid whose viscosity is to be measured. The sphere is excited in torsional oscillation and the subsequent motion observed. In principle the viscosity of a Newtonian fluid may be obtained from either the period or the damping of this motion. In 1959 [1][1] an analysis of the absolute torsional pendulum viscometer was published giving design criteria for the sphere and wire suspension which made the period sensitive to viscosity. That paper pointed out that modern techniques of measuring time intervals with great accuracy make this a promising method of measuring viscosity.

This paper describes the apparatus and the procedures used in calibrations and measurements. Difficulties encountered in obtaining a high degree of accuracy are discussed. The most reliable measurements reported are those obtained for Octoil S, a fluid with nominal kinematic viscosity of 19 centistokes (cSt). These measurements were subsequently compared with an absolute measurement with a capillary instrument [2]. Measurements of a few other fluids were also reported with error estimates, primarily as a consistency check. A few measurements by the method of decrement are reported, but without complete error estimates.

2. Apparatus and Method of Measurement

The apparatus was designed to exhibit relatively high dependence of period on viscosity for a range from 10 to 150 cSt. Above and below this range, the dependence is markedly weaker. Figure 1 is a photograph of the complete apparatus showing the hollow sphere hanging above the thermostatted and vacuum tight housing within which it normally operates and the optical devices and timer used in measuring the period. Figure 2 is a schematic cross section of the thermostatted housing showing the sphere hanging on the torsion wire in the normal operating position. In operation, the sphere is excited in torsional oscillation, and the period is measured. The kinematic viscosity is then given by:

$$\nu = R^2\sqrt{\frac{K}{I_0}}\,\hat{\eta}(\tau, \alpha)$$

$$\tau = \sqrt{\frac{K}{I_0}}\left(\frac{T}{2\pi}\right),\ \alpha = \frac{I}{I_0} \qquad (1)$$

where ν is the kinematic viscosity, K is the torsion constant of the suspension, R is the internal radius of the hollow sphere, T is the period of the oscillation, I is the moment of inertia of the empty sphere, and I_0 is the moment of inertia of the test fluid considered as a

*Retired from the Institute for Basic Standards, National Bureau of Standards, Washington, D.C. 20234.

[1] Figures in brackets indicate the literature references at the end of this paper.

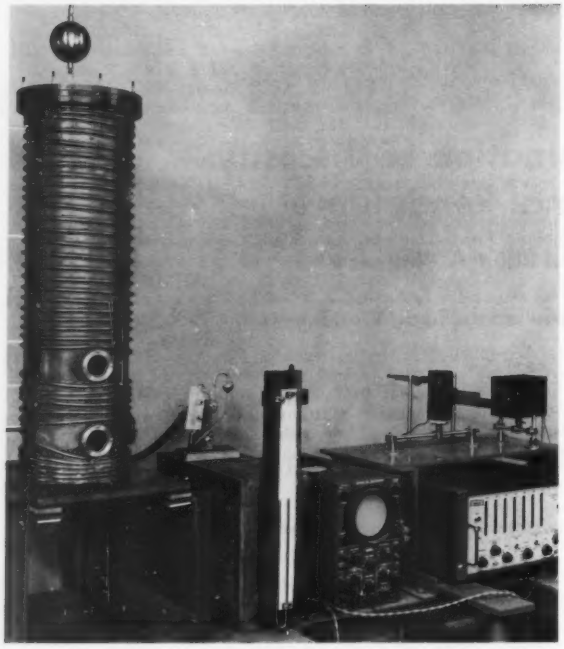

FIGURE 1. *Photograph of the torsional pendulum viscometer.* The sphere has been withdrawn above the thermal chamber.

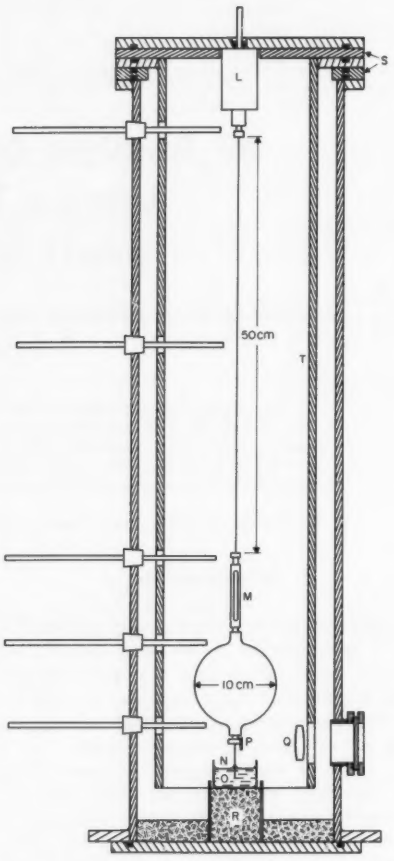

FIGURE 2. *Cross-section of thermal chamber of viscometer with sphere in operating position.*

rigid sphere. The dimensionless quantity $\hat{\eta}$ is a mathematical function of the two dimensionless variables τ and α. An accurate determination of viscosity requires measurements of all the physical quantities entering into these equations. The calculation of $\hat{\eta}$ (τ, α) can be done to the necessary accuracy by numerical methods using a modern digital computer. Details of this calculation are given in [1], (where η is used for our $\hat{\eta}$).

2.1. The Torsion Constant of the Suspension

The torsion wire was of an alloy of 92 percent platinum and 8 percent tungsten. This alloy was shown by Kestin, et al. [3] to be especially suitable for use as a torsion wire by reason of its low internal friction and stable elastic constant. The wire was a 51-cm length of 0.051-cm diam which was heat treated (to about 1300 °F) to relieve stresses after which the ends were hard soldered into threaded fittings.

The calibration of this viscometer requires an extremely accurate evaluation of the torsion constant K. It was necessary, therefore, to measure the constant at various temperatures and for various tensile loads on the wire. For this purpose, a number of cylinders of calculable moment of inertia were made. The torsion constant of this wire was measured by timing the oscillations of these cylinders. Steel and brass stock were found to be unsuitable[2] for making these rods, presumably because the material was not sufficiently homogeneous. Aluminum alloy 6061 and oxygen-free high-conductivity copper were found to be suitable materials. Six cylinders were used as shown in table 1, with moments of inertia ranging from about 11,000 to 1,200 g · cm² and weights ranging from 2,100 to 510 g.

The measurements of period were made with the cylinders oscillating in torsion while suspended in the position of the sphere shown in figure 2. The air pressure was reduced to less than 0.2 mm of mercury within the thermal jacket to eliminate any significant effects of the atmosphere on the period (see section 4). The temperature of the torsion wire was taken to be that indicated by the mercury in glass thermometers through the thermal jacket shown in figure 2. The temperature was controlled for a day or more before measurements were made to insure that the apparatus was in thermal equilibrium. The period measurements were made with the optical and timing systems used in the viscosity measurements. These systems are described in section (2.4).

[2] Several measurements of the torsion constant were made with a cylinder machined down in radius between each measurement. When plotted against the weights of the cylinders, the measurements for steel and brass cylinders did not fall on the same smooth curve as did measurements using aluminum or copper cylinders.

TABLE 1. *Calibrating rods*

Rod number	Material	Diameter at 25 °C	Weight in vacuo	Weight before drilling ends, in vacuo	Moment of inertia
		inches	*grams*	*grams*	$g \cdot cm^2$
1	6061 alloy	1.717794	511.31	513.43	1221.80
2	6061 alloy	1.758891	535.58	537.55	1341.14
3	6061 alloy	3.010187	1574.36	1576.52	11520.30
3a	6061 alloy	2.655604	1224.80	1226.96	6978.06
4	OFHC Copper	1.758936	1773.51	1780.19	4441.65
5	OFHC Copper	1.907257	2093.75	2099.75	6159.75

The torsion constant of the wire was found to conform to the equation

$$K = 11471.5 - 0.0208\, g - 2.6(t - 25)$$

where K is the torsion constant in dyne cm, g is the tensile load on the wire in grams and t is the temperature in degrees Celsius.

This expression for the torsion constant is accurate to better than ± 0.015 percent through the necessary range of temperature around 25 °C and through the range of tensile load spanned by the cylinders in table 1. The dimensions of the cylinders were measured at 20 °C to ± 20 microinches and the masses to ± 10 milligrams. Even for measurements made with the smallest cylinder we estimate that the errors in these measurements contribute an error of at most ± 0.004 percent of the torsion constant. We estimate a further error of ± 0.002 percent from a possible error of, at most, 10 percent in the calculation of the temperature correction of the moment of inertia. The largest error in the calculation of the moment of inertia comes, however, from the calculation of the correction for the drilled holes, brass fittings, wax used to affix the mirror, etc. This correction amounts to 1.3 $g \cdot cm^2$. A 10-percent error in this calculation, which is a reasonable but generous estimate, would cause an error of ± 0.010 percent in the moment of inertia of the smallest cylinder. Errors of less than 5 μs in the measured period and errors of less than 0.05 °C in the temperature assigned to the wire caused a negligible error in the torsion constant.

2.2. The Construction of the Sphere and the Determination of Its Radius

Initially, a sphere was constructed of aluminum by machining two hemispherical cavities threaded to screw together at the equator. There was no way to be sure, however, that the fit at the threads was exact enough to prevent the flow of a significant amount of fluid into the seam between the hemispheres. Ultimately a nickel sphere was made without this seam by electroplating over a spun aluminum form. The form was machined to a sphere and ground to a tolerence of 0.001 in, then fitted with nickel polar hubs concentric to the same tolerance. It was then plated with a flash plating of copper followed by a plating of nickel to a thickness of about 0.1 in. The aluminum form was removed by washing with caustic solution flowed through holes in the polar hubs. The exterior of the sphere was then turned down so that the final sphere had a wall thickness of 0.085 in and a nominal diameter of 10 cm. A rough calculation shows that these walls are easily stiff enough to prevent a significant change of shape under load.

The plating process was carried out at an elevated temperature (45 °C to 60 °C) so that the actual internal radius of the sphere was larger than the radius of the form at 25 °C which was $4.9535 \pm .0025$ cm. Since the difference between thermal expansion coefficients of aluminum and nickel is roughly 1×10^{-5}/ °C, the radius of the sphere at 25 °C should be about 4.955 cm. The calculation of the radius in this way is not very accurate, however, and a more direct measurement is needed.

For this purpose, the mass of distilled and boiled (approximately air-free) water needed to fill the sphere at 25 °C was measured by weighing the sphere empty and full. The level of the water was adjusted to a fiducial mark in the sight glass at the top of the sphere while it was immersed in a bath of oil thermostatted at 25.00 °C. A value of 0.9970478 g/cm^3 was used for the density of water and account was taken of air buoyancy and the volume of water in the sight glass and in the holes in the polar hubs. The measurement was repeated with two oils of low vapor pressure using values of density as measured by the Metrology Section of NBS. These measurements give a volume of the sphere at 25 °C of 509.515 cm$^3 \pm 0.002$ percent, which is the volume of a sphere of radius 4.9548 cm. The uncertainty of ± 0.002 percent assigned includes the spread of a number of weighings. The uncertainty in the density of water is negligible.

A value for the equatorial radius of the sphere can be found by filling the sphere with an oil of high viscosity and measuring the period. This is approximately equivalent to measuring the moment of inertia of a rigid sphere. Oil N with a viscosity of about 10 St was used for this purpose. The moment of inertia was calculated from eq (1) using the viscosity measured by a capillary instrument. This value of viscosity need not be extremely accurate since a one percent error will lead to an error in effective radius of only about 0.005 percent.[3] The equatorial radius measured in this way was 4.95525 cm. The difference between this and the radius of a sphere equal in volume to that measured is less than 0.01 percent and this difference may be taken as the uncertainty in the radius of the sphere. In fact, the evidence is that the figure of the "sphere" was close to that of a prolate spheroid with the equatorial radius slightly greater than the polar radius. Consequently, in all subsequent calculations we used a moment of inertia for the fluid calculated from the mass of the measured volume of fluid and the measured equatorial radius.

2.3. The Moment of Inertia of the Empty Sphere

The moment of inertia of the empty sphere was found

[3] In fact, the independent value of the viscosity of N oil measured by the decrement method (see section 4) was within a half percent of the capillary value.

to be 4074.45 g · cm² ±0.022 percent by timing the period of torsional oscillations at 25 °C in vacuum. This value is based on the average of a number of observations of the period of the empty sphere in a vacuum and on the previously determined value of K. An error of ±0.007 percent corresponds to the spread of a number of measurements made at different times. It is accounted for, in part, by the condensed or absorbed material on the sphere wall which apparently varied each time the sphere was subjected to a vacuum (the measured weight varied by about ±0.005 percent), and, further, by small changes in the mounting of the mirror. There is also a possible error of 0.015 percent associated with the value of the spring constant K. This error will not contribute to the scatter in the observations of period. The actual timing errors involved in measuring the period of the empty sphere were completely negligible, since they amounted to only 2×10^{-4} percent of the period (see section 2.4).

Equation (1) applies to a sphere of fluid contained in a rigid shell of moment of inertia I. Thus, in calculating I, the effective moment of inertia of the small amounts of fluid in hub and sight glass should be added to the moment of inertia of the empty sphere. In practice, these corrections for the nickel sphere are negligible because the small cylinders of fluid are all on the axis of rotation. For the original aluminum sphere, however, the unknown amount of fluid which leaked into the equatorial seam could produce a sensible effect.

2.4. The Period of the Oscillations

Measurements of period were made using an electronic timer with an optical lever and photomultiplier. Light from the 0.005-in diameter straight filament of a shielded lamp shines through a window and lens (Q in figure 2) to a small galvanometer mirror (P in figure 2) fastened to a brass fitting on the lower pole of the sphere. The filament image is reflected through the lens and window to a horizontally adjustable vertical slit 0.005 in wide in an opaque film on the outside of a slotted black box enclosing a photomultiplier tube. The output from the photomultiplier tube is wired to the timer and to an oscilloscope. The photomultiplier and electronic timer arrangement was checked against the NBS standard frequency and found to measure time intervals to within 5 μs. Errors from this source are completely negligible, since only intervals of several seconds duration were measured. The principal difficulties of the measurement of period are to be found in the mechanical arrangements.

Actually, half periods were measured by timing the intervals between zero crossings of the light beam. At the beginning of the oscillations, there is a transient effect, referred to as a "zero-point drift" in the analysis of the apparatus [1], which dies out in a few oscillations. This effect is illustrated in figure 3 which shows some data for the aluminum alloy sphere filled with water. (The effect is especially large with low viscosity fluids and spheres of low moment of inertia.) The time interval between zero crossings is plotted against the number of the zero crossing at the beginning of the interval. The transient effect causes the even half periods to be larger than the odd ones. This effect can be used to adjust the slit, first by rough mechanical adjustment and finally by setting the trigger voltage of the timer. When the even and odd half periods approach the same limiting value, as they do in figure 3, the slit is set to give a correct zero position.

Figure 4 shows a similar plot for the nickel sphere filled with Octoil, but for two different starting amplitudes. No effects of starting amplitude are evident although the starting effect of the previous paragraph is present. This fact is important in establishing that secondary flows due to inertial effects in the fluid are not causing a measurable effect on the period. Figure 5 shows a similar plot for N oil. For this liquid, with a viscosity some 50 times that of Octoil, a pronounced amplitude effect can be observed. The data after starting light amplitudes[4] of 12 to 36 degrees were obtained at the same temperature and pressure within a forty minute period of time, and these data show an increase of sphere period with pass number until the amplitude has decreased to about 8 degrees. The data for a starting amplitude of the light of 8 degrees (obtained at a different ambient pressure and slightly different temperature) shows no change of period with pass number.[5] In measuring the period of the sphere filled with Octoil, half periods before the 5th pass are not used because of excessive "starting effect" and half-periods beyond the 9th pass were not used because of the very small amplitude. Thus, the average of half periods starting with the 5th, 6th, 7th, and 8th passes (having light beam amplitudes in the range from 6 down to 3 degrees at the start of timing), were used in the calculation of viscosity.

Some measurements of period were made with the apparatus at atmospheric pressure. In such cases a correction to the observed period was ascribed to the air drag on the outer surface of the sphere. This correction was determined from data on the period of the

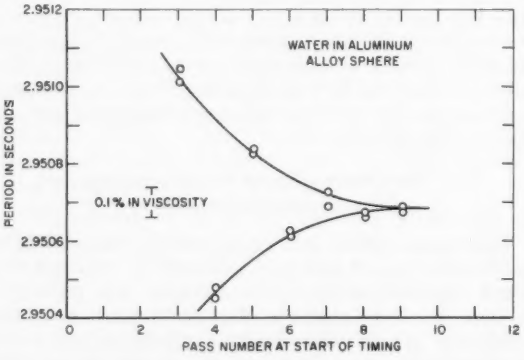

FIGURE 3. *Period from time between zero-crossings plotted against number of zero-crossing at beginning of pass.*
This example of water in the aluminum sphere illustrates the transient effect.

[4] The angular amplitude of the oscillations of the light beam are twice those of the sphere.
[5] Note that the experimental scatter for these measurements on a liquid with viscosity well outside the design range of the sphere has increased from less than 0.1 percent to about 0.5 percent.

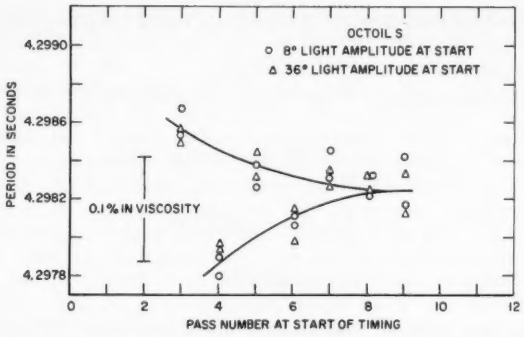

FIGURE 4. *Period plotted against pass number for Octoil S showing transient effect but no amplitude effect.*

sphere while empty and while filled with air-free oil N at pressures ranging from 0.2 mm of Hg to atmospheric.[6] The data obtained with the empty sphere were interpreted as having 48 percent of the air drag correction caused by the air within the sphere, since that is the percentage of surface area exposed in the internal cavity. With these data a correction could be calculated for a given period and air pressure by linear interpolation. At 760 mm of Hg these corrections amounted to 550 μs. for Octoil and 470 μs. for N oil.

Vibration from nearby traffic could cause pendulum motions of the sphere and interfere with the measurement of period. A needle from the lower polar hub of the sphere (or cylinder when calibrating the torsion wire) extending into a container of high viscosity mineral oil (about 10 St at 25 °C) effectively damped the swinging motion with no measurable effect on the period of the oscillation. As a further precaution, the whole apparatus was mounted on a base consisting of two 30-in concrete cubes (visible in figure 1) connected by four heavyweight steel railroad rails embedded in the concrete at each end. Vibration-insulating pads of laminated rubber and cork composition under the corners of each concrete cube separated the base from the concrete floor.

2.5. Miscellaneous

Octoil S is a commercial di(2-ethylhexyl) sebacate that has been highly purified by molecular distillation. It was chosen because its low vapor pressure (about 6×10^{-7} mm Hg at 25 °C) made it suitable for use under vacuum conditions down to about 10^{-3} mm Hg, and its viscosity (about 19 cSt at 25 °C) is within the 10 to 150 cSt design range of the spheres.

Oil N is a Pennsylvania bright stock similar in viscosity to the discontinued SAE 70 motor oil. It was chosen because its low volatility under vacuum and its viscosity (about 1000 cSt) made it suitable for determining the effective inner radius of the sphere. (See section 2.2) The viscosity is low enough to permit filling and emptying of the sphere with reasonable ease and is high enough so that the period of oscillation of the filled sphere depends only slightly on viscosity.

Pressures below 1 mm of mercury were measured by a McLeod gage. Pressures between 1 mm and 1 atm were determined by suitable manometers, one of which is shown in figure 1. Atmospheric pressure was measured by a conventional mercury barometer. A mechanical vacuum pump was used to obtain the pressures less than atmospheric.

Mercury-in-glass thermometers (K in figure 2), graduated in tenths of degrees Celsius and calibrated in hundredths of degrees, were used for measuring the temperature inside the housing at appropriate positions. The calibration took into account the horizontal position of the thermometers and corrected for the ambient pressure at the bulb.

Whenever the sphere was filled, it was immersed in a constant temperature oil bath at 25.00 ± .01 °C while the oil level in the sphere sight glass was adjusted to a fiducial line. A syringe with a long needle was used for adding or removing oil. The bath temperature was controlled by a large-bulb mercury-in-glass thermoregulator with fixed enclosed platinum points. The sphere and sight glass could be used as a dilatometer to calculate changes in density associated with temperature and pressure variations.

When the wire constant was being determined, when the moment of inertia of the empty sphere was being measured, or when the sphere was being used for viscosity determinations, oil was pumped from the constant temperature oil bath through the copper coil surrounding the sphere housing. The thermoregulator in the oil bath was set at 24.7 °C to allow for a 0.3 °C temperature rise in the oil line following the pump, while a similar thermoregulator set at 24.9 °C and enclosed in a perforated heavy-wall copper tube located at the base of the housing, near the copper coil, controlled the room air conditioner. This arrangement maintained the ambient temperature of the housing at 25.0 °C.

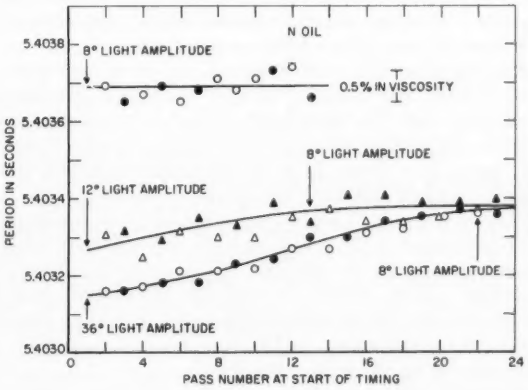

FIGURE 5. *Period plotted against pass number for N oil showing amplitude effect.*

The data at 8° light amplitude was taken at temperature different than for the other data.

[6] Account must be taken of the change of viscosity with pressure (see section 3).

3. Calculation of Viscosity from Measured Period

The equation giving kinematic viscosity (= viscosity/density), in terms of the measured period, T, and parameters of the sphere is repeated here, with b, the equatorial radius, replacing R, the radius of a perfect sphere of the same volume (see section 2.2)

$$\nu = b^2\sqrt{\frac{K}{I_0}}\,\hat{\eta}(\alpha,\tau)$$

$$\alpha = \frac{I}{I_0},\ I_0 = \frac{2}{5}\rho V b^2$$

$$\tau = \frac{T}{2\pi}\sqrt{\frac{K}{I_o}}$$

b = equatorial radius = 4.95525 cm $\delta\, b/b = \pm 1.0 \times 10^{-4}$ (sec. 2.2)
K = torsion constant of wire = 11455.54 dyn-cm $\delta\, K/K = \pm 1.5 \times 10^{-4}$ (sec. 2.1)
I = measured moment of inertia of empty sphere = 4074.445 g · cm² $\delta\, I/I = \delta\, K/K$
I_0 = moment of inertia of liquid in sphere moving as rigid body
V = volume of sphere excluding sight glass and hubs = 509.515 cm³
ρ = density of test fluid
$\delta I_0/I_0 = \delta\rho/\rho + \delta\, V/V + 2\delta\, b/b$
$\delta V/V = \pm 2 \times 10^{-5}$
$\delta\rho/\rho = \pm 2 \times 10^{-5}$

The above uncertainties refer to systematic[7] errors only, that is those associated with constants of the apparatus and the density of the test fluid. The systematic error in period was less than five microseconds and the periods were two seconds or longer. That in weighings was less than 1 mg in values of 270 grams or greater. Neither contribute significantly to the total systematic error, though there were differences between replicate determinations due to variations in the mass of the sphere (see section 2.3).

The functional relationships between $\hat{\eta}$, α, and τ comes from the solution of the equations of motion assuming that the fluid motion has no component in planes containing the axis of rotation of the sphere (no secondary flow). It is an implicit relation which can be used to calculate the τ's corresponding to given values of $\hat{\eta}$ and α. A set of such solutions was computed and tabulated with a fine enough grid so that linear interpolation was permissible. Thus, using an observed period T (from which τ could be calculated) and a known α, a corresponding value of $\hat{\eta}$ could be found from the computed tables by interpolation and a corresponding value of ν obtained.

Example of calculation of viscosity from period:

Air-free Octoil S at 0.24 mm Hg, 24.97 °C. $\rho = 0.91014$ g/cm³
Observed period, $T = 4.297637$ s.
The parameters of the sphere listed above are then:

$$I_0 = \frac{2}{5}V\rho b^2 = 4554.660\ \text{g} \cdot \text{cm}^2$$

$$\tau = \frac{1}{2\pi}\sqrt{\frac{K}{I_0}} = 1.084750$$

$$\alpha = I/I_0 = 0.894566$$

In the table of calculated values of τ is a line with $\alpha = 0.89450$, $\tau = 1.084737$, $\hat{\eta} = 0.0050100$, and in this region of the table $\Delta\hat{\eta}/\Delta\tau = 0.07042$, $\Delta\hat{\eta}/\Delta\alpha = -0.03380$. Thus, a linear interpolation gives us for the $\hat{\eta}$ corresponding to the observed τ and α:

$$\hat{\eta} = 0.0050086$$

from which we calculate

$$\nu = \hat{\eta}b^2\,(K/I_0)^{1/2} = 19.504\ \text{cst.}$$

The systematic error associated with this value may be calculated in terms of the independent constants of the experiment b, K, ρ, and V as

$$\frac{\delta\nu}{\nu} = \left(1 - \frac{\tau}{\hat{\eta}}\frac{\partial\hat{\eta}}{\partial\tau} - 2\frac{\alpha}{\hat{\eta}}\frac{\partial\hat{\eta}}{\partial\alpha}\right)\left(\frac{\delta b}{b} + \frac{\delta\rho}{\rho}\right) + \frac{1}{2}\left(1 + \frac{\tau}{\hat{\eta}}\frac{\partial\hat{\eta}}{\partial\tau} + 2\frac{\alpha}{\hat{\eta}}\frac{\partial\hat{\eta}}{\partial\alpha}\right)\left(\frac{\delta K}{K} + \frac{\delta V}{V}\right) = \pm 6.2 \times 10^{-4},$$

this 0.06 percent is the sum of the absolute values of the four independent contributions, that associated with K giving 0.03 percent, that with b giving 0.02 percent, while the other two contributions are each less than 0.01 percent.

In order to compare this value of viscosity to that obtained at atmospheric pressure with a capillary instrument, one must know the effect of pressure on the viscosity. At 25.00 °C and pressures below 10 mm of Hg, the viscosities of Octoil S and N oil are lower than that at atmospheric pressure by 0.20 percent and 0.30 percent respectively. This value can be calculated for Octoil from published measurements of viscosity and density as a function of pressure for both Octoil and Plexol, a less refined commercial grade of the same chemical. These liquids are labeled samples 1–A and 19–D respectively in an ASTM report on pressure effects on lubricating fluids [4]. The effect of pressure on the viscosity of N oil was measured with relative viscometers in our laboratory, and the effect on the density of both oils measured using the sphere as a dilatometer.

Corrections of ρ and ν for the effect of being air-free were also needed for both oil N and Octoil S. For air-free oil N at 25.00 °C the density was greater by

[7] These errors will not produce a scatter among replicate determinations of the viscosity of a given fluid.

0.00007 g/cm³ and the viscosity was greater by 0.038 St (0.36 percent) than that of air saturated oil N; for Octoil S the corresponding density difference is 0.000010 g/cm³ and the viscosity difference is 0.00068 St (0.35 percent). With oil N, these corrections were estimated from relative measurements with a capillary viscometer and from weighings of a known volume in the NBS density laboratory. Air-free Octoil S (much lower in viscosity than oil N) apparently dissolved air rapidly while being transferred from the sphere to capillary viscometers or volumetric flasks. Accordingly, for Octoil S these corrections were estimated from relative measurements made with the sample in the sphere and at atmospheric pressure.

4. Determination of the Viscosity of N oil by Measurement of Decrement

Since the viscosity of oil N is used in the determination of the radius of the sphere (see section 2.2) the apparatus was adapted to give an independent value of this viscosity through measurement of the decrement of the torsional oscillation.

The apparatus was designed for the determination of viscosities by measurement of periods, and originally, no provision was made for determining decrement. We found, however, that quite accurate decrements could be measured through timing successive passes of the light beam through a small interval near the zero rest position. The single 0.005-in slit in front of the photomultiplier tube was replaced with two similar slits with their centers 0.065 inches apart. At rest, the light beam triggering edge was adjusted midway between the two slits. In motion, the light beam triggering edge started the timer as it passed the center of one slit and stopped it as it passed the corresponding position in the second slit. The 0.065-in interval was chosen to be large enough for good accuracy of timing and small enough so that the average velocity over the interval would be nearly the same as the instantaneous velocity at the zero rest position.

For computing the viscosity from decrement, the ratios of timings for the 0.065-in light beam travel near the zero rest position, for successive passes in the same direction, were used. The ratio was measured for beam travel in each direction and then averaged to minimize the error caused by any inexactitude in centering of the interval. If t_n denotes the time for nth traverse of the interval, D denotes a decrement defined by

$$D = (\log_e t_n / t_{n+1})/\pi.$$

This decrement must be corrected for the damping caused by the internal friction of the torsion wire and the viscous "air-drag."

Decrement measurements were made with the empty sphere oscillating in air from atmospheric pressure down to 0.008 mm Hg. The damping decreased with decreasing pressure at pressures above 1.0 mm Hg, remained almost constant while the pressure was between 1.0 and 0.1 mm, and again decreased as the pressure was decreased below 0.1 mm. Measurements of the period of the empty sphere showed no change throughout the range of pressures from 1.0 to 0.01 mm Hg. Presumably, the effects of pressure changes down to pressures of 1.0 mm of Hg are primarily through changes of the density of air while those for pressures below 0.1 mm of Hg are associated with the changing viscosity or mean free path of the air. Data were obtained with oil N_{35} and Octoil S at pressures down to about 0.1 mm Hg.

In the range of 0.1 to 1 mm Hg ambient pressure, the magnitude of the corrections to the decrement, D, were estimated as:

correction due to internal friction of wire 0.000067
correction due to air drag on sphere 0.000031.

These should be compared to a total decrement for oil N of about 0.04.

The viscosity of oil N obtained by this decrement method was within 0.5 percent of the value obtained by capillary methods relative to the currently accepted value for the viscosity of water at 20 °C.

5. Results

The collection of measured values of kinematic viscosity of Octoil S is shown in table 2. These measurements were made at various times over a period of about two years. Values measured with the original machined aluminum sphere are included and are marked with one or two asterisks to indicate two conditions of smoothness of the interior surface.[8] Since the temperature and pressure varied slightly for the different measurements, we compare them in terms of the difference between the viscosity measured in the sphere and that measured in a relative capillary viscometer, calibrated in terms of the generally accepted value for the viscosity of water, at the same temperature and pressure [2]. Measurements were also made on several test fluids outside the design range of the apparatus to see if the deviations are consistent with our analysis of the instrument. These fluids, water and two of the standard viscosity fluids formerly distributed by NBS, each had a vapor pressure at room temperature which excluded the possibility of operating the instrument in vacuum. Consequently, all the determinations of viscosity on these three fluids involved a period corrected to account for air drag (see section 2.4.). The results are shown in table 3. Determinations of viscosity by the decrement method are found in table 4.

A systematic error of ± 0.06 percent was estimated for the measurement of the viscosity of Octoil S as noted in section 3. Calculations for water, Oil D, and Oil L yielded values ranging from ±0.05 to ±0.07 percent, an insignificant variation, with an average for the four calculated values of ±0.065 percent. We may therefore assign an estimated systematic error of ±0.07 percent to the measurement of any fluid in this range of viscosity (1 to 90 cSt).

[8] The aluminum sphere consisted of two hemispheres which screwed together at the equator. The resulting seam between the hemispheres introduced an error in the measured viscosity which was probably as much as 0.1 percent.

TABLE 2. *Comparison of viscosity of Octoil S (in centistokes) measured by sphere period (absolute method) and capillary (relative method with value calculated based on viscosity of water at 20 °C = 1.004 cSt)*

Fluid and condition	Ambient pressure	$\nu_{sphere.}$ from period measurements	$\frac{\nu_{sphere} - \nu_{cap}}{\nu_{cap}} \times 100$
	mm Hg	*cSt*	*percent*
Octoil S, air-saturated	758	19.475	0.404
	757	19.477	.414
(ν_{cap} = 19.397)	745	19.468	.366
	738	19.468	.364
	735	19.470	.375
Average	atmos	19.472	0.385
Octoil S, air-free	766	19.541	0.389
	766	19.539	.382
(ν_{cap} = 19.465)	766	19.537	.369
	756	19.544	.404
	759	19.548	.427
	759	19.547	.419
	760	19.550	.435
	740	19.541	.390
	755	19.540	.383
Average	atmos	19.543	0.400
Octoil S, air-free	0.24	19.484	0.297
(ν_{cap} = 19.426)	.16	19.497	.368
	2.0	19.497	.363
	0.9	19.510	.433
Average	vac	19.497	0.365
Octoil S, average, all	.....	.....	0.388
Octoil S,* air-free	756	19.533	0.347
	756	19.517	.269
(ν_{cap} = 19.465)	756	19.513	.245
	755	19.508	.221
	753	19.524	.303
	753	19.525	.307
Average	atmos	19.520	0.282
Octoil S,* air-free	0.15	19.495	0.356
	.15	19.488	.321
(ν_{cap} = 19.426)	.13	19.483	.293
	.12	19.492	.342
	.11	19.495	.354
Average	vac	19.491	0.333
Octoil S,* average, all	.....	.....	0.305
Octoil S,** air-free	756	19.570	0.538
	756	19.572	.549
(ν_{cap} = 19.465)	760	19.556	.465
Average	atmos	19.566	0.517
Octoil S,** air-free	1.0	19.522	0.493
	0.22	19.524	.504
(ν_{cap} = 19.426)	0.22	19.528	.524
Average	vac	19.525	0.507
Octoil S,** average, all	.....	.....	0.512

* In aluminum alloy sphere as machined.
** In aluminum alloy sphere after polishing interior.

TABLE 3. *Comparison of viscosities (in centistokes) measured by sphere period (absolute method) and capillary (relative method with value calculated based on viscosity of water at 20 °C = 1.004 cSt).*

Fluid and condition	Ambient pressure	ν_{sphere}, from period measurements	$\frac{\nu_{sphere} - \nu_{cap}}{\nu_{cap}} \times 100$
	mm Hg	*cSt*	*percent*
L_{31}, air-saturated	752	86.991	0.275
	752	87.020	.309
(ν_{cap} = 86.752)	752	86.996	.281
	755	87.047	.340
	758	86.965	.246
	758	86.983	.266
Average	atmos	87.000	0.286
Water, air-saturated	745	0.90020	0.813
	746	.89992	.782
(ν_{cap} = 0.89294)	752	.89928	.710
	754	.89857	.631
	759	.89855	.628
	759	.89828	.598
	753	.90087	.888
	756	.90199	1.013
	756	.90196	1.010
	754	.90191	1.005
Average	atmos	0.90015	0.808
Water, air-free	760	0.89518	0.251
	760	.89544	.280
(ν_{cap} = 0.89294	759	.89518	.251
	754	.90050	.847
	754	.90041	.837
	752	.90147	.955
	751	.90215	1.031
	751	.90168	.978
	752	.89693	.447
	751	.89681	.433
	751	.89654	.403
	757	.89699	.454
	759	.90098	.900
	758	.90139	.946
	759	.90128	.934
	761	.89989	.778
	755	.89632	.378
	755	.89723	.480
	759	.89663	.413
Average	atmos	0.89858	0.631
D_{14}, air-saturated	752	3.1859	0.512
	751	3.1856	.502
(ν_{cap} = 3.1697)	751	3.1855	.498
	742	3.1856	.502
Average	atmos	3.1857	0.504
D_{14}, air-saturated	756	3.1913	0.511
	755	3.1885	.422
(ν_{cap} = 3.1751)	754	3.1934	.577
	752	3.1932	.569
	756	3.1937	.585
	748	3.1936	.584
Average	atmos	3.1923	0.541
D_{14}, average, all	.....	.....	0.526

TABLE 4. *Comparison of viscosities (in centistokes) measured by decrement method and capillary (relative method with value calculated based on viscosity of water at 20 °C = 1.004 cSt).*

Fluid and condition	Ambient pressure	ν_{sphere} from decrement measurements	$\frac{\nu_{sphere}-\nu_{cap}}{\nu_{cap}}\times 100$
	mm Hg	*cSt*	*percent*
N_{35}, air-free	762	1054.3	0.603
	761	1052.8	.457
(ν_{cap} = 1048.0)	753	1053.8	.555
Average	atmos	1053.6	0.538
N_{35}, air-free	632	1052.3	0.460
	524	1050.7	.354
	303	1050.0	.374
	164	1051.2	.540
	145	1051.8	.606
	59	1050.4	.510
	21	1050.2	.497
Average	.....	.....	0.477
N_{35}, air-free	2.5	1050.4	0.528
	2.0	1050.1	.500
(ν_{cap} = 1044.9)	0.45	1050.5	.540
	.25	1051.4	.623
Average	vac	1050.6	0.548
N_{35}, average, all	.....	.....	0.510
Octoil S, air-free	762	19.391	−0.382
	762	19.395	− .360
(ν_{cap} = 19.465)	760	19.391	− .382
	760	19.452	− .067
	760	19.432	− .167
	758	19.479	.070
	754	19.483	.093
Average	atmos	19.432	−0.171
Octoil S, air-free	645	19.460	0.004
	531	19.450	− .016
	431	19.469	.107
	363	19.516	.365
	317	19.463	.107
	154	19.453	.100
	150	19.486	.265
	37	19.467	.200
Average	.....	.....	0.142
Octoil S, air-free	9	19.468	0.216
	9	19.446	.102
(ν_{cap} = 19.426)	8	19.427	.005
	3	19.422	− .019
	2	19.493	.344
	0.33	19.441	.075
	.29	19.423	− .014
Average	vac	19.446	0.101
Octoil S, average, all	.....	.....	0.029

In addition there was observed, of course, a variability between replicate measurements of the same fluid. There are primarily two factors which are responsible for this. First we expect small variations in the actual temperature of the fluid and the torsion wire which we estimate to be ±0.005 °C and ±0.05 °C respectively. This will affect the viscosity of the fluid being measured and the torsion constant of the wire. The effect on dimensions of the sphere is not significant. The second factor, and the major one, is the observed variation in the weight of the sphere which seems to account for the variability of 0.007

percent in the moment of inertia of the empty sphere when measured in vacuum. For measurements at atmospheric pressure this variability in the measured moment of inertia increased to 0.01 percent. Presumably these variations in I will also occur between measurements of viscosity and we have calculated the variability in the measured viscosity by making this assumption.

Measurements of viscosity by the period method are plotted in figure 6. The results are presented in terms of the percent deviation of individual measurements from the results of relative viscometry with capillary instruments taking the viscosity of water as 1.002 centipoise (1.004 centistokes) at 20 °C.

The dashed lines are centered on the mean of the observed points for each liquid to indicate the estimate of spread of errors calculated above. The agreement between the observed variability and that estimated is as close as we could expect. For water, Octoil S, and Oil L the agreement is almost exact. For Oil D the observed spread is smaller than that estimated, probably because of the limited number of observations. The calculated systematic error and variability for period measurements on Oil N were 3.9 percent and 1.1 percent respectively. The spread of a few observations of the period with Oil N in the sphere were consistent with the latter value; the dashed lines are continued toward this range of viscosity merely to indicate that we expected, and observed, greater variability on both sides of the design range.

In an attempt to see if the smoothness of the inner surface of the sphere might have any influence on the observed period, the original tool marks in the aluminum sphere were polished off, changing the roughness [9] from the original 20 microinches to 5 microinches. Of course, a new set of constants for the sphere had to be determined after this polishing. Table 2 includes values of viscosity obtained with the aluminum sphere both before (*) and after (**) this polishing procedure. The difference of about 0.2 percent is consistent with a reasonable set of error estimates for the aluminum sphere, in which we know that there is an uncertainty in the determination of I due to the seam between the two hemispheres (see section 2.3). If the roughness of our spheres did influence our measurements, we would

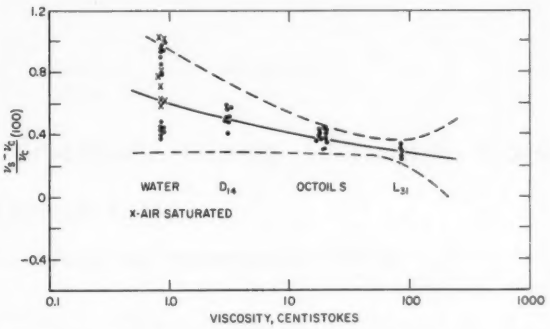

FIGURE 6. *The difference in percent between the measurement of viscosity with the sphere and the relative value by capillary measurement.*

The zero corresponds to capillary measurements based on the current standard of 1.002 cP for the viscosity of water at 20 °C.

expect greater roughness to correspond to higher values of viscosity. The difference observed here was in the opposite direction. It is clear from figure 6 that all the measurements of viscosity made by timing the period of the sphere are mutually consistent among themselves. It is also clear from figure 6 that our measurements of the viscosity in the design range of the apparatus (Octoil S and Oil L) are 0.3 percent or 0.4 percent higher than the relative measurements with a capillary instrument taking the viscosity of water as 1.002 cP (1.004 cSt) at 20 °C. These errors are beyond our estimate of the maximum possible error. We can only conclude that there is an unidentified systematic error in one or both of these methods of measuring viscosity.

6. References

[1] Kearsley, E. A., An analysis of an absolute torsional pendulum viscometer, Trans. Soc. Rheol. **III**, 69–80 (1959).

[2] Marvin, R. S., The accuracy of measurements of viscosity of liquids, J. Res. Nat. Bur. Stand. (U.S.). **75A** (Physics and Chem.), No. 6, 535–540 (Nov.–Dec. 1971).

[3] Kestin, J., and Moszynski, J. M., An experimental investigation of the internal friction of thin platinum alloy wires at low frequencies, Brown University Report, AF 891/11, July 1958.

[4] ASME Pressure Viscosity Report, II, Viscosity and density of over 40 lubricating fluids of known composition at pressures to 150,000 Psi and temperatures to 425 °F (1953).

(Paper 75A6–685)

[9] These values represent the arithmetical average of the irregularities in surface height as measured with a profilometer.

443-082 OL - 71 - 2

JOURNAL OF RESEARCH of the National Bureau of Standards—A. Physics and Chemistry
Vol. 75A, No. 6, November-December 1971

An Absolute Determination of Viscosity Using Channel Flow

Robert W. Penn and Elliot A. Kearsley

Institute for Basic Standards, National Bureau of Standards, Washington, D.C. 20234

(July 28, 1971)

The viscosity of a sample of di(2-ethylhexyl) sebacate has been determined by measuring the pressure at taps along a closed channel containing the flowing liquid. By means of relative viscosity measurements in conventional capillary viscometers, we are able to express our results in terms of the viscosity of water at 20 °C. We find a value of 0.010008 poise. An appendix outlines the calculation of upper and lower bounds for the geometrical flow constant.

Key words: Absolute measurement; calculation of bounds; calibration; Poiseuille flow; standard; viscosity; viscous flow.

1. Introduction

The history of the absolute measurement of the viscosity of water at the National Bureau of Standards began about 1931 when a committee chaired by E. C. Bingham recommended that a new determination be made. Work proceeded spasmodically until 1952 when Swindells, Coe, and Godfrey [1][1] published the results of their work, and the recommended value for the viscosity of water at 20 °C was changed from 1.005 centipoise (cP) to 1.002 cP. In 1957 Kearsley pointed out that all of the previous measurements had been made by very similar experiments and that there was a possibility that an unknown systematic error affected all of the results. At that time work was started on two different absolute measurements. One of these involved measuring the period of a liquid-filled sphere oscillating in torsion. The other involved measuring the pressure at taps along a capillary. Work proceeded, again spasmodically, on both of these experiments. In 1959, Kearsley published the analysis of the torsional sphere viscometer [2]. Results of that work are presented in an adjacent paper [3]. In 1968 we decided to construct an accurate channel in order to avoid some of the difficulties of measuring the radius and radius distribution of small capillaries. At the suggestion of Mr. T. R. Young of the Metrology Division we settled on a channel formed by pressing two cylindrical rods against a flat plate. This suggestion led to the work which we report here.

2. Experimental Procedure

Figure 1 shows a cross section of the channel we used. Two 2-cm diameter stainless steel rods were clamped against a 2-cm thick plate glass flat and sealed with epoxy resin to produce a cuspoid-triangular channel one meter long. This geometry allowed us to put the pressure taps out in the corners of the channel in a region of low velocity so that any disturbance of the flow would be minimized. The new geometry required us to calculate the geometrical flow constant. This was accomplished by computer calculation of upper and lower bounds, which agreed to better than five significant figures. Details of this calculation are presented in appendix 1.

The channel was placed in the apparatus shown in figure 2. A large, well insulated, water filled thermostat was constructed. The channel was fed from a water jacketed stand pipe which produced a constant pressure head. The stand pipe was fed by a pump which took the oil (a commercial grade of di(2-ethylhexyl) sebacate) from a large reservoir through an oil filter, then through a 50 ft coil of copper tubing to bring the oil to the bath temperature, and then to the top of the stand pipe. Overflow returned to the reservoir.

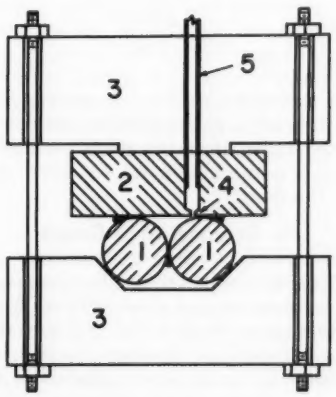

FIGURE 1. *Cross section of channel assembly.*
1, Stainless steel rods. 2, Plate glass flat. 3, Plastic clamps. 4, Pressure tap. 5, Copper tubing to pressure gage.

[1] Figures in brackets indicate the literature references at the end of this paper.

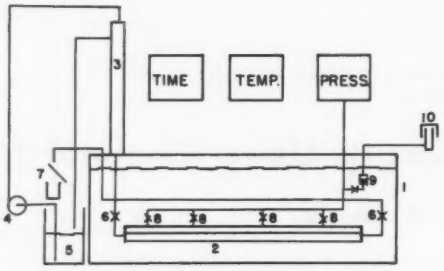

FIGURE 2. *Schematic diagram of the channel flow assembly.*

1. Thermostat. 2. Channel assembly. 3. Water jacketed stand pipe. 4. Pump. 5. Oil reservoir. 6. Flow control valves. 7. Solenoid operated diverter. 8. Pressure tap valves. 9. Oil-air interface. 10. Dead weight piston gage.

The channel was fed from the standpipe by plumbing which allowed us to run the flow in either direction. The flow was controlled by a needle valve near the entrance end of the channel. The effluent was returned to the reservoir. A solenoid operated device was used to divert the effluent stream so that accurately timed samples could be taken in beakers for weighing.

The measurement of pressure transmitted through the small pressure taps (0.08-cm diam) required the use of a high impedance pressure gage. A liquid filled fused quartz bourdon tube was used. This gage could be connected to any one of the four pressure taps to measure its pressure with respect to the efflux tube level by opening the tap valves one at a time. By closing all of the tap valves and opening the connection to an oil air interface, the quartz bourdon gage could be connected to a dead weight piston gage for calibration before and after a series of test runs.

Temperature was controlled by a proportional controller which balanced an electric heater against the heat loss to a constant temperature cooling coil. Temperature was measured with a quartz crystal thermometer which was calibrated against a platinum resistance thermometer before and after a series of test runs.

We now have all of the quantities necessary to calculate the kinematic viscosity of our test fluid:

$$\nu = \frac{\Gamma \Delta P R^4 T}{LM}. \qquad (1)$$

Γ is the (dimensionless) geometrical constant, 3.64872×10^{-3}; $\Delta P/L$ is the pressure gradient; R is the radius of the rods; M is the mass of fluid flowing in time, T; and ν is the kinematic viscosity, the viscosity divided by the density.

3. Discussion of Errors

Figure 3 shows the final results for measurements taken on two days in two directions of flow with four different flow rates from 1.5 to 5.2 g/s. These rates correspond to Reynolds numbers between 6.5 and 22. A detailed display of data is included in appendix 2. A statistical analysis of the pressure measurements show: (1) There is no significant day-to-day variation; (2) The variability of the individual pressure measurements does not correlate with flow rate; (3) There is no difference in average gradient for the two directions; (4) There is a statistically significant correlation of viscosity with flow rate for the left to right direction but not for the right to left direction. The total spread of the data in figure 3 is 0.06 percent of the mean. The standard deviation of their average is only 0.02 percent. In order to estimate the absolute accuracy of the measurements, we will examine the accuracy with which we know each of the various factors in eq 1.

3.1. The Geometrical Flow Constant

As mentioned above, we have calculated the geometrical factor to five significant figures. We have three ways to estimate how well we realized the geometry. The first was obtained from measurements of the diameters of the rods along four different diameters at thirteen places on the rods. The measurements were made by comparison with a gage block which was calibrated by the Length Measurements Section. Its dimension was known to within $\pm 10^{-6}$ inches. The comparison was made using a dial gage with a precision of $\pm 10^{-5}$ inches. The two rods differ in average diameter by 10^{-4} in. This difference would produce only a negligible error in the area of the channel and in the calculated viscosity. The diameter measurements show a standard deviation of 6×10^{-5} in and a maximum range of 3×10^{-4} in. The reciprocal of the root mean fourth power of the reciprocal diameters is found to be the same as the mean diameter to seven significant figures. From the standard deviation in diameter we calculate an uncertainty in viscosity of 0.032 percent due to the uncertainty in the value of R. This does not include the effects of radial flows due to irregularities in the cross section which we do not know how to estimate.

A second estimate of the accuracy of the geometry of the channel was obtained from an examination of the optical interference pattern between the rods and plate with sodium light which showed the distance of separation due to irregularities. Figure 4 shows a typical interference pattern. The rods were clamped to the glass plate by means of 12 equally spaced plastic [2]

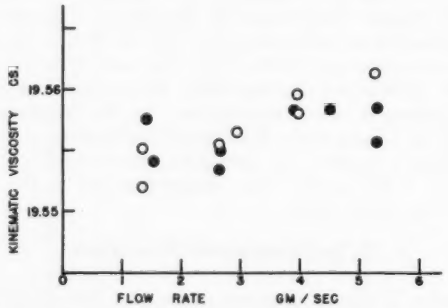

FIGURE 3. *Kinematic viscosity of oil sample at various flow rates.*
Closed circles, flow right to left. Open circles, flow left to right.

[2] Plastic components of the apparatus were constructed from commercially available poly(methyl methacrylate) materials.

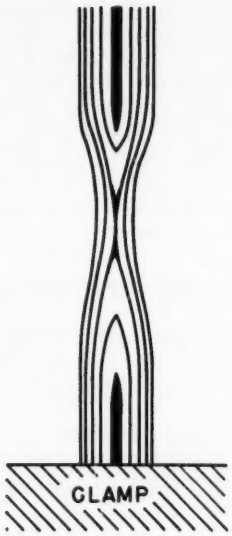

FIGURE 4. *Typical interference pattern between a steel rod and the glass plate showing second order separation.*

clamps 2-cm wide. Invariably, the zero order fringe indicated intimate contact between rods and plate in the regions under the clamps and within 1 cm of a clamp. Of the remaining 52 cm of the channel, the first, second, third, and fourth order fringes closed in about 26 cm, 14 cm, 10 cm, and 2 cm, respectively. By taking a weighted average of the reciprocals of the squares of the cross sections augmented by such separation, one estimates that the observed viscosity would be reduced by 0.025 percent. It is not clear how these separations are related to the variations in diameter of the rods, to nonstraightness of the rods, or to nonflatness of the glass plate.

Finally, using linear elasticity theory, we can estimate the penetration of the rods into each other and into the glass plate. These effects could reduce the cross-sectional area of the channel by less than 10^{-4} percent and so produce an error of less than $\pm 2\times10^{-4}$ percent in viscosity. Such penetration would, of course, tend to compensate for errors due to separation which were observed by means of the optical interference patterns. One cannot say with certainty how much these irregularities will disturb the flow; however, we estimate that we know the geometry of the channel well enough to assign an uncertainty of ± 0.04 percent from these sources.

3.2. Flow Rate Measurements

Uncertainties in flow rate can be estimated in several ways. First, duplicate determinations made before and after a series of pressure measurements show a standard deviation of 0.01 percent. Second, uncertainties in weighing 100- to 500-gram samples using calibrated weights are less than ± 0.005 percent. Our time interval measurements were made with a digital counter controlled by the National Bureau of Standards' standard frequency. Therefore the uncertainty in the time required to move the diverting mechanism constitutes the principal timing error.[3] From measurement of the mass of this mechanism and the forces used to move it we calculate that it takes about 0.02 s to move the diverter between its on and off positions. The flow during 0.02 s is 0.02 percent of the total flow. The uncertainty in flow rate due to the timing error is certainly less than this.

3.3. Pressure Gradient Measurements

Errors in the pressure gradient measurement could arise from errors in measurements of pressure, from uncertainty in measurements of the distances between the pressure taps, or from irregularities in the cross section of the channel, such as a possible constriction between two of the taps.

a. Distances Between Pressure Taps

The distances between the pressure taps in the glass plate were measured with a cathetometer. The cathetometer was checked against a standard Invar meter in 1952 with no correction larger than 10^{-3} cm. The midpoints of the holes were located to within $\pm 2\times10^{-3}$ cm from an arbitrary reference point near one end of the channel. The holes were approximately 0.08 cm in diameter. Since we wish to determine a pressure gradient, we have assumed that we measure the pressure at each of the holes at the same point with respect to its midpoint. We then determine the pressure gradient by a least squares technique of fitting the pressure measurements to a linear function of distance along the channel. The same values of pressure gradient are obtained to six digits whether the errors are attributed to pressure measurements or to measurements of position of the holes. The statistical analysis of the pressure measurements indicates that there is a barely significant systematic deviation of the individual pressure measurements from the constant gradient line. The pressure reading deviations from the center two taps are consistently positive for one direction of flow and negative for the other direction. These deviations from the constant gradient line could be explained by uncertainties of 8×10^{-3} cm in the position of the holes. This is approximately one-tenth of the diameter of the holes. Deviations from this source are indistinguishable from those due to irregularities in the cross section of the channel.

b. Pressure Measurements

Pressure measurements were made with a liquid filled, fused quartz bourdon gage with a resolution of about ± 0.1 N/m^2. Pressure measurements were reproducible to within ± 0.1 N/m^2 both during the viscosity measurements and during the calibration of this gage against a dead weight piston gage. The effective area

[3] The diverter was removed from the oil stream during the timed period, thus drainage from it did not contribute to error.

of the piston gage certified by the manufacturer, and checked by the Pressure Measurement Section of NBS, is within 0.01 percent of its nominal value. The weights used were found to be accurate within 0.005 percent of their nominal values.

Since air was used in the piston gage, the calibration was made through an oil-air interface of 4-cm diameter which might introduce an uncertainty of ± 0.1 N/m^2 due to surface tension effects. A reproducible periodicity of ± 0.5 N/m^2 amplitude in the calibration curve was traced to the gears in the system used to measure the angular displacement of the quartz bourdon tube. The calibration curve was found to be reproducible over the period of the measurements to within ± 0.15 N/m^2, or ± 0.03 percent for the smallest pressure differences measured.

Since all of the systematic deviations of pressure measurements from the constant gradient line are barely significant statistically, we have chosen to use an average of all of the pressure gradient determinations weighted by the inverse of their individual standard deviations. The standard deviation of this average is only 0.02 percent. We estimate the absolute accuracy of this average to be ± 0.06 percent.

3.4. Temperature Measurements

Temperature was controlled in the thermostat at 25 °C by means of a proportional controller with reset action which uses a platinum resistor as a sensing element. Temperature was measured with a digital thermometer which uses a quartz crystal as a sensing element. This thermometer indicated temperature within the bath constant to $\pm 10^{-3}$ °C for periods up to 8 hr. Rapid temperature fluctuations of about ± 0.003 °C were found at the end of the bath near the heater and cooling coil. The average temperature here was the same as that of the rest of the bath. The digital thermometer was calibrated against a platinum resistance thermometer in a well stirred oil bath. The platinum thermometer had been calibrated in 1960 in terms of the International Temperature Scale of 1948. A triple point temperature check and bridge calibration were made in 1969.

Temperature measurements were made both in the circulating bath and in copper temperature wells, shown in figure 5, which had good thermal contact with the test oil but were relatively isolated from the water of the bath. These wells were placed in the oil stream at both ends of the channel. No significant difference was found between the two wells; however, both well temperatures consistently read 0.004 °C higher than the bath temperature. The same difference was found whether or not oil was flowing in the channel. It was attributed to self-heating of the temperature probe in the unagitated water in the wells. We believe we know the temperature of the oil to better than ± 003 °C which would produce an uncertainty in viscosity of ± 0.012 percent.

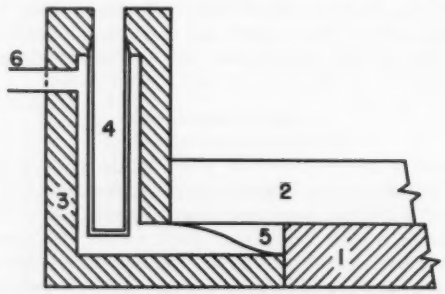

FIGURE 5. *Diagram of channel entrance section.*

1, Steel rod. 2, Plate glass flat. 3, Plastic entrance adapter. 4, Copper thermometer well. 5, Plastic streamline fillet. 6, Oil entrance tube.

3.5. Summary of Error Estimation

We list in table 1 the various sources of error which we have considered. These errors can be combined to a total probable error of approximately ± 0.1 percent.

TABLE 1. *Systematic errors*

Error source	Estimated accuracy
	Percent
Geometry of channel	±0.04
Flow rate	±0.02
Pressure measurements	±0.06
Temperature measurements	±0.012
Total absolute value	±0.13
Root total squares	±0.075

One effect which might be expected in these measurements is that the pressure at the hole nearest the entrance end of the channel might deviate from the others due to entrance effects. This effect is apparently seen in a significant dependence of pressure gradient on flow rate for left to right flow direction where the first hole is only 7 cm from the entrance. We attempted to minimize this effect by streamlining the entrance to the channel with plastic fillet pieces shown in figure 5. No effect is seen for right to left flow where the first hole is 28 cm from the entrance. Eliminating this effect by leaving out the data from the first hole would increase our final result by only 0.01 percent.

Corrections were applied to the raw data for air buoyancy on the weights of oil samples and on the weights used in calibrating the pressure gage. The local acceleration of gravity was calculated from the value determined by Tate [4] assuming a gravity gradient of 3×10^{-6}s^{-2}. Temperature corrections were applied using a decrement of 4 percent per degree which was determined in a capillary viscometer.

4. Results

The direct result of this work is a value for the kinematic viscosity of one sample of commercial grade di(2-ethylhexyl) sebacate at 25 °C. This value was found to be 19.555 centistokes. By means of conventional relative viscosity measurements [5], this value can be compared with the viscosity of water at 20 °C. Such measurements were made immediately before and after our absolute measurements. Neglecting errors in the relative viscometry, we calculate the

viscosity of water of 20 °C to be 1.0008 ± 0.0010 centipoise (cP). The corresponding value from the torsional sphere viscometer [3] is 1.006 ± 0.001 cP. The discrepancy suggests the presence of an unidentified systematic error in one or both of these measurements of at least 0.25 percent. The comparison is discussed in detail by Marvin [6].

We gratefully acknowledge the assistance of many members of the staff of NBS. Particularly, we would like to thank Marion Brockman, who assisted with many of the measurements, Henry Pierce, who made density and relative viscosity measurements, and James Filliben of the Statistical Engineering Section, who assisted with the analysis of our results.

5. Appendix 1. Calculation of Bounds for the Geometrical Flow Constant

For unaccelerated viscous flow of an incompressible fluid through a channel the Navier-Stokes equations may be reduced to:

$$\nabla^2 v = \frac{1}{\eta}\frac{dP}{dz} = -K \qquad \text{(A-1)}$$

where $v(x, y)$ is the velocity profile, η is the viscosity, dP/dz is the pressure gradient in the direction of flow, and K is a positive constant. The total flow

$$Q = \int_S v dS \qquad \text{(A-2)}$$

over the cross-sectional area, S, of the channel. By Green's Theorem, since $v = 0$ on the boundary, by the adherence condition

$$\int_S (v\nabla^2 v + \nabla v \cdot \nabla v) dS = \int_\beta v \nabla v \cdot d\beta = 0 \qquad \text{(A-3)}$$

where β is the boundary of the channel, and $d\beta$ is in the direction of the outward normal. Combining equations (A-1), (A-2), and (A-3), we obtain

$$Q = \frac{1}{K}\int_S \nabla v \cdot \nabla v dS. \qquad \text{(A-4)}$$

From equations (1) and (A-1) which define Γ and K, respectively,[4] it is possible to express the relationship between K and Γ as

$$\Gamma = \frac{Q}{KR^4}. \qquad \text{(A-5)}$$

[4] The equations $M/T\rho = Q$ and $\Delta P/L = -\partial P/\partial z$ relate the quantities of the two equations.

Since Γ is a dimensionless geometric constant, we can arbitrarily set K and R equal to one and Γ will be numerically equal to the corresponding value of Q.

5.1. Upper Bound

To obtain an upper bound for Q, one chooses a trial velocity function, ψ, which satisfies the differential equation (A-1), but does not necessarily satisfy the boundary condition. Then, by Green's Theorem and the adherence condition

$$\int_S (v\nabla^2\psi + \nabla v \cdot \nabla\psi) dS = \int_\beta v \nabla\psi \cdot d\beta = 0. \qquad \text{(A-5)}$$

By Schwarz' inequality:

$$K\int_S v dS = \left| \int_S (\nabla v \cdot \nabla\psi) dS \right|$$

$$\leq \left(\int_S (\nabla v \cdot \nabla v) dS \cdot \int_S (\nabla\psi \cdot \nabla\psi) dS \right)^{1/2}$$

$$KQ \leq \left(KQ \cdot \int_S (\nabla\psi \cdot \nabla\psi) dS \right)^{1/2}$$

$$Q \leq \frac{1}{K}\int_S (\nabla\psi \cdot \nabla\psi) dS. \qquad \text{(A-6)}$$

Equation (A-6) defines an upper bound for the total flow.

5.2. Lower Bound

To generate a lower bound for Q one chooses another trial velocity function, φ, which satisfies the boundary condition, $\varphi = 0$ on β, but does not necessarily satisfy the differential equation (A-1). Then, by Green's Theorem:

$$\int_S (\varphi\nabla^2 v + \nabla\varphi \cdot \nabla v) dS = \int_\beta \varphi \nabla v \cdot d\beta = 0 \qquad \text{(A-7)}$$

since $\varphi = 0$ on β. Again, by Schwarz' inequality

$$\left(K\int_S \varphi dS \right)^2 = \left(\int_S (\nabla\varphi \cdot \nabla v) dS \right)^2$$

$$\leq \int_S (\nabla\varphi \cdot \nabla\varphi) dS \cdot \int_S (\nabla v \cdot \nabla v) dS$$

$$\frac{\left(K\int_S \varphi dS \right)^2}{\int_S (\nabla\varphi \cdot \nabla\varphi) dS} \leq \int_S (\nabla v \cdot \nabla v) dS = KQ.$$

Thus,

$$\frac{K\left(\int_S \varphi dS\right)^2}{\int_S (\nabla\varphi \cdot \nabla\varphi) dS} \leqslant Q \qquad \text{(A–8)}$$

which defines a lower bound for the total flow.

5.3. Optimization of Bounds

For the upper bound we can choose as a trial function

$$\psi = by^2 + \Sigma \alpha_n h_n \qquad \text{(A–9)}$$

where $b = K/2$, α_n is an arbitrary coefficient and h_n is a harmonic polynomial of degree n in x and y.

$$\nabla^2 h_n = 0.$$

There are two such polynomials of each degree; one is even and one is odd in y. In the present problem we may choose our axes such that the channel is symmetric about the x axis, with origin at the point of contact between the cylinders. Then we need not include the polynomial which is odd in y.

The integral

$$Q_U = \frac{1}{K}\int_S (\nabla\psi \cdot \nabla\psi) dS$$

will be quadratic in the α_n's. Q_U can be written in matrix component notation with the usual summation convention as:

$$KQ_U = \alpha_l H_{lm} \alpha_m + 4b\alpha_l Y_l + 4b^2 \int_S y^2 dS \qquad \text{(A–10)}$$

where the arbitrary coefficients α_n form a vector; H is the symmetric matrix,

$$H_{nm} = \int_S \left(\frac{\partial h_n}{\partial x}\frac{\partial h_m}{\partial x} + \frac{\partial h_n}{\partial y}\frac{\partial h_m}{\partial y}\right) dS;$$

and Y is a vector,

$$Y_n = \int_S \left(y \frac{\partial h_n}{\partial y}\right) dS.$$

To find the values of the arbitrary coefficients which minimize Q, we differentiate eq (A–10) with respect to α and set the derivatives equal to zero to obtain

$$K\frac{\partial Q_U}{\partial \alpha_i} = 2H_{il}\alpha_l + 4bY_i = 0. \qquad \text{(A–11)}$$

We can solve for the coefficient vector,

$$\alpha_i = -2bH^{-1}_{il} Y_l.$$

This result can be put into eq (A–10) to yield the desired upper bound.

For the lower bound, we can choose a trial function

$$\varphi = F \cdot G$$

where F is a function which vanishes on the boundary β and G is an arbitrary function. We have used [5]

$$F = (x^2+y^2-2y)\ (x^2+y^2+2y)\ (x-1)$$

and

$$G = \sum_{i,j=0}^{n,m} a_{ij} x^i y^{2j}.$$

Then, since F vanishes on β,

$$\frac{Q_L}{K} = \frac{\left(\int_S FG dS\right)^2}{\int_S (G^2 \nabla F \cdot \nabla F - F^2 G \nabla^2 G) dS} \qquad \text{(A–12)}$$

is the functional to be maximized by adjusting the a_{ij}'s. This can be done by minimizing the denominator under the condition that

$$\int_S FG dS = 1$$

by Lagrange's method of undetermined multipliers. If we call the denominator of (A–12) D *and* $\int_S FG dS = N$ then

$$\frac{\partial D}{\partial a_{ij}} + \lambda \frac{\partial N}{\partial a_{ij}} = 0 \qquad \text{(A–13)}$$

$$N = 1$$

form a set of $(n+1)\ (m+1)+1$ equations which are linear in the a_{ij}'s. If we relabel a_{ij}:

$$a_{ij} = \alpha_{(m+1)i+j}\ ,$$
$$\lambda = \alpha_{(n+1)\,(m+1)}$$

then eqs (A–13) can be written as

$$\left|\begin{array}{c|c|c|c|c} \dfrac{\partial^2 D}{\partial\alpha_i \partial\alpha_j} & \dfrac{\partial N}{\partial \alpha_i} & & & \begin{matrix}0\\0\\0\\\cdot\\\cdot\\\cdot\end{matrix} \\ & & \alpha_i & = & \\ \hline \left(\dfrac{\partial N}{\partial \alpha_i}\right)^T & 0 & & & 1 \end{array}\right| \qquad \text{(A–14)}$$

where the matrix on the left is indicated as a par-

[5] This F is the lowest order polynomial which vanishes on β. It is important that F does not vanish within S in order that the bound given in (A–12) be a close one.

titioned matrix. The problem is thus reduced to finding the inverse of this matrix and from that to calculate the optimum α_n's through (A–14) and then the bound through (A–12). In fact, the element at the bottom of the diagonal of this inverse matrix is the reciprocal of the bound.

For both of the bounds the matrix elements involved are composed of sums of integrals of the form

$$I_{nm} = \int\int x^n y^m dy dx$$

over the cross-sectional area of the channel. This integral can be expressed as a sum of beta functions [7] since:

$$I_{nm} = B_{nk} C_{km}$$

where

$$C_{km} = \frac{(-1)^k (m)!}{(m-k+1)!\, k!}$$

and

$$B_{nk} = \mathrm{B}\left(\frac{n+1}{2}, \frac{k}{2}+1\right) = \frac{\Gamma\left(\frac{n+1}{2}\right)\Gamma\left(\frac{k}{2}+1\right)}{\Gamma\left(\frac{n+k+3}{2}\right)}.$$

Both of these calculations were coded for the UNIVAC 1108 computer. With the inclusion of the first 21 harmonic polynomials for the upper bound and 31 terms up to x^5y^8 in the lower bound calculation, the two bounds converged to 3.64872 ($\pm$0.00002) $\times$ 10^{-3}

6. Appendix 2. Data

Tables A1 and A2 show flow rate and pressure data taken on two days. Table A3 lists measurements of the distances of the midpoints of the four pressure taps from one end of the channel. The individual masses of oil listed in tables A1 and A2 have not been corrected for air buoyancy. The average flow rates have been so corrected. The appropriate factor is 1.0012. The pressure measurements have been corrected for the nonlinearities in the quartz bourdon gage. They have not been corrected for the local gravity of 980.0972 cm/s^2 nor for air buoyancy on the calibrating weights. The appropriate factor is 0.99927. The viscosity values listed should also be so corrected. They are shown in the table for the operating temperature of 25.035 °C. They should be multiplied by 1.0014 to adjust them to 25 °C. The appropriate factor to convert the pressure gradient-flow rate ratios to kinematic viscosity is 207.404.

Run number eight gave a value of viscosity more than three standard deviations from the average of the other fifteen runs. Although we could find no reason for this difference we have assumed that it is not due to random error and we have not included it in our final average.

TABLE A1. *Flow rate and pressure data for day 1.*

Flow direction			Right to left				Left to right			
Run number			2	4	5	7	1	3	6	8
	Nominal		1.5	3	4.5	6	1.5	3	4.5	6
	Mass (g)		132.141	254.568	371.234	565.633	128.786	252.383	379.414	510.885
	Time (s)		95.36	96.89	95.48	107.42	95.13	95.24	96.09	97.68
Flow Rate, g/s	Mass (g)		147.660	285.531	411.833	534.506	142.801	315.619	416.731	530.851
	Time (s)		106.57	108.67	105.91	101.51	105.58	118.98	105.55	101.51
	Average		1.3873	2.6306	3.8929	5.2719	1.3548	2.6545	3.9531	5.2360
	Tap	1	0.02812	0.08318	0.17314	0.22018	0.16386	0.41412	0.57984	0.78724
		4	.11360	.24531	.41309	.54508	.08040	.25054	.33610	.46483
		2	.05388	.13209	.24546	.31816	.13873	.36486	.50632	.69004
Pressure, psi		3	.09702	.21393	.36660	.48214	.09652	.28222	.38334	.52730
		1	.02813	.08320	.17317	.22020	.16385	.41410	.57980	.78724
		4	.11362	.24529	.41310	.54514	.08042	.25054	.33610	.46483
		2	.05386	.13206	.24546	.31818	.13871	.36480	.50634	.69006
		3	.09710	.21390	.36660	.48212	.09646	.28221	.38335	.52730
		1	.02813	.08318	.17315	.22020	.16385	.41406	.57980	.78722
		4	.11362	.24531	.41308	.54508	.08040	.25052	.33610	.46483
		2	.05388	.13210	.24546	.31816	.13873	.36480	.50632	.69004
		3	.09708	.21390	.36660	.48214	.09650	.28220	.38336	.52730
Pressure Gradient Flow rate	Value $\times 10^6$		94234	94222	94238	94225	94222	94221	94236	94141
	Std er $\times 10^6$		19	13	5	10	36	11	9	.....
Kinematic viscosity	Stokes		0.19545	0.19542	0.19545	0.19543	0.19542	0.19542	0.19545	.....

TABLE A2. *Flow rate and pressure data for day 2.*

Flow direction			Right to left				Left to right			
Run number			9	12	13	16	10	11	14	15
	Nominal		1.5	3	4.5	6	1.5	3	4.5	6
	Mass (g)		164.799	248.408	427.531	521.915	159.538	316.214	415.209	505.133
	Time (s)		107.24	94.47	94.92	98.72	118.38	108.20	105.28	96.45
Flow Rate, g/s	Mass (g)		146.345	278.677	470.861	565.833	134.698	275.726	375.640	556.020
	Time (s)		95.23	105.98	104.55	107.02	99.92	94.34	95.24	106.17
	Average		1.5386	2.6326	4.5093	5.2933	1.3495	2.9261	3.9487	5.2434
	Tap	1	0.02750	0.08296	0.17316	0.21586	0.16358	0.41372	0.57895	0.78789
		4	.12234	0.24524	0.45112	0.54216	0.08046	0.23340	0.33552	0.46466
		2	.05609	0.13194	0.25696	0.31424	0.13858	0.35937	0.50552	0.69050
		3	.10394	0.21377	0.39722	0.47888	0.09656	0.26837	0.38269	0.52730
Pressure, psi										
		1	0.02750	0.08298	0.17318	0.21586	0.16360	0.41376	0.57893	0.78789
		4	.12234	0.24524	0.45114	0.54214	0.08048	0.23344	0.33553	0.46468
		2	.05609	0.13194	0.25700	0.31426	0.13860	0.35946	0.50556	0.69049
		3	.10392	0.21377	0.39724	0.47888	0.09658	0.26840	0.38269	0.52730
		1	0.02750	0.08298	0.17318	0.21586	0.16362	0.41382	0.57892	0.78789
		4	.12232	0.24520	0.45114	0.54216	0.08048	0.23346	0.33552	0.46466
		2	.05606	0.13192	0.25700	0.31426	0.13862	0.35946	0.50552	0.69050
		3	.10394	0.21376	0.39724	0.47888	0.09660	0.26842	0.38270	0.52732
Pressure Gradient / Flow Rate	Value×10⁶		94217	94213	94237	94238	94207	94229	94244	94252
	Std er×10⁶		10	22	14	16	9	10	3	10
Kinematic viscosity	Stokes		0.19541	0.19540	0.19545	0.19545	0.19539	0.19543	0.19547	0.19548

TABLE A3. *Positions of pressure taps*

Tap No.	Distance (meters)
1	0.93434
2	.73731
3	.40711
4	.28030

7. References

[1] Swindells, J. F., Coe, J. R., and Godfrey, T. B., Absolute viscosity of water at 20 °C, J. Res. NBS **48**, No. 1, 1–31 (1952) RP2279.

[2] Kearsley, E. A., An analysis of an absolute torsional pendulum viscometer, Trans. Soc. Rheol. **3**, 69–80 (1959).

[3] White, H. S., Kearsley, E. A., An absolute determination of viscosity using a torsional pendulum, J. Res. Nat. Bur. Stand. (U.S.), **75A** (Phys. and Chem.), No. 6, 541–551 (Nov.-Dec. 1971).

[4] Tate, D. R., Acceleration Due to Gravity at the National Bureau of Standards, Nat. Bur. Stand. (U.S.), Monogr. 107, 24 pages (June 1968).

[5] Hardy, R. C., NBS Viscometer Calibrating Liquids and Capillary Tube Viscometers, Nat. Bur. Stand. (U.S.), Monogr. 55, 22 pages (Dec. 1962).

[6] Marvin, R. S., The accuracy of viscosity measurements of liquids, J. Res. Nat. Bur. Stand. (U.S.), **75A**, (Phys. and Chem.), No. 6, 535–540 (Nov.-Dec. 1971).

[7] Handbook of Mathematical Functions, Nat. Bur. Stand. (U.S.), Appl. Math. Ser. 55, p. 258 (June 1964).

(Paper 75A6–686)

JOURNAL OF RESEARCH of the National Bureau of Standards—A. Physics and Chemistry
Vol. 75A, No. 6, November-December 1971

A New Determination of the Atomic Weight of Zinc*

George Marinenko

Institute for Materials Research, National Bureau of Standards, Washington, D.C. 20234

and

The American University, Washington, D.C. 20016

and

Robert T. Foley

The American University, Washington, D.C. 20016

The atomic weight of zinc determined coulometrically for 5 metallic reference samples is 65.377 ± 0.003 where the uncertainty figure is the 95 percent confidence interval for the mean plus an allowance for known possible sources of systematic error.

Key words: Atomic weight; coulometry; zinc, atomic weight.

1. Introduction

The presently accepted value for the atomic weight of zinc is 65.3_7 [1, 2].[1] The above value is based primarily on $ZnCl_2/2Ag$ [3], $ZnCl_2/2AgCl$ [3], $ZnBr_2/Zn$ [4], and $ZnCl_2/Zn$ [5] combining weight ratios. Two mass spectrometric determinations of the isotopic abundances [6, 7] yield a significantly different value for the atomic weight of zinc—65.387. Since mass spectrometric measurements were carried out without the absolute calibration of the instruments the Commission recommended retaining the chemically determined value [8].

An electrochemical method for the determination of the electrochemical equivalent and the atomic weight of zinc has been utilized in this work, which will aid in narrowing down the existing uncertainty in this important constant.

The suitability of electrochemical methods for the determination of atomic weights was implied in the original work of Faraday. In 1833 he established that the law of definite proportions holds even when the chemical reactions are not carried out directly but are induced by the passage of electric current through the electrolysis cells [9]. The amount of chemical change produced at the electrodes of a cell is directly proportional to the quantity of charge passed.

Explicit utilization of Faraday's laws for the determination of atomic weights was recognized very early in the development of quantitative electrochemistry. Thus, for example, Laird and Hulett state [10]:

"*Faraday's law, that a definite quantity of electricity is associated with one gram equivalent of any ion, is, as far as we know, strictly accurate, probably as accurate as the law of conservation of mass. There is evidence that not even as small a quantity of electricity as* 10^{-16} *coulomb passes from an electrolyte to an electrode without a corresponding chemical change taking place . . .*"

Using electrolytic deposition of Cd in series with a silver coulometer, Laird and Hulett were able to obtain precise Cd/Ag ratios, and assigning a value for the atomic weight of silver they were able to calculate the atomic weight of cadmium. A similar approach had been used by Gladstone and Hibbert earlier [11] for the determination of Zn/Ag and Zn/Cu ratios, and subsequently, the atomic weight of zinc. Unfortunately, we now know that silver deposition coulometers and copper coulometers, though precise for a given set of experimental conditions, are not very accurate due to the differences in the amount of occluded mother liquor in the deposit obtained in different laboratories. This aspect of silver deposition coulometers is discussed by Hamer [12]. A more direct approach to the determination of the electrochemical equivalent is through the use of absolute current and time measurements, employed by Craig and coworkers [13] in the determination of the electrochemical equivalent of silver and the faraday. The anodic silver coulometer obviates mother liquor occlusion errors but at the same time it requires tedious collection and weighing of material which

*This work was conducted in partial fulfillment of the requirements for Ph D. degree.

[1] Figures in brackets indicate the literature references at the end of this paper.

flakes off in the course of the dissolution of the anode. The absolute current measurement was also employed by one of the authors of this work, in the determination of the electrochemical equivalents of benzoic acid and oxalic acid [14].

This communication reports only a small fraction of data obtained to date on the redetermination of the atomic weight of zinc. The primary purpose of this paper is to report the progress which has been made in this work. However, even at this point it is possible to present a significantly improved value of the atomic weight of zinc. Other available data which are not presented in this paper are in excellent agreement with the results reported here.

2. Summary of Preliminary Investigations

The nature and experimental detail of some preliminary investigations will be discussed in future publications. Nevertheless, it is germane to the subject at hand to outline the results of these preliminary studies here.

(1) The presence of oxygen (air) in the electrolyte has a significant effect on the rate of spontaneous corrosion of zinc. This in turn affects the experimentally determined electrochemical equivalent and the atomic weight of zinc. For this reason air was removed from the electrolyte be purging with nitrogen. A nitrogen atmosphere was maintained in the coulometer in all final determinations of the electrochemical equivalent of zinc.

(2) Commercial grade zincs without any a priori processing yield a higher electrochemical equivalent (on the order of 0.01%) than the same materials subjected to vacuum fusion. This could easily be explained by the presence of gases (notably oxygen) in the commercial material which are removed under vacuum fusion conditions.

(3) Zinc anodes amalgamated on the surface undergo electrochemical dissolution without any detectable fall-off of material in the course of electrolysis.

(4) The difference between the free energies of the reaction

$$Zn(Hg) \rightarrow Zn^{++} + 2e \,|\, U^\circ = -0.799V)$$

and the next conceivable reaction

$$Hg + 2OH^- \rightarrow HgO + H_2O + 2e (U^\circ = +0.098V)$$

is sufficiently large that even at current densities as high as several amperes per square centimeter the former reaction proceeds at 100.000 percent current efficiency. This was verified experimentally by measurements of the working anode potentials at different current densities, using first pure mercury anode and then zinc amalgam anodes. Coulometric experiments conducted at current densities ranging from 10^{-5} to 1.0 $A \cdot cm^{-2}$ substantiate this conclusion since no significant dependence between current density and the electrochemical equivalent of zinc could be found.

(5) Other investigated parameters include current (from 10^{-4} to 1.0 A), time of electrolysis (from 3 to 7×10^4 s), electrode area (from 0.5 to 10 cm^2), total amount of change passed through the cell (up to 3×10^4 C), purity of material, and mass of dissolved zinc (up to 10 g). Only the electrode area has a significant effect resulting from the dissolution of ZnO formed on the surface of the amalgam during handling of the electrode in air. The magnitude of this effect was evaluated (10.7 ± 1.5 μg cm^{-2}) and appropriate correction applied.

3. Method

The approach taken in this investigation is rather straightforward in its conception—to determine the mass of zinc dissolved anodically during the passage of a constant electrical current through the following electrochemical cell:

$$Zn(Hg)|ZnCl_2 \text{ (3 molal, aq)}, NH_4Cl \text{ (25 wt \%, aq)}|Hg.$$

The quantitative reaction which is of specific interest here is

$$Zn(Hg) \rightarrow Zn^{++} + 2e; \qquad (1)$$

and the accompanying cathodic reaction is simply the reverse of reaction (1):

$$Hg + Zn^{++} + 2e \rightarrow Zn(Hg). \qquad (2)$$

In such a cell the composition of electrolyte remains unaltered throughout the whole experiment.

The passage of two faradays of charge through the cell dissolves 1 mol of zinc from zinc amalgam. The coulometric circuit enabling passage of charge through the cell within an accuracy of 0.0002 percent has been described earlier [14]. The coulometer used in this work is shown in figure 1. A weighed zinc amalgam anode is suspended in the coulometer (1). The mercury pool cathode (2) is located at the bottom of the coulometer. The ground glass flat joint (3) in the coulometer is provided for insertion of a porous membrane filter which is used in some experiments to establish the existence or the absence of any significant fall-off of the material from the anode in the course of its electrochemical dissolution. The electrolyte is deaerated and a nitrogen atmosphere maintained in the coulometer throughout the experiment.

Zinc anodes are weighed by substitution on a 20-g capacity microbalance. The uncertainty of the mass measurement process (standard deviation) is 3×10^{-6} g. The smallest changes in the mass of Zn anodes in the experiments reported here were on the order of 2 g.

A constant current of known magnitude is passed through the coulometer for a precalculated period of time sufficient to produce a desired change in mass of the anode roughly equivalent to the mass of a single weight in the calibrated set of weights (e.g. 2 g). After termination of electrolysis, the zinc anode is carefully removed from the coulometer, washed first

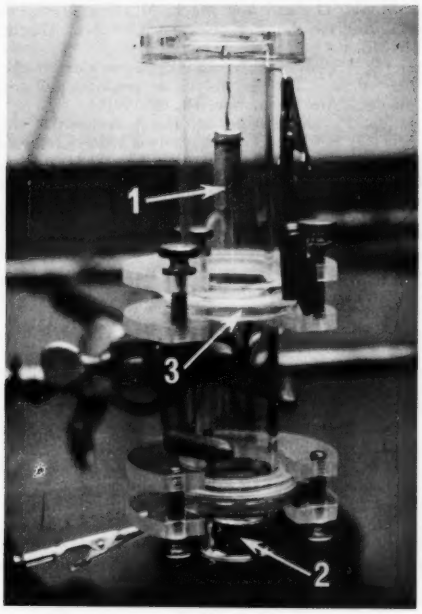

FIGURE 1. *Coulometer for the determination of the atomic weight of zinc.*

1 – zinc anode; 2 – mercury pool cathode; 3 – ground glass flat joint.

in 0.1 molar NH_4Cl solution and then in hot distilled water and reweighed. Appropriate corrections for the effects of buoyancy of air are applied. Thus the charge to mass ratio can be readily computed.

4. Results

The results of experiments with metallic zinc samples of five different origins are summarized in the table. The first column in the table gives the original number of the experiment. Material code and the origin of material are given in columns two and three respectively. The last column, column four, gives the determined values of the atomic weight of zinc in each experiment.

The material designated as 1 is high purity zinc issued by the National Bureau of Standards as Standard Reference Material (SRM) 682. The material was produced by Cominco American, Inc. from a special lot of high-grade electrolytic zinc. It was purified by vacuum distillation, zone-refining and degasification. The overall assessment of impurities indicates that the material is 99.9999 percent Zn [15]. The material designated as 2 is a special high-grade metal (99.995% Zn) produced by the Electrolytic Zinc Company of Australasia Ltd. [16]. Materials 3, 4 and 5 were produced in Peru, Yugoslavia, and Italy respectively.

The calculated values of the atomic weight of zinc in column four are based on the coulometrically determined electrochemical equivalent of zinc and adopted value of the faraday. For the determination of charge consumed in the electrochemical reaction, the value of electrical current is based on the NBS ohm and U.S. legal volt of 1969.

Time measurement is based on 100 kHz frequency maintained by NBS. Mass measurements were performed by substitution using a set of weights calibrated at NBS. The value of the faraday employed in these calculations is 96486.70 C mol^{-1} [17].

5. Discussion

The mean value of the atomic weight of zinc based on coulometric data reported here is 65.37736. A two-sided 95 percent confidence interval for the mean, 0.00086, reflects adequately the uncertainty in this value due to the random sources of error. The accuracy of the result, however, depends not only on the random error of measurement, but also on the biases which could exist in the various stages of the measurement process and in the constants which are employed in calculation of the results.

The assessment of the uncertainties due to all known sources of possible systematic error (uncertainties in electrical standards, time, mass and the faraday) indicates that these sources can contribute as much as 0.002 percent (0.00131 amu) error. Thus, the two components of error yields an uncertainty figure of 0.0022 in the atomic weight of zinc.

It is thus felt that on the basis of this work the atomic weight of zinc can be assigned the value

$$65.377 \pm 0.003.$$

All the experimental values reported here lie well within the assigned uncertainty bounds. Further reduction in the uncertainty of this constant is anticipated when processing of all data is completed. Nevertheless, even the present uncertainty is an order of magnitude lower than that of the presently accepted value. (See table 1.)

On the basis of data presented here, there appears to be no significant difference between the values of atomic weight for materials of different origins even at the 10 percent level of significance. The published results of mass spectrometric investigations [7] also indicate no significant differences in the isotopic composition of zinc produced by electrolytic and chemical reduction processes. To insure that the value obtained in this research is truly representative of the terrestrial zinc, an experimental survey of primary zinc bearing minerals from world-wide sources is now in progress. This study is conducted on virgin minerals which have not been subjected to metallurgical processing (other than flotation), since the latter could produce isotope separation (isotope separation can conceivably occur in such processes as distillation which is commonly used in purification of zinc).

The authors express their gratitude to D. W. Kohls of The New Jersey Zinc Company, A. S. Gill of Elec-

TABLE 1. *Atomic weight of zinc determined by coulometry*

Experiment No.	Material code	Origin of material	Atomic weight of zinc
139	1	Canada	65.3759
140	1	Canada	65.3761
141	1	Canada	65.3782
142	2	Australia	65.3783
143	2	Australia	65.3778
144	3	Peru	65.3786
145	3	Peru	65.3764
146	4	Yugoslavia	65.3761
147	4	Yugoslavia	65.3751
148	5	Italy	65.3784
149	5	Italy	65.3783
150	1	Canada	65.3791
		Mean	65.3773_6

Pertinent Statistical Data
Standard deviation of a single determination $s = 0.00134$.
Standard deviation of the mean $s/\sqrt{n} = 0.00039$.
Two sided 95 percent confidences interval for the mean based on 11 degrees of freedom $ts/\sqrt{n} = \pm 0.00086$.

trolytic Zinc Company of Australasia Limited, W. Tunney, Jr. of St. Joseph Lead Company, and J. F. Harris of Cominco Limited for their donation of zinc samples from different origins. We also express our thanks to J. Mandel of the National Bureau of Standards for his help in statistical evaluation of our results and to A. R. Cook of International Lead Zinc Research Organization for his interest in this work.

6. References

[1] International Commission on Atomic Weights, Final Version of the Report 28–9–1967, Comptes Rendus XXIV IUPAC Conference, Prague, Sept. 4–10, 1967, pp. 130–141.
[2] IUPAC adopts new look in atomic weights, Chem. Eng. News **48,** No. 4, 38 (1970).
[3] Hönigschmid, O., and von Mack, M., Des Atomgewicht des Zinks. Analyse des Zinkchlorids, Z. Anorg. Allgem. Chem. **246,** 363 (1941).
[4] Baxter, G. P., and Grose, M. R., A revision of the atomic weight of zinc. The electrolytic determination of zinc in zinc bromide, J. Am. Chem. Soc. **38,** 868 (1916).
[5] Baxter, G. P., and Hodges, J. H., A revision of the atomic weight of zinc. II. The electrolytic determination of zinc in zinc chloride, J. Am. Chem. Soc. **43,** 1242 (1921).
[6] Leland, W. T., and Nier, A. O., The relative abundances of the zinc and cadmium isotopes, Phys. Rev. **73,** 1206 (1948).
[7] Hess, D. C., Inghram, M. G., and Hayden, R. J., The relative abundance of zinc isotopes, Phys. Rev. **74,** 1531 (1948).
[8] Cameron, A. E., and Wichers, E., Report of the International Commission on Atomic Weights (1961), J. Am. Chem. Soc. **84,** 4175 (1962).
[9] Faraday, M., Identity of electricities derived from different sources, Phil. Trans. Series 2, **3,** 23 (1833).
[10] Laird, J. S., and Hulett, G. A., The electrochemical equivalent of cadmium, Trans. Am. Electrochem. Soc. **22,** 385 (1913).
[11] Gladstone, J. H., and Hibbert W., On the atomic weight of zinc, J. Chem. Soc. **55,** 443 (1889).
[12] Hamer, W. J., Resumé of values of the Faraday, J. Res. Nat. Bur. Stand. (U.S.) **72A,** (Phys. and Chem.), No. 4, 435 (1968).
[13] Craig, D. N., Hoffman, J. I., Law, C. A., and Hamer, W. J., Determination of the value of the faraday with a silver-perchloric acid coulometer, J. Res. Nat. Bur. Stand. (U.S.) **64A,** (Phys. and Chem.), No. 1, 381 (1960).
[14] Marinenko, G., and Taylor, J. K., Electrochemical equivalents of benzoic and oxalic acid, Anal. Chem. **40,** 1645 (1968).
[15] This high purity standard reference material, SRM No. 682, is available from the Office of Standard Reference Materials, National Bureau of Standards, Washington, D.C. 20234, along with the Certificate of Analysis at a unit price of $90.
[16] Gill, A. S., Acting General Superintendent of Electrolytic Zinc Company of Australasia Ltd., Private Communication.
[17] Taylor, B. N., Parker, W. H., and Langenberg, D. N., Determination of e/h, using macroscopic quantum phase coherence in superconductors: implications for quantum electrodynamics and the fundamental phyical constants, Rev. Mod. Phys. **41,** 375 (1969).

(Paper 75A6–687)

JOURNAL OF RESEARCH of the National Bureau of Standards—A. Physics and Chemistry
Vol. 75A, No. 6, November–December 1971

High-Speed (Subsecond) Measurement of Heat Capacity, Electrical Resistivity, and Thermal Radiation Properties of Niobium in the Range 1500 to 2700 K*

Ared Cezairliyan

Institute for Materials Research, National Bureau of Standards, Washington, D.C. 20234

(August 10, 1971)

Measurements of heat capacity, electrical resistivity, hemispherical total emittance, and normal spectral emittance of niobium in the temperature range 1500 to 2700 K by a subsecond duration pulse heating technique are described. Results obtained on the above properties are reported and are compared with those in the literature. A sharp increase in heat capacity above 2000 K was observed. Electrical resistivity showed a negative departure from linearity in the curve of electrical resistivity against temperature. Estimated inaccuracy of measured properties is: 2 percent for heat capacity, 0.5 percent for electrical resistivity, and 3 percent for hemispherical total and normal spectral emittances.

Key words: Electrical resistivity; emittance; heat capacity; high-speed measurements; high temperature; niobium; thermal radiation properties; thermodynamics.

1. Introduction

Because of the difficulties involved in performing accurate experiments at high temperatures by conventional techniques, a high-speed method was developed to measure heat capacity, electrical resistivity, hemispherical total emittance, and normal spectral emittance of electrical conductors. In this paper, application of this technique to measurements on niobium in the temperature range 1500 to 2700 K is described.

The method is based on rapid resistive self-heating of the specimen from room temperature to near its melting point. During the short experiment, which lasts less than 1 s, current flowing through the specimen, potential across the specimen and specimen temperature are measured. The experimental quantities are recorded with a digital recording system, which has a time resolution of 0.4 ms, and a full-scale signal resolution of one part in 8000. Details regarding the construction and operation of the measurement system, the methods of measuring experimental quantities, and other pertinent information, such as formulation of relations for properties, etc. are given in earlier publications [1, 2].[1]

2. Measurements

Measurements were performed on two specimens designated as niobium-1 and niobium-2. Each specimen was a tube of the following nominal dimensions; length, 4 in (101 mm); outside diameter, 0.25 in (6.3 mm); and wall thickness, 0.02 in (0.5 mm). A small rectangular hole (0.5×1 mm) fabricated in the wall at the middle of the specimen approximated blackbody conditions for the high-speed photoelectric pyrometer [3].

The measurements were made in the temperature interval 1500 to 2700 K (approximately 50 K below the melting point). To optimize the operation of the pyrometer, this temperature interval was divided into six ranges: I, 1500 to 1650 K; II, 1600 to 1800 K; III, 1750 to 1950 K; IV, 1900 to 2200 K; V, 2100 to 2550 K; and VI, 2400 to 2700 K.

In each of the first five temperature ranges, two experiments were conducted on niobium-1 and one on niobium-2; in the last range, one experiment was conducted on each specimen. A total of three additional experiments in the ranges II, III, and IV were performed on niobium-1 in which the surface radiance of the specimen was measured.

Before the start of the experiments, each specimen was annealed by subjecting it to 30 heating pulses (up to 2400 K). All the experiments were conducted with the specimens in a vacuum environment of approximately 10^{-4} torr.

To optimize the operation of the measurement system, the heating rate of the specimens was varied depending on the desired temperature range by adjusting the value of the resistance in series with the specimen. Duration of the current pulses in the experiments ranged from 390 to 450 ms; and the average heating rate of the specimens was approximately

*This work was supported in part by the Directorate of Aeromechanics and Energetics of the U.S. Air Force Office of Scientific Research under contract ISSA–70–0002.

[1] Figures in brackets indicate the literature references at the end of this paper.

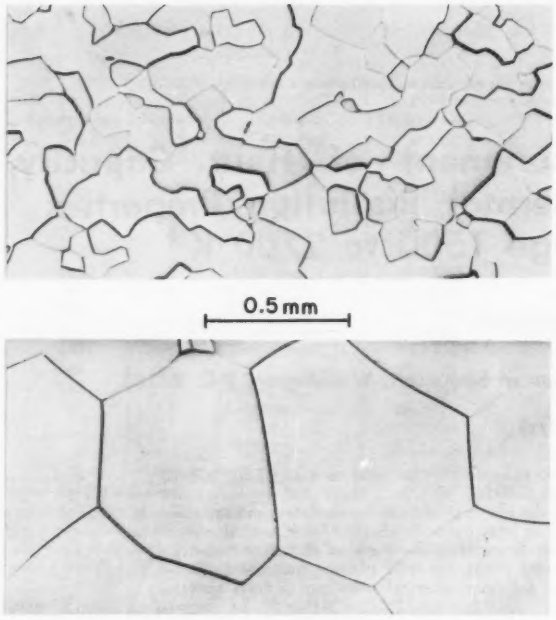

FIGURE 1. *Photomicrographs of the niobium specimen before (upper photograph) and after (lower photograph) the entire set of experiments.*

5200 Ks^{-1}. Radiative heat losses from the specimens amounted to approximately 1 percent at 1500 K, 3 percent at 2000 K, and 10 percent at 2700 K of the input power.

Characterization of one of the specimens (niobium-1) was made by the following methods: photomicrography, spectrochemical analysis, and residual resistivity ratio. Photomicrographs of the specimen, shown in figure 1, indicate that considerable grain growth took place as the result of pulse heating to high temperatures. Chemical analyses were made of the specimen before and after the entire set of experiments. Comparison of results does not indicate any detectable change in impurity concentration. A list of the nature and composition of impurities in the specimen is given in table 1. The residual resistivity ratio (ratio of electrical resistivity at 273 K to the residual resistivity) of the specimen, measured before the experiments, was 11.

The data on voltage, current, and temperature were used to obtain third degree polynomial functions for each quantity in terms of time, which then provided the input information for the determination of properties.

3. Experimental Results

This section presents the thermophysical properties determined from the measured quantities. All values are based on the International Practical Temperature Scale of 1968 [4]. In all computations, the geometrical quantities are based on their room temperature (298 K) dimensions. The experimental results are represented by polynomial functions in temperature obtained by least squares approximation of the individual points. The final values on properties at 100 degree temperature intervals computed using the functions are presented in table 2. Results obtained from individual experiments, by the method described previously [2], are given in the appendix (tables A–1, A–2, and A–3).

3.1. Heat Capacity

Heat capacity was computed from data taken during the heating period. A correction for power loss due to thermal radiation was made using the results on hemispherical total emittance. The standard deviation of the individual data points from a third degree polynomial function in the range 1500 to 2700 K for each specimen is 0.7 percent for niobium-1 and 0.9 percent for niobium-2. The average absolute difference between the results on two specimens is 0.7 percent. The function for heat capacity (standard deviation = 0.8%) that represents the combined results of the two specimens in the temperature interval 1500 to 2700 K is:

$$c_p = -3.395 + 4.855 \times 10^{-2} T - 2.531 \times 10^{-5} T^2 + 5.035 \times 10^{-9} T^3 \quad (1)$$

where T is in K and c_p is in J mol^{-1} K^{-1}. In the computations of heat capacity, the atomic weight of niobium was taken as 92.91.

3.2. Electrical Resistivity

The electrical resistivity of niobium was determined from the same experiments that were used to calculate heat capacity. The standard deviation of the individual data points from a second degree polynomial function in the range 1500 to 2700 K for each specimen is 0.2 percent for both niobium-1 and niobium-2. The average absolute difference between the results on two specimens is 0.5 percent. The function for electrical resistivity (standard deviation = 0.3%) that represents

TABLE 1. *Impurities in niobium specimen*

Impurity	Amount ppm	Impurity	Amount ppm
Al	5	Mo	5
As	< 5	Ni	< 1
B	< 1	Pb	< 1
Bi	< 5	Sb	< 10
Ca	< 1	Si	< 5
Cd	< 5	Sn	3
Co	< 1	Ta	450
Cr	< 1	Te	< 5
Cu	< 1	Ti	< 1
Fe	< 3	V	< 1
Hf	< 50	W	< 100
Mg	< 1	Zn	< 10
Mn	< 1	Zr	< 5

470 < Total < 680

TABLE 2. *Heat capacity, electrical resistivity, hemispherical total emittance and normal spectral emittance of niobium*

Temp. K	c_p J mol^{-1} K^{-1}	ρ^a 10^{-8} Ω m	ϵ^a	$\epsilon_{N,\lambda}$
1500	29.48	57.58		
1600	30.11	60.41		
1700	30.73	63.20	0.217	0.353
1800	31.35	65.96	.230	.352
1900	32.02	68.68	.242	.352
2000	32.75	71.37	.254	.351
2100	33.57	74.02	.264	.351
2200	34.53	76.63	.274	.351
2300	35.64	79.20	.282	.350
2400	36.94	81.74	.290	
2500	38.46	84.25	.297	
2600	40.23	86.71	.303	
2700	42.28	89.14		

[a] Based on ambient temperature (298 K) dimensions.

the combined results of the two specimens in the temperature interval 1500 to 2700 K is:

$$\rho = 10.74 + 3.396 \times 10^{-2} T - 1.823 \times 10^{-6} T^2 \quad (2)$$

where T is in K, and ρ is in 10^{-8} Ωm. In the computations of the specimen's cross-sectional area, which is needed for the computations of electrical resistivity, the density of niobium was taken as 8.57×10^3 kg m^{-3} [5]. The measurements, before pulse experiments, of the electrical resistivity of the two niobium specimens at 293 K with a Kelvin bridge were in agreement within 0.1 percent. Electrical resistivity of niobium at 293 K obtained by averaging the results of the two specimens is 15.9×10^{-8} Ωm.

3.3. Hemispherical Total Emittance

Hemispherical total emittance was computed for niobium-1 using data taken during both heating and initial free cooling periods. The function for hemispherical total emittance (standard deviation = 0.4%) that represents the results in the temperature range 1700 to 2650 K is:

$$\epsilon = -0.144 + 2.88 \times 10^{-4} T - 4.46 \times 10^{-8} T^2 \quad (3)$$

where T is in K.

3.4. Normal Spectral Emittance

Normal spectral emittance was computed for niobium-1 using data from three sets of two experiments, one in which the pyrometer was aimed at the surface of the specimen, and another in which it was aimed at the blackbody hole in the specimen. The measurements were made at the effective wavelength of the pyrometer interference filter (650 nm; bandwidth 10 nm). The function for normal spectral emittance (standard deviation = 0.6%) that represents the results in the temperature range 1700 to 2300 K is:

$$\epsilon_{N,\lambda} = 0.361 - 4.77 \times 10^{-6} T \quad (4)$$

where T is in K.

4. Estimate of Errors

Estimates of errors in measured and computed quantities lead to the following estimates of errors in the properties over the temperature range 1500 to 2700 K: heat capacity, 2 percent; electrical resistivity, 0.5 percent; hemispherical total emittance, 3 percent; normal spectral emittance, 3 percent. Details regarding the estimates of errors and their combination in high-speed experiments using the present measurement system are given in a previous publication [2]. Specific items in the error analysis were recomputed whenever the present conditions differed from those in the earlier publication.

In all the earlier experiments with the present high-speed system, the lowest temperature at which measurements were made was 1900 K. In the present work, the measurements were extended down to 1500 K without creating any significant uncertainties in temperature measurements. The imprecision [2] of temperature measurements was 0.7 K at 1500 K, and 0.5 K at 1900 K. The imprecision of voltage and current measurements was less than 0.02 and 0.03 percent, respectively, over the entire temperature range.

5. Discussion

The heat capacity and electrical resistivity results of this work are compared graphically with those in the literature in figures 2 and 3, respectively. Numerical comparisons are given in tables 3 and 4. Heat capacity results of this work are, in general, lower than those of most other investigators, with the exception of Kraftmakher [8]. Electrical resistivity results are in good agreement with those of others. Estimates of errors in papers cited lead to an estimate of inaccuracies in previously reported heat capacity and electrical resistivity of approximately 5 to 10 and 1 to 3 percent, respectively.

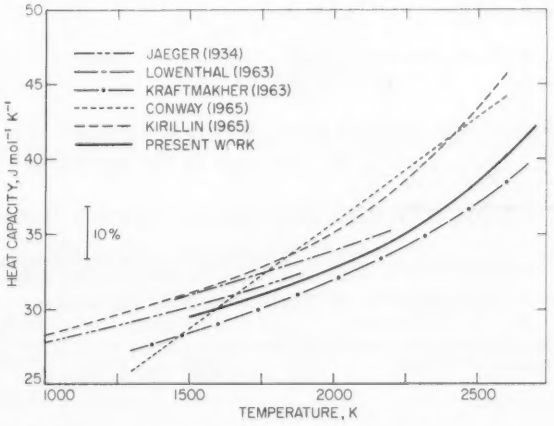

FIGURE 2. *Heat capacity of niobium reported in the literature.*

[2] Imprecision refers to the standard deviation of an individual point as computed from the difference between measured value and that from the smooth function obtained by the least squares method.

443-082 OL - 71 - 3

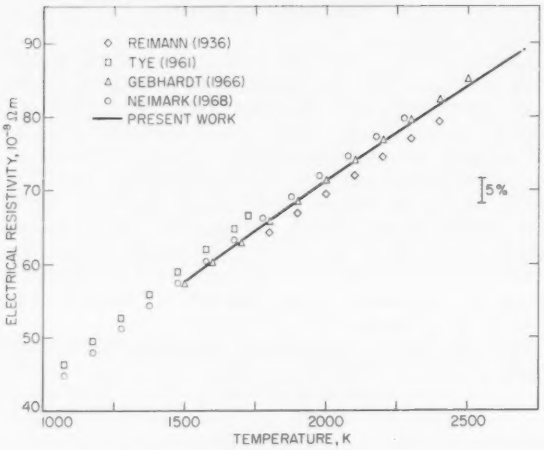

FIGURE 3. *Electrical resistivity of niobium reported in the literature.*

The present result of the electrical resistivity of niobium corresponding to 293 K is 15.9×10^{-8} Ωm; those reported in the recent literature range from 14.6×10^{-8} Ωm [13] to 16.9×10^{-8} Ωm [12].

The results for hemispherical total emittance and normal spectral emittance of this work and those in the literature are presented in figures 4 and 5, respectively. Deviations in the results of various investigators may largely be attributed to the differences in specimen surface conditions.

Similar to the earlier results on molybdenum [2], tantalum [21], and tungsten [22] obtained with the present measurement system, heat capacity of niobium at high temperatures is considerably higher than the Dulong and Petit value of $3R$. Some of this departure is due to $c_p - c_v$ and the electronic terms. However, they do not account for the entire difference. Heat capacity above the Debye temperature may be expressed by

$$c_p = A - \frac{B}{T^2} + CT + \Delta c \qquad (5)$$

where the constant term is 3R (24.943 J mol^{-1} K^{-1}), the term in T^{-2} is the first term in the expansion of the Debye function, the term in T represents $c_p - c_v$ and electronic contributions, and the quantity Δc represents excess in measured heat capacity at high temperatures, which is not accounted for by the first three terms. The coefficients $B(9.6 \times 10^4)$ and $C(2.9 \times 10^{-3})$ were obtained from data on heat capacity at 200 K and 1000 K given by Hultgren et al. [23].

Using eq (5) and the heat capacity results of this work, the quantity Δc was computed for temperatures above 1500 K. The results for Δc in J mol^{-1} K^{-1} are: 0.2 at 1500 K, 2.0 at 2000 K, 6.3 at 2500 K, and 9.5 at 2700 K.

Although the mechanisms of vacancy generation become important at high temperatures, it was not possible to attribute the high heat capacity values entirely to vacancies. To demonstrate this, a crude estimate of the contribution of vacancies to heat capacity was made using the method described in a previous publication [2]. The results indicate that vacancy contribution would be small, less than 0.05 J mol^{-1} K^{-1} at 2000 K and 0.5 J mol^{-1} K^{-1} at 2700 K, and would not account for the high heat capacity values. If the entire difference between measured and computed [using the first three terms in eq (5)] heat capacities is attributed to vacancies, values of 1.3 eV for vacancy formation energy and 3.5 percent for vacancy concentration at the melting point are obtained. Both of these values seem to be unrealistic for niobium.

To give a simple expression for the heat capacity of niobium over a wide temperature range, an empirical term for the quantity Δc in eq (5) was substituted. Trials indicated that a term in T^5 describes the experimental results better than a term in T^4. The coefficient of this term was obtained from the results of the present work in conjunction with the values given by Hultgren et al. [23] at temperatures below 1000 K. Then eq (5) for the range 300 to 2700 K becomes

$$c_p = 24.943 - \frac{9.6 \times 10^4}{T^2} + 2.9 \times 10^{-3} T + 6.4 \times 10^{-17} T^5 \qquad (6)$$

where T is in K and c_p is in J mol^{-1} K^{-1}. Average absolute deviation of the individual points from the function over the temperature range considered is 0.4 percent. Equation (6) is presented graphically in figure 6.

TABLE 3. *Niobium heat capacity difference (previous literature minus present work values) in percent*

Investigator	Ref.	Year	Method	Temperature, K						
				1500	1700	1900	2100	2300	2500	2700
Jaeger and Veenstra	6	1934	drop	+2.4	+1.8	+1.3				
Lowenthal	7	1963	modul.	+4.8	+4.1	+3.6	+2.6	+0.7		
Kraftmakher	8	1963	modul.	−3.6	−3.4	−3.1	−2.9	−3.2	−4.0	−5.5
Conway and Hein	9	1965	drop	−2.6	+2.6	+7.2	+10.6	+12.0	+11.0	
Kirillin et al.	10	1965	drop	+5.2	+5.1	+6.3	+8.2	+10.4	+12.3	+13.6

TABLE 4. *Niobium electrical resistivity difference (previous literature minus present work values) in percent*

Investigator	Ref.	Year	Temperature, K					
			1500	1700	1900	2100	2300	2500
Reiman	11	1936			−2.7	−2.8	−2.9	
Tye	12	1961	+3.6	+3.9				
Gebhardt et al.	13	1966	−0.6	−0.6	−0.5	−0.1	+0.4	+1.0
Neimark and Voronin	14	1968	+1.0	+1.4	+1.6	+1.7	+1.6	

Earlier work on tantalum [21], which also belongs to Group V, indicated that the quantity Δc in eq (5) is best represented by a term in T^5. However, the results on molybdenum [2] and tungsten [22], which belong to Group VI, indicated that the same quantity is best described by a term in T^4. The significance of this is not apparent at this time.

Electrical resistivity of niobium, in the range of present measurements, showed a negative departure from linearity in the curve of electrical resistivity against temperature. A similar trend was also observed for tantalum [21].

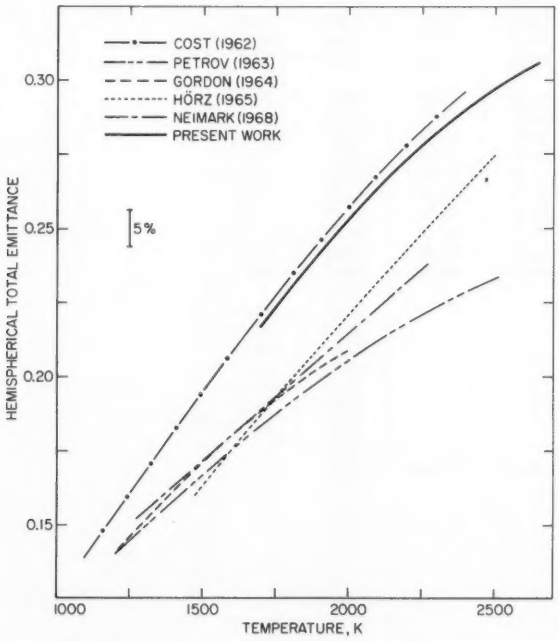

FIGURE 4. *Hemispherical total emittance of niobium reported in the literature.*

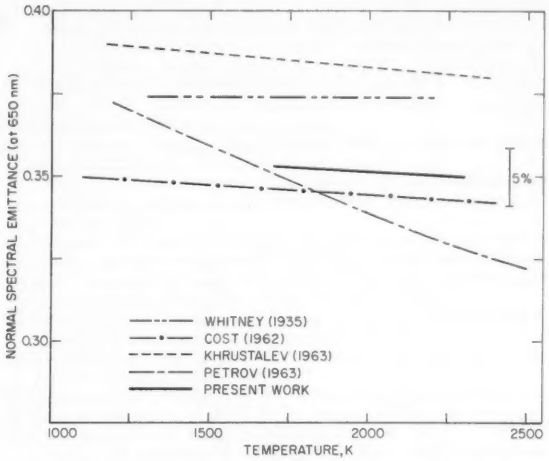

FIGURE 5. *Normal spectral emittance of nibium at λ = 650 nm reported in the literature.*

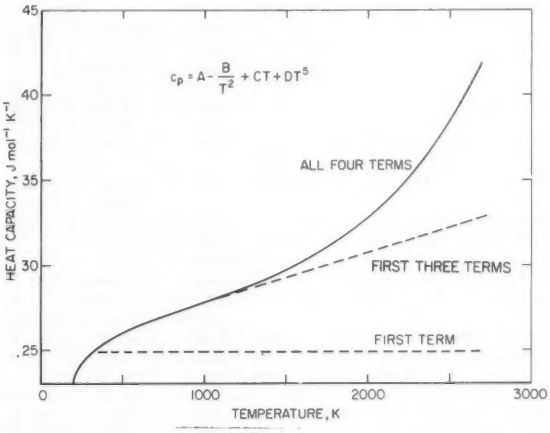

FIGURE 6. *Heat capacity of niobium according to equation (6).*

The author expresses his gratitude to C. W. Beckett for his continued interest and encouragement of research in high-speed methods of measuring thermophysical properties. The contributions of M. S. Morse in connection with electronic instrumentation are also greatly appreciated.

6. Appendix

TABLE A–1. *Experimental results on heat capacity and electrical resistivity of niobium* [a]

Range	Specimen	Niobium-1				Niobium-2	
	Run	1		2		1	
	T	c_p	ρ	c_p	ρ	c_p	ρ
I	1500	29.56	57.48	29.39	57.49	29.51	57.82
	1550	29.72	58.89	29.69	58.89	30.05	59.22
	1600	30.11	60.28	30.14	60.28	30.58	60.63
	1650	30.74	61.67	30.75	61.67	31.09	62.04
II	1600	29.87	60.34	29.99	60.35	29.99	60.71
	1650	30.15	61.71	30.22	61.72	30.47	62.08
	1700	30.52	63.09	30.55	63.09	30.93	63.46
	1750	31.01	64.45	31.01	64.44	31.39	64.83
	1800	31.60	65.80	31.59	65.81	31.83	66.19
III	1750	30.65	64.48	30.55	64.48	30.85	64.86
	1800	31.03	65.83	31.07	65.81	31.29	66.20
	1850	31.48	67.16	31.59	67.15	31.78	67.55
	1900	32.00	68.50	32.11	68.49	32.31	68.89
	1950	32.61	69.83	32.62	69.82	32.90	70.24
IV	1900	31.91	68.59	31.66	68.61	31.69	69.01
	1950	32.19	69.92	32.07	69.92	32.22	70.33
	2000	32.55	71.23	32.53	71.23	32.76	71.64
	2050	32.98	72.54	33.03	72.54	33.33	72.95
	2100	33.50	73.83	33.58	73.84	33.93	74.25
	2150	34.12	75.12	34.19	75.14	34.56	75.55
	2200	34.87	76.42	34.85	76.43	35.23	76.84
V	2100	33.58	73.98	33.37	73.98	33.61	74.37
	2150	34.00	75.27	33.87	75.27	34.10	75.66
	2200	34.46	76.55	34.41	76.55	34.62	76.94
	2250	34.97	77.83	34.97	77.82	35.18	78.21
	2300	35.53	79.09	35.58	79.08	35.79	[illegible].47
	2350	36.16	80.35	36.24	80.34	36.46	80.72
	2400	36.86	81.60	36.96	81.59	37.19	81.97
	2450	37.66	82.84	37.75	82.83	38.01	83.21
	2500	38.57	84.07	38.62	84.06	38.91	84.45
	2550	39.63	85.29	39.60	85.30	39.94	85.69
VI	2400	36.73	81.69			37.01	82.08
	2450	37.21	82.92			37.39	83.31
	2500	37.85	84.13			37.98	84.53
	2550	38.68	85.34			38.82	85.74
	2600	39.74	86.54			39.99	86.94
	2650	41.10	87.75			41.60	88.15
	2700	42.89	88.97			43.21	89.37

[a] Temperature in K, heat capacity in J mol^{-1} K^{-1}, electrical resistivity in 10^{-8} Ωm.

TABLE A–2. *Experimental results on hemispherical total emittance of niobium-1*

T K	ϵ
1715	0.219
1715	.217
1715	.220
1714	.218
1890	.240
1889	.239
1889	.243
1889	.242
2058	.261
2057	.260
2057	.260
2056	.259
2328	.286
2326	.284
2326	.284
2325	.283
2655	.307
2653	.307
2653	.306
2651	.305

TABLE A–3. *Experimental results on normal spectral emittance of niobium-1 at* $\lambda = 650$ *nm*

T K	$\epsilon_{N,\lambda}$
1694	0.354
1712	.354
1730	.353
1747	.353
1765	.353
1783	.353
1801	.353
1818	.354
1836	.354
1853	.349
1874	.349
1895	.349
1916	.350
1937	.351
1957	.352
1978	.353
1998	.354
2019	.355
2038	.350
2069	.348
2099	.348
2129	.348
2158	.349
2187	.349
2216	.350
2244	.352
2272	.353
2300	.354

7. References

[1] Cezairliyan, A., Design and operational characteristics of a high-speed (millisecond) system for the measurement of thermophysical properties at high temperatures. J. Res. Nat. Bur. Stand. (U.S.) **75C** (Eng. and Instr), No. 1, 7 (1971).

[2] Cezairliyan, A., Morse, M. S., Berman, H. A., and Beckett, C. W., High-speed (subsecond) measurement of heat capacity, electrical resistivity, and thermal radiation properties of molybdenum in the range 1900 to 2800 K, J. Res. Nat. Bur. Stand. (U.S.) **74A** (Phys. and Chem.), No. 1, 65 (1970).

[3] Foley, G. M., High-speed optical pyrometer, Rev. Sci. Instr. **41**, 827 (1970).

[4] International Practical Temperature Scale of 1968, Metrologia **5**, 35 (1969).

[5] Tietz, T. E. and Wilson, J. W., Behavior and properties of refractory metals, p. 28. (Stanford University Press, California, 1965).

[6] Jaeger, F. M., and Veenstra, W. A., The exact measurement of the specific heats of solid substances at high temperatures, VI, the specific heats of vanadium, niobium, tantalum, and molybdenum. Rec. Trav. Chim. **53**, 677 (1934).

[7] Lowenthal, G. C., The specific heat of metals between 1200 K and 2400 K, Australian J. Phys. **16**, 47 (1963).

[8] Kraftmakher, Ya. A., Vacancy formation in niobium. Solid State (USSR), **5**, 696 (1963).

[9] Conway, J. B., and Hein, R. A., Enthalpy measurements of solid materials to 2400 C by means of drop technique in advances in thermophysical properties at extreme temperatures and pressures, S. Gratch, ed., p. 131. (ASME, New York, 1965).

[10] Kirillin, V. A., Sheindlin, A. E., Chekhovskoi, V. Ya., and Zhukova, I. A., Experimental determination of the enthalpy of niobium in the temperature range 600 to 2600 K, High Temperature, **3**, 357 (1965).

[11] Reimann, A. L., Some high-temperature properties of niobium, Phil. Mag. **22**, 34 (1936).

[12] Tye, R. P., Preliminary measurements on the thermal and electrical conductivities of molybdenum, niobium, tantalum, and tungsten, J. Less-Common Metals **3**, 13 (1961).

[13] Gebhardt, E., Dürrschnabel, W., and Hörz, G., J. Nucl. Mat. **18**, 119 (1966).

[14] Neimark, B. E., and Voronin, L. K., Thermal conductivity, specific electrical resistivity, and total emissivity of refractory metals at high temperatures, High Temperature **6**, 999 (1968).

[15] Cost, J. R., Emissivities of niobium and niobium-nitrogen solids solutions, Trans. Metall. Soc. AIME **224**, 634 (1962).

[16] Petrov, V. A., Chekhovskoi, V. Ya., and Sheindlin, A. E., Experimental determination of the degree of blackness of niobium at temperatures of 1200 to 2500 K, High Temperature **1**, 416 (1963).

[17] Gordon, A. R., and Muchnik, G. F., Determination of the emissivity of niobium as a function of the roughness of the surface, High Temperature **2**, 505 (1964).

[18] Hörz, G., Dürrschnabel, W., and Gebhardt, E., Hemispherical total emittance of niobium, J. Nucl. Mat. **17**, 277 (1965).

[19] Whitney, L. V., The temperature scales of columbium, thorium, rhodium and molybdenum at 0.667 μ, Phys. Rev. **48**, 458 (1935).

[20] Khrustalev, B. A., Kolchenogova, I. P., and Rakov, A. M., Spectral coefficients of tantalum, molybdenum and niobium radiation, High Temperature **1**, 13 (1963).

[21] Cezairliyan, A., McClure, J. L., and Beckett, C. W., High-speed (subsecond) measurement of heat capacity, electrical resistivity, and thermal radiation properties of tantalum in the range 1900 to 3200 K, J. Res. Nat. Bur. Stand. (U.S.) **75A** (Phys. and Chem.), No. 1, 1 (1971).

[22] Cezairliyan, A., and McClure, J. L., High-speed (subsecond) measurement of heat capacity, electrical resistivity, and thermal radiation properties of tungsten in the range 2000 to 3600 K, J. Res. Nat. Bur. Stand. (U.S.), **75A** (Phys. and Chem.), No. 4, 283 (1971).

[23] Hultgren, R., Orr, R. L., Anderson, P. D., and Kelly, K. K., Selected Values of Thermodynamic Properties of Metals and Alloys, (Wiley, New York, 1963).

(Paper 75A6–688)

JOURNAL OF RESEARCH of the National Bureau of Standards—A. Physics and Chemistry
Vol. 75A, No. 6, November–December 1971

Stable Radical-Anions Derived from Glyoxal *Bis*(phenylhydrazones)*

Alexander J. Fatiadi

Institute for Materials Research, National Bureau of Standards, Washington, D.C. 20234

(May 10, 1971)

A series of resonance-stabilized, hydrazyl radical-anions has been observed for the first time; they were prepared by an electron-transfer reaction involving treatment of glyoxal bis(phenylhydrazones) in methyl sulfoxide with a base and a trace of oxygen. The stability of these radical-anions appears to be dependent on the nature of the *para* substituents on the phenylhydrazine moiety.

Key words: Bis(phenylhydrazone); e.s.r.; glyoxal; methyl sulfoxide; oxygen; radical-anion.

1. Introduction

In the series of stable hydrazyl radicals, a neutral radical, namely, 1,1-diphenyl-2-picrylhydrazyl (DPPH), and its analogs are the best known and the most thoroughly studied [1, 2];[1] recently, e.s.r. studies established the existence of stable, hydrazinium radical-cations in colored solutions of tetraphenylhydrazine dissolved in strong acids [3]. The present report describes the preparation and some of the properties of some new, stable, hydrazyl radical-anions.

2. Experimental Procedure

2.1. Apparatus

Ultraviolet and visible spectra were recorded with a Beckman DK–2 or Cary 14 spectrophotometer.[2] Electron-spin resonance spectra were recorded with a Varian Model 4500 EPR spectrometer with 100-kHz field-modulation and detection. The klystron frequency was measured with a transfer oscillator and a frequency counter. The magnetic field was measured by a proton gaussmeter monitored by the same frequency counter.

The solutions were examined in a Varian Model V–4548 aqueous-solution sample-cell. All experiments in solution required a trace of oxygen; freshly prepared solutions of bis(phenylhydrazones) in methyl sulfoxide (2.5 to 5.0 m*M*) were mixed with base (5% aqueous potassium hydroxide or 5% potassium *tert*-butoxide in methyl sulfoxide) and exposed to air for about 30 s. Initial e.s.r. spectra were recorded about 1 min after mixing.

2.2. Materials

Methyl sulfoxide (Matheson spectrograde) and a reagent-grade potassium *tert*-butoxide (Mine Safety Appliances Research Corp.) were used directly.

Glyoxal bis(phenylhydrazones) were prepared by condensation of 40 percent aqueous glyoxal (Union Carbide Chemicals) with phenylhydrazine or with *p*-bromo-, *p*-chloro-, 2,5-dichloro, *p*-nitro- or *m*-nitrophenylhydrazine in the presence of a catalytic amount of acetic acid; the crude bis(phenylhydrazones) were purified by repeated recrystallization from ethanol or ethanol-acetic acid.

The $C_6D_5NHNH_2$ was prepared according to the following scheme:

$$C_6D_5NO_2 \xrightarrow[HCl]{Sn} C_6D_5NH_2 \cdot HCl \xrightarrow[(3)\ \text{ether extraction}]{(1)\ NaOH;\ (2)\ \text{steam distillation}}$$

$$C_6D_5NH_2 \xrightarrow[0°]{NaNO_2,\ HCl} C_6D_5\overset{+}{N}{\equiv}NCl^-$$

$$\xrightarrow{Na_2SO_3} C_6D_5NHNH_2 \cdot HCl\ (45\%\ \text{overall yield}).$$

3. Results and Discussion

Treatment of a solution of glyoxal bis(phenylhydrazone) **1a** in methyl sulfoxide (Me_2SO) (10^{-2} to 10^{-3} *M*, $\lambda_{max}^{Me_2SO}$ 382 nm, $\epsilon_{mM} \sim 49$) with a strong base (5% aqueous potassium hydroxide or potassium *tert*-butoxide in Me_2SO) and a trace of oxygen produced a deep violet-purple solution exhibiting bands at λ_{max} 455 and 562 nm with rapidly changing intensity. E.s.r. examination of the solution revealed that the deep-purple color, and consequently a batho-

* Part II. Stable Free Radicals. For part I, see Chem. Commun. 456 (1968).

[1] Figures in brackets indicate the literature references at the end of this paper.

[2] Certain commercial instruments or chemicals are mentioned in this paper; this does not imply recommendation or endorsement by the National Bureau of Standards.

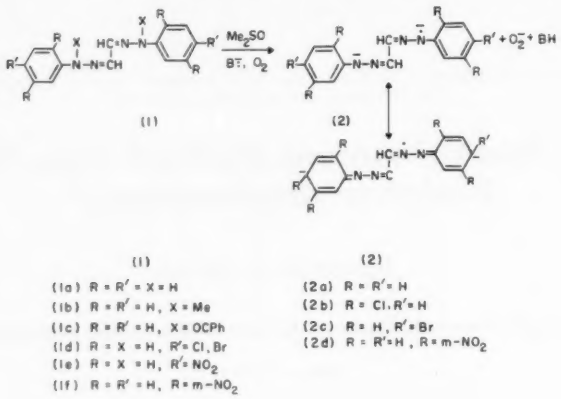

(1)

(1a) R = R′ = X = H
(1b) R = R′ = H, X = Me
(1c) R = R′ = H, X = OCPh
(1d) R = X = H, R′ = Cl, Br
(1e) R = X = H, R′ = NO_2
(1f) R = R′ = H, R = m-NO_2

(2)

(2a) R = R′ = H
(2b) R = Cl, R′ = H
(2c) R = H, R′ = Br
(2d) R = R′ = H, R = m-NO_2

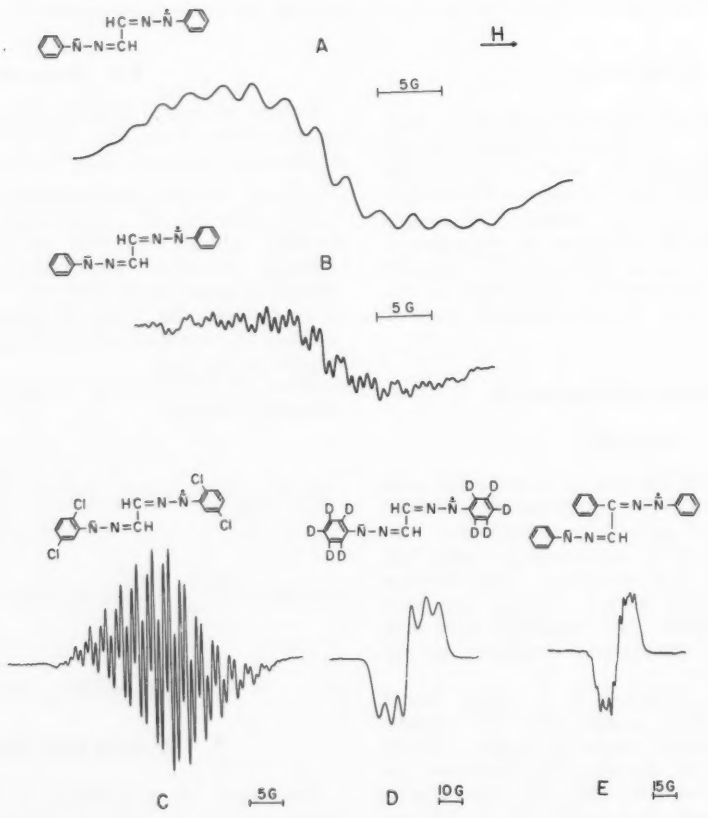

FIGURE 1. *Radical-anions from glyoxal bis(phenylhydrazones); A, from* **1a** *(3.2 mM, in* Me_2SO*-5 percent aqueous* KOH*); B, from* **1a** *(2.8 mM, in* Me_2SO-$KOBu^t$*); C, from 2,5-dichloro derivative of* **1a** *(3 mM, in* Me_2SO-$KOBu^t$*); D, from* **1a**, *completely substituted with deuterium on the benzene ring (5 mM, in* Me_2SO-$KOBu^t$*); E, from phenylglyoxal bis(phenylhydrazone).*

chromic shift in the visible spectrum, is partly associated with the presence of a paramagnetic species having the hyperfine structure shown in figures 1A and 1B.

Cooling and rapid filtration of the concentrated, alkaline solution from **1A** yielded a somewhat air-sensitive, purple-violet, paramagnetic dipotassium salt (**2** ↔ **2a**). From the fact that neither the *N*-methyl nor the *N*-benzoyl derivative of glyoxal bis(phenylhydrazone) (**1b** and **1c**, respectively) showed either a color change or the presence of paramagnetic species following treatment with base, it was concluded that the purple radical-anion from **1a** must arise following the abstraction of acidic imino protons (X in **1a**) by base. The dianion character of the radical anion (**2** ↔ **2a**) was deduced from the fact that methylation or benzoylation of the latter gave the di-*N*-methyl (**1b**) (mp. 224 °C) or di-*N*-benzoyl (**1c**) (mp. 312 °C. derivative of glyoxal bis(phenylhydrazone) in 45 and 60 percent yield, respectively.

The contribution of the resonance form (**2** ↔ **2a**) to the stability of the radical anion from **1a** was deduced from a study of radical anions derived from the substituted bis(phenylhydrazones). The most stable radical-anions were obtained from (a) the unsubstituted glyoxal bis(phenylhydrazone) **1a**, (b) those having the *para*-position in the benzene ring unsubstituted (for example, the 2,5-dichloro derivative, **2b**), or (c) those in which the *para*-position was substituted with an electron-withdrawing group, for example, the *p*-nitro derivative **1e**. Derivatives having electron-donating groups on the phenylhydrazino group (for example, the *p*-chloro or *p*-bromo derivatives **1d**) produced, on treatment with base, little or no bathochromic shift and gave little or no e.s.r. signal. These observations are in agreement with the substituent effect proposed by Walter [4], in which it was considered that electron-withdrawing groups (e.g., *p*-NO_2) enhance the stability of the hydrazyl radical by delocalization of an unpaired electron. It may be mentioned, however, that in contrast to neutral and cationic hydrazyl radicals having *p*-Cl or *p*-Br substituents, the corresponding anion-radical of type **2c** was not observed following treatment of the glyoxal *p*-Cl- or *p*-Br-substituted bis(phenylhydrazones) **1d** with base.[3] Formation of a radical anion (**2** ↔ **2a**) from the bis(phenylhydrazone) **1a** in the presence of oxygen and base appears to be a straightforward example of electron transfer; similar electron transfer occurs in the formation of radical anions from formazans [5]. The contribution of the resonance form (**2** ↔ **2a**) to the stability of the radical anion from **1a** was also supported by the fact that examination of the residue obtained after acidification with dilute hydrochloric acid of the alkaline paramagnetic solution from **1a** revealed the presence of a trace of the oxidation product 1,2-bis(phenylazo)ethylene **5**. This indicates that only a negligible proportion of a tautomer anion (as shown) is involved in the resonance form.

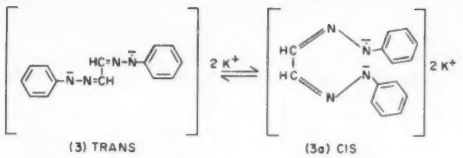

(3) TRANS (3a) CIS

(4) (4a)

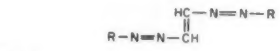

R=C_6H_5

(5)

$$HC=N-\bar{N}C_6H_5 \leftrightarrow H\dot{C}-N=NC_6H_5 \xrightarrow{O_2} H\dot{C}-N=NC_6H_5 \rightarrow \mathbf{5} + \dot{O}_2^-$$

or the resonance form

$$H\dot{C}-N=NC_6H_5 \leftrightarrow HC=N-\dot{N}C_6H_5$$

(only half of **1a** is depicted).

The radical anion from **1a** (or its analogs **2b** or **2d**) is stable in air for over an hour (dilute solution in Me_2SO); in concentrated solution, especially with limited access of air, the e.s.r. signals persist for at least 24 h; signals were not observed in methanol, *p*-dioxane, or their aqueous mixtures as solvent.

Bis(phenylhydrazone) **1a** gave the e.s.r. spectra shown in figures 1 and 2. The 15-line spectra A and A–1 (aqueous potassium hydroxide) with intensities of ~1:2:6:10:14:18:22:24:22:18:14:10:6:2:1 were observed. Structure A represents a centrosymmetric, resonance-stabilized, radical anion having two different pairs of nitrogen atoms (N=CH and N–Ph); the e.s.r. spectrum (A and A–1, figs. 1 and 2) can be explained by assuming interaction of the unpaired electron with two pairs of equivalent nitrogen atoms; this spectrum is consistent with $a^N = 4.95$ and 4.95 G, $a^H = 4.95$, 4.95, 2.35, and 2.35 G. Spectrum B (fig. 1) (prepared with anhydrous potassium *tert*-butoxide in methyl sulfoxide) is consistent with $a^N = 5.70$ and 5.70 G; $a^H = 5.70$, 5.70, 1.41, 1.41, 0.70, and 0.70 G.[4] The radical intermediate may be represented as a resonance-stabilized, acyclic

[3] A very weak, one-line e.s.r. spectrum [ΔH (width) = 21.6 G, $g_{av} = 2.007$] was observed for the radical anion from the bis(*p*-chloro-*o*-methoxyphenylhydrazone) of glyoxal.

[4] The 15-line spectra A and A–1 (figs. 1 and 2) are indicative of the unpaired electron interacting with two pairs of equivalent nitrogen atoms and two equivalent hydrogen atoms (or their equivalent pairs) or $(N-N)_2H_2$.

The observed 40-line spectra for B and C (fig. 1, which could have some overlap) fits $(N-N)_2H_7$, whereas $(N-N)_2H_6$ should give a 35-line pattern.

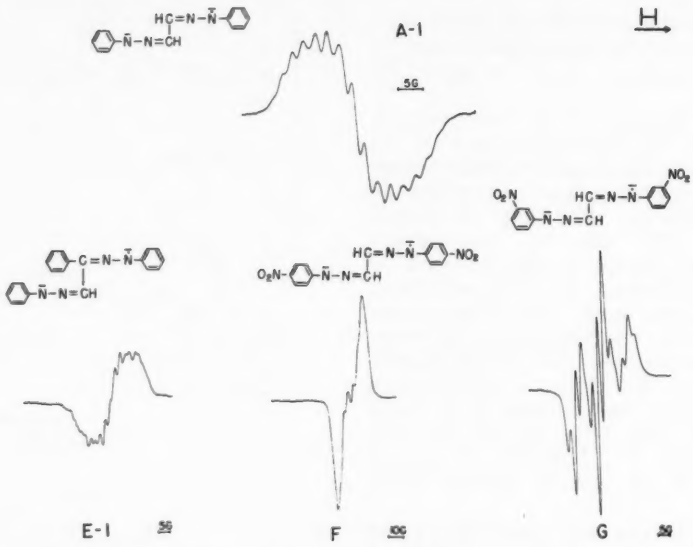

FIGURE 2. *Radical-anions from glyoxal bis(phenylhydrazones): A–1, from* **1a** *(3.8 mM, in* Me_2SO*-5 percent aqueous* KOH*); E–1, from phenylglyoxal bis(phenylhydrazone) (3.3 mM, in* Me_2SO-$KOBu^t$*); F, from* p-NO_2 *phenylglyoxal bis(phenylhydrazone* **1e***, 2.75 mM, in* Me_2SO-$KOBu^t$*); G,* m-NO_2 *derivative* **2d** *(3.5 mM, in* Me_2SO-$KOBu^t$*).*

structure (*trans-cis* structures **3** ↔ **3a**), mainly sterically favored *anti-anti* form **3** [6]; three geometrical isomers of the glyoxal bis(phenylhydrazones) are possible: *anti*, *syn*, and *amphi*, (see reference [6, 10c] for the discussion). However, some cyclic 1, 2, 3, 4-tetrazine structure (**4** ↔ **4a**) cannot be excluded completely. Further examination of the residue obtained after neutralization of the original purple solution from **1a** with aqueous hydrochloric acid, showed, in addition to the starting material, only a trace of the azo derivative **5**; the mixture contained [by preparative t.l.c. on Silica Gel G with 1:4 (v/v) ethanol–benzene] a small proportion of an orange component [5] believed to be a derivative of the cyclic 1,2,3,4-tetrazine [8–10]. The cyclic structures of the radical intermediates from formazans and tetrazolium salts involving 4-nitrogen nuclei were proposed by Maender and Russell [4a]; the stable radical derived from the cyclic 1,2,4,5-tetrazines (also comprising 4 nitrogen-nuclei) were recently reported [11]; the radical anion derived, for example, from 2,5-dialkyl-substituted 1,2,4,5-tetrazine showed an e.s.r. feature consisting of 63 lines [12].

N.M.R. studies of the bis(phenylhydrazones) of glyoxal (**1a**) in methyl sulfoxide gave evidence for the existence of a chelated and a nonchelated N–H group, prototype structures **3** ↔ **3a** [6] [7]; addition of a strong base, however, produced a paramagnetic solution, and caused disappearance of the N–H chelated bond. For example, an N.M.R. signal due to a chelated N—H in **1a** at 12.55 ppm (in methyl sulfoxide, after equilibration) [7], disappears on addition of 0.1 ml of 5 percent solution of potassium *tert*-butoxide (in Me_2SO) to the probe; the same happens to a signal at 12.25 ppm (chelated H–H) in *p*-NO_2 derivative **1e.**

The oxidative radical dimerization and coupling in the phenylhydrazine series is well known [13–17].

A symmetrical radical-anion **2b** derived from glyoxal bis[(2,5-dichlorophenyl)hydrazone] gave the e.s.r. features shown in figure 1C; this is also explained by assuming interaction of the unpaired electron with two pairs of equivalent nitrogen atoms $a^N = 6.35$ and 6.35 G; $a^H = 6.35$, 6.35, 1.65, 1.65, 0.82, and 0.82 G.

The hyperfine splitting constant (h.f.s.c.), which is a function of the spin densities, is somewhat larger for the radical **2b** ($a^N = 6.35$ G) than for the radical derived from the unsubstituted bis(phenylhydrazone) of glyoxal **1a** ($a^N = 4.95$ G or 5.70 G, see table 1). This can be explained by the electron-donating character of the 2,5-dichloro substituents, which results in an increase in the spin density on the 4 nitrogen nuclei of the molecule (the *para*-position in the benzene ring of **2b** is free to participate in the resonance).

In an attempt to find an unequivocal proof for the magnetic equivalence of four nitrogen atoms or their pairs in radical-anions **2a** and **2b** (fig. 1A, 1B, and 1C), the e.s.r. spectrum of glyoxal bis(phenylhydrazone) completely substituted with deuterium on the benzene ring was measured; this gave an incomplete pattern (fig. 1D); the spectrum did not show 4 nitrogen nuclei, and the quintet observed having h.f.s.c. $a^N = 5.45$ G is evidently a portion derived from two magnetically equivalent nitrogen atoms.

The radical anion derived from phenylglyoxal bis-

[5] Irradiation (366 nm) of a 1 percent solution of **1a** in benzene, gave a blue fluorescent component, in addition to a starting material and **5** [t.l.c. 3:1(v/v) benzene-methyl alcohol]; the mixture also contained a brown-orange component (by preparative t.l.c.) that on treatment with $KOBu^t$–Me_2SO produced an e.s.r. spectrum similar to A (fig. 1). The compound may have a structure (**4** ↔ **4a**).

TABLE 1. *Hyperfine splitting constants and g_m values[a] of radical anions of substituted bis(phenylhydrazones) of glyoxal at 25 ± 3°*

Compound No.	Spectrum	Solvent	g_m value[b]	Hyperfine structure a^N (G)	No. of equivalent nitrogen atoms[g]
2a	A–1[d]	[c]1	2.0035 ± 0.0001	4.95, 4.95	Two pairs.
	B[e]	2	2.0041 ± 0.0001	5.70, 5.70	Two pairs.
2b	C	2	2.0044 ± 0.0002	6.35, 6.35	Two pairs.
	D	2	2.0042 ± 0.0003	5.45	Two.
	E	2	2.0043 ± 0.0001	(f)	
	E–1	2	2.0044 ± 0.0001	4.40, 4.40	Two pairs.
2d	G	2	2.0053 ± 0.0002	7.05	Four.
	F	2	2.0059 ± 0.0003	(f)	

[a] Indicated errors of all values in this table are standard deviations of the average for three determinations; for example, for the a^N values the average deviation is ±0.15.
[b] g_m is defined as the middle point of the hyperfine lines of the spectrum.
[c] 1, Me_2SO-aqueous KOH; 2, Me_2SO-KOBu^t.
[d] Radical concentration (range from 12 to 38%), based on starting bis(phenylhydrazones), was determined by comparison with a diphenylpicrylhydrazyl standard solution.
[e] E.s.r. spectrum of **2a** measured at 77 K gave one line ($g_\perp = 1.99$, $\Delta H = 19.3$ G).
[f] Poorly resolved splitting.
[g] Distribution of Intensity.

(1) For Equivalent Nitrogens

No. of N	No. Lines	Pattern
1	3	1 : 1 : 1
2	5	1 : 2 : 3 : 2 : 1
3	7	1 : 3 : 6 : 7 : 6 : 3 : 1
4	9	1 : 4 : 10 : 16 : 19 : 16 : 10 : 4 : 1

(2) For Equivalent Hydrogens

No. of H	No. Lines	Pattern
1	2	1 : 1
2	3	1 : 2 : 1
3	4	1 : 3 : 3 : 1
4	5	1 : 4 : 6 : 4 : 1

(phenylhydrazone) (fig. 1E) did not show a well-resolved e.s.r. spectrum, a e.s.r. spectrum of the same radical-anion that is somewhat better resolved is shown in (fig. 2E–1). The 15-line pattern can be explained by assuming interaction of the unpaired electron with two pairs of equivalent nitrogen atoms, the spectrum (E–1) is consistent with $a^N \sim 4.40$ and 4.40 G. $a^H \sim 4.40$, 4.40, 2.60, and 2.60.[6]

The radical anions derived from glyoxal bis[(*p*-nitrophenyl)hydrazone]**1e** (spectrum F, fig. 2) showed a poorly resolved e.s.r. spectrum (apparently a portion of a 9-line pattern) a split (in the middle of a strong line) into three weak lines having a separation $a^N \sim 4.25$ G, $g_m = 2.006$. On the other hand, the radical anion derived from the *m*-nitro derivative **1f** (spectrum G fig. 2) showed a well-resolved, 9-line pattern indicative of interaction of the unpaired electron with four magnetically equivalent nitrogen atoms, with the hyperfine splitting constant $a^N = 7.05$ G.

The author thanks N. Adams (NBS) for the e.s.r. measurements, and R. Schaffer for his interest in this work.

[6] The average deviations: a^N 4.40 ± 0.25, a^H 2.60 ± 0.22.

4. References

[1] Buchachenko, A. L., Stable Radicals, pp. 100–144 (consultants Bureau, New York, 1965).
[2] Forrester, A. R., Hay, J. M., and Thomson, R. H., Organic Chemistry of Stable Free Radicals, pp. 137–179 (Academic Press, New York, 1968).
[3] (a) Razuvaez, G. A., Abakumov, G. A., and Pestunovich, V. A., J. Struct. Chem. **5**, 278 (1964); (b) Ref. [2], pp. 122–125.
[4] Walter, R. J., J. Amer. Chem. Soc. **88**, 1923 (1966); Ref. [2], pp. 5, 115–116.
[5] (a) Maender, O. W. and Russell, G. A., J. Org. Chem. **31**, 442 (1966); (b) Russell, G. A., Radical Ions, Kaiser, E. T. and Kevan, L. Ed., p. 87 ff (Interscience, New York, 1968).
[6] Chapman, O. L., King, R. W., Welstead, W. J., Jun., and Murphy, T. J., J. Amer. Chem. Soc. **84**, 4968 (1964).
[7] Fatiadi, A. J. and Isbell, H. S., Carbohyd. Res. **5**, 302 (1967).
[8] Katritzky, A. R. and Lagowski, J. M., Heterocyclic Chemistry, p. 129 (John Wiley, New York, 1960).
[9] Zollinger, H., Azo and Diazo Chemistry, pp. 108–109, 146–148 (Interscience Publishers, New York, 1961).
[10] (a) Roberts, J. D., Chem. Ber. **94**, 273 (1961); (b) I. Lalezari, A. Shafice, and M. Yalpani, Tetrahedron Letters, 3049 (1969) (c) R. B. Woodward and C. Winter, Tetrahedron Letters, 2697 (1969) (d) C. Winter and J. Wiecko, Tetrahedron Letters, 155 (1969).
[11] Kuhn, R. and Trischman, H., Angew. Chem. **75**, 294 (1963).
[12] Malkus, H., Battiste, M. A., and White, R. M., Chem. Commun. (1970) 479.
[13] Milligan, T. W. and Minor, B. C., J. Org. Chem. **27**, 4663 (1962).
[14] Smith, P. A. S., The Chemistry of Open-Chair Organic Nitrogen Compounds, Vol. **2**, pp. 150–172 (W. A. Benjamin, Inc., New York, 1966).
[15] Sidgwick, N. V., The Organic Chemistry of Nitrogen, pp. 505–531 (Oxford, London, 1966).
[16] Grundron, M. F. and Scott, M. D., J. Chem. Soc. 5674 (1964).
[17] Bloch, J. C., Tetrahedron Letters 4041 (1969).

(Paper 75A6–689)

JOURNAL OF RESEARCH of the National Bureau of Standards—A. Physics and Chemistry
Vol. 75A, No. 6, November-December 1971

Temperature Dependence of Photocurrents Produced by X and Gamma Rays in Silicon Radiation Detectors

Karl Scharf and Robert K. Mohr*

Institute for Basic Standards, National Bureau of Standards, Washington, D.C. 20234

(August 9, 1971)

The temperature dependence of dc photocurrents produced by x and gamma rays in silicon radiation detectors of the *n-p*, *p-i-n*, and surface-barrier type was investigated in a temperature range between 20 and 50 °C. Photodiode photocurrents, assumed as being equal to the *generated* currents I_g, showed a positive temperature dependence in all detectors investigated. Their temperature coefficient at 25 °C varied between +0.004 per °C and +0.002 per °C. The temperature dependence of short-circuit currents I_{sc} measured by a compensation method, was positive and nearly linear for *n-p* type detectors but nonlinear and negative for *p-i-n* and surface-barrier type detectors. It is shown, that this different behavior of individual detectors is due to the influence of the strongly temperature-dependent junction current I_j which under the short-circuit mode is drained off the generated current I_g. The junction current is a function of the internal series resistance R_s and the junction resistance R_j of the irradiated detector ($I_j = I_{sc}\, R_s/R_j$). With increasing resistance ratio R_s/R_j, the current ratio I_j/I_g increases and the temperature coefficient α_{sc} of the short-circuit current decreases. Temperature coefficients $(\alpha_{sc})_{25}$ measured in the different detectors at 25 °C and a current density 6×10^{-7} A/cm² decreased with increasing resistance ratio from +0.004 per °C to −0.005 per °C. Resistance ratios R_s/R_j of the detectors investigated ranged between 0.01 and 0.24 approximately. Thus, $(\alpha_{sc})_{25}$ measured in an individual detector can be changed by changing its *effective* series resistance. A decrease of $(\alpha_{sc})_{25}$ with increasing I_{sc} was observed in detectors with larger resistance ratios. This was apparently due to the voltage dependence of R_j at higher junction voltages produced by larger short-circuit currents.

Key words: Gamma rays; photocurrents; radiation; radiation detector; radiation dosimetry; silicon radiation detector; temperature dependence; x rays.

1. Introduction

Silicon radiation detectors operated as direct-current measuring devices can conveniently be used for measurements of exposure rates of x and gamma rays larger than approximately 0.1 R/min [1, 2].[1] Under this mode of operation, exposure rates are determined by measuring steady-state direct currents produced by irradiation in the detector circuit. These radiation-produced signal currents, in general called here *photocurrents*, are related to the exposure rate of the respective radiation incident on the detector. Detectors can be used as photodiodes [3] when photocurrents are large compared with the dark current produced without irradiation by an external bias voltage. Otherwise, detectors are operated as photovoltaic cells [4]. In this case no external bias voltage is applied at the detector and the total load current measured under irradiation is the photovoltaic photocurrent. However, its magnitude as well as its temperature dependence are functions of the external load resistance used. It is therefore recommended that exposure rates be determined by measuring the photovoltaic *short-circuit current* which is proportional to exposure rate over a wide range. Short-circuit currents can be determined by extrapolating photovoltaic current measurements to zero load resistance [4], but are usually approximated by photovoltaic currents measured at small load resistances [1].

An important problem in exposure rate measurements with dc operated silicon radiation detectors is the temperature dependence of photocurrents, in particular that of short-circuit currents. In previous investigations [3, 4], short-circuit currents as well as photodiode photocurrents produced by x rays in diffused silicon radiation detectors of the diffused *p-n* junction type were found to increase with increasing temperature varying approximately from 20 to 50 °C. Other authors reported similar measurements with silicon radiation detectors of different types but differed in their findings. For instance, temperature-independent short-circuit currents were observed in diffused *p-n* junction [5] and surface-barrier type [1] detectors as well as in *p-i-n* type detectors with shallow lithium drifts [5, 6], but short-circuit currents showing a negative temperature dependence were

*Present address: University of Massachusetts, Amherst, Mass. 01002.

[1] Figures in brackets indicate the literature references at the end of this paper.

observed in *p-i-n* type detectors with deep lithium drifts [5]. No definite explanation could be given for such different behavior of individual detectors.

In this paper an investigation is reported of the temperature dependence of short-circuit currents and photodiode photocurrents produced by x and gamma rays in silicon radiation detectors of different types. An electrical compensation method, described in a previous paper [8], was used for a direct and precise measurement of the short-circuit current. Under this method, the voltage drop produced by the photovoltaic current across the external load resistance is compensated by an applied bias voltage. Then, the *apparent* load resistance and the detector input voltage under irradiation are equal to zero and the current in the external circuit is equal to the short-circuit current. By using this method, it was possible to eliminate any influence of the external load resistance on the temperature dependence of short-circuit currents. In particular, it is shown that differences in the temperature dependence of short-circuit currents observed with detectors of different types can be related to the different values of internal series and junction resistances of individual detectors.

2. Circuit Equations

Circuit equations for the direct-current operation of a radiation detector can be derived from the simplified equivalent circuit of a detector shown in figure 1. The detector is represented by a dc current generator shunted by a rectifying diode of a resistance R_j,

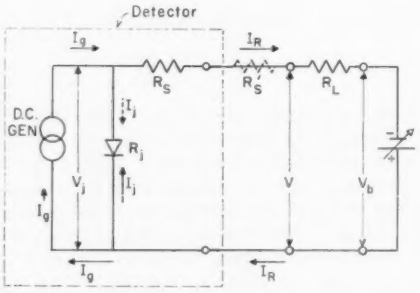

FIGURE 1. *Simplified equivalent circuit of an irradiated silicon radiation detector.*

called here the junction resistance, and an internal series resistance R_s. Sometimes it may be desirable to add, as shown, an additional series resistance R'_s in the circuit as will be discussed below.

The junction resistance R_j is a nonohmic resistance. According to the theory of an ideal diode, the voltage-dependence of a current I_j passing through a diode junction is given by the relation

$$I_j = I_o\,[\exp(qV_j/kT) - 1] \qquad (1)$$

where V_j is the voltage across the junction, I_j the junction current, T the absolute temperature, k the Boltzman constant, q the electronic charge, and I_o the reverse saturation current of the diode. Both V_j and I_j are assumed to be positive in the forward direction (broken arrow) and negative in the reverse direction (solid arrow) of the rectifying diode junction. The dynamic junction resistance derived from eq (1) as

$$dV_j/dI_j = (kT/qI_o)\,\exp\,(-qV_j/kT) \qquad (2)$$

is a nonlinear function of the junction voltage V_j and decreases or increases with increasing voltage depending on whether V_j is in the forward or reverse direction of the junction. However, for voltages $V_j << kT/q$, it may be assumed that R_j is a voltage-independent ohmic resistance

$$R_j = (kT)/(qI_o) \qquad (3)$$

The junction resistance R_j is strongly temperature dependent because of its dependence on I_o which increases exponentially with increasing temperature T. At a temperature of 300 K, $(kT)/q$ is equivalent to 26 mV which means that at room temperature eq (3) is applicable only if V_j is of the order of a few millivolts.

The internal series resistance R_s is assumed here to be an ohmic resistance. It consists of the bulk resistance of the detector, contact resistance, and sheet resistance along the thin contact layer and is usually considered to be negligibly small compared with R_j. As shown in this investigation, this assumption is apparently not justified in the case of silicon radiation detectors which are made of high-resistivity silicon and are provided with very thin electrical surface contacts.

The bias voltage V_b applied to the detector through a load resistance R_L (fig. 1) is either equal to zero (photovoltaic mode) or is a reverse voltage of finite value (short-circuit mode and photodiode mode). In the latter case V_b produces without irradiation a reverse load current, called here the *dark current* I_D, which is not shown in figure 1. When irradiating the detector, a current I_g is generated in the reverse direction of the diode junction, causing an increase in the external reverse load current. If I_R is the total reverse load current under irradiation (fig. 1) then the photocurrent I, defined here as the radiation-produced reverse current signal, is obtained as

$$I = I_R - I_D. \qquad (4)$$

In this equation it is assumed that I, I_R, and I_D are reverse currents determined at the voltage V which is applied under irradiation across the detector terminals (fig. 1). Values of I_R and I_D can be obtained from current-voltage characteristics of the detector measured with and without irradiation. If $V_b = 0$ or $V = 0$, then, as discussed below, I_D is either a forward current or is equal to zero and

$$I = I_R. \tag{5}$$

The generated current I_g is proportional to the number of electron-hole pairs produced in the detector by the radiation and collected by the electrical junction field per unit time, and is therefore proportional to the exposure rate. It increases at a small rate when the junction voltage V_j increases in the reverse direction, thereby increasing the effective charge collecting volume. However, the generated current I_g cannot be directly measured except when operating the detector as a photodiode and using high bias voltages. Thus, exposure rate measurements have to be based on the measurement of the photocurrent I which is usually different from I_g.

The relation between I_g and I can be obtained by determining the relation between I_g and I_R. This can be done by considering the following equation for the voltages V and V_j applied under irradiation across the detector terminals and the diode junction respectively. Taking into account the internal series resistance R_s, then according to the equivalent circuit (fig. 1)

$$\begin{aligned} V &= V_b - I_R R_L \\ V_j &= V_b - I_R (R_L + R_s) = V - I_R R_s. \end{aligned} \tag{6}$$

Due to the voltage drop produced by I_R across R_s, V and V_j are different for a given I_R. Since under the dc modes $V_b \leq 0$ and $I_R < 0$, it follows from eq (6) that for a given I_R, V and V_j are forward or reverse voltages, i.e., are positive or negative depending on the value of V_b. In the case of a forward biased junction a forward junction I_j is drained off the reverse generated current I_g (fig. 1) and

$$I_R = I_g - I_j. \tag{7}$$

In the case of a reverse biased junction, a reverse junction current I_j is added to I_g and

$$I_R = I_g + I_j. \tag{8}$$

In using eqs (4) to (8) one obtains the following circuit equations for the different dc modes of operation:

(a) Under the *photovoltaic* mode, $V_b = 0$. Thus, according to eq (6), V and V_j are positive. Therefore, I_D and I_j, which are functions of V and V_j respectively, are forward circuits and eqs (5) and (7) are applicable for this mode. Furthermore, the voltage V_j is a function of R_L and R_s. This means that I_j and consequently the photovoltaic photocurrent (eq (7)) are dependent on the load resistance R_L, as mentioned above.

(b) Under the *short-circuit* mode, which is the main subject of this investigation, the short-circuit current is measured by an electrical compensation method. Under this method, a reverse bias voltage, now called the compensation voltage V_c, is applied under irradiation so that

$$V_b = V_c = I_R R_L. \tag{9}$$

Then the voltage drop produced by I_R across the load resistance R_L is compensated and according to eq (6)

$$V = 0 \text{ and } V_j = -I_R R_s. \tag{10}$$

At $V = 0$, the dark current $I_D = 0$ and V_j is positive or a forward voltage because I_R is negative. Thus, as under the photovoltaic mode, eqs (5) and (7) can also be applied under the short-circuit mode, noting that I_R measured at $V = 0$ is called now the *short-circuit* current, I_{sc}.

Assuming in particular that, at the small junction voltages encountered under this mode, the junction resistance R_j may be considered to be an ohmic resistance, then one obtains the junction current as

$$I_j = I_{sc} R_s / R_j \tag{11}$$

and the short-circuit current according to eq (7) as

$$I_R \equiv I_{sc} = I_g (1 + R_s/R_j)^{-1}. \tag{12}$$

Compared with the photovoltaic current, the short-circuit current has the advantage that it is independent of R_L and is dependent only on the internal resistances R_s and R_j which are characteristics unique to each individual detector. The short-circuit current I_{sc} is smaller than I_g but is proportional to I_g as long as the ratio R_s/R_j remains constant. This condition is usually fulfilled when V_j remains within the voltage range of constant junction resistance R_j. According to eq (9), I_{sc} can be determined by measuring the compensation voltage V_c which for a given value of I_{sc} may be increased by increasing R_L, thereby increasing the accuracy of exposure rate measurements carried out with silicon radiation detectors.

(c) Under the *photodiode* mode $|V_b| > |I_R| R_L$. In this case the detector voltage V and the dark current I_D are in the reverse direction, but depending on whether $|V| \gtrless |I_R| R_s$, the junction voltage V_j is under irradiation either in the reverse or the forward direction. Thus combining eqs (4), (7), and (8) which are applicable to this mode, one obtains the photodiode photocurrent

$$I = I_g - (I_D \pm I_j) \tag{13}$$

where the minus sign in the bracketed term refers to a reverse biased junction. A distinction is made here between the dark current I_D determined by the current-voltage characteristic of the detector measured without irradiation and the current I_j passing through the junction under irradiation. They are related to different voltages V and V_j respectively and are therefore of different values as shown below.

It should be noted that in all the above circuit equations, I_R, I, and I_D are values determined as functions of the detector voltage V, while I_g and I_j are related to the corresponding junction voltage V_j which, due to the voltage drop across R_j is different from V (eq (6)). However, when I_D approaches a voltage-independent saturation value at larger reverse detector voltages, then $(I_D - I_j) \rightarrow 0$ and $I \rightarrow I_g$. Thus, considering photodiode currents at larger reverse detector voltages and neglecting the small voltage dependence of I_g

in the voltage interval between V and V_j, one may with good approximation assume that for a given voltage V the photodiode current

$$I = I_g. \tag{14}$$

The influence of the internal detector resistance R_s on measured photocurrents is further illustrated in figure 2, showing assumed current-voltage characteristics for a radiation detector having been measured without and with irradiation at constant exposure rate. For convenience, reverse current and voltage values are indicated by positive coordinates. Currents are given by the *external* characteristics (solid lines) as functions of the measured detector voltage V, and by the *internal* characteristics (broken lines) as functions of the junction voltage V_j. For a given current I_R, the corresponding voltages V and V_j differ by the voltage drop of the current across the internal series resistance R_s, assumed here to be extremely large. For given values of external bias voltage and load resistance, the corresponding values of I_R and V are given by the coordinates of the point of intersection between the *external* characteristic $I_R = f(V)$ and the load line crossing the voltage axis at the respective bias voltage V_b, or the compensation voltage V_c in the case of the short-circuit current. In figure 2, I_g is as an approximation assumed to be voltage-independent and consideration is given only to the behavior of the short-circuit current I_{sc} and the photodiode current I.

When applying at the detector the compensation voltage V_c, then $V=0$ at the detector and $I_D=0$, and the measured current is equal to the short-circuit current I_{sc}. But, as discussed above, $I_{sc} < I_g$ because due to the corresponding voltage V_j, a forward current I_j is deducted from I_g. If a reverse bias voltage $|V_b| > |V_c|$ is applied, the detector voltage V will be in the reverse direction. At small reverse voltages, V_j and I_j are in the forward direction but decrease and change into the reverse direction with increasing reverse voltage V. Then the respective photodiode photocurrent I is obtained from the *external* characteristics as the difference between I_R and I_D at the voltage V. The generated current I_g is read from the *internal* characteristics as the difference between the respective current I_R and the junction current I_j at the voltage V_j corresponding to V. As long as the dark current I_D does not achieve saturation, $I_D > I_j$, and consequently $I < I_g$. It is obvious from figure 2 that V_j and I_j cannot be obtained from the measured external characteristics unless R_s is known and that is usually not the case.

3. Experimental Procedure

Most of the detectors investigated were commercially available silicon radiation detectors. Measurements reported here were carried out with two different *n-p* type detectors, two *p-i-n* type detectors and one surface-barrier type detector. The *n-p* type detectors

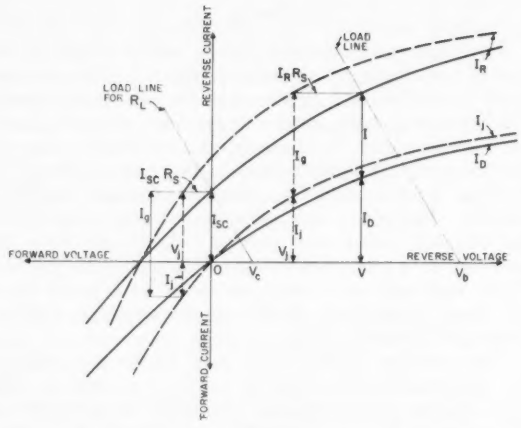

FIGURE 2. *Hypothetical current-voltage characteristics of a radiation detector showing external load currents measured with and without irradiation as functions of detector voltage* V *(solid lines) and junction voltage* V_j *(broken lines) respectively.*

with surface areas of 2.1 cm² and 0.3 cm² respectively were of the encapsulated type with thin protective aluminum coatings on the surfaces. One of the *p-i-n* detectors, hereafter referred to as *p-i-n* detector (No. 1) was a lithium-drifted detector with a passivated surface and a specified depletion depth of 2 mm. The other *p-i-n* detector, hereafter referred to as *p-i-n* detector (No. 2) was a lithium-drifted detector with a specified depletion depth of 1 mm. The surface-barrier type detector was a ceramic ring-mounted gold-silicon detector disc placed between pressure contacts. The surface-barrier detector was made of *n*-type silicon of a high unspecified resistivity. All the other detectors were made of 1000 Ω-cm *p*-type silicon.

For measurements with x rays, detectors were mounted in a metallic vacuum-tight container [2] which was placed inside a thermostatically controlled drying oven (fig. 3). The radiation beam first passed through the nonmetallic oven wall before entering and leaving the container through thin aluminum windows. A lead diaphragm was placed over the entrance window for collimation of the beam. Inside the container the detector was held by a metallic ring mounted on a Bakelite rod. In order to minimize oxidation of detector surfaces, the air pressure in the container was maintained at approximately 10^{-5} torr. For measurements with γ rays, detectors were placed inside a thermostatically controlled environmental test chamber and exposed to radiation at atmospheric pressure. In both cases the stabilized temperature of the detector was measured with a thermistor-type telethermometer with its probe attached to the metal casing of the detector. All detectors were covered with light-tight aluminum covers of electronic equilibrium thickness [9].

Radiation sources were, if not otherwise stated, a 250 kV tungsten target x-ray tube operated by a stabi-

[2] The metallic container was originally designed in connection with a previous investigation [3].

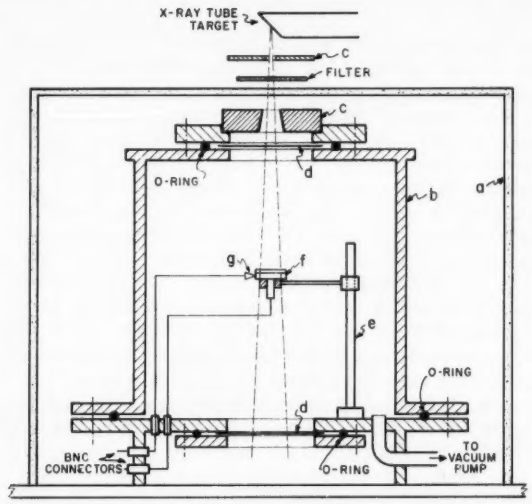

FIGURE 3. *Mounting of radiation detector in vacuum-tight metallic container.*
(a) Drying oven; (b) metallic container; (c) removable lead diaphragm; (d) thin Al-windows for entrance and exit of radiation beam; (e) Bakelite rod with metallic supporting ring; (f) detector; (g) thermistor thermometer probe.

lized constant voltage supply, and a ^{137}Cs γ-ray source.

Short-circuit currents were measured by a compensation method [8]. Currents observed under the photodiode mode of operation were determined by potentiometric measurement of the voltage drop across a known load resistance.

4. Temperature Dependence of Photocurrents

The temperature dependence of short-circuit currents and photodiode photocurrents measured with silicon radiation detectors of different types in a temperature range between 20 and 50 °C is shown in figure 4. Photocurrents are given in relative values and are normalized to unity at 25 °C. Measurements were made with lightly filtered 100 kV x rays at an approximate exposure rate of 8 R/min. Photodiode photocurrents determined at a bias voltage of 10 V were obtained from current-voltage characteristics measured at different temperatures.

Short-circuit currents (solid lines) as well as photodiode photocurrents (broken lines) measured with a diffused *n-p* type detector show a positive temperature dependence and increase with increasing temperature. For the other detectors investigated, photodiode photo-currents also show a positive temperature dependence, but short-circuit currents decrease at varying rates with increasing temperature. The *p-i-n* detector (No. 2) shows a very small temperature dependence for the short-circuit current. But short-circuit currents measured with the *p-i-n* detector (No. 1) and the surface-barrier detector show a strongly negative temperature dependence.

Photodiode photocurrents shown in figure 4 were measured at relatively small bias voltages. One may therefore assume that charge collection under the photodiode as well as under the short-circuit mode of operation was mainly achieved by diffusion of minority carriers from the detector base into the depletion region. Thus, the qualitatively different behavior observed under different modes of operation can apparently not be explained by different intrinsic electronic properties of individual detectors, such as mobility and lifetime of minority carriers. An explanation has rather to consider the dependence of the short-circuit current on the strongly temperature-dependent junction current which is a function of the internal series and junction resistance of each individual detector.

5. Temperature Coefficients of Photocurrents

In order to compare the temperature dependence of photocurrents measured with detectors of different types, the temperature coefficient α of the photocurrents at a given temperature is considered here.

In the case of a *forward* biased junction, as encountered under the photovoltaic and short-circuit mode, the temperature coefficient α can be derived from eq (7). If α, β, and γ are the temperature coefficients of I, I_g, and I_j respectively, defined as

$$\alpha = (dI/dT)/I; \qquad \beta = (dI_g/dT)/I_g; \; \gamma = (dI_j/dT)/I_j \tag{15}$$

then by differentiation of eq (7) one obtains

$$\alpha = (\beta I_g - \gamma I_j)/I \tag{16}$$

or

$$\alpha \gtrless 0 \text{ if } (I_g/I_j) \gtrless (\gamma/\beta). \tag{17}$$

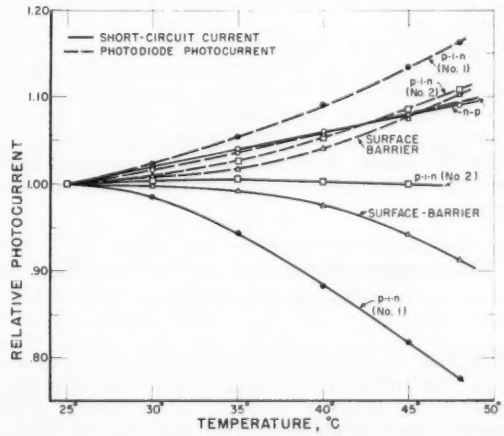

FIGURE 4. *Temperature dependence of short-circuit currents (solid lines) and photodiode photocurrents (broken lines) produced by lightly filtered 100 kV x rays in silicon radiation detectors of different types.*
The reverse bias voltage used for the measurement of photodiode photocurrents was $V_b = 10$ V.

443-082 OL - 71 - 4

The temperature coefficient β of I_g as derived from photodiode current measurements (fig. 4) is positive, and so is the temperature coefficient of I_j which increases rapidly with increasing temperature. However, the temperature coefficient α of photocurrents I can either be positive or negative depending on the value of the ratio (I_g/I_j).

Under the photovoltaic mode, I_j is a function of the load resistance R_L and consequently $\alpha=f(R_L)$ as has been shown in a previous paper [4]. However, under the short-circuit mode, I_j is independent of R_L and so is the temperature coefficient α_{sc} of the short-circuit current. Assuming a constant junction resistance R_j, one obtains from eqs (11), (12), and (16) the temperature coefficient of the short-circuit current as

$$\alpha_{sc}=\beta+(R_s/R_j)(\beta-\gamma) \tag{18}$$

which is dependent only on parameters characteristic of the individual detector. The temperature coefficient α_{sc} of the short-circuit current is smaller than the temperature coefficient β of the generated photocurrent because γ is positive and much larger than β. The contribution of γ to the value of α_{sc} can also be derived as a function of the temperature coefficients of the internal resistances. By differentiation of eq (12) one obtains

$$\alpha=\beta+[R_s/(R_j+R_s)](\delta_j-\delta_s) \tag{19}$$

if δ_j and δ_s are the temperature coefficients of the junction and series resistance respectively and are defined by relations similar to those given in eq (15). The value of δ_j is negative but δ_s can be positive or negative depending on the structure of the detector. Equation (19) is similar to eq (18) but here α_{sc} is a function of the ratio of R_s and the zero-voltage resistance (R_s+R_j) which is equal to the slope dV/dI_D at $V=0$ of the external characteristic $I_D=f(V)$ shown in figure 2.

In the case of a *reverse* biased junction, as in the photodiode mode, eq (16) could be used for values of I measured at small voltages by substituting (I_D-I_j) for I_j. However, for large voltages, one can assume that $I=I_g$. In this case the temperature coefficient α of the photodiode photocurrent may be assumed to be equal to the temperature coefficient β of the generated current.

6. Measurement of α as a Function of Different Parameters

According to equations discussed in the previous section, the temperature coefficient of photocurrents observed in a radiation detector is a function of the junction current I_j which is determined by the voltage V_j existing across the junction under irradiation. In order to verify these relations, the dependence of the temperature coefficient α on different parameters influencing V_j (eq (6)) was investigated. Measurements were carried out with the same detectors that were used for measurements shown in figure 4. If not otherwise stated, measurements were carried out with lightly filtered 100 kV x rays.

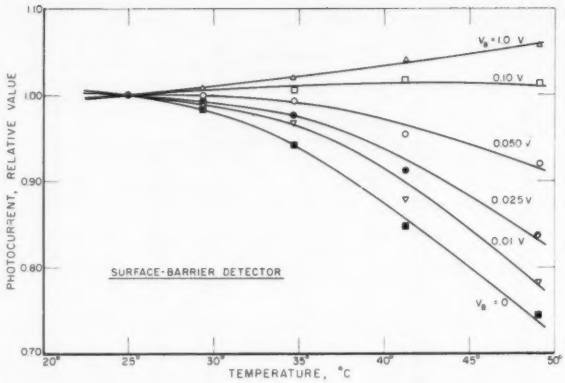

FIGURE 5. *Temperature dependence of photocurrents produced by lightly filtered 100 kV x rays in a surface-barrier detector at different detector voltages.*

(a) *Detector voltage.* The temperature dependence of photodiode photocurrents measured with the surface-barrier type detector at constant exposure rate for different detector voltages is shown in figure 5. Voltages V existing at the detector under irradiation and corresponding photocurrents were derived from reverse current-voltage characteristics measured at different temperatures with and without irradiation. Photocurrents are given in relative values normalized to unit at 25 °C. The strongly negative temperature dependence of the short-circuit current at $V=0$, changes gradually with increasing V into the positive temperature dependence of the photodiode photocurrent. The temperature coefficient α_{25} at a given voltage is equal to the slope of the respective curve at 25 °C.

Similar measurements made with detectors of other types are summarized in figure 6, showing α_{25} as a

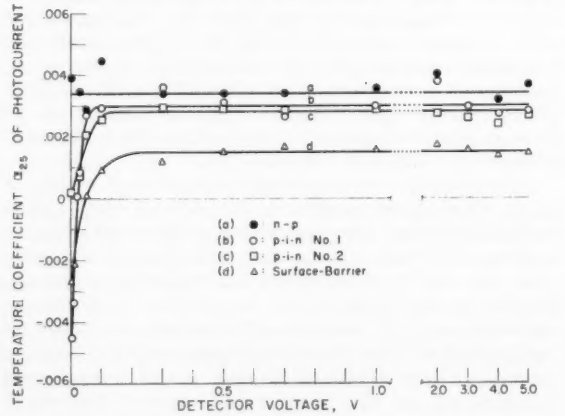

FIGURE 6. *Temperature coefficient α_{25} at 25 °C of photocurrents produced by lightly filtered 100 kV x rays in silicon radiation detectors of different types measured as a function of detector voltage.*

Values of α_{25} at $V=0$ refer to short-circuit currents.

function of V. Values of α_{25} for short-circuit currents ($V=0$) are either positive or negative but change with increasing V into positive values becoming approximately constant at higher voltages. For the diffused n-p type detector (2.1 cm^2), α_{25} is nearly voltage-independent over the voltage range investigated. Constant values of α_{25} are reached at relatively small voltages of the order of one volt for all detectors. Apparently at this point $I=I_g$ and α_{25} becomes equal to the temperature coefficient of β_{25} of the generated photocurrent I_g. These "plateau" values of α_{25} are of the same order of magnitude for the different detectors but differ slightly apparently due to differences in electronic properties of individual detectors.

(b) *Series resistance.* In order to change the *effective* series resistance of a detector, additional resistances R'_s were inserted in the circuit as shown in figure 1. These resistances with a negligible temperature coefficient were not incorporated in the detector and were always kept at room temperature. Then photocurrents measured at $V=0$ can be assumed to be approximately equal to the short-circuit current I'_{sc} of the respective detector having an internal resistance $(R_s+R'_s)$.

The temperature dependence of I'_{sc} measured with the diffused n-p type detector at constant exposure rate is shown in figure 7 as a function of R'_s. Photocurrents are again given in relative values and the slope of each curve at 25 °C is the temperature coefficient of I'_{sc} measured with the respective additional resistance R'_s. For $R'_s=0$, the temperature coefficient of I'_{sc} is positive and decreases with increasing R'_s changing to negative values at larger R'_s. This behavior is in agreement with eq (17) because at constant exposure rate, i.e., constant I_g, and constant voltage $V=0$, the junction voltage increases with increasing R'_s thereby increasing I_j and decreasing the ratio I_g/I_j. The temperature dependence of I'_{sc} is similar to that of photovoltaic currents measured with different load resistances [4].

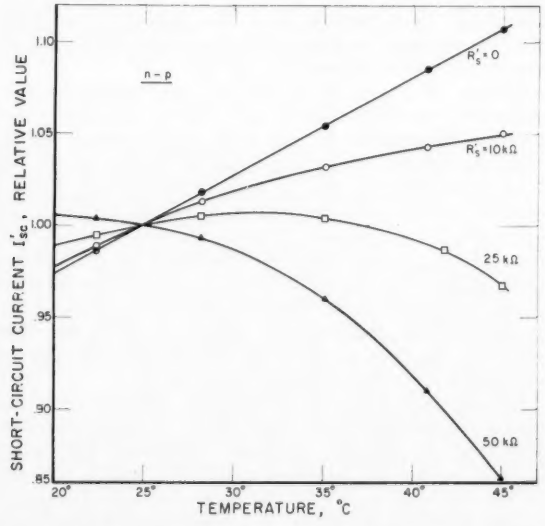

FIGURE 7. *Temperature dependence of short-circuit currents* I'_{sc} *produced by lightly filtered 100 kV x rays in a diffused silicon* n-p *type detector, measured with different additional series resistances* R'_s.

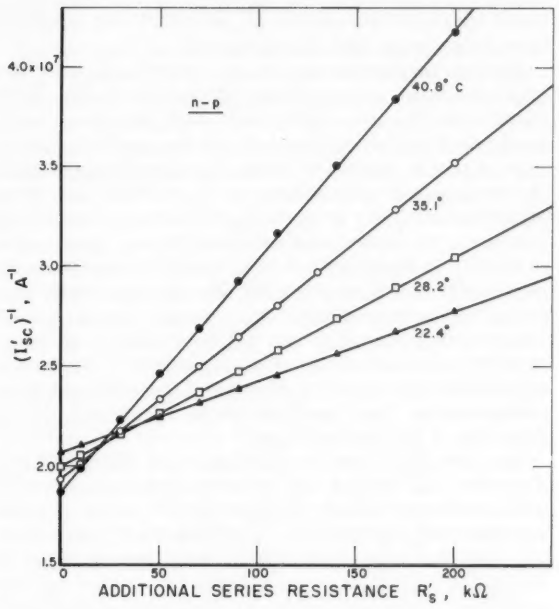

FIGURE 8. *Dependence of* $(I'_{sc})^{-1}$ *on additional series resistance* R'_s *at different temperatures derived from measurements with a diffused silicon* n-p *type detector.*

The short-circuit current of the n-p type detector can be made nearly temperature-independent within a certain temperature range by adding a suitable series resistance R'_s as shown in figure 7. This optimum resistance can conveniently be determined by using a relation derived from eq (12):

$$(1/I'_{sc}) = (R_j+R_s+R'_s)/(I_gR_j) = (1/I_{sc})+R'_s/(I_gR_j) \tag{20}$$

where I'_{sc} and I_{sc} are the short-circuit currents measured with and without an additional resistance R'_s.

According to eq (20), at constant exposure rate and constant temperature $(I'_{sc})^{-1}$ is a linear function of R'_s provided that R_j remains constant. Graphs of $(I'_{sc})^{-1}$ as a function of R'_s which were derived from measurements shown in figure 7 are given in figure 8. Graphs are linear for all temperatures indicating that over the resistance range investigated the junction resistance R_j remains constant at each temperature. The change from a positive to a negative temperature dependence of I'_{sc} with increasing R'_s is indicated by the crossing of the lines. They do not cross at a single point, but points of intersection are spread over a

small range of resistances R_s' for which the temperature dependence of I_{sc} is very small.

Similar measurements were carried out with the other detectors with qualitatively similar results. With increasing R_s', α_{25} decreases and becomes more negative. Graphs determined for the surface-barrier type detector shown in figure 9 indicate this change in temperature dependence of I_{sc}' but do not show an intersection because at $R_s'=0$, $(\alpha_{sc})_{25}$ is already negative. At lower temperatures, these graphs are nonlinear indicating that the junction resistance R_j decreases with increasing R_s'. This is apparently due to an increasing voltage drop across the series resistance which makes the junction voltage so large that R_j becomes voltage-dependent and eq (3) is not applicable any more. Linearity of graphs at higher temperatures can apparently be explained by a decrease in junction voltage.

Similar observations were made with the *p-i-n* type detector (No. 1). For the *p-i-n* type detector (No. 2) irradiated with heavily filtered 100 kV x rays at a low exposure rate, graphs of $(I_{sc}')^{-1}$ versus R_s' are linear (fig. 10), but become nonlinear when the detector is irradiated with lightly filtered 240 kV x rays (fig. 11) at a high exposure rate. The explanation given above for the nonlinear cases is supported by measurements discussed in the following section.

(c) *Short-circuit current.* Temperature coefficients $(\alpha_{sc})_{25}$ of short-circuit currents measured at 25 °C with detectors of different type and size at different current levels are shown in figure 12. In order to make measurements for detectors of different areas more comparable, $(\alpha_{sc})_{25}$ is shown as a function of short-circuit current density, considering that in the case of a fully irradiated detector, I_g and I_{sc}, as well as I_j are proportional to the detector area. Short-circuit currents changing by about three orders of magnitude were produced by x rays obtained at different tube voltages and different filtrations. The smallest short-circuit currents of the order of 10^{-9} A/cm² were produced by ^{137}Cs gamma rays. The quality of radiation may be assumed to have only a negligible influence on the temperature dependence of I_{sc}.

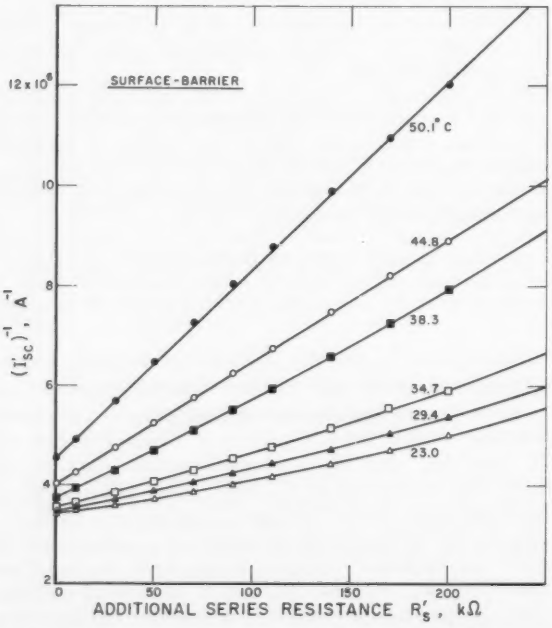

FIGURE 9. *Dependence of* $(I_{sc}')^{-1}$ *on additional series resistance* R_s' *at different temperatures, measured in a silicon surface-barrier type detector.*

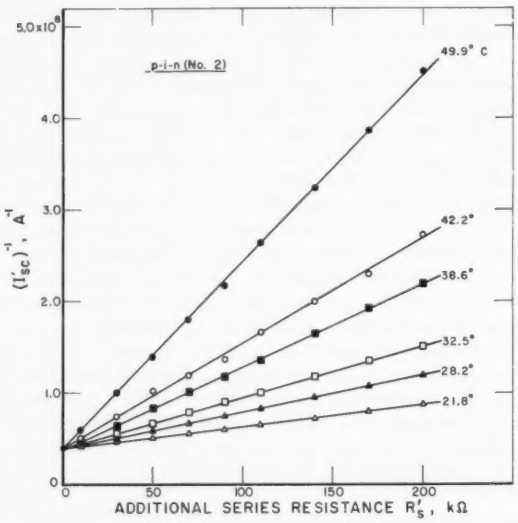

FIGURE 10. *Dependence of* $(I_{sc}')^{-1}$ *on additional series resistance* R_s' *measured with* p-i-n *type detector No. 2, using heavily filtered 100 kV x rays at an approximate exposure rate of 0.6 R/min.*

Values of $(\alpha_{sc})_{25}$ of I_{sc} remain approximately constant for the diffused *n-p* type detector (0.3 cm²) and change only slightly for the *p-i-n* type detector (No. 2) over the current range investigated. However, for the *p-i-n* type detector (No. 1) and for the surface-barrier type detector, $(\alpha_{sc})_{25}$ decreases markedly with increasing short circuit current. This negative current dependence of $(\alpha_{sc})_{25}$ can again be explained by the voltage drop of the short-circuit current across a large internal series resistance in the detector. With increasing short-circuit current, the junction voltage equal to this voltage drop reaches a value for which the junction resistance R_j becomes voltage dependent.

(d) *Internal detector resistances.* The relation between the temperature dependence of photocurrents produced in silicon radiation detectors and their internal series and junction resistance has in a qualitative way been shown by the measurements discussed in the previous sections. A quantitative relation between these resistances and the temperature coefficient $(\alpha_{sc})_{25}$ of short-circuit currents can be obtained by determining the resistance ratio R_s/R_j and the zero-

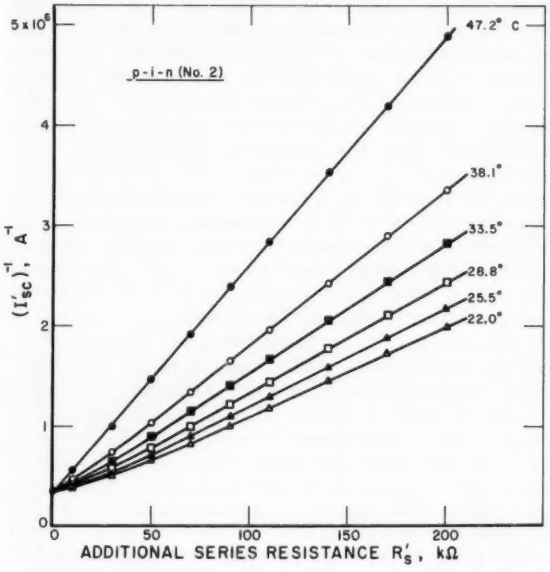

FIGURE 11. *Dependence of* $(I'_{sc})^{-1}$ *on additional series resistance* R'_s *measured with p-i-n type detector (No. 2), using lightly filtered 240 kV x rays at an approximate exposure rate of 65 R/min.*

voltage resistance (R_s+R_j) of a detector from its measured current-voltage characteristics. From these values, the series resistance R_s and the junction resistance R_j can then be calculated. According to eq (12), R_s/R_j can be obtained from the ratio I_g/I_{sc} where I_{sc} is the measured short-circuit current and I_g is the generated photocurrent at $V=0$ which is derived from photodiode photocurrents measured at detector voltages of a few volts by extrapolation to zero detector-voltage. This extrapolation was based on the measured voltage-dependence of I_g which for all detectors investigated was found to satisfy the relation [3]

$$(I_g)_V = a+b(V+V_0)^{1/2} \qquad (21)$$

where $(I_g)_V$ is the generated current at the detector voltage V, a and b are constants, and V_0 is the built-in potential difference across the junction, assumed here as an approximation to be $V_0=0.5$ V.

Resistance values determined in this way for the different detectors investigated, and the respective temperature coefficients of short-circuit currents are given in table 1. Values of $(\alpha_{sc})_{25}$ at a short-circuit density of approximately 6×10^{-7} A/cm^2 were taken from curves shown in figure 12. The high series resistances of the surface-barrier type and the *p-i-n* type detector (No. 1) may be due to surface oxide layers or nonohmic contacts on these detectors. The relative low junction resistances of both *p-i-n* type detectors may be explained by an inhomogeneous distribution of lithium ions forming low-resistivity channels shunting the junction field region. It should be noted that measured values of R_s and R_j are *effective* values which are determined by a combination of different series and shunt resistances not specifically considered here.

According to table 1, and as shown in figure 13, $(\alpha_{sc})_{25}$ is not changing in a way similar to that of the individual values of R_s or R_j, but decreases monotonically with the increasing ratio of these resistances. This result is in agreement with eq (18), though according to this equation a linear dependence of $(\alpha_{sc})_{25}$ on R_s/R_j may have been expected. The nonlinearity of the relation between $(\alpha_{sc})_{25}$ and the resistance ratios as shown in figure 13, may be due to differing temperature coefficients β and γ of the currents I_g and I_j in individual detectors and to the voltage dependence of R_j at higher junction voltages. Junction voltages $(V_j=I_{sc}R_s)$ calculated for the different detectors investigated are shown in table 1. At the given current level, the junction voltages V_j in the *n-p* type detector and the *p-i-n* type detector (No. 2) are rather small. However, for the *p-i-n* type detector (No. 1) and the surface-barrier type detector, values of V_j are much higher and in such a range that R_j and R_s/R_j may be assumed to be voltage dependent. This confirms the explanation given earlier for the current dependence of $(\alpha_{sc})_{25}$ observed with these detectors. It should be noted that in such cases, values of R_j determining the zero voltage resistance (R_s+R_j) and those determining the current ratios I_g/I_{sc} are different. Thus, the "true" values of the zero-voltage junction resistances R_j may be larger, and the values of the corresponding series resistances R_s and resistance ratios R_s/R_j may be smaller than those given in table 1 and used in figure 13.

7. Exposure Rate Dependence of I_{sc}

The value of the temperature coefficient of the short-circuit current I_{sc} (eq (18)) has been derived from eq (12) showing the dependence of I_{sc} on the resistance ratio R_s/R_j. Hence, any voltage dependence of R_j

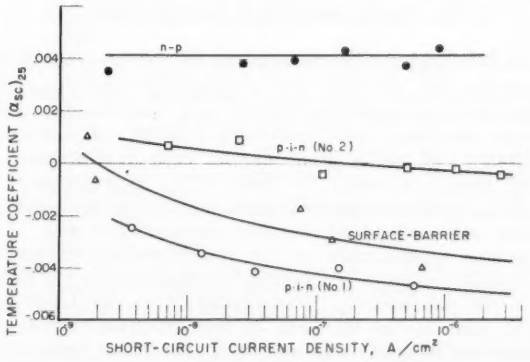

FIGURE 12. *Temperature coefficient* $(\alpha_{sc})_{25}$ *at 25 °C of short-circuit currents measured with detectors of different types as a function of short-circuit current density.*

TABLE 1. *Temperature coefficients* $(\alpha_{sc})_{25}$ *of short-circuit currents measured in silicon radiation detectors at 25 °C at a current density of* 6×10^{-7} *A/cm², and detector data*

Item	Detector type			
	n-p	*p-i-n* (No. 2)	Surface B.	*p-i-n* (No. 1)
$(\alpha_{sc})_{25}$.....$(°C)^{-1}$...	+0.0040	−0.0002	−0.0033	−0.0047
Area.....cm^2...	0.3	1.1	2.3	2.5
R_s/R_j.....	0.011	0.044	0.092	0.245
(R_j+R_s).....kΩ...	830	147	866	61
R_j.....kΩ...	821	141	793	49
R_s.....kΩ...	9	6	73	12
V_j.....mV...	1.6	4.0	100.7	18.0

should influence I_{sc} as well as $(\alpha_{sc})_{25}$. In order to prove this point, measurements of the exposure rate dependence of I_{sc}, were carried out for the different detectors as shown in figures 14 and 15. For small short-circuit currents produced by ^{137}Cs gamma rays, I_{sc} is a linear function of exposure rate for all detectors. However, for large short-circuit currents produced at high exposure rates of lightly filtered 30 kV x rays obtained from a beryllium window-type tube, the exposure rate dependence of I_{sc} is non-linear for detectors which have a high resistance ratio and show a relatively large current dependence of $(\alpha_{sc})_{25}$ (fig. 14). This nonlinearity can again be explained by the increase of R_s/R_j with increasing exposure rate, i.e., increasing short-circuit current, due to the voltage dependence of R_j. According to eq (12), I_{sc} remains proportional to I_g, i.e., to exposure rate, only as long as the resistance ratio R_s/R_j remains constant. Short-circuit currents observed with the *p-i-n* type detector (No. 2) (fig. 14) show only a slight deviation from a linear exposure rate dependence, but for the *n-p* type detector (2.1 cm^2) which had a resistance ratio of about 0.015, I_{sc} is proportional to exposure rate over the whole range investigated (fig. 15).

8. Summary and Conclusions

The following conclusions can be drawn from this investigation of the temperature dependence of photocurrents produced by x and gamma rays in silicon radiation detectors of the diffused *n-p*, lithium drifted *p-i-n*, and surface barrier type in a temperature range between 20 and 50 °C approximately.

(1) Generated photocurrents derived from photodiode measurements showed an increase with increasing temperature in all detectors investigated. Although there is no complete explanation for this positive temperature dependence it is, at least in part, due to an increase in the effective diffusion length of minority carriers with increasing temperature, as has previously been shown [3].

(2) The temperature dependence of the short-circuit current was similar to that of the generated current in the diffused *n-p* type detectors only, but was in a varying degree non-linear and negative for the other detectors. It is shown that this different behavior can be explained by the influence of the strong positive temperature-dependence of the junction current which in the short-circuit mode is deducted from the generated photocurrent. This junction current is a function of the internal series resistence R_s and the junction resistance R_j of the respective detector. With increasing resistance ratio R_s/R_j, the junction current increases and the temperature coefficient of the short-circuit current decreases. Assuming a temperature coefficient at 25 °C of about 10 percent per °C for the junction current and about 0.4 percent per °C for the generated photocurrent, then the temperature coefficient $(\alpha_{sc})_{25}$ of the short-circuit current should become negative when the junction current is larger than about 4 percent of the generated photocurrent (eq (16)) or R_s is larger than approximately the same fraction of R_j. These values were confirmed by determining the resistance ratios from the current-voltage characteristics of the individual detectors.

(3) Values of the temperature coefficients β_{25} of the *generated* photocurrent, determined by measurements of photodiode photocurrents, varied approximately between +0.004 per °C and +0.002 per °C for the different detectors (fig. 6). Values of $(\alpha_{sc})_{25}$ for short-circuit currents changed with increasing resistance ratio of individual detectors of different types from about +0.004 per °C to −0.005 per °C.

(4) Detectors with larger series resistances showed a current dependence of $(\alpha_{sc})_{25}$ decreasing with increasing short-circuit currents. This can be explained by a decrease of R_j at higher forward junction voltages resulting in an increase of the resistance ratio and a corresponding decrease of $(\alpha_{sc})_{25}$. This explanation was confirmed by the measurement of the exposure rate dependence of the short-circuit current which is also a function of the resistance ratio. For

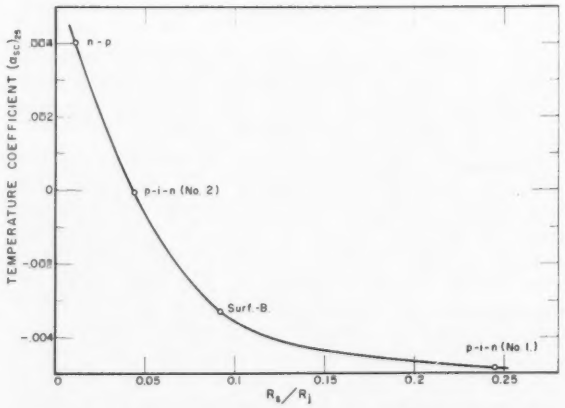

FIGURE 13. *Temperature coefficient* $(\alpha_{sc})_{25}$ *at 25 °C and current density* 6×10^{-7} *A/cm² of short-circuit currents measured with detectors of different types as a function of the ratio of their individual series and junction resistance* R_s/R_j.

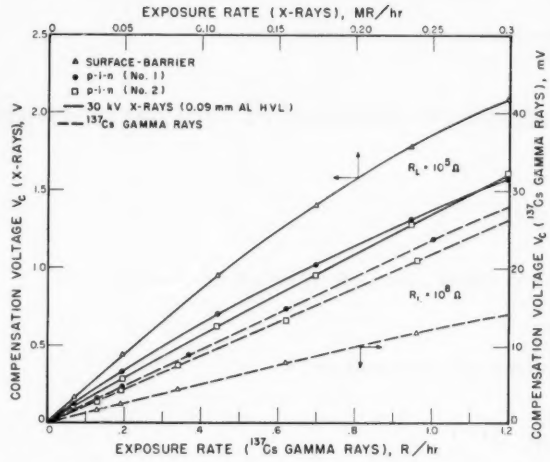
EXPOSURE RATE (X-RAYS), MR/hr
SURFACE-BARRIER
p-i-n (No. 1)
p-i-n (No. 2)
30 kV X-RAYS (0.09 mm AL HVL)
137Cs GAMMA RAYS
$R_L = 10^5\ \Omega$
$R_L = 10^8\ \Omega$
COMPENSATION VOLTAGE V_c (X-RAYS), V
COMPENSATION VOLTAGE V_c (^{137}Cs GAMMA RAYS), mV
EXPOSURE RATE (^{137}Cs GAMMA RAYS), R/hr

FIGURE 14. *Exposure rate dependence of compensation voltage, determining the short-circuit currents, as measured with silicon* p-i-n *and surface-barrier type detectors at high exposure rates of lightly filtered 30 kV x rays and at low exposure rates of* ^{137}Cs *gamma rays.*

detectors with high resistance ratios, the exposure rate dependence is linear at low current levels and becomes non-linear at large currents.

(5) According to the above findings it is possible to change the value of $(\alpha_{sc})_{25}$ by changing the resistance ratio. By adding to a detector an additional resistance of small temperature dependence, the short-circuit currents showing a positive $(\alpha_{sc})_{25}$ can be made nearly independent of temperature within a certain temperature range. In the case of a negative $(\alpha_{sc})_{25}$, the additional resistance must be of the thermistor type having a strong negative temperature dependence. However, by using an additional resistance, care must be taken that a linear exposure rate dependence is retained in the range of interest.

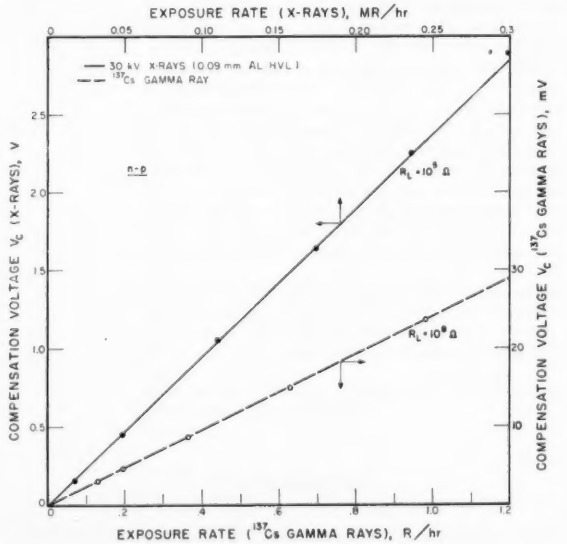
EXPOSURE RATE (X-RAYS), MR/hr
30 kV X-RAYS (0.09 mm AL HVL)
137Cs GAMMA RAY
n-p
$R_L = 10^8\ \Omega$
$R_L = 10^9\ \Omega$
COMPENSATION VOLTAGE V_c (X-RAYS), V
COMPENSATION VOLTAGE V_c (^{137}Cs GAMMA RAYS), mV
EXPOSURE RATE (^{137}Cs GAMMA RAYS), R/hr

FIGURE 15. *Exposure rate dependence of compensation voltage, determining the short-circuit currents as measured with a diffused silicon* n-p *type detector at high exposure rates of lightly filtered 30 kV x rays and at low exposure rates of* ^{137}Cs *gamma rays.*

(6) By measuring the resistance ratio of an individual detector, its behavior with regard to temperature and exposure rate dependence can be predicted qualitatively.

(7) The diffused *n-p* type detectors showed the best performance characteristic with regard to temperature and exposure rate dependence of short-circuit currents. Obviously no generalization can be made for the behavior of individual detectors of different types. But the larger resistance ratios observed with the other detectors seem to be typical, being due either to large series resistances as in the case of surface-barrier type detectors, or to relatively small junction resistances as in the case of *p-i-n* type detectors.

9. References

[1] Parker, R. P. and Morley, B. J., Silicon *p-n* junction surface barrier detectors and their application to the dosimetry of x- and gamma-ray beams, Proc. Solid State and Chemical Radiation Dosimetry in Medicine and Biology Symp., Vienna, October 3–7, 1966, pp. 167–183 (International Atomic Energy Agency, Vienna, 1967).

[2] Fowler, J. F., Solid state electrical conductivity dosimeters, Chapter 14, in Radiation Dosimetry, 2nd Edition, Eds. F. H. Attix and W. C. Roesch, pp. 291–305 (Academic Press, New York, 1966).

[3] Scharf, K., and Sparrow, J. H., Steady-State response of silicon radiation detectors of the diffused *p-n* junction type to x rays. II: Photodiode mode of operation, J. Res. Nat. Bur. Stand. (U.S.), **70A** (Phys. and Chem.) No. 2, 181–191 (March–April 1966).

[4] Scharf, K. and Sparrow, J. H., Steady-State response of silicon radiation detectors of the diffused *p-n* junction type to x rays. I: Photovoltaic mode of operation, J. Res. Nat. Bur. Stand. (U.S.), **68A** (Phys. and Chem.) No. 6, 683–701 (Nov.–Dec. 1964).

[5] Laughlin, J. S., Biological and clinical dosimetry, Bull. Am. Phys. Soc. (Series 2), **11**, No. 6, 4963 (Nov. 1966).

[6] Bailey, N. A., and Kramer, G., The lithium-drifted silicon *p-i-n* junction as an x-ray and gamma-ray dosimeter, Radiation Research, **22**, No. 1, 53–79 (May 1964).

[7] Whelpton, D., and Watson, B. W., A *p-n* junction photovoltaic detector for use in radiotherapy, Phys. Med. Biol. **8**, No. 1, 33–42 (April 1963).

[8] Scharf, K., Exposure rate measurements of x- and gamma-rays with silicon radiation detectors, Health Phys. **13**, No. 6, 575–586 (June 1967).

[9] White, G. N., Measurement of exposure dose, Chapter 5 in Principles of Radiation Dosimetry, pp. 62–64 (John Wiley & Sons, Inc., New York 1959).

(Paper 75A6–690)

JOURNAL OF RESEARCH of the National Bureau of Standards—A. Physics and Chemistry
Vol. 75A, No. 6, November–December 1971

Isomerization Processes in Ions of the Empirical Formula $C_4H_8^{+}$ *

S. G. Lias

Institute for Materials Research, National Bureau of Standards, Washington, D.C. 20234

and

The American University, Washington, D.C. 20016

and

P. Ausloos

Institute for Materials Research, National Bureau of Standards, Washington, D.C. 20234

(June 9, 1971)

Ions of the formula $C_4H_8^+$ have been generated with different initial energies by ionizing ethylene ($C_2H_3^+ + C_2H_4 \rightarrow C_4H_8^+$, where the $C_4H_8^+$ ion is formed with an initial energy of > 11.51 eV), cyclobutane (initial energy of $C_4H_8^+$, > 10.84 eV), methylcyclopropane (> 10.15 eV), 1-C_4H_8 (> 9.58 eV), and i-C_4H_8 (> 9.06 eV) with 11.6–11.8 eV photons, and in some cases also with 10 eV photons and with gamma radiation. The structures of the ions have been determined from the structures of the C_4H_8 products formed in charge transfer reaction between the ions and charge acceptors such as dimethylamine and nitric oxide, as well as from the structures of the butanes formed in D_2^- transfer reactions with methylcyclopentane-d_{12} ($C_4H_8^+ + C_6D_{12} \rightarrow C_4H_8D_2 + C_6D_{10}^+$).

At low pressures the $C_4H_8^+$ ions initially formed in ethylene, cyclobutane, and methylcyclopropane isomerize to the thermodynamically most stable configurations, i-$C_4H_8^+$ and 2-$C_4H_8^+$. The 2-$C_4H_8^+$ structure predominates in all the experiments. As the pressure is raised, the i-$C_4H_8^+$ ion yield diminishes as that of 2-$C_4H_8^+$ increases, indicating that when the precursor of the i-$C_4H_8^+$ ion is collisionally deactivated, it ends up as 2-$C_4H_8^+$. At high pressures, 1-$C_4H_8^+$ ions are intercepted; their yield increases with increasing pressure, indicating that 1-$C_4H_8^+$ is an intermediate which isomerizes further unless it is collisionally deactivated. The 1-$C_4H_8^+$ ion formed in methylcyclopropane (initial energy > 10.15 eV) is more easily deactivated than that formed in cyclobutane (initial energy > 10.84 eV). That the isomerization of the 1-$C_4H_8^+$ ion to lower energy structures such as i-$C_4H_8^+$ and 2-$C_4H_8^+$ requires excess internal energy is demonstrated by the fact that in the photolysis with 10 eV photons, a negligible amount of isomerization is observed, but with 11.6–11.8 eV photons, more than half of the 1-$C_4H_8^+$ ions isomerize to the 2-$C_4H_8^+$ structure at a pressure of 2 torr. Isomerization of the low energy i-$C_4H_8^+$ ions formed in the photolysis of i-C_4H_8 to other structures is relatively unimportant at 11.6–11.8 eV.

Taking the ratio i-$C_4H_8^+$/2-$C_4H_8^+$ as an indicator of the amount of energy removed by collisions from the intermediate $C_4H_8^+$ species under conditions where only i- and 2-$C_4H_8^+$ ions are intercepted, it is shown that the efficiency of energy transfer from the ions to helium, hydrogen, neon, krypton, xenon, nitrogen, and carbon dioxide is related to the polarizability of the added deactivator.

Key words: Butene; cyclobutane; ion structure; isomerization; methylcyclopropane; photoionization; photolysis; radiolysis.

1. Introduction

Determinations of the structures of organic ions have been the subject of a great deal of interest in the literature recently [1].[1] In particular, n.m.r. spectra of organic ions formed in very strong acids are now being recorded [2]. More classical studies, using analysis of the products formed from ionic reactions in thermal organic systems in the liquid phase [3], or from ions generated by high energy radiation in the gas phase [4], have recently elucidated isomerization mechanisms of the $C_3H_7^+$ and $C_4H_9^+$ carbonium ions. Indirect evidence bearing on ionic structures has been inferred from mass spectrometric results; in particular, many studies recently have attempted to derive information about ionic structures from

* This research, which was supported by the U.S. Atomic Energy Commission, was presented by S. G. Lias in partial fulfillment of the requirements for the Ph.D. degree at the American University, Washington, D.C. 20006.

[1] Figures in brackets indicate the literature references at the end of this paper.

the modes and rates of reaction of ions as observed in ion cyclotron resonance mass spectrometry [5].

This investigation is devoted to a detailed examination of the structures and isomerization reactions of the ions having the empirical formula, $C_4H_8^+$. These ions are not known to be formed in thermal chemical reactions, and to our knowledge have not been studied except in systems where they are generated by high-energy radiation. Several years ago, it was reported [6] that when ethylene was irradiated in the presence of a compound having an ionization energy lower than or equal to 9.54 eV, the $C_4H_8^+$ ion formed in the reaction:

$$C_2H_4^+ + C_2H_4 \rightarrow C_4H_8^+ \qquad (1)$$

would transfer its charge to the additive, A, to form neutral butene molecules:

$$C_4H_8^+ + A \rightarrow C_4H_8 + A^+ \qquad (2)$$

whose structures were assumed to correspond to the structures of the precursor $C_4H_8^+$ ions. Using the same technique, it was then demonstrated that the $C_4H_8^+$ ions formed in the radiolysis [7] or photoionization [8] of cyclobutane

$$c\text{-}C_4H_8 \xrightarrow{\text{radiation}} C_4H_8^+ + e \qquad (3)$$

acquired the same butene structures as those seen for the $C_4H_8^+$ ions in the ethylene system. In those early studies it was reported that the $C_4H_8^+$ ions formed in ethylene and cyclobutane acquired the 2-$C_4H_8^+$ and 1-$C_4H_8^+$ structures. A mass spectrometric study compared the rate of charge transfer to NO from the $C_4H_8^+$ ions in cyclobutane with the rates of the same reaction for the 1-$C_4H_8^+$, 2-$C_4H_8^+$, and i-$C_4H_8^+$ ions, and seemingly corroborated these results [9]. However, more recently it was noted [10] that when the $C_4H_8^+$ ions formed in the photoionization of cyclobutane at a pressure of 20 torr were allowed to undergo D_2^- transfer reactions with methylcyclopentane-d_{12}, the butane products consisted of $CH_3CHDCHDCH_3$ from the 2-$C_4H_8^+$ reaction:

$$2\text{-}C_4H_8^+ + C_6D_{12} \rightarrow CH_3CHDCHDCH_3 + C_6D_{10}^+ \qquad (4)$$

and i-$C_4H_8D_2$, which could only result from a reaction of the i-$C_4H_8^+$ ion:

$$i\text{-}C_4H_8^+ + C_6D_{12} \rightarrow (CH_3)_2CDCH_2D + C_6D_{10}^+. \qquad (5)$$

A reexamination of the butenes formed in the charge exchange experiments indicated that the product originally identified as 1-butene was indeed actually isobutene, reconfirming the formation of i-$C_4H_8^+$ ions in cyclobutane. It was later noted that the i-$C_4H_8^+$, rather than the 1-$C_4H_8^+$, ion is also formed in irradiated ethylene [11]. (The original misassignment came about because 1-C_4H_8 and i-C_4H_8 have nearly identical retention times on the gas chromatographic columns used for analysis in these studies.)

The structures of the $C_4H_8^+$ ions formed in the dissociation of cyclohexane and methylcyclopentane parent ions were recently determined by an examination of the structures of the butanes formed in D_2^- transfer reactions, (such as 4 and 5), as well as by the structures of the butenes formed in charge transfer reactions [12]. This study was carried out at a single pressure, so pressure effects on the distribution of the isomeric $C_4H_8^+$ ions could not be observed; because in the 10 eV photolysis of 1-C_4H_8 and 2-C_4H_8 in the presence of methylcyclopentane-d_{12}, no evidence was seen [12] for isomerization of 1-$C_4H_8^+$ to the 2-$C_4H_8^+$ structure, or 2-$C_4H_8^+$ to the 1-$C_4H_8^+$ structure, isomerizations between the different C_4H_8 structures were not considered.

More recently, a study has appeared [11] in which $C_4H_8^+$ ions generated in the photoionization of ethylene (reaction 1) are intercepted by charge exchange with dimethylamine, or toluene. Because the yield which could be attributed to the i-$C_4H_8^+$ ion was seen to increase relative to the 2-$C_4H_8^+$ yield as the concentration of charge acceptor was increased, the results were interpreted in terms of a $C_4H_8^+$ entity which would undergo a rapid equilibrium between the 2-$C_4H_8^+$ and i-$C_4H_8^+$ structures:

$$2\text{-}C_4H_8^+ \rightleftarrows i\text{-}C_4H_8^+. \qquad (6)$$

It was suggested that the equilibrium position is affected by the internal energy of the ion, which is gradually diminished as the entity undergoes successive collisions.

Because such a rapid equilibrium between two skeletally different isomers has not been seen for carbonium ions [1], and because detailed information about isomerization process in $C_nH_{2n}^+$ ions is generally lacking, it was considered worthwhile to undertake a study of isomerization processes in these ions. In particular, it was felt that since $C_4H_8^+$ ions formed in ethylene can undergo further reaction with the parent molecule:

$$C_4H_8^+ + C_2H_4 \rightarrow C_6H_{12}^+ \qquad (7)$$

it would be of interest to observe the charge transfer and D_2^- transfer products of $C_4H_8^+$ ions in cyclobutane, where such competing processes are absent; $C_4H_8^+$ ions do not react with cyclobutane [10]:

$$C_4H_8^+ + c\text{-}C_4H_8 \not\rightarrow \text{no reaction}. \qquad (8)$$

Further, an examination of pressure effects on the structures of $C_4H_8^+$ ions over a wide pressure range seemed warranted.

In the results reported here, $C_4H_8^+$ ions are generated in cyclobutane, ethylene, methylcyclopropane and the butenes, through photoionization with 11.6–11.8 eV photons as well as through γ-radiolysis. The $C_4H_8^+$ (or $C_4D_8^+$) ions are intercepted both by charge transfer and by D_2 transfer reactions with added alkanes. The pressure of these systems is varied from about 0.1 torr to 1 atm, and in some systems, unreactive deactivator gases are added. As will be seen below, the composite picture which emerges from these various results not only indicates that isomerization process in the $C_4H_8^+$ ions are relatively slow in the energy range accessible for these experiments and can be collisionally quenched, but demonstrates that the isomerization reactions involve several different C_4H_8 structures, not just the 2-$C_4H_8^+$ and *i*-$C_4H_8^+$ configurations.

2. Experimental Procedure

All the hydrocarbons used in this study were rigorously purified by gas chromatography, and low temperature distillation. The irradiation and analytical procedures were the same as those described in earlier publications from this laboratory [13]. The argon resonance lamps, equipped with 0.35 mm thick LiF windows, were fabricated according to the procedure described recently [14]. The 104.8 and 106.7 nm lines emanating from the lamp were of equal intensity, within 10 percent. Impurity lines constituted less than 1 percent of the radiation. After approximately 20 experiments, the transmission of the window was reduced by 50 percent from its initial value because of *F*-center formation. Bleaching of the window with a mercury lamp restored the output of the lamp to its original intensity. Impurity lines did not appear even after extensive usage. The intensity at which most of the experiments were carried out was 10^{13} quanta per second.

The radiolysis experiments were carried out in the NBS cobalt-60 gamma source, which, at the time these experiments were performed, provided 1.7×10^{17} eV/s per gram of hydrocarbon.

Quantitative analyses were carried out by injecting aliquots of the irradiated samples onto a 40 ft squalane column operated at 20 °C in a gas chromatograph equipped with a flame ionization detector. This column did separate 1,3-butadiene from 1-butene and isobutene, but did not separate 1-butene from isobutene. In some experiments, the combined peak of these two butenes was trapped out at liquid nitrogen temperature at the exit of the column and analyzed on a mass spectrometer. The methylcyclopropane was only partially separated from the *cis*-2-butene, but fairly good estimates of the yield of methylcyclopropane could be obtained, especially in experiments in which *cis*-2-butene is a minor product. The identity of the methylcyclopropane product was also confirmed by mass spectrometric analysis, and by injection of several of the samples on an alumina and on a sulfolane column, which separated the methylcyclopropane from the butenes.

All photolysis and radiolysis experiments were carried out in the presence of 3–5 percent oxygen, which effectively scavenges free radicals and prevents their forming hydrocarbon products.

The NBS high pressure photoionization mass spectrometer [10] was used to determine the modes of decomposition of cyclobutane ions, the modes of reaction of the fragment ions with cyclobutane, and the rates of certain reactions of importance to the interpretation of the results reported here.

Product yields are given in ion pair yield units, that is, in molecules (M) of product formed per positive ion (N_+) generated by the radiation in the *parent compound*. In the case of the photolysis experiments, ion pair yield determinations were made using the techniques discussed before [15]. The ion pair yield of a given product (X), is related to its quantum yield and the quantum yield of ionization in the parent compound:

$$\Phi(X)/\Phi_+ = M(X)/N_+.$$

The quantum yield of ionization at 11.6–11.8 eV of ethylene [6c] is 0.20, of cyclobutane [16] is 0.52, and of methylcyclopropane [16], 0.44.

In the case of cyclobutane, it was found that the quantum yield of ethylene plus acetylene was 0.91, independent of pressure from 0.2 to 1 torr. When the intensity of the lamp was kept constant, and 5 percent of dimethylamine was added to the cyclobutane, neither the ratio of ethylene to acetylene nor the absolute yields of these two products changed. Therefore, in photolysis experiments in the presence of larger amounts of dimethylamine, the combined yields of these two products were taken as the base for calculation of the product yields; in this way the fact that dimethylamine absorbed some of the energy was automatically corrected for. The same procedure was followed for experiments in which methylcyclopentane was the additive. In that case, the hydrocarbon additive did contribute to the formation of ethylene; however, because the methylcyclopentane was deuterated, a mass spectrometric analysis of the ethylene formed in the photolysis of *c*-C_4H_8–*c*-$C_5D_9(CD_3)$ mixtures verified that the yield of ethylene plus acetylene originating from cyclobutane did indeed remain constant.

It should be pointed out that this yield of ethylene plus acetylene is much lower than that reported in the earlier study [8] of the photolysis of cyclobutane. At the time that study was carried out, it was not realized that ion current measurements made at high sample pressures are generally not valid [15b]; therefore, all the absolute yields reported in that study are too high.

2.1. Ion Interception Techniques

In the discussion which follows, the yields of $C_4H_8^+$ ions of different structures (i.e. *i*-$C_4H_8^+$, 2-$C_4H_8^+$, 1-$C_4H_8^+$, etc.) will be followed under various conditions. In all cases, these yields have been derived from experiments in which (a) it is assumed that the C_4H_8 product formed in a charge transfer reaction

(reaction 2) has a structure which corresponds to the structure of the precursor $C_4H_8^+$ ion, or (b) the yields of the butanes formed in H_2^- or D_2^- reactions (such as 4 and 5) have been related to the yields of precurso- ions.

Charge acceptors used in this study are dimethylamine and, in a few ethylene experiments, nitric oxide. In the case of NO, it has been reported [10] that at a pressure of ~ 0.1 torr, only 15–20 percent of the $C_4H_8^+$ ions from cyclobutane undergo charge transfer with NO, the remainder reacting to form an adduct $C_4H_8NO^+$ ion. Adduct formation may possibly also occur with dimethylamine; adduct formation has been reported for the $C_4H_8^+$-trimethylamine reaction pair in one study [9], but was not confirmed in a study from this laboratory [10] (and trimethylamine has been reported to react with $C_4H_7^+$ ions in exactly the same way as dimethylamine [11]). Because the results obtained with NO are in fair agreement with those in which dimethylamine was added, and because the results of the charge transfer experiments in general are, within experimental error, in agreement with what is seen in the H_2^- (or D_2^-) transfer experiments, adduct formation between $C_4H_8^+$ ions and the charge acceptor apparently does not materially alter the relative amounts of the different C_4H_8 isomers which are observed. Also, at pressures below about 100 torr, in cyclobutane the overall yields of products formed in charge exchange reactions with dimethylamine are in good agreement with the yields of products from H_2^- (or D_2^-) transfer reactions in methylcyclopentane additive experiments. However, because of possible complications from adduct formation, as well as the fact that the unambiguous analysis of all the C_4H_8 isomers is difficult with the analytical techniques used here, the results from the charge exchange experiments will generally be considered mainly as corroborative evidence for conclusions drawn from the H_2^- (D_2^-) transfer experiments.

The experiments in which the $C_4H_7^+$ ions were trapped by H_2^- (or D_2^-) transfer reactions were mainly carried out with methylcyclopentane-d_{12} as the reactive additive. As was noted before, it has been demonstrated conclusively [12] that the product $CH_3CHDCHDCH_3$ results only from a reaction of a 2-$C_4H_7^+$ ion with c-$C_5D_9(CD_3)$ (reaction 4) while $(CH_3)_2CDCH_2D$ results from reaction of an i-$C_4H_7^+$ ion (reaction 5). Furthermore, 1-$C_4H_8^+$ ions react with c-$C_5D_9(CD_3)$ to give $CH_2DCHDCH_2CH_3$:

$$1\text{-}C_4H_8^+ + C_6D_{12} \rightarrow CH_2DCHDCH_2CH_3 + C_6D_{10}^+ \quad (9)$$

which is easily distinguishable by mass spectrometry [12] from the n-$C_4H_8D_2$ product formed in reaction 4 of the 2-$C_4H_8^+$ ion. It has been demonstrated in the mass spectrometer [10, 17] that the only reactions between the $C_4H_8^+$ ions and methylcyclopentane are H_2^- transfer reactions (analogous to the D_2^- transfer reactions 4, 5, and 9) and H^- transfer reactions:

$$C_4H_7^+ + C_6H_{12} \rightarrow C_4H_9 + C_6H_{11}^+. \quad (10)$$

The H^- (or D^-) transfer reactions 10 lead to the formation of butyl radicals, which in our experiments will be scavenged by added oxygen; however, because of the occurrence of reaction 10, the yields of butane products formed in the H_2^- (D_2^-) transfer reactions must be corrected upwards to obtain the correct $C_4H_8^+$ ion yields. Such corrections have been made for all the results presented below. The ratios of H^- transfer to H_2^- transfer (or D^-/L_2^-) for the C_4H^+ (or $C_4D_8^+$) isomeric ions with methylcyclopentane are [10, 16]: 1-$C_4H_8^+$ —0.23; 2-$C_4H_8^+$—only H_2^- transfer; i-$C_4H_8^+$—0.14.

In certain experiments, cyclohexane has been added as an interceptor of $C_4H_8^+$ ions. It has been shown [12] that 2-$C_4H_8^+$ ions do not react with cyclohexane, while 1-$C_4H_8^+$ ions do undergo reaction 9 at a rate about one-fifth of the collision rate when C_6D_{12} is cyclohexane. (i-$C_4H_8^+$ ions react with cyclohexane to form isobutane, but at a very low rate.) Thus, the formation of n-butane in an experiment with cyclohexane additive demonstrates the presence of 1-$C_4H_8^+$ ions. (This has been confirmed by isotopic analyses of butane produced in reaction with c-C_6D_{12} in the experiments discussed below.) The ratio [10, 17] of H^-/H_2^- transfer reactions for the 1-$C_4H_8^+$-c-C_6H_{12} reaction pair is 0.06.

In the following discussion, no distinction will be made between *cis*- and *trans*-2-$C_4H_8^+$. When *cis*- and *trans*-2-C_4H_8 are photolyzed individually in the presence of dimethylamine, it is seen that isomerization between the two structures occurs readily.

2.2. Results and Discussion: Effect of Interceptor Concentration

Figure 1 shows the yields of the i-$C_4H_8^+$ and 2-$C_4H_8^+$ ions formed in the radiolysis of c-C_4H_8 at a pressure of 22 torr, as determined by varying amounts of added methylcyclopentane-d_{12}, which intercepts the ions according to reactions 4, 5 and to a minor extent, 10

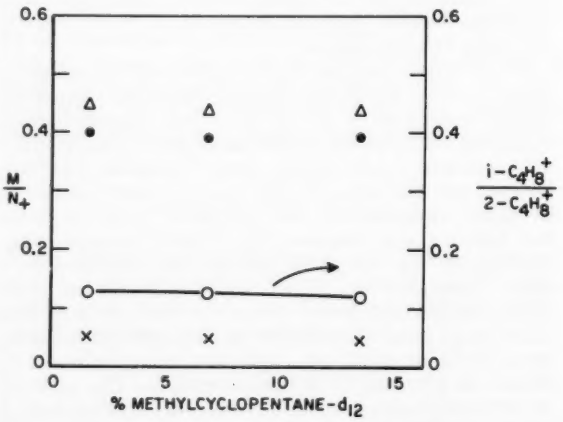

FIGURE 1. *The radiolysis of* c-C_4H_8-c-$C_5D_9(CD_3)$-O_2 *mixtures at a total pressure of 22 torr.*

The effect of methylcyclopentane concentration on the yields of intercepted i-$C_4H_8^+$ (X), 2-$C_4H_8^+$ (•), total $C_4H_8^+$ (△), and the ratio i-$C_4H_8^+$/2-$C_4H_8^+$ (○).

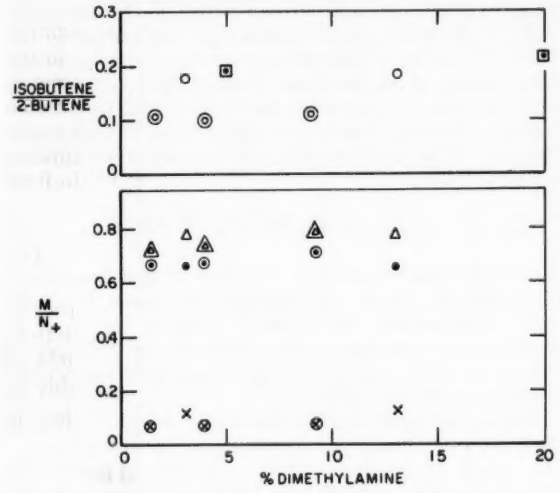

FIGURE 2. *The 11.6–11.8 eV photolysis of cyclobutane-dimethylamine mixtures in the presence of oxygen*

The effect of dimethylamine concentration on the yields of intercepted i-$C_4H_8^+$ ions (X), 2-$C_4H_8^+$ ions (•), and total $C_4H_8^+$ ions (△) in c-$C_4H_8^+$, as well as the yields of i-$C_4H_8^+$ (⊗), 2-$C_4D_8^+$ (◎), and total $C_4D_8^+$ (△) in c-C_4D_8. The ratios of isobutene ion to 2-butene ion are also shown: c-C_4H_8 experiments at 9 torr (○), c-C_4D_8 experiments at 4 torr (◎), and c-C_4H_8 experiments at 0.5 torr (⊡). (In the latter two experiments, absolute product yields were not measured.)

as mentioned above. It is seen that the yields of the two isomeric ions do not vary at all as a function of the concentration of interceptor. This result was verified in the 11.6–11.8 eV photolysis of c-C_4H_8 (at 9 torr and at 0.5 torr) and c-C_4D_8 (at 4 torr) in the presence of varying amounts of dimethylamine (fig. 2) which intercepts the ions through reaction-2 to form butene products. The invariance with interceptor concentration of the total yields which can be attributed to the isobutene and 2-butene ions in the cyclobutane systems demonstrates that in this system, where the ions can only react with the added reactive compound, the $C_4H_8^+$ ($C_4D_8^+$) ions are effectively intercepted.

This is in marked contrast to the result reported earlier and discussed in the Introduction, that the ratio of i-C_4H_8 to 2-C_4H_8 observed in ethylene varies as a function of the concentration of added dimethylamine at low dimethylamine concentration; the results of a similar series of experiments, in which ethylene at a pressure of 11 torr was photolyzed at 11.6–11.8 eV in the presence of varying amounts of dimethylamine, are given in figure 3. In the ethylene system, the fact that the total yields of $C_4H_8^+$ ions intercepted (fig. 3 and reference [11]) increase as a function of interceptor concentration (in the same low concentration range where the change in the i- to 2-$C_4H_8^+$ ratio is seen) suggests that the effect observed can be explained if ethylene competes for interception of the i- and 2-$C_4H_8^+$ ions when the concentration of additive is low (reaction 7). It has been reported [18] that reaction 7 between i-$C_4H_8^+$ ions and ethylene is faster than the analogous reaction of 2-$C_4H_8^+$ ions. Thus, one would predict, qualitatively, that at low concentrations of added interceptor, the ethylene would compete more effectively for the i-$C_4H_8^+$ ions than for the 2-$C_4H_8^+$ ions, producing concentration effects like those which are actually observed. Actually, the results given in the earlier study [11] and in figure 3 are what would be predicted if the rate constant of reaction 7 is $\sim 0.3 \times 10^{-10}$ cm³/molecule · s for i-$C_4H_8^+$ ions and $\sim 0.03 \times 10^{-10}$ cm³/molecule · s for 2-$C_4H_8^+$ ions[2] (assuming that the rate constant for reaction 2 with dimethylamine is 1.3×10^{-9} cm³/molecule · s[18b]). These rate constants are higher by about an order of magnitude than the rate constant which can be derived for these reactions from earlier measurements in a tandem mass spectrometer [18a]; however, the results of recent studies of reactions of thermal ions carried out in the NBS photoionization mass spectrometer [10, 17] indicate that the rate constants of the reactions of the energetic ions formed in a tandem instrument often vary widely from those observed for ions at thermal energies. In order to verify that the rate constant for reaction 7 involving thermal i-$C_4H_8^+$ ions is actually higher than the earlier literature value would indicate, i-$C_4H_8^+$ ions were generated by 10 eV photons in the NBS high pressure photoionization mass spectrometer in the presence of bulk C_2D_4 (which is not ionized at this energy). Although the results were too complex to be interpreted in detail, it was observed that both the condensation reaction

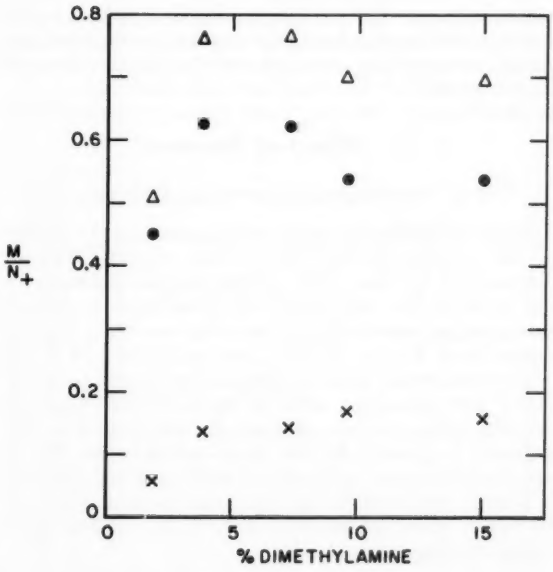

FIGURE 3a. *The 11.6–11.8 eV photolysis of ethylene-dimethylamine mixtures in the presence of oxygen at a pressure of 11 torr.*

The effect of dimethylamine concentration on the yields of intercepted i-$C_4H_8^+$ ions (X), 2-$C_4H_8^+$ ions (•), and total $C_4H_8^+$ ions (△).

[2] Since this paper was submitted for publication, a value of 0.37×10^{-10} cm³/molecule · s has been determined for the rate constant of the reaction (2-$C_4H_8^+$ + 2-C_4H_8) by L. W. Sieck of this laboratory. Taking this value, and the relative rate constants for these reactions determined by J. M. S. Henis (J. Chem. Phys. **52**, 282 (1970)), one obtains a value of 0.026×10^{-10} for the rate constant of Reaction 7 involving 2-$C_4H_8^+$ ions.

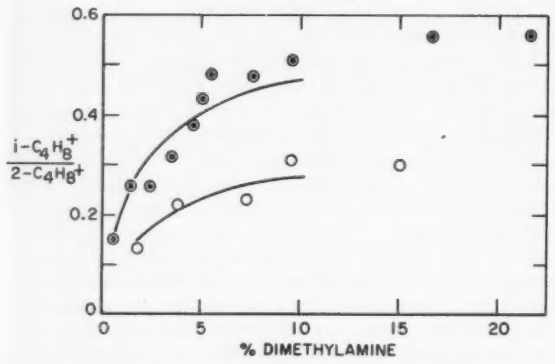

FIGURE 3b. *The ratio of* i-$C_4H_8^+$/2-$C_4H_8^+$ *intercepted in the 11.6–11.8 eV photolysis of ethylene by varying concentrations of dimethylamine as measured in this study* (○) *at a pressure of 11 torr, and in reference* [11] (⊙) *at a pressure of 2.8 torr.*

The solid lines show the ratios calculated on the assumption that the rate constant of reaction 7 is $0.3 + 10^{-10}$ cm³/molecule · s for *i*-$C_4H_8^+$ ions and $0.03 + 10^{-10}$ cm³/molecule · s for 2-$C_4H_8^+$ ions.

(reaction 7) and various D or D^+ exchange reactions—some of which led to the re-formation of butene ions—occurred; the overall rate constant of interaction between these partners was 2.7×10^{-10} cm³/molecule · s at pressures up to 0.05 torr. Although our calculated rate constant of 0.3×10^{-10} for reaction 7 involving *i*-$C_4H_8^+$ ions was not verified, the results obtained would indicate that this rate constant may be entirely feasible for the condensation reaction in the pressure region used for the photolysis and radiolysis experiments.

3. Effect of Pressure

3.1. A. Fragmentation of the $C_4H_8^\ddagger$ Ions

Figure 4 shows the effect of pressure on the yields of the *i*-$C_4H_8^\ddagger$ ($C_4D_8^\ddagger$) and 2-$C_4H_8^\ddagger$ ($C_4D_8^\ddagger$) ions as determined by the yields of the butane products in the 11.6–11.8eV photolysis of cyclobutane–methylcyclopentane mixtures. It is seen that over the pressure range from 0.1 to 10 torr, the total yield of $C_4H_8^\ddagger$ ($C_4D_8^\ddagger$) ions intercepted increases greatly; this suggests that a low pressures, some of the $C_4H_8^\ddagger$ ions undergo decomposition, but are collisionally deactivated as the pressure is raised. As has been noted before [8, 9], when cyclobutane is irradiated with 11.25 eV photons in a mass spectrometer at a pressure of approximately 10^{-5} torr, about 30 percent of the $C_4H_8^\ddagger$ ions undergo fragmentation to form $C_4H_7^+$:

$$C_4H_8^\ddagger \rightarrow C_4H_7^+ + H \qquad (11)$$

or $C_3H_5^+$:

$$C_4H_8^\ddagger \rightarrow C_3H_5^+ + CH_3. \qquad (12)$$

In order to check on the fragmentation mechanisms occurring in cyclobutane at the argon resonance lines, 11.6–11.8 eV, as well as the fates of the fragment ions, cyclobutane was irradiated at this energy in the NBS high pressure photoionization mass spectrometer. The results, given in figure 5, show the fragmentation and ion-molecule reaction mechanisms in pure cyclobutane. The allyl ion formed in process 12 disappears because of a rapid reaction with cyclobutane to form propene [18a]:

$$C_3H_5^\ddagger + C_4H_8 \Rightarrow C_3H_6 + C_4H_7^\ddagger. \qquad (13)$$

The $C_4H_7^\ddagger$ ions formed in reaction 13 and fragmentation process 11 do not undergo any rapid reactions with cyclobutane; the gradual drop in the yield of $C_4H_7^\ddagger$ as the pressure is raised (fig. 5) can probably be traced to collisional quenching of the parent ion decomposition processes 11 and 12.

Returning now to the photolysis results shown in figure 4, one should see a compensating diminution in the yield of propene (from reaction 13) over the pressure range from 0.1 to 10 torr if indeed the observed increase in the total yield of $C_4H_8^\ddagger$ ($C_4D_8^\ddagger$) ions intercepted is due to a collisional quenching of dissociation process 12; this is seen, as shown in the figure.

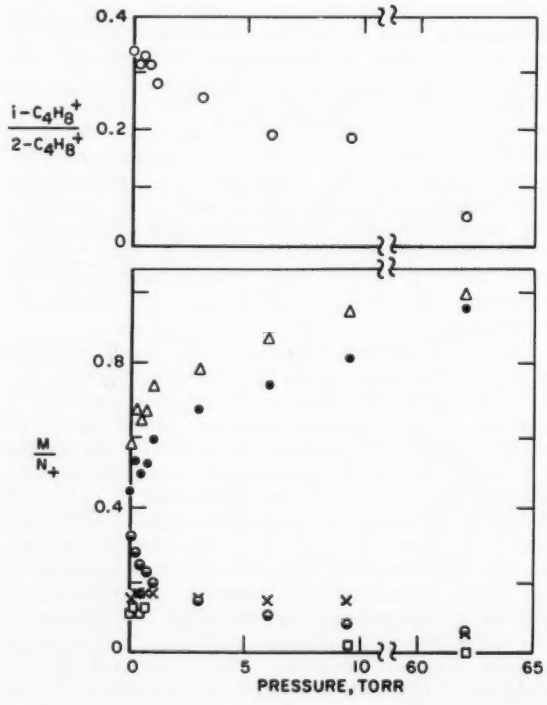

FIGURE 4a. *The 11.6–11.8 eV photolysis of a* c-C_4H_8-c-C_5D_{10}(CD_3) *(1:0.20) mixture in the presence of oxygen*

The effect of pressure on the yield of intercepted *i*-$C_4H_8^+$ (X) and 2-$C_4H_8^+$ (•) and total $C_4H_8^+$ (△) ions, as well as the yields of propylene (◒) and methylcyclopropane (□). The ratios of isobutene ion to 2-butene ion are also shown (○).

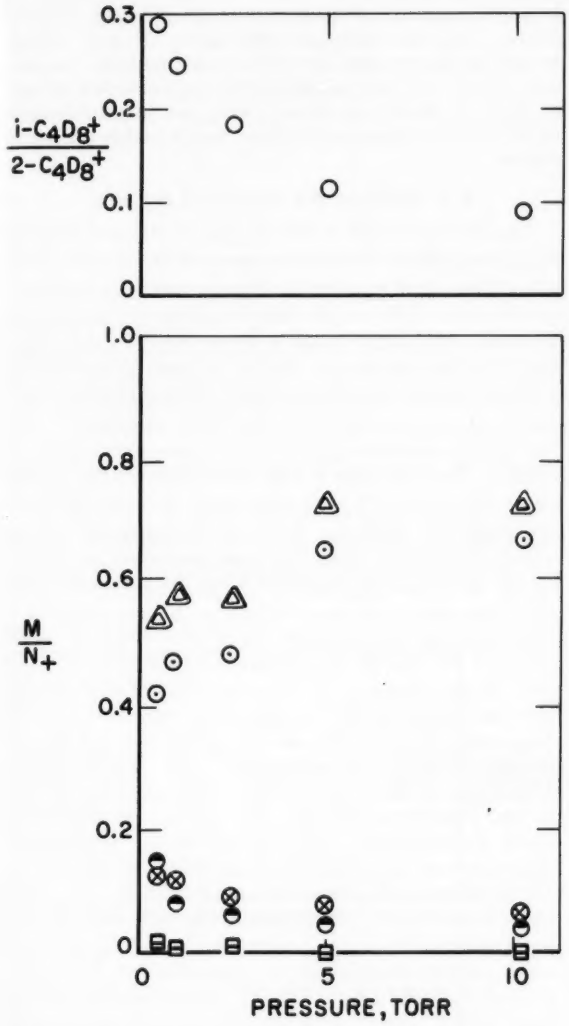

FIGURE 4b. *The 11.6–11.8 eV photolysis of a* c-C_4D_8-c-$C_5D_6(CD_3)$ *(1:0.05) mixture in the presence of oxygen.*

The effect of pressure on the yield of intercepted *i*-$C_4D_8^+$ (⊗), 2-$C_4D_8^+$ (⊙), and total $C_4D_8^+$ (△) ions as well as the yields of propylene (◓), and methylcyclopropane (⊟). The ratios of isobutene ion to 2-butene ion are also shown (○).

In these experiments, in which methylcyclopentane is the added interceptor, the $C_4H_7^+$ ($C_4D_7^+$) ions formed by reaction 11 or 13 may undergo a hydride transfer reaction to form C_4H_7D (C_4D_8) products; they will not contribute to the formation of butane products.

In low pressure experiments in which the $C_4H_8^+$ ($C_4D_8^+$) ions are intercepted by dimethylamine, the $C_4H_7^+$ ($C_4D_7^+$) ions formed in reactions 11 and 13 might be expected to react to form butadienes. Small amounts of 1,3-butadiene ($M/N_+ \approx 0.046$ in *c*-C_4H_8 photolysis) and 1,2-butadiene ($M/N_+ \approx 0.0026$ in *c*-C_4H_8 photolysis) are observed in such experiments, but the yields do not differ significantly from the yields of these products observed in methylcyclopentane additive experiments (where the 1,3-butadiene yield is ≈ 0.055 and that of 1,2-butadiene ≈ 0.0020 under similar conditions). At any rate, the $C_4H_7^+$ ($C_4D_7^+$) ions formed at low pressures in the presence of dimethylamine do not apparently contribute appreciably to the formation of the butene products; this is shown by the results given in figure 6, which gives the yields of the *i*-C_4D_8 and 2-C_4D_8 products (see reaction 2) formed in the 11.6–11.8 eV photolysis of a *c*-C_4D_8-$(CH_3)_2NH$ mixture over the 0.1–10 torr pressure range. The yields which are attributed to the *i*- and 2-$C_4D_8^+$ ions intercepted in these experiments are in close agreement with the yields which were attributed to these same ions in the D_2^- transfer experiments shown in figure 4b. This agreement also demonstrates that apparently both compounds intercept the $C_4D_8^+$ ions quantitatively under these conditions.

In the photolysis of ethylene over this pressure region, from 0.1 to 10 torr, it was shown some time ago [6c] that the overall yields of $C_4H_8^+$ ions intercepted by NO increase drastically as a function of pressure up to about 10 torr, indicating that the $C_4H_8^+$ ions formed in reaction 1 undergo dissociation at low pressure and are collisionally stabilized as the pressure is increased. This result is confirmed here in experiments in which the $C_4H_8^+$ ions in ethylene were intercepted by dimethylamine and by methylcyclopentane, both shown in figure 7. The $C_4H_8^+$ ions formed in ethylene have more internal energy than the cyclobutane parent ions (table 1), and it is to be expected that they also should dissociate in this pressure region.

It is significant that the yields, as well as the ratios, of ions intercepted in these ethylene experiments by

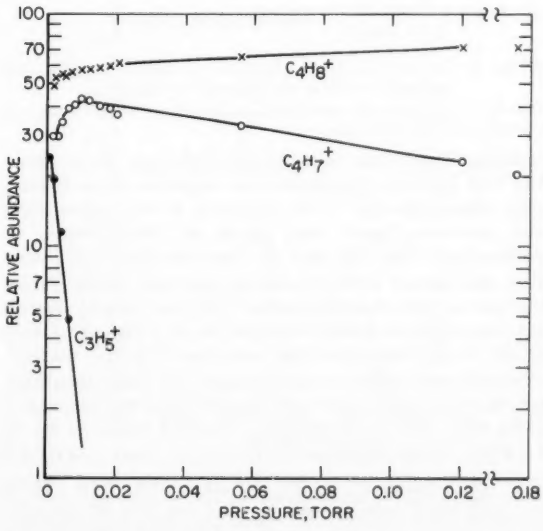

FIGURE 5. *The relative abundance of ions observed as a function of pressure in* c-C_4H_8 *irradiated with 11.6–11.8 eV photons in the NBS high pressure photoionization mass spectrometer.*

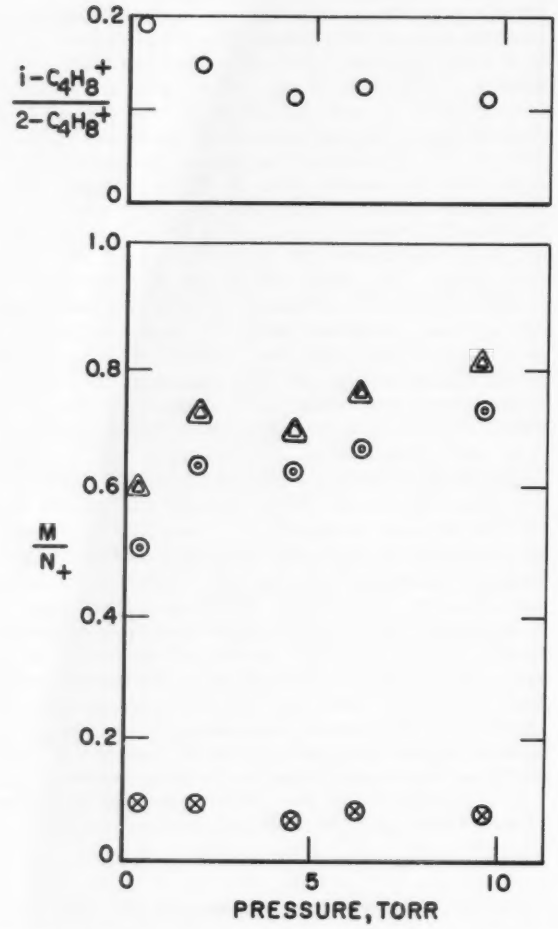

FIGURE 6. *The 11.6–11.8 eV photolysis of a* c-C_4D_8-$(CH_3)_2NH$ *mixture (1:0.09) in the presence of oxygen.*

The effect of pressure on the yields of intercepted *i*-$C_4D_8^+$ (⊗), 2-$C_4D_8^+$ (⊙), total $C_4D_8^+$ (△) and the ratio *i*-$C_4D_8^+$/2-$C_4D_8^+$ (○).

methylcyclopentane are greatly different from those observed in the dimethylamine additive experiments (both shown in fig. 7) in contrast to the agreement seen between these two kinds of experiments in cyclobutane (figs. 4b and 6). Because the $C_4H_8^+$ ions react only about 3–6 percent as fast with methylcyclopentane as with dimethylamine [12], one would predict that the ethylene would compete much more effectively for the $C_4H_8^+$ ions (through reaction 7) in the methylcyclopentane additive experiments. In fact, assuming that the rate constants for reaction 7 are (as estimated above from the dimethylamine results given in fig. 3) 0.3×10^{-10} cm³/molecule · s for *i*-$C_4H_8^+$ ions and 0.03×10^{-10} cm³/molecule · s for 2-$C_4H_8^+$ ions, and taking the measured rate constants [17] for the D_2^- transfer reactions between these ions and methylcyclopentane-d_{12} (and estimating from the results given in reference [11] that the total ion pair yields of the *i*- and 2-$C_4H_8^+$ ions at a pressure of 2.8 torr are 0.20 and 0.38, respectively), one can calculate the yields of ions which would be intercepted by 10 percent methylcyclopentane-d_{12} at 2.8 torr; as shown by the encircled points in figure 7, these calculated yields are in good agreement with the measured butane yields in this pressure region.

3.2. Yields of the Isomeric $C_4H_8^+$ Ions

The relative yields of the *i*-$C_4H_8^+$ ($C_4D_8^+$) and 2-$C_4H_8^+$ ($C_4D_8^+$) ions depend on the pressure of the system, even when the overall pressure is high enough that fragmentation of the $C_4H_8^+$ ($C_4D_8^+$) ions is effectively quenched. This can be readily seen in figure 4a, by comparing the 9.5 torr experiment (M/N_+ of total $C_4H_8^+ = 0.95$) with the 62 torr experiment (M/N_+ of total $C_4H_8^+ = 1.0$); the yield of intercepted *i*-$C_4H_8^+$ drops drastically, and the drop is compensated by an increase in the yield of 2-$C_4H_8^+$. There is also a significant diminution in the ratio *i*-$C_4H_8^+$/2-$C_4H_8^+$ with increasing pressure for ions generated in ethylene, even in the pressure range where all fragmentation has been inhibited, as shown by the results given in figure 8 for the radiolysis and

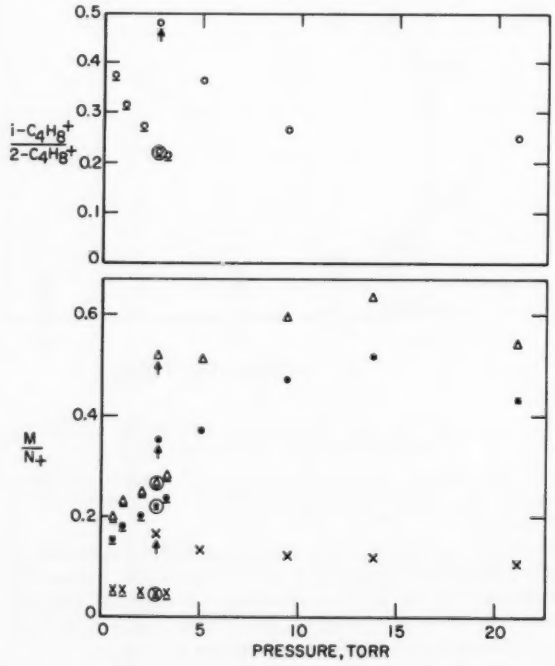

FIGURE 7. *The effect of pressure on the yields of* i-$C_4H_8^+$ (X), 2-$C_4H_8^+$ (●), *total* $C_4H_8^+$ (△), *and the ratio* i-$C_4H_8^+$/2-$C_4H_8^+$ (○) *intercepted in the 11.6–11.8 eV photolysis of ethylene by 10 percent methylcyclopentane-*d_{12} *(underlined points) or by 7 percent dimethylamine.*

Arrows designate experimental points for 7.6 percent dimethylamine experiment from Reference 11. Encircled points are yields one would predict for a methylcyclopentane additive experiment, assuming the estimated rate constants for reaction 7 given in the discussion.

TABLE 1. *Heats of formation of* $C_4H_8^+$ *isomers*

$C_4H_8^+$ Isomer	ΔH_f eV
$C_2H_4^+ + C_2H_4$	11.51
c-$C_4H_8^+$	10.84
c-$C_3H_5(CH_3)^+$ [a]	10.15
1-$C_4H_8^+$	9.58
i-$C_4H_8^+$	9.06
cis-2-$C_4H_8^+$	9.06
tr-2-$C_4H_8^+$	9.02

All values, except c-$C_3H_5(CH_3)^+$, from J. L. Franklin, J. G. Dillard, H. M. Rosenstock, J. T. Herron, K. Draxl, and F. H. Field, National Standard Reference Data System—NBS, **26**, U.S. Govt. Printing Office (1969).

[a] The heat of formation of the methylcyclopropane ion is calculated assuming that the ionization potential of the neutral molecule is 9.9 eV (F. H. Field, footnote in J. L. Franklin, J. Chem. Phys. **22**, 1304 (1954)). This value, which was chosen because we observed ionization of pure methycyclopropane irradiated with 10.0 eV photons ($\Phi_+ = 0.13$ [16]), is within the limits of error of the more recent value of 10.1 ± 0.02 eV (G. G. Meisels, J. Y. Park, and B. G. Geissner, J. Am. Chem. Soc. **92**, 254 (1970)).

photolysis of ethylene in the presence of charge acceptor.

In order to examine the effect of pressure over a much wider pressure range, a series of radiolysis experiments were performed on a c-C_4H_8-c-$C_5D_9(CD_3)$ (1:0.050) mixture (fig. 9). An isotopic analysis of the n-butane formed at higher pressures revealed that these butanes consisted of a mixture of CH_3CHD-$CHDCH_3$ formed in reaction 4 of the 2-$C_4H_8^+$ ion, and $CH_2DCHDCH_2CH_3$ formed in reaction 9 of the 1-$C_4H_8^+$ ion. The presence of 1-$C_4H_8^+$ ions was confirmed by the results of two other series of experiments. First, (fig. 10), when a c-C_4D_8-$(CH_3)_2NH$ (1:0.08) mixture was irradiated at different pressures ranging from 7 torr to 418 torr, the combined yield of intercepted (i-$C_4D_8^+ + 1$-$C_4D_8^+$) increased. Mass spectrometric analysis confirmed that the increase could be attributed to 1-butene. The presence of 1-$C_4H_8^+$ ions was also confirmed by the observation of n-butane [20] in irradiated c-C_4H_8 in the presence of 5 percent cyclohexane; as mentioned above, cyclohexane will intercept 1-$C_4H_8^+$ ions through a $H_2^-(D_2^-)$ transfer reaction, but is unreactive toward 2-$C_4H_8^+$ ions [10, 12, 17]. The yield of 1-$C_4H_8^+$ ions, as determined in both the methylcyclopentane and cyclohexane additive experiments (fig. 9) increased as a function of pressure, while the yield of intercepted i-$C_4H_8^+$ ions dropped off rapidly.

In the high pressure experiments given in figures 9 and 10, the total yield of products which can be attributed to $C_4H_8^+$ ion precursors diminishes with pressure. There are two possible explanations for this: collisional stabilization of adduct ions formed in the $C_4H_8^+$-interceptor encounter, or collisional stabilization of the parent c-$C_4H_8^+$ ions. It should be pointed out that in the liquid [21] and solid [22] phase radiolysis of ethylene, as well as in the solid phase photolysis [22] at 11.6–11.8 eV, cyclobutane is observed as an important product. (In the solid phase photolysis at 8.4 eV, where ionization of ethylene is unimportant, cyclobutane is not observed, so it may be inferred that it has an ionic precursor.) Cyclobutane grows in as a product in the radiolysis of ethylene at very high pressures [23] (> 1 atm). It is tempting to postulate that the $C_4H_8^+$ ion formed in reaction 1 is stabilized in the cyclobutane structure and somehow ends up as neutral cyclobutane. However, it must be pointed out that the mode of formation of the cyclobutane product in ethylene may be plausibly explained in other ways [22].

4. Isomerization Mechanisms of $C_4H_8^+$ Ions

From the results discussed above, it is now possible to derive certain information about the isomerization mechanisms operative in $C_4H_8^+$ ions. These results suggest a mechanism in which the initially formed $C_4H_8^+$ ions rearrange to lower energy structures (see table 1) at a rate which is approximately of the same order of magnitude as the collision rate (10^7–10^{10} s^{-1}). As the pressure is increased, some of the processes which require longer times to occur (i.e. rearrangement to the i-$C_4H_8^+$ structure, for example)

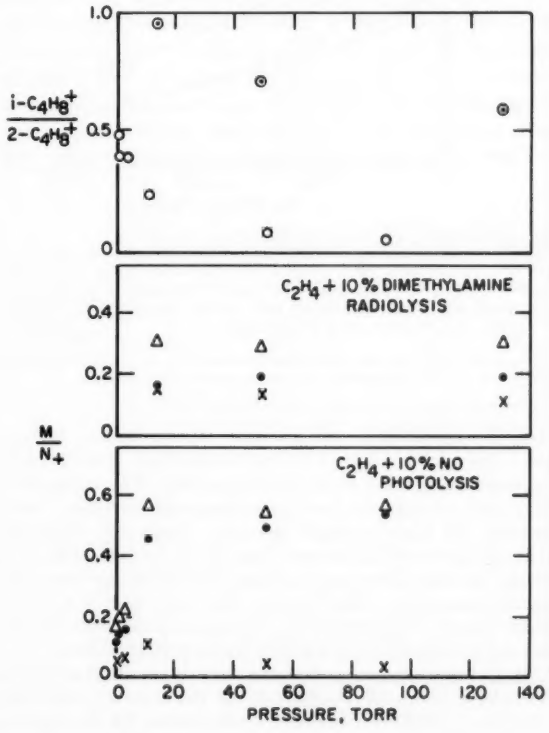

FIGURE 8. *The effect of pressure on the yields of intercepted* i-$C_4H_8^+$ (X), *and* 2-$C_4H_8^+$ (●) *and total* $C_4H_8^+$ (△) *ions in the 11.6–11.8 eV photolysis and the radiolysis of ethylene-charge acceptor mixtures in the presence of oxygen.*

The i-$C_4H_8^+$/2-$C_4H_8^+$ ratio in the photolysis (○) and radiolysis (○) is also shown.

443-082 OL - 71 - 5

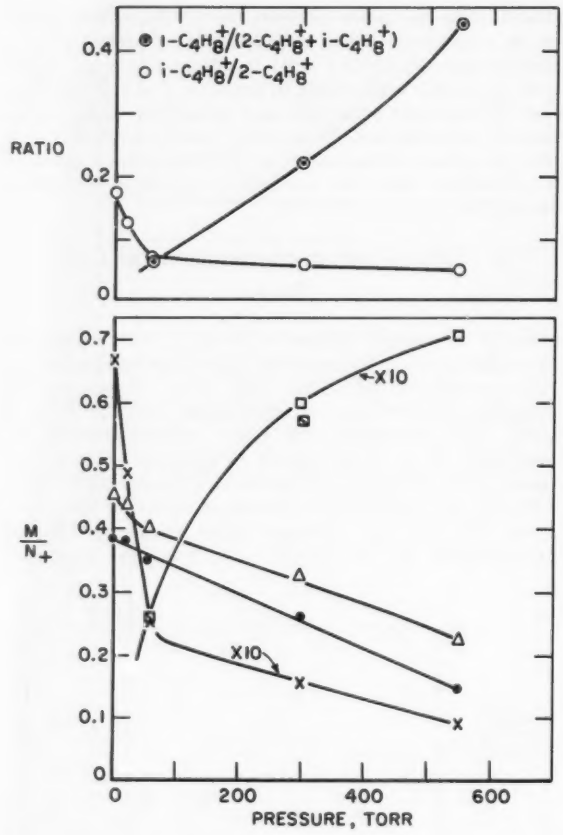

FIGURE 9. *The effect of pressure on the yields of intercepted* i-$C_4H_8^+$ (X), 2-$C_4H_8^+$ (●), 1-$C_4H_8^+$ (□), *and total* $C_4H_8^+$ (△) *in the radiolysis of a* c-C_4H_8-c-C_5D_9 (CD_3) (*1:0.05*) *mixture in the presence of 3 percent oxygen, as well as the ratios,* i-$C_4H_8^+$/2-$C_4H_8^+$ (○) *and* 1-$C_4H_8^+$/(2-$C_4H_8^+$ + i-$C_4H_8^+$) (⊙).

Also shown are the yields of 1-$C_4H_8^+$ (⊠) as determined from the *n*-butane yields in the radiolysis of a c-C_4H_8-c-C_6H_{12} mixture, in the presence of 3 percent oxygen.

may be quenched, while some of the higher energy ions (i.e., 1-$C_4H_8^+$) are deactivated or intercepted before having time to isomerize further. The unimolecular rate constants for isomerizations increase with energy. At high enough energies, however, dissociation of the ions will occur (that is, in cyclobutane, the onset of fragme..tation is about 0.7 eV above the ionization potential). This means that very fast (i.e., very high energy) isomerization processes may not be observed in experiments such as those reported here.

It is not surprising that the rate of isomerization is the same order of magnitude as the rate of collision. For the $C_4H_8^+$ ion formed in cyclobutane by absorption of 11.6–11.8 eV photons, the main fragmentation process (fig. 5) is the loss of a methyl radical (process 12). Clearly, this fragmentation must involve a rearranged $C_4H_8^+$ structure, and one may therefore assume that the isomerization is at least as fast as the dissociation, which the data given in figure 5 indicate occurs with a rate of the order of 10^6–10^7 s^{-1}. At higher energies, where the rate of fragmentation will be faster, rearrangement becomes much less important, as indicated by the fact that the $C_2H_4^+$ ion is a much more important ion in the 70 eV mass spectral cracking pattern of cyclobutane [18c] (this ion comprises only 1.5 percent of the total ionization in the 11.6–11.8 eV experiments given in fig. 5) than in any of the other isomeric C_4H_8 compounds. It has been noted before that the cyclohexane ion undergoes rearrangement before undergoing low energy fragmentation processes, but maintains the parent structure in high energy dissociations [12].

This mechanism, of course, assumes that 1-$C_4H_8^+$ ions can isomerize to other structures, contrary to the observation reported earlier that when 1-$C_4H_8^+$ ions are formed by photolyzing 1-C_4H_8 with 10 eV photons, isomerization processes are not observed [12]. In order to check on this, 1-C_4H_8 was photolyzed in the presence of dimethylamine with 10 eV and with 11.6–11.8 eV photons; the yields of the 2-$C_4H_8^+$ ions intercepted (reaction 2) are given in table 2. (Analysis of *i*-C_4H_8

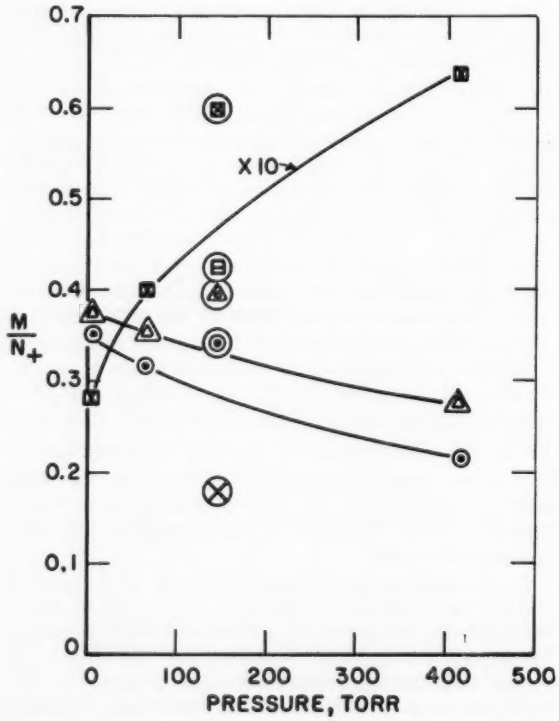

FIGURE 10. *The effect of pressure on the yields of intercepted* (i-$C_4D_8^+$ + 1-$C_4D_8^+$) *ions* (⊠), 2-$C_4D_8^+$ *ions* (⊙), *and total* $C_4D_8^+$ *ions* (▲) *in the radiolysis of a* c-C_4D_8-$(CH_3)_2NH$ (1:0.08) *mixture in the presence of oxygen.*

Encircled points show, for comparison, the yields of i-$C_4D_8^+$ (X), 1-$C_4D_8^+$ (⊟), 2-$C_4D_8^+$, total $C_4D_8^+$, and the sum (i-$C_4D_8^+$ + 1-$C_4D_8^+$) intercepted by 5 percent methylcyclopentane in the radiolysis of c-C_4D_8.

TABLE 2. *The photolysis of butene-dimethylamine (1:1) mixtures at a pressure of 2 torr; the interception of* 2-$C_4H_8^+$ *ions*

	$M/N_+(2\text{-}C_4H_8^+)$	
	10.0 eV	11.6–11.8 eV
1-C_4H_8	0.05	0.63
1-C_4H_8 + 180 torr Ne		.52
i-C_4H_8	.002	.050
i-C_4H_8 + 130 torr Ne		.025

could not be carried out.) It is seen that, indeed, when the ions are formed by absorption of 10 eV photons, isomerization to the 2-$C_4H_8^+$ structure is unimportant, but when the photon energy is raised to 11.6–11.8 eV, at a pressure of 2 torr more than half the ions do rearrange to the 2-$C_4H_8^+$ structure. Furthermore, the importance of this isomerization can be diminished by increasing the pressure, as was demonstrated by photolyzing the 1-C_4H_8-$(CH_3)_2NH$ mixture in the presence of added neon (table 2). Thus, the isomerization of the 1-$C_4H_8^+$ ion to the 2-$C_4H_8^+$ structure requires that the ions have excess energy; removal of energy by collisions diminishes the probability that the isomerization will occur. The $C_4H_8^+$ ions formed in ethylene and in cyclobutane will have at least 1.93 and 0.67 eV excess energy above the energy of the 1-$C_4H_8^+$ ion (table 1). It is easy to visualize plausible pathways by which such ions could rearrange to the 1-$C_4H_8^+$ structure; for instance:

$$c\text{-}C_4H_8^+ \rightarrow [+CH_2CH_2CH_2CH_2\cdot]^*$$

$$\rightarrow [CH_3\overset{+}{C}HCH_2CH_2\cdot]^*$$

$$\rightarrow CH_3CH_2CH^+=CH_2. \qquad (14)$$

Once the ion has attained the 1-$C_4H_8^+$ structure, the results indicate that it will continue to rearrange to the 2-$C_4H_8^+$ (and probably also to the *i*-$C_4H_8^+$) structure, unless sufficient energy is removed by collisions before these rearrangements occur, or unless the excited ion is intercepted before rearrangements occur. In order to distinguish between these two possible interpretations of the observed increase in the yield of 1-$C_4H_8^+$ ions intercepted as the pressure is increased, a series of radiolysis experiments was performed in which the concentration of dimethylamine added to *c*-C_4H_8 was varied at a pressure of 300 torr, where, as shown above (fig. 9) a significant yield of 1-$C_4H^+{}_8$ ions can be intercepted. If at high pressures, we are simply intercepting excited 1-$C_4H_8^+$ ions before they have time to isomerize, we should see the yield of intercepted ions increase as the concentration of dimethylamine is increased (i.e. as the time before interception is decreased), but if the ions are collisionally deactivated before interception, there should be little effect of interceptor concentration. The results (fig. 11) indicate that a change in interceptor concentration has, at most, only a slight effect on the ratio of 1-$C_4H_8^+$ to 2-$C_4H_8^+$ ions intercepted. The ratio 1-$C_4H_8^+$/2-$C_4H_8^+$ at 2 percent dimethylamine (where 1 collision in 49 is with interceptor) is only about 10 percent lower than at 16 percent dimethylamine (where 1 collision in 5 is with interceptor). We can conclude, then, that most of the 1-$C_4H_8^+$ ions intercepted have been collisionally deactivated.

If the isomerization mechanism proposed here is valid, then it would be expected that if one could form $C_4H_8^+$ ions having a somewhat lower initial energy than those generated in cyclobutane and ethylene, then the intermediate 1-$C_4H_8^+$ ion should be more easily deactivated. The methylcyclopropane ion is such an ion (table 1). Therefore, a methylcyclopropane-methylcyclopentane-d_{12} mixture was photolyzed with 11.6–11.8 eV photons in the presence of varying amounts of xenon (fig. 12). The methylcyclopropane ion apparently isomerizes through the same pathway(s) followed by the $C_4H_8^+$ ion generated in ethylene and by the cyclobutane parent ion. That is, at low pressures, all ions intercepted are in the *i*-$C_4H_8^+$ and 2-$C_4H_8^+$ configurations, with the latter predominating. As the pressure is increased the importance of the *i*-$C_4H_8^+$ ion diminishes relative to that of the 2-$C_4H_8^+$ ion, and eventually, the 1-$C_4H_8^+$ ion grows in at the expense of the *i*- and 2-$C_4H_8^+$ ions. Because the yields of ions intercepted were strongly dependent on the concentration of interceptor, suggesting that the ions react with the parent methylcyclopropane molecule, methyl-

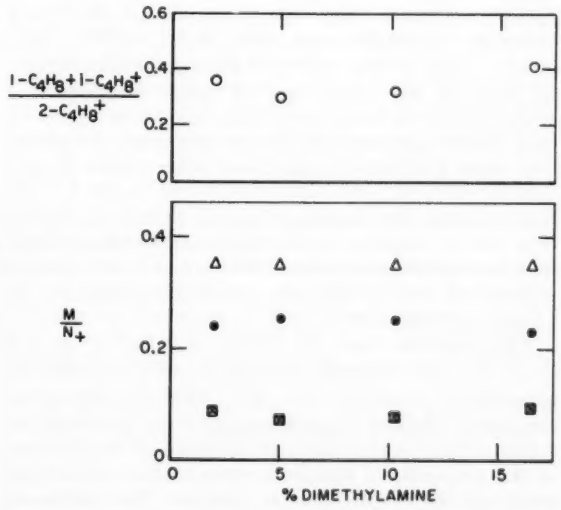

FIGURE 11. *The effect of dimethylamine concentration on the yields of intercepted* 2-$C_4H_8^+$ (●), 1-$C_4H_8^+$ + i-$C_4H_8^+$ (⊠), *and total* $C_4H_8^+$ (△), *as well as the ratio* (1-$C_4H_8^+$ + i-$C_4H_8^+$)/2-$C_4H_8^+$, *in the radiolysis of* c-C_4H_8-$(CH_3)_2NH$ *mixtures in the presence of oxygen at a total pressure of 300 torr.*

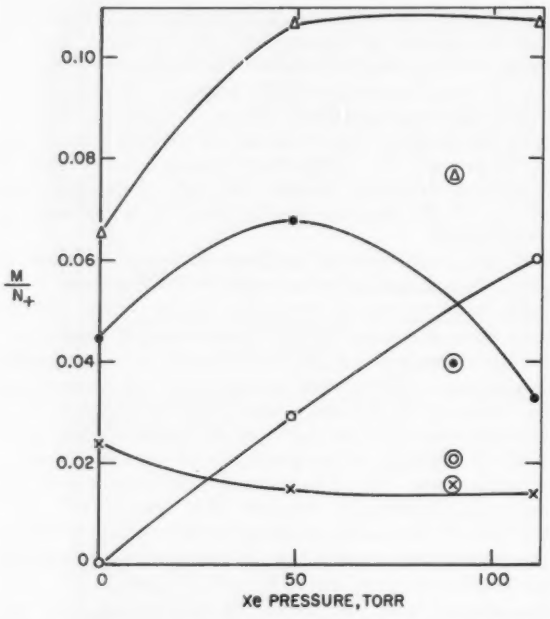

FIGURE 12. *The 11.6–11.8 eV photolysis of 2 torr of a methylcyclopropane-methylcyclopentane-d_{12} (1:0.12) mixture (in the presence of 3 percent oxygen), in the presence of added xenon.*

Points show the yields of i-$C_4H_8^+$ (X), 2-$C_4H_8^+$ (●), 1-$C_4H_8^+$ (○), and total $C_4H_8^+$ (△), derived from the yields of the appropriate butane products. Encircled points indicate an experiment performed in the presence of added helium.

cyclopropane was ionized with 11.6–11.8 eV photons in the NBS high pressure photoionization mass spectrometer. The $C_4H_8^+$ ion was seen to react with the parent molecules with a rate constant of 6×10^{-11} cm^3/molecule · s; product ions were $C_5H_{10}^+$ (69%), $C_5H_9^+$ (8.8%), $C_6H_{11}^+$ (8.0)%, $C_6H_{12}^+$ (7.6%), and $C_7H_{13}^+$ (6.6%). Because of the occurrence of these reactions, the actual yields of intercepted ions shown in figure 12 have little significance. It is important, however, that when 110 torr of xenon have been added, 56 percent of all $C_4H_8^+$ ions intercepted are in the 1-$C_4H_8^+$ configuration. By contrast, in the 11.6–11.8 eV irradiation of a similar cyclobutane-methylcyclopentane mixture in the presence of 150 torr of xenon, only 2 percent of the $C_4H_8^+$ ions intercepted are in the 1-$C_4H_8^+$ configuration.

The question may be raised of whether or not the $C_4H_8^+$ ions initially formed in ethylene and cyclobutane isomerize to the methylcyclopropane structure. Methylcyclopropane was not observed as a product in the photolysis or radiolysis of cyclobutane in the presence of charge acceptor. However, in the photolysis of cyclobutane at relatively low pressures (0.1–10 torr) in the presence of methylcyclopentane as an interceptor (fig. 4), methylcyclopropane was seen as a product. This product was not seen in the photolysis of a similar mixture below the ionization potential (i.e., at 10 eV), so it may be inferred that it has an ionic precursor. It is feasible that excited methylcyclopropane ions may undergo charge transfer with methylcyclopentane [24], but undergo ring opening when colliding with polar molecules such as dimethylamine. At any rate, the yield of the methylcyclopropane product (fig. 4) is strongly diminished by an increase in pressure, and has essentially vanished at a pressure of 10 torr; if this product does reflect the yield of methylcyclopropane ions in the system, one must conclude that ring closure in the excited $C_4H_8^+$ ions is a slow process which is readily quenched by collisions.

No methylcyclopropane was formed in any ethylene experiment, either in pure ethylene or in the presence of dimethylamine or of methylcyclopentane. A recent paper [25] reports that methylcyclopropane is formed in the 10.2 eV photolysis of ethylene through a reaction of an excited C_2H_4 species with ethylene. A careful examination of the products formed in the 10.0 eV photolysis of ethylene failed to confirm the presence of this product. The quantum yield of this product must be less than 2×10^{-4}.

The results given above demonstrate that at low pressures most of the $C_4H_8^+$ ions formed in ethylene and cyclobutane end up in the i- and 2-$C_4H_8^+$ structures, and that the isomerization to the i-$C_4H_8^+$ structure occurs from some excited entity which, after undergoing collisions, has a lowered probability of rearranging to the i-$C_4H_8^+$ structure and an increased probability of ending up in the 2-$C_4H_8^+$ structure. This excited precursor of the i-$C_4H_8^+$ ion is most likely the 1-$C_4H_8^+$ ion, but we can not exclude the possibility that some of the i-$C_4H_8^+$ may have the 2-$C_4H_8^+$ ion as precursor although this is probably unlikely. Taking the ratio i-$C_4H_8^+$/2-$C_4H_8^+$ as an approximate measure of the energy of the ions under given conditions, we see from the results given in table 3 that, as one would expect, at a given pressure the internal energy content of an ion is lower for ions with a lower initial energy. It is interesting that for $C_4H_8^+$ ions formed in ethylene, the average energy of the ion at a given pressure is much greater in the radiolysis than in the photolysis experiments. This probably reflects the fact that in the photolysis, these ions can be formed with, at most 1 eV excess energy, while in the

TABLE 3. *The ratio of intercepted isobutene to 2-butene ions as a function of the energy with which the ion is initially formed*

Ion Source	Ion minimum initial energy	i-$C_4H_8^+$/2-$C_4H_8^+$ (or i-$C_4D_8^+$/2-$C_4D_8^+$)	
		10 torr	50 torr
C_2H_4 Radiolysis	11.51 eV	[a] 0.5–1.0	[a] 0.3 ~ 0.7
C_2H_4 Photolysis		~.26	.08
c-C_4H_8 Radiolysis	10.84 eV	.13	.07
c-C_4H_8 Photolysis		~.13	~.07
c-C_4D_8 Photolysis		.09	...

[a] Nitric oxide additive experiments give the low values, and dimethylamine additive experiments give the high values.

radiolysis much higher energy ethylene ions may be formed and undergo reaction 1; the ethylene ion does not fragment unless it has 2.9 eV excess energy). In the cyclobutane experiments on the other hand, the results given in table 3 indicate that the ions are formed with about the same energy in the photolysis and radiolysis. This is not surprising, since in cyclobutane the onset of fragmentation is only about 0.7 eV above the ionization potential, so there is less likelihood for very energetic ions to survive as $C_4H_8^+$ species.

Further corroborative evidence for the mechanism proposed here is given by the isotope effects observed in some of the experiments reported above. for instance, in figure 2, it is seen that the yield, relative or absolute, of the isobutene ion intercepted in c-C_4D_8 is lower than that intercepted in c-C_4H_8, even though the pressure of the C_4D_8 experiments is less than half that of the C_4H_8 experiments. The results shown in figure 4 demonstrate that the pressure effect on the relative yield of the isobutene ion is indeed much more pronounced for the deuterated cyclobutane molecule than for the nondeuterated. It is to be expected that the deuterated ion would lose energy through collisions more readily than the nondeuterated ion, because of a closer spacing of vibrational levels in the excited deuterated species.

Finally, one must ask whether the i-$C_4H_8^+$ and 2-$C_4H_8^+$ ions, once formed, undergo any further rearrangements. In order to obtain a partial answer to this question, i-C_4H_8 was photolyzed with 10 eV and with 11.6–11.8 eV photons in the presence of dimethylamine; the results are given in table 2. It was seen that in the 10 eV photolysis, isomerization of the i-$C_4H_8^+$ ion to the 2-$C_4H_8^+$ structure is negligible, as reported before. When the energy of the photons was raised, 5 percent of the i-$C_4H_8^+$ ions were seen to isomerize to the 2-$C_4H_8^+$ structure. This rearrangement was, however, quenched by the addition of neon. A more detailed discussion of the isomerization reactions and pressure effects of $C_4H_8^+$ ions generated in butenes will be presented elsewhere [26].

5. Collisional Deactivation of Intermediate $C_4H_8^+$ Ions by Added Gases

It is of interest, to examine the relative efficiencies of various gases in removing energy from the excited intermediate ion(s). Therefore, a c-C_4H_8-c-$C_5D_9(CD_3)$ (1:0.05) mixture, with 3 percent oxygen added as a radical scavenger, was irradiated with 11.6–11.8 eV photons in the presence of varying amounts of helium, hydrogen, neon, nitrogen, krypton, xenon, and carbon dioxide. (As mentioned above, 1-$C_4H_8^+$ ions are not observed to any significant extent in these experiments; in the presence of 150 torr of xenon, only 2 percent of the $C_4H_8^+$ ions intercepted are in the 1-$C_4H_8^+$ structure.) The overall product yields observed in the nitrogen and neon additive experiments are given in table 4. As above, the ratio i-$C_4H_8^+$/2-$C_4H_8^+$ was taken as an approximate measure of the deactivation of the ions. It was noted that the extent of lowering of the ratio at a given pressure seemed to depend approximately on the polarizability of the deactivating gas but was not apparently related to any other parameter (such as the rate of collision, the mass of the neutral species, etc.); this is shown in figure 13 for experiments in which 8 torr, 20 torr, and 50 torr of deactivator have been added to 0.2 torr of the hydrocarbon mixture. Thus, from these results we can conclude that the effectiveness of energy transfer from the excited ion to the collision partner depends on the polarizability of the added gas. This is not surprising, since it might be expected that a collision with a more polarizable species would be more "sticky" and that such "sticky" collisions would facilitate energy transfer.

A quantitative treatment of the data for these experiments is not actually feasible at the present time. That is, the relevant detailed mechanisms and unimolecular

TABLE 4. *The 11.6–11.8 eV photolysis of 0.2 torr of a cyclobutane-methylcyclopentane-d_{12}-O_2 (1:0.05:0.04) mixture in the presence of added unreactive gases*

Additive	Relative polarizability	Pressure torr	Quantum yields							$\frac{i\text{-}C_4H_{10}}{n\text{-}C_4H_{10}}$
			Ethylene	Acetylene	i-C_4H_{10}	n-C_4H_{10}	c-$C_3H_5(CH_3)$	i-C_4H_8 + 1-C_4H_8	2-C_4H_8	
None	.....	0.2	0.56	0.35	0.094	0.30	0.046	0.017	0.031	0.313
Neon	0.392	20.	.57	.34	.068	.33	.028	.014	.016	.206
		105.	.58	.33	.059	.41	.018	.018	.024	.143
		398.	.59	.32	.045	.44	.0058	.023	.028	.102
Nitrogen	1.730	8.	.57	.34	.073	.35	.029	.014	.0082	.209
		20.	.56	.35	.068	.35	.013	.011	.013	.194
		105.	.58	.33	.051	.41	.0086	.028	.024	.124
		345.	.61	.30	.020	.28	.000	.029	.015	.072

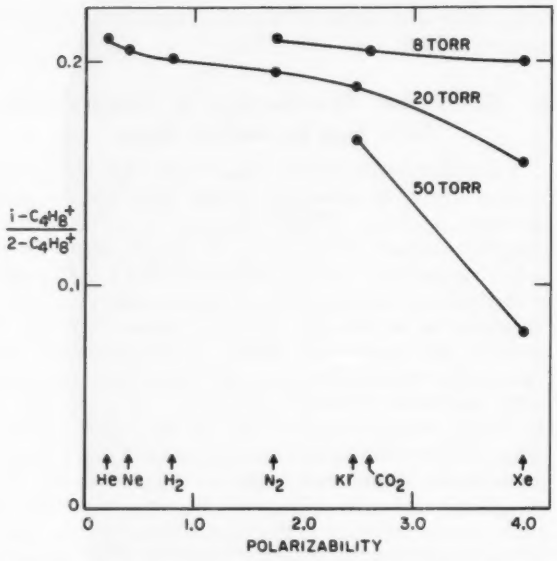

FIGURE 13. *The ratio of* i-$C_4H_8^+$/2-$C_4H_8^+$ *intercepted by 5 percent methylcyclopentane-*d_{12} *in* c-C_4H_8 *irradiated with 11.6–11.8 eV photons at a pressure of 0.2 torr in the presence of 8, 20, or 50 torr of added foreign gas plotted as a function of the polarizabilities of the added compounds.*

rate constants for the isomerization reactions to form i-$C_4H_8^+$ and 2-$C_4H_8^+$ are not only unknown, but dependent on the internal energy of the rearranging species. It is not possible now to estimate the energy or the energy distribution of these excited entities.

Similar experiments examining the deactivation of the $C_4H_8^+$ ions formed in the ethylene system would be quite difficult to interpret, since the precursor $C_2H_4^+$ ions would also be deactivated by the added gases, thus shifting the energy distribution of the product $C_4H_8^+$ ions toward lower energies. Therefore, any effects observed would be composites of the deactivation of the $C_2H_4^+$ ions and the $C_4H_8^+$ ions. Ethylene ions formed at 11.6–11.8 eV do have excess internal energy which is retained in the product $C_4H_8^+$ ions. Indeed, it has been seen [18b] that the relative importance of dissociation processes 11 and 12 differs for $C_4H_8^+$ ions formed in ethylene irradiated with 10.0 and with 11.6–11.8 eV photons.

The authors thank L. Wayne Sieck for performing the mass spectrometric experiments reported here, and R. E. Rebbert for his assistance with some of the photolysis experiments.

6. References and Notes

[1] Ausloos, P., in Ion Molecule Reactions, J. L. Franklin, Ed., (Plenum Press, New York, N.Y., 1970).

[2] Olah, G. A., and von R. Schleyer, P., Carbonium Ions, Vol. **II**, (Interscience, New York, N.Y., 1970).

[3a] Karabatsos, G. J., Orzech, C. E., Jr., Fry, J. L., and Meyerson, S., J. Am. Chem. Soc. **92**, 606 (1970).

[3b] Karabatsos, G. J., Fry, J. L., and Meyerson, S., ibid. **92**, 614 (1970).

[3c] Karabatsos, G. J., Hsi, N., and Meyerson, S., ibid. **92**, 621 (1970).

[3d] Karabatsos, G. J., Mount, R. A., Rickter, D. O., and Meyerson, S., ibid. **92**, 1248 (1970).

[4] Lias, S. G., Rebbert, R. E., and Ausloos, P., ibid. **92**, 6430 (1970).

[5a] Eadon, G., Diekman, J., and Djerassi, C., ibid. **92**, 6205 (1970).

[5b] Wilkins, C. L., and Gross, M. L., ibid. **93**, 895 (1971), and references cited therein.

[6a] Meisels, G. G., J. Chem. Phys. **42**, 3237 (1965).

[6b] Meisels, G. G., Adv. in Chem. **58**, 243 (1966).

[6c] Gorden, R., Jr., and Ausloos, P., J. Chem. Phys. **47**, 1799 (1967).

[7] Doepker, R. D., and Ausloos, P., ibid., **44**, 1641 (1966).

[8] Doepker, R. D., and Ausloos, P., ibid., **43**, 3814 (1965).

[9] Hughes, B. M., and Tiernan, J. O., ibid., **51**, 4373 (1969).

[10] Sieck, L. W., Searles, S. K., and Ausloos, P., J. Am. Chem. Soc. **91**, 7627 (1969).

[11] Gill, P. S., Inel, Y., and Meisels, G. G., J. Chem. Phys. **54**, 2811 (1971).

[12] Lias, S. G., and Ausloos, P., J. Am. Chem. Soc. **92**, 1840 (1970).

[13] Lias, S. G., and Ausloos, P., J. Chem. Phys. **43**, 2748 (1965).

[14] Gorden, R., Jr., Rebbert, R. E., and Ausloos, P., Nat. Bur. Stand. (U.S.), Tech. Note 496, 55 pages (Oct. 1969).

[15a] Ausloos, P., Rebbert, R. E., and Lias, S. G., J. Phys. Chem. **72**, 3904 (1968).

[15b] Ausloos, P., and Lias, S. G., Rad. Res. Rev. **1**, 75 (1968).

[16] Herman, J., Herman, K., and Ausloos, P., J. Chem. Phys. **52**, 28 (1970).

[17] Sieck, L. W., and Searles, S. K., J. Am. Chem. Soc. **92**, 2937 (1970).

[18a] Tiernan, T. O., and Futrell, J., J. Phys. Chem. **72**, 3080 (1968).

[18b] Sieck, L. W., private communication.

[18c] Meisels, G. G., Park, J. Y., and Geissner, B. G., J. Am. Chem. Soc. **92**, 254 (1970).

[19] Natalis, P., Steiner, B., and Inghram, M. G., private communication.

[20] That this n-butane product does originate largely from reaction of the 1-$C_4H_8^+$ ion with cyclohexane was confirmed in an experiment in which c-C_4D_8 was irradiated in the presence of c-C_6H_{12} at a pressure of 300 torr, and the n-butane product was analyzed isotopically. The n-butane indeed consisted mainly of $CD_2HCDHCD_2CD_3$ from a reaction analogous to 9 but with the deuteration reversed. A small amount of n-C_4D_{10} was also observed. The yield of this product ($M/N_+ \approx 0.004$) corresponded approximately to the yields of n-butane which are observed in all cyclobutane experiments in which the butane-forming H_2^- (D_2^-) transfer reactions are absent. The mode of formation of the n-C_4D_{10} is unknown, but its yield is so small that it constitutes only a small fraction of the n-butane formed through H_2^- (D_2^-) transfer reactions in the presence of methylcyclopentane or cyclohexane.

[21] Holroyd, R. A., and Fessenden, R. W., J. Phys. Chem. **67**, 2743 (1963).

[22] Gorden, R., Jr. and Ausloos, P., J. Res. Nat. Bur. Stand. (U.S.), **75A** (Phys. and Chem.), No. 3, 141–146 (May-June 1971).

[23] Lias, S., Ph.D. Thesis, American University (1971).

[24] The enthalpy of this charge transfer reaction can not be calculated exactly since the heat of formation of the methylcyclopentane ion is unknown. However, from the observation made during the course of this study that methylcyclopentane is not ionized by 10.0 eV photons, we can assign a minimum value of 8.85 eV to its heat of formation. Therefore, the postulated charge transfer with methylcyclopropane ions is endothermic by at least 0.1 eV. If the

reaction does occur in the experiments reported here, it must involve excited methylcyclopropane ions.
[25] Inel, Y., Siddiqi, A., and Meisels, G. G., J. Phys. Chem. **75,** 1317 (1971).
[26] Ausloos, P., Lias, S. G., and Sieck, L. W., NBS J. Res., to be published.

(Paper 75A6–691)

JOURNAL OF RESEARCH of the National Bureau of Standards—A. Physics and Chemistry
Vol. 75A, No. 6, November-December 1971

The Photochemistry of Propane at High Photon Energies (8.4-21.2 eV)*

R. E. Rebbert, S. G. Lias, and P. Ausloos

Institute for Materials Research, National Bureau of Standards, Washington, D.C. 20234

(June 28, 1971)

Neon and helium resonance lamps, which deliver photons of 16.7–16.8 eV and 21.2 eV energy, respectively, have been used to photolyze C_3H_8, C_3D_8, C_3H_8-C_3D_8 (1:1) mixtures, and $CD_3CH_2CD_3$ and the results obtained at the two energies are compared. In particular, it is noted that although the quantum yield of ionization in propane is unity at 16.7–16.8 eV, when the energy is raised still further to 21.2 eV, the probability of ionization apparently diminishes to 0.93, an observation which suggests that at 21.2 eV, superexcited states may be reached whose dissociation into neutral fragments competes with ionization.

The quantum yields of the lower hydrocarbon products formed in the presence of a radical scavenger in C_3H_8 and C_3D_8 are reported, and are compared with quantum yields of products formed in the vacuum ultraviolet photolysis at lower energies. (Quantum yields of products formed at 8.4 eV and 10.0 eV are reported here for the first time.) Acetylene is formed as a product in the decomposition of the neutral excited propane molecule, and its yield increases in importance with increasing energy; at 16.7–16.8 eV, where all product formation can be traced to ionic processes, acetylene is formed in negligible yields. It is concluded that ionic processes in propane do not lead to the formation of acetylene, and the observation of this product in radiolytic systems may be a reliable indicator of the relative importance of neutral excited molecule decomposition processes.

From the results obtained with the C_3H_8-C_3D_8 (1:1) mixture, and with $CD_3CH_2CD_3$, details of the ion-molecule reaction mechanisms and the unimolecular decomposition of the propane ion are derived.

Key words: Ion-molecule reaction; photoionization; propane; quantum yields; rare-gas resonance radiation; unimolecular dissociation.

1. Introduction

In the past, most photolysis studies in the vacuum ultraviolet region have been carried out at energies below 11.8 eV (104.8 nm). The lamps commonly used in this energy region are rare gas resonance lamps, which deliver the resonance lines of xenon (8.4 eV, 147.0 nm), krypton (10.0 eV, 123.6 nm), or argon (11.6–11.8 eV, 106.7–104.8 nm). Higher energy resonance lamps could not be made because of the lack of suitable windows which would transmit photons above 11.8 eV in energy. Recently, in this laboratory, enclosed neon and helium lamps have been fabricated; their operational characteristics have been described in detail [1].[1] These lamps, which deliver the neon and helium resonance lines (16.7–16.8 eV and 21.2 eV, respectively), are fitted with windows made of thin (2000–4000 Å) films of aluminum.

Photolysis studies in this high energy region are, of course, still very rare. Only a few studies, limited in scope, of the chemical effects brought about in methane [2–4] and in argon-propane mixtures [5] by helium resonance radiation have been published. One of these studies [2] was carried out with a differentially pumped windowless helium lamp; under such conditions, the investigator is restricted to a low pressure range. No studies at pressures above the millitorr range utilizing neon resonance radiation have so far appeared in the literature.

This paper reports the results of a study where, for the first time, a compound is exposed to both neon and helium resonance radiation, and the chemical effects at the two energies are compared. Propane was chosen as the subject compound because the unimolecular and bimolecular (ionic and free radical) processes occurring in this system have been extensively investigated [6] and are well understood. In the high energy region used in this study, chemical effects will be brought about nearly exclusively through ionic processes. A comparison of the effects brought about by photons of two different energies may highlight subtle differences, and, therefore, increase our understanding

*Supported in part by the U.S. Atomic Energy Commission, Washington, D.C. 20545
[1] Figures in brackets indicate the literature references at the end of this paper.

of the activation processes in the high energy range. These results should also be of value in interpreting results obtained in systems exposed to high energy radiation (x rays, gamma rays, energetic electrons, etc.) where end product formation is brought about not only through ionic processes similar to those observed here, but also through the unimolecular decomposition of superexcited molecules.

2. Experimental Procedure

The reaction vessel and the resonance lamps used in this study have been described before [1]. Both the neon and helium resonance lamps were provided with 2000 Å aluminum windows which were entirely leak-free, and could withstand a pressure differential between the reaction vessel and the interior of the resonance lamp of 100 torr or more. At the start of the study the photon flux of the helium and neon resonance lamps was, respectively, 5×10^{13} and 7×10^{12} quanta/s. It was ascertained that the helium and neon lamps were essentially monochromatic throughout the study by introducing neon and helium, respectively, into the first compartment of a double cell arrangement described before [1]. It was ascertained that neon gas placed in the sample cell absorbed the neon resonance radiation and was transparent to the radiation emanating from the helium lamp, while helium was transparent to the photons from the neon lamp and absorbed those from the helium lamp. In the course of an experiment, either at the neon or the helium line, the decay in the light flux was no more than five percent from beginning to end.

The analytical procedures, as well as the purification of the materials used in this study, have been described [7].

In most experiments, quantum yield determinations of the end product were made which were based on saturation ion currents measured periodically during the course of an irradiation [1, 7]. In these experiments, approximately 15 torr of a nonabsorbing inert gas (helium in the neon resonance line experiments, and vice versa) was added; it has been shown that the addition of such an inert will generally improve the definition of the plateau of the saturation ion current [1, 8], and therefore lead to a more accurate determination of the quantum yields of the end products formed in the photolysis.

Allene and methylacetylene were noted as products at 8.4 to 11.8 eV, but their quantum yields were not determined.

3. Results and Discussion

3.1. Units

In a photolysis experiment carried out at an energy below the ionization energy of the compound of interest, a quantum yield of a given product, Φ, is simply the probability that the particular product will result when an excited molecule undergoes unimolecular decomposition in the system under a particular set of conditions. In photoionization experiments, where some quanta produce ions, it has been found convenient in the past [7] to use two systems of units depending on whether a process involving a neutral excited molecule or an ionic process is being considered. Thus, the yields of products resulting fron nonionic processes were expressed in units of $M(X)/N_{ex}$, or molecules M of product X formed per neutral excited molecule dissociating in the system, N_{ex}; for photolysis in the subionization region $M(X)/N_{ex}$ is simply the quantum yield. Ionic product yields, on the other hand, have generally been expressed in ion pair yield units, that is, as $M(X)/N_+$, or molecules M of product X formed per positive ion formed in the system, N_+.

Experimentally, an ion-pair yield is easily measured since N_+ is directly determined by measuring the saturation ion current:

$$N_+ = I\times t(\mathrm{s})\times 6.24\times10^{18}\ \mathrm{ions/C}$$

(where I is the saturation ion current in amps and C is coulombs). If the quantum yield of ionization, Φ_+, is known, then $M(X)/N_{ex}$ can be determined from the relationship:

$$\frac{M(X)}{N_{ex}}=\frac{M(X)}{N_+}\times\Phi_+\times\frac{1}{1-\Phi_+}=\Phi\times\frac{1}{1-\Phi_+}$$

The overall quantum yield is thus:

$$\Phi=\frac{M(X)}{N_{ex}+N_+}$$

In this paper, we are concerned mainly with results obtained at very high energies where all, or almost all, product formation results from ionic processes; under these conditions the quantum yields and ion pair yields are essentially identical. The products formed at these energies are, however, compared with products observed in the photolysis at lower energies. All product yields are expressed in quantum yield units. Thus, in the 8.4 and 10.0 eV experiments, no ionization occurs, and there is no complication about the yield units. At 11.6–11.8 eV, on the other hand, only 73 percent (table 1) of the quanta absorbed lead to neutral excited molecule formation. Therefore, an

TABLE 1. *Ionization quantum yields and extinction coefficients of propane* [a]

Photon energy	ϵ cm^{-1}atm^{-1}	Φ_+
11.6–11.8 eV	n.d.	0.27 [b]
16.7–16.8 eV	2950	1.00
21.2 eV	2240	0.93

[a] Argon lamp: 70 percent 11.6 eV, 30 percent 11.8 eV.
[b] C. E. Klots, to be published.

estimation of the probability that the decomposition of the superexcited propane molecule formed at this energy would lead to the formation of a given product requires that the overall quantum yields be divided by 0.73; the quantum yields can be translated into ion pair yields, if the product of interest is of ionic origin, by dividing by 0.27.

3.2. Ionization Quantum Yields

In table 1 are given the extinction coefficients and ionization quantum yields of propane at the argon, neon, and helium resonance lines, 11.6–11.8 eV (106.7–104.8 nm), 16.7–16.8 eV (74.4–73.6 nm) and 21.2 eV (58.4 nm), respectively [8]. It is noteworthy that when the photon energy is increased from 11.6–11.8 eV to 16.6–16.7 eV, the quantum yield of ionization increases from 0.27 to a value of unity, but when the photon energy is further increased to 21.2 eV, the quantum yield of ionization seems to decrease to a value lower than unity. The value reported for 21.2 eV is based on the saturation ion current measurements shown in figure 1. At this wavelength, hydrogen has an ionization quantum yield of unity [8–10]; because at the helium resonance line, hydrogen has a low extinction coefficient [8, 9, 11] ($\epsilon = 185$), the saturation current measured in hydrogen has a well defined plateau extending over a range of several hundred volts (fig. 1). Therefore, the hydrogen saturation ion current is an ideal standard against which to compare saturation ion currents measured in other compounds at the same light flux. Under pressure conditions where all incident photons are absorbed, the quantum yield of ionization of the unknown is given simply by the ratio of the two platueu values of the saturation ion current measurements. As the figure clearly shows, the plateau of the saturation ion current measured in propane at this energy is not as well defined as that for hydrogen, but seems to fall below the plateau measured in hydrogen.

A recent study from this laboratory [8] reported that the ionization quantum yields of C_1 to C_4 alkanes at the neon resonance lines (16.7–16.8 eV) are all unity. The apparent drop in the importance of ionization in propane as the energy is raised to 21.2 eV is also observed in these other alkanes [12, 13]. This is an interesting observation which, if correct, suggests that in alkanes which have absorbed a 21.2 eV photon, superexcited states may be reached which dissociate so rapidly that decomposition can compete with ionization. Overall product distributions such as those shown in the table do not, of course, in themselves give us much information about photolytic mechanisms. Additional information, such as that obtained from deuterium labeling experiments is required in order to trace the modes of formation of a given product. Such experiments have demonstrated [17–19] that neutral excited propane molecules undergo the following primary processes:

$$C_3H_8^* \rightarrow C_2H_6 + CH_2 \quad (1)$$

$$\rightarrow CH_4 + C_2H_4 \quad (2)$$

$$\rightarrow H_2 + C_3H_6 \quad (3)$$

$$\rightarrow CH_3 + C_2H_5 \quad (4)$$

$$\rightarrow H + C_3H_7 \quad (5)$$

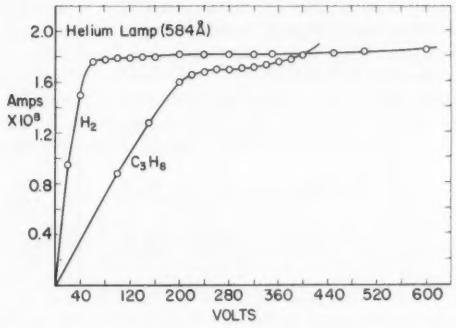

FIGURE 1. *Saturation ion currents measured in 5 torr of hydrogen and in 0.2 torr of C_3H_8 in the presence 20 torr of helium, irradiated with the 21.2 eV helium resonance line.*

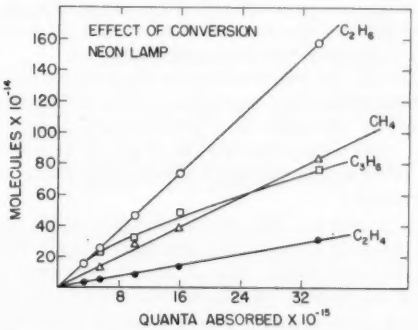

FIGURE 2. *Molecules of ethane, methane, propylene, and ethylene formed in the 16.7–16.8 eV photolysis of a propane-oxygen-helium (1.0:0.03:8.3) mixture at a total pressure of 28 torr, as a function of the number of quanta absorbed by the propane.*

3.3. Photolytic Product Yields

Figure 2 shows the number of molecules of various lower hydrocarbon products formed as a function of the number of 16.7–16.8 eV quanta absorbed in a propane-oxygen-helium (1.0:0.03:8.3) mixture at a propane pressure of 3 torr. The amounts of the methane, ethane, and ethylene products formed increase linearly with the number of photons absorbed. Propylene, on the other hand, does not show such a linear relationship. This behavior may be accounted for by several factors. For instance, it has been shown before [5] that one precursor of propylene in propane is the propyl ion, and this ion may react with accumulated products at high conversions. Another plausible

TABLE 2. *Quantum yields of end products in the photolysis of* C_3H_8

Photon energy	Propane	Scavenger	Methane	Acetylene	Ethylene	Ethane	Propylene
8.4 eV	C_3H_8	O_2	0.040	0.028	0.080	0.015	0.23
10 eV	C_3H_8	O_2	.115	.073	.22	.043	.17
11.6–11.8 eV	C_3H_8	O_2	.22	.22	.27	.0585	.13
16.7–16.8 eV	C_3H_8	O_2	.27	.001	.084	.46	.32
		NO	.29	.001	.072	.42	.36
	C_3D_8	O_2	.29	.001	.052	.43	.14
		NO	.27	.001	.060	.48	.23
21.2 eV	C_3H_8	O_2	.29	.018	.113	.37	.405
		NO	.27	.018	.13	.37	.40
	C_3D_8	O_2	.28	.023	.092	.41	.23
		NO	.31	.020	.095	.40	.24

Pressure = 3.0 torr.

explanation of the fact that the propylene yield drops off at high conversions is that propylene product may be removed by reaction with ions or H atoms in the system. It has been shown [15, 16] that H atoms add to propylene faster than to ethylene or acetylene. Apparently, at the relatively low pressures at which the experiments are carried out, oxygen is not a very effective interceptor of hydrogen atoms.

In table 2, the experiments were carried out under conditions where no more than 3×10^{15} quanta were absorbed by propane at a pressure of 3 torr in the reaction cell. Thus, the yields of propylene shown in table 2 have not been much affected by these secondary processes.

Table 2 shows the quantum yields of products formed in C_3H_8 and C_3D_8 irradiated with 8.4, 10.0, 11.6–11.8, 16.7–16.8, and 21.2 eV photons in the presence of 5 percent O_2 or NO added as a radical scavenger. As the photon energy is increased the amount of energy to be distributed among the fragments will be larger and secondary decompositions will become more prevalent. For instance the formation of acetylene, whose quantum yield of production is seen to increase with energy from 8.4 to 11.6–11.8 eV, can be attributed to the decomposition of C_2H_4 and C_3H_6 formed in primary processes 2 and 3 respectively. It is of interest that at 16.7–16.8 eV, where only ionic processes lead to end product formation, the quantum yield of acetylene is negligible (~0.001). This observation is not unexpected because as shown by Cermak and Herman [20] none of the fragmentation processes of the $C_4H_8^+$ ion formed by collision with metastable neon atoms yields C_2H_2 as a neutral product. Furthermore, there are no known ion-molecule reactions involving fragments from $C_3H_8^+$ which would ultimately result in the formation of C_2H_2 [21–27].

Thus, the result that acetylene formation from ionic processes (i.e., in the 16.7–16.8 eV photolysis) in propane is negligible, confirms the assumption made earlier [18], that all acetylene formed in the radiolysis of propane has neutral excited propane molecules, rather than ions, as precursor. The estimate that the ratio of neutral excited molecule formation to ionization is 0.4 in the radiolysis of propane [18], based on this assumption is, thus, probably approximately correct.

Considering that acetylene formation can apparently all be ascribed to a neutral excited propane precursor, it is interesting that the yield of acetylene increases ten-fold when the photon energy is raised from 16.7–16.8 eV to 21.2 eV (table 3). This is in agreement with the tentative conclusion reached above, that at 21.2 eV as many as 7 percent of the activated species may dissociate as neutral excited molecules before an electron can be ejected.

It is of interest to note that according to the quantum yield data given in table 2, the probability of the elimination of an alkane from neutral excited propane (processes (1) and (2)) increases with the energy of the photon [28]. The increase probably occurs at the expense of the H_2 elimination process (3). In a recent study on the far ultraviolet photolysis of ethane [29] a similar trend was seen. In that case, however, all molecular elimination processes decrease at the expense of direct bond cleavage processes as the energy is increased further. Similar trends can be expected for propane. The data given in table 2 do not allow a more detailed analysis of the primary processes occurring in propane in the 8.4–11.8 eV energy range. Quantum yields of all free radicals have to be known as well. A partial analysis of the role of free radicals in the decomposition of neutral excited propane is given elsewhere [18, 19, 30, 31].

3.4. Isotopic Labeling Experiments

In table 3 are given the isotopic distributions of the major lower hydrocarbon products formed in the photolysis of a C_3H_8-C_3D_8 (1 : 1) mixture in the presence of a radical scavenger with 16.7–16.8 and 21.2 eV photons.

The product ethane is known [5, 27, 32] to be formed in the reactions of ethyl ions with propane:

$$C_2D_5^+ + C_3H_8 \rightarrow C_2D_5H + C_3H_7^+ \quad (6)$$

and in the ethylene ion reaction:

$$C_2D_4^+ + C_3H_8 \rightarrow C_2D_4H_2 + C_3H_6. \quad (7)$$

It can be estimated from the relative amounts of C_2D_5H and $C_2D_4H_2$ formed in these experiments at 16.7–16.8 eV, that about 75 percent of the ethane resulted from the ethyl ion reaction, and about 25 percent from the ethylene ion reaction. On this basis, since the ethyl ion does not undergo any alternate reactions with propane [27] we can estimate roughly that the ion pair yield of the ethyl ion in the 16.7–16.8 eV photolysis of propane is about 0.32–0.34; the ion pair yield of this ion observed in the mass spectrometric study in which propane ions were generated by collision with metastable neon atoms [20] was 0.37. Using the same reasoning, it can be estimated that at 21.2 eV, 89 percent of the ethane originates from the reaction of an ethyl ion precursor. This gives an approximate ion pair yield for the ethyl ion in the photolysis at 21.2 eV of ~ 0.33; when $C_3H_8^+$ ions are generated in a mass spectrometer through collision with metastable helium atoms [20], the ion pair yield of ethyl ions observed was 0.25.

TABLE 3. *Photolysis of* C_3H_8-C_3D_8 *(1:1); isotopic compositions of products*

Photon Energy	Ethanes			Methanes	Propylenes	Ethylenes
	C_2D_6	C_2D_5H	$C_2D_4H_2$	CD_3H/CD_4	C_3D_5H/C_3D_6	C_2D_3H/C_2D_4
16.7-16.8 eV	1.00	0.75	0.25	0.057	0.32	0.63
21.2 eV	1.00	.95	.12	.051	.33	.46

Prescure = 3 torr.
5 percent O_2 added.

The yields of ethanes formed in reactions such as 7 from ethylene ion precursors do not directly give us the yield of the ethylene ion, since this ion can also undergo an H^- (or D^-) transfer reaction with propane:

$$C_2D_4^+ + C_3D_8 \rightarrow C_2D_5 + C_3D_7^+ \quad (8)$$

to form an ethyl radical, which in these experiments will be scavenged. However, in one experiment H_2S was added to C_3D_8 irradiated with 21.2 eV photons. In this system, the deuterated ethyl radical formed in reaction 8 will react with H_2S to form C_2D_5H:

$$C_2D_5 + H_2S \rightarrow C_2D_5H + HS \quad (9)$$

while all other ethane-forming reactions will give fully deuterated ethane, C_2D_6. From the observed yield of C_2D_5H, it could be deduced that for an ethylene ion reacting with propane-d_8, the ratio of D^-/D_2^- transfer reactions is 0.9. This value is in reasonably good agreement with the results of Sieck and Searles [33], who recently ascribed a value of 0.8 to this ratio on the basis of results obtained in the NBS high pressure photoionization mass spectrometer. (They found that the ratio of H^-/H_2^- transfer reactions for ethylene ions reacting with C_3H_8 was 1.15.) On this basis, we can estimate ion pair yields for the ethylene ion generated in the 16.7–16.8 eV photolysis or the 21.2 eV photolysis of propane of about 0.22 and 0.08, respectively. The corresponding ion pair yields of ethylene ions generated in a mass spectrometer by collision with metastable neon and helium atoms are 0.20 and 0.17.

Because the methane formed in the photolysis of C_3H_8-C_3D_8 (1:1) mixture contains very little partially deuterated product, it must be formed almost exclusively in the unimolecular decompositions:

$$C_3H_8^+ \rightarrow CH_4 + C_2H_4^+ \quad (10)$$

$$C_3H_7^+ \rightarrow CH_4 + C_2H_3^+. \quad (11)$$

Process (11) and/or further decomposition of $C_2H_4^+$ formed in process (10) must be of importance in view of the fact that the estimated quantum yields of $C_2H_4^+$ are lower than the quantum yield of molecular methane (table 2).

From studies on $CD_3CH_2CD_3$, the fragmentation of the propane ion to form an ethylene ion (process 10) is known to occur through two mechanisms. The lower energy process (A.P. = 11.8 eV) [34] is a 1,3 elimination of methane from the propane ion:

$$CD_3CH_2CD_3^+ \rightarrow CD_4 + CD_2CH_2^+ \quad (12)$$

and the higher energy process (A.P. = 12.2 eV) [34] is a 1,2 elimination:

$$CD_3CH_2CD_3^+ \rightarrow CD_3H + C_2D_3H^+. \quad (13)$$

It is of interest then that the observed ratio CD_3H/CD_4 (table 4) indeed increases from 0.69 at 16.7–16.8 eV to 0.76 at 21.2 eV. In an earlier study [34], it was noted that $CD_3CH_2CD_3^+$ ions generated by charge exchange with Xe^+ ions (12.1–13.4 eV) underwent processes 12 and 13 to give a CD_3H/CD_4 ratio of 0.35.

Because the ethylene and propylene contain large fractions of partially deuterated products (table 3), it is evident that an important mode of formation of these products is bimolecular ion-molecule reactions such as, for instance:

TABLE 4. *Photolysis of* $CD_3CH_2CD_3$; *isotopic composition of methane*

Photon Energy	CD_3H/CD_4
16.7–16.8 eV	0.69
21.2 eV	.76

Pressure = 3 torr.
5 percent O_2 added.

$$C_2D_3^+ + C_3H_8 \rightarrow C_2D_3H + C_3H_7^+ \quad (14)$$

$$C_3D_5^+ + C_3H_8 \rightarrow C_3D_5H + C_3H_7^+. \quad (15)$$

Reaction 14 is thought to proceed through formation of a condensation ion, $C_5D_3H_8^+$, which will dissociate to form other partially deuterated ethylenes besides C_2D_3H [27]. Reaction 15 is a simple hydride transfer reaction.

For a more detailed discussion on the neutral end-product resulting from ion-molecule reactions we refer the reader to earlier studies [5, 18, 27, 32, 35].

4. References

[1] Gorden, R. Jr., Rebbert, R. E., and Ausloos, P., Nat. Bur. Stand. (U.S.), Tech. Note 496, 55 pages (Oct. 1969).
[2] Back, R. A., and Walker, D. C., J. Chem. Phys. **37,** 2348 (1962).
[3] Jensen, C. A., and Libby, W. J., J. Chem. Phys. **9,** 2831 (1968).
[4] Rebbert, R. E., and Ausloos, P., J. Am. Chem. Soc. **90,** 7370 (1968).
[5] Lias, S. G., Rebbert, R. E., and Ausloos, P., J. Chem. Phys. **52,** 773 (1970).
[6] Fundamental Processes in Radiation Chemistry, P. Ausloos, Ed., (Interscience Publishers, New York, N. Y., 1968).
[7] Ausloos, P., Rebbert, R. E., and Lias, S. G., J. Phys. Chem. **72,** 3904 (1968).
[8] Rebbert, R. E., and Ausloos, P., J. Res. Nat. Bur. Stand. (U.S.), **75A** (Phys. and Chem.), No. 5, 481–486 (Sept.-Oct. 1971).
[9] Bennett, S. W., Tellinghuisen, J. B. Phillips, L. F., J. Phys. Chem. **75,** 719 (1971).
[10] Cook, G. R., and Metzger, P. H., J. Opt. Soc. Am. **54,** 968 (1964).
[11] Cook, G. R., Metzger, P. H., Ogawa, M., Becker, R. A., and Ching, B. K., Aerospace Corp. Report No. TDR-469 (9260-01)-4 (1965).
[12] Rebbert, R. E., and Ausloos, P., unpublished results.
[13] Metzger, P. H., and Cook, G. R., J. Chem. Phys. **41,** 642 (1964).
[14] Schoen, R. I., J. Chem. Phys. **37,** 2032 (1962).
[15] Cowfer, J. A., Keil, D. K., Michael, J. V., and Yeh, C., J. Phys. Chem. **75,** 1584 (1971) and references cited therein.
[16] Daby, E. E., Niki, H., and Weinstock, B., J. Phys. Chem. **75,** 1601 (1971) and references cited therein.
[17] McNesby, J. R., and Okabe, H., Advan. Photochem. **3,** 157 (1964).
[18] Ausloos, P., and Lias, S. G., J. Chem. Phys. **44,** 521 (1966).
[19] Ausloos, P., and Lias, S. G., Ber. Bun. Physik. Chem. **72,** 187 (1968).
[20] Cermak, V. and Herman, Z., Coll. Czechoslov. Chem. Commun. **30,** 169 (1965).
[21] Ryan, K. R., and Futrell, J. H., J. Chem. Phys. **42,** 819 (1965).
[22] Petterson, E., and Lindholm, E., Arkiv. Fysik **24,** 49 (1963).
[23] Munson, M. S. B., Franklin, J. L., and Field, F. H., J. Phys. Chem. **68,** 3098 (1964).
[24] Derwish, G. A. W., Galli, A., Giardini-Guidoni, A., and Volpi, G. G., J. Chem. Phys. **41,** 2998 (1964).
[25] Aquilanti, V., and Volpi, G. G., J. Chem. Phys. **44,** 2307 (1966).
[26] Sieck, L. W., and Futrell, J. H., J. Chem. Phys. **45,** 560 (1966).
[27] Bone, L. I., and Futrell, J. H., J. Chem. Phys. **46,** 4084 (1967).
[28] At 11.6–11.8 eV fragmentation of the $C_3H_8^+$ ion may contribute to the formation of CH_4. However at the pressures used in this study, the unimolecular decomposition of $C_3H_8^+$ is entirely quenched.
[29] Lias, S. G., Collin, G. J., Rebbert, R. E., and Ausloos, P., J. Chem. Phys. **52,** 1841 (1970).
[30] Vorachek, J. H., and Koob, R. D., J. Phys. Chem. **74,** 4455 (1970).
[31] Dhingra, A. K., and Koob, R. D., J. Phys. Chem. **74,** 4490 (1971).
[32] Ausloos, P., Lias, S. G., and Sandoval, I. B., Disc. Faraday Soc. **36,** 66 (1963).
[33] Sieck, L. W., and Searles, S. K., J. Am. Chem. Soc. **92,** 2937 (1970).
[34] Futrell, J. H., and Tiernan, T. O., J. Chem. Phys. **39,** 2539 (1963).
[35] Bone, L. I., Sieck, L. W., and Futrell, J. H., The Chemistry of Ionization and Excitation, G. R. A. Johnson and G. Scholer, Eds., Taylor and Francis Ltd., London (1967).

(Paper 75A6–692)

JOURNAL OF RESEARCH of the National Bureau of Standards—A. Physics and Chemistry
Vol. 75A, No. 6, November–December 1971

Publications of the National Bureau of Standards*

Selected Abstracts

Barbrow, L. E., Coordinator, **U.S. Metric Study Interim Report. Department of Defense,** *Nat. Bur. Stand. (U.S.), Spec. Publ. 345–9, 132 pages (June 1971) $1.25, SD Catalog No. C13.10:345–9.*

Key words: Department of Defense; International System of Units; metric conversion; metric system; metrication; metrication, costs and benefits of; metrication, impact of; SI; U.S. Metric Study.

This publication reports the results of a Department of Defense study, conducted pursuant to the U.S. Metric Study Act, to determine and evaluate the advantages and disadvantages, including impact on operational capability, that would attend adoption of the International System of units of weights and measures (otherwise known as the Modernized Metric System) for use in the Department (DoD). The report includes estimates for each of the major components of the DoD of the costs of a transition to metric system usage. In addition to discussing the specific advantages and disadvantages that would be expected within the Department, the report describes the dependence of the DoD on the National Industrial Base, and discusses how this interaction would be involved in a national metrication effort.

Barbrow, L. E., Coordinator, **U.S. Metric Study Interim Report. The manufacturing industry,** *Nat. Bur. Stand. (U.S.), Spec. Publ. 345–4, 172 pages (July 1971) $1.25, SD Catalog No. C13.10: 345–4.*

Key words: International System of Units; manufacturing industry; metric conversion; metric system; metric usage; metrication; metrication, attitudes toward; metrication, costs and benefits of; metrication, impact of; SI; U.S. Metric Study.

This publication reports the results of a study to assess the impacts of increasing metric usage—past, present and future—on U.S. manufacturing industry. The study, conducted pursuant to the U.S. Metric Study Act, is based on responses from more than 2,000 manufacturing companies. Information was obtained on: past and present experience with use of the metric system, including advantages and disadvantages thereof, and the views of the firms with regard to future U.S. policy—whether the country should continue its laissez faire approach to metric usage, or should undertake some sort of national program to encourage more widespread use of metric weights and measures. A separate survey of a smaller number of selected firms obtained detailed information as to estimated cost impact of a national metrication effort.

Bell, F. C., Wollin, H. F., Editors, **Report of the 55th National Conference on Weights and Measures 1970,** *Nat. Bur. Stand. (U.S.), Spec. Publ. 342, 315 pages (April 1971) $1.75. SD Catalog No. C13.6/3:342.*

Key words: Conference, weights and measures—laws; weights and measures—regulations; weights and measures—technical requirements; weights and measures—history; weights and measures.

This is a report of the proceedings (edited) of the Fifty-fifth National Conference on Weights and Measures, sponsored by the National Bureau of Standards, held in Salt Lake City, Utah, July 13–17, 1970, and attended by state, county, and city weights and measures officials and representatives of the Federal Government, business, industry, railroads, and associations.

Bennett, L. H., Swartzendruber, L. J., **Interactions between small magnetic clusters in copper-rich Cu-Ni-Fe alloys,** *J. Appl. Phys.* **42,** *No. 4, 1547–1548 (March 15, 1971).*

Key words: Alloys; clustering; copper; iron; local moments; Mössbauer effect; nickel.

Traces of iron in "nonmagnetic" Cu-rich Cu-Ni alloys produce small magnetic clusters largely limited to an Fe site and its Ni nearest neighbors, as observed in Mössbauer *source* experiments. The present work concerns ^{59}Fe Mössbauer absorber data for higher Fe concentrations (¼%–3%), in the 10%–30% Ni range, which demonstrates the existence of a magnetic-moment distribution centered about two distinct moment values. For the lower Fe concentrations, the smaller and more abundant of these moments is identical to that observed in the source experiments and is associated with isolated small Fe-Ni clusters. The other moment is about twice as large and can be ascribed to coupled pairs of these small clusters. These results are almost free of effects of metallurgical clustering. By appropriate heat treatment, clustered samples are obtained with different moment distributions and higher Curie temperatures.

Brauer, G. M., Huget, E. F., **Heats of immersion of the components of tooth structure,** *J. Dental Res.* **50,** *No. 3, 776 (May–June* 1971).

Key words: Heats of immersion; heats of immersion of tooth structure; reactivity of anorganic whole tooth; reactivity of dentin.

Heats of immersion measurements for dentin and anorganic whole tooth powders of known specific surface were used in this study to determine quantitatively the nature and degree of surface modification produced by polar organic compounds and inorganic oxidizing agents in an aqueous environment. The experimental procedure and equipment, as well as the techniques for the preparation and physical characterization of dentin and anorganic whole tooth powders have been described elsewhere (Huget, Brauer & Loebenstein, J Dent Res **47:** 291–301, 1968).
The data are compatible with previous observations that suggested preferential interaction of certain ions and functional groups with the organic matrix of dentin. The reactions occurring at the surface of dentin are similar to those exhibited by purified collagen.

Brenner, D. J., **A technique for measuring the surface temperature of transistors by means of fluorescent phosphor,** *Nat. Bur. Stand. (U.S.), Tech. Note 591, 49 pages (July 1971) 50 cents, SD Catalog No. C13.46:591.*

Key words: Surface temperature; temperature measurement; temperature-sensitive phosphor; thermographic phosphor; transistor-chip temperature.

A technique that uses temperature-sensitive phosphor (TSP) to make quantitative measurements of transistor-chip surface temperatures over the range of 170–210 °C is described. The experimental procedure consisted of depositing a thin coating of phosphor on uncapped power transistors, and then photographing the visible fluorescence generated under near-ultraviolet (uv) excitation. The cooler regions produced a brighter fluorescence than the hotter areas. The surface temperatures of operating transistors were determined by comparing, on a point-by-point basis, the photographic density of operating photographs to the density of a family of calibration photographs. Repeated temperature measurements always fell within a 4 °C overall error range when the phosphor surface was scanned with a 25 x 25 μm aperture. The error band dropped to less than 2 °C when a 50 x 50 μm aperture was used. Coarseness of the phosphor coating seemed to limit spacial resolution to about 20 μm. Any

narrow temperature range between 20 and 400 °C can probably be measured by selecting a suitable level of uv irradiation and/or a suitable phosphor.

Cezairliyan, A., **Short-time (ms) fluctuations of radiance temperature of graphite arc,** *Appl. Opt.* **10,** *No. 5, 1178 (May 1971).*

Key words: Graphite arc; high-speed measurements; high temperatures, pyrometry radiance standards.

Short-time fluctuations of the radiance temperature graphite arcs are investigated with a millisecond resolution photoelectric pyrometer. Standard deviation of the fluctuations around their mean is found to be 4 K. The range of low and high temperatures for four experiments extended from 3799 K to 3808 K, with an average of 3804 K on IPTS–68.

Cezairliyan, A., Morse, M. S., Beckett, C. W., **Measurement of melting point and electrical resistivity (above 2,840 K) of molybdenum by a pulse heating method,** *(Proc. Conf. Thermophysical Properties, Manchester, England, April 7–10, 1970), Rev. Int. Hautes Tempér. Réfract* **t. 7,** *382–388 (1970).*

Key words: Electrical resistivity; high-speed; high temperatures; melting point; methods; molybdenum; properties.

A pulse heating method is used to measure the melting point and electrical resistivity of molybdenum in the temperature range 2,840 melting point in approximately 0.8 s. Specimen temperature is measured with a high-speed photoelectric pyrometer. During the heating period, voltage, current, and temperature are recorded with a high-speed digital data acquisition system which has a full-scale signal resolution of approximately one part in 8,000, and a time resolution of 0.4 ms. Results are compared with those in the literature. Estimated inaccuracy in the melting point (2,889 K) and in electrical resistivity is 10 K and 0.5 percent, respectively.

Chandler, H. H., Bowen, R. L., Paffenbarger, G. C., **Development of a radiopaque denture base material,** *J. Biomed. Mater. Res.* **5,** *253–265 (March 1971).*

Key words: Bonding; composites; denture base materials; diagnosis; light translucency; physical properties; radiopacity.

Radiopaque glass-resin compositions were made for evaluation as denture base materials. The addition of silane-treated, radiopaque, powdered glass to clear poly(methyl methylacrylate) resulted in composites that had greater optical translucency than commercially available pink denture base resins. These formulations could be pigmented and opacified to produce materials that simulated oral soft tissues in color and translucency. Other composites were made using various monomer, polymer and glass combinations. Those made from mixes of BIS–GMA, methyl methacrylate, poly(methyl methylacrylate) and radiopaque glass had excellent translucency but handling characteristics were less ideal. Removal of very small glass particles (less than a few μm) appeared to improve optical translucency. A radiographic survey of 12 specimens that contained from 29 to 57% of the radiopaque glass indicated that all had sufficient radiopacity to aid in localization of swallowed or aspirated dentures made from such materials. Finishing procedures on composite specimens were more difficult and time-consuming and did not produce surfaces as smooth as those obtained on poly(methyl methylacrylate). The finished surfaces felt smooth to the tongue but might stain more easily in the mouth.

Chandler, H. H., Bowen, R. L., Paffenbarger, G. C., **The need for radiopaque denture base materials: A review of the literature,** *J. Biomed. Mater. Res.* **5,** *245–252 (March 1971).*

Key words: Denture foreign bodies; type, cause, prevention; prosthetic materials; radiopaquing agents; radiopaque denture base materials.

The need for esthetic and functionally acceptable radiopaque denture base materials is reflected by numerous reports of patients who ingested or aspirated portions of dentures and reports of difficulties encountered in the removal of these dentures because they could not be located radiographically. The type of denture most commonly ingested or aspirated is a maxillary partial consisting of a palatal piece to which is attached one or more anterior teeth. It may or may not have clasps. Ingestion or aspiration of the foreign body commonly occurs with either broken or ill-fitting dentures are being worn. Few cases have been reported where patients swallowed portions of complete dentures. Previous attempts at providing radiopacity have included addition of heavy metal salts or radiopaque inserts to denture base resins. None of these attempts has been entirely successful. Elimination of dentures as foreign bodies requires a greater effort toward preventive measures by the dentist and the patient. When dentures are swallowed or inhaled, the dentist should immediately seek medical assistance for the patient. The common symptomless period following ingestion or aspiration should not lead the dentist to believe that there will not be serious subsequent complications.

Clark, R. E., Tascher, J. M., **U.S. Metric Study Interim Report. Federal Government: Civilian agencies,** *Nat. Bur. Stand. (U.S.), Spec. Publ. 345–2, 328 pages (July* 1971) *$2.25, SD Catalog No. C13.10:345–2*

Key words: Federal Government; International System of Units; metric conversion; metric system; metric usage; metrication; metrication, attitudes toward; metrication, costs and benefits of; metrication, impact of; SI; U.S. Metric Study.

This publication reports the findings of a survey to ascertain the views of the civilian agencies of the Federal Government on the issues raised by the U.S. Metric Study Act. With regard to internal operations of the Federal agencies, the report covers present metric (International System of Units, or SI) usage and its advantages and disadvantages, expectations of future changes in measurement usage if the U.S. continues its laissez faire policy toward the SI, and attitudes toward a possible nationally coordinated metrication program. In the latter connection, the report contains estimates of added cost or savings impacts on agency internal operating budgets to be expected from a nominally 10-year planned metrication program, both during the transition and thereafter. The survey also assessed the impacts of metric usage and of its increase on the areas of responsibility of the Federal agencies in the society at large (e.g., communications, science and technology, health, labor affairs, international affairs and trade), and on the agencies' interfaces therewith.

Devereux, C. W., Technical Standards Coordinator, **Steel bi-fold closet door units, frames, and trim,** *Nat. Bur. Stand. (U.S.), Prod. Stand. 38–70, 12 pages (May 1971) 15 cents, SD Catalog No. C13.20/2:38–70.*

Key words: Bi-fold doors, steel; closet doors, steel bi-fold; doors, steel bi-fold; steel bi-fold doors.

This Voluntary Product Standard covers sizes, types, materials, construction, hardware, and finishing of steel bi-fold closet door units and frames intended to be stock items not subject to variations according to the customer's special requirements. Methods of marking and labeling are included so that products which comply with the standard may be clearly identified. Provisions for the erection of doors, frames, and accessories are not included in the standard, but certain recommendations for storage and erection as generally endorsed by the manufacturers are given for information and guidance.

Domalski, E. S., **Thermochemical properties of peroxyacetyl (PAN) and peroxybenzoyl nitrate (PBN),** *Environ. Sci. Tech. Communications* **5,** *443–444 (1971).*

Key words: Bond additivity method; group additivity method; peroxyacetyl nitrate; peroxybenzoyl nitrate; thermochemical properties.

The thermochemical properties of peroxyacetyl nitrate (PAN) and peroxybenzoyl nitrate (PBN) were estimated by means of bond and group additivity schemes. Values are given at 298.15 K for the follow-

ing properties: $\Delta Hf°$ (g), $Cp°$ (g), $S°$ (g), $Cp°$ (liq), ΔHvap, and ΔH sublim.; these values were used to calculate $\Delta Sf°$ (g), $\Delta Gf°$ (g), $\Delta Cp°$[(liq) − (g)], $\Delta Hf°$ (liq), and $\Delta Hf°$ (s), which are also cited.

Eisele, J. W., Technical Standards Coordinator, **School Chalk,** *Nat. Bur. Stand. (U.S.), Prod. Stand. 30–70, 14 pages (May 1971) 15 cents, SD Catalog No. C13.20/2:30–70.*

Key words: Calcium carbonate; calcium sulfate; chalk; chroma; toxicity; whiting.

This standard provides requirements for the dimensions, material, breaking strength, characteristics, toxicity, workmanship, and chroma (as applicable) for six types and several classes and grades of school chalk. Test methods for determining the material content, breaking strength, and chroma are provided. Standard packages are given, and methods for labeling to indicate compliance with the standard are provided.

Evenson, K. M., Radford, H. E., Moran, M. M., Jr., **CH free radicals detected by infrared laser magnetic resonance,** *Appl. Phys. Letters* **18,** *No. 10, 426–429 (May 15, 1971).*

Key words: CH; far infrared; free radical; laser; laser magnetic resonance.

CH radicals in an oxyacetylene flame have been detected by a magnetic resonance absorption method, with a water-vapor laser as the source oscillator at a frequency of 2.5 THz. The absorption spectrum is identified with the pure rotational transition, J, $K = (5/2, 2) \rightarrow (7/2, 3)$ at a wavelength of 118.6 μm.

Fong, E., **A preliminary design of a date retrieval language to handle a generalized data base: DRL,** *Nat. Bur. Stand. (U.S.), Tech. Note 590, 26 pages (July 1971) 35 cents, SD Catalog No. C13.46:590.*

Key words: Data base; data retrieval; data structure; information storage and retrieval; language extension; preprocessor; programming language.

DRL (Data Retrieval Language) is a high-level programming language for information retrieval. The language includes a data description language which can describe fixed-length hierarchical data structures, and DRL includes a data retrieval statement whereby a user can retrieve data by specifying conditions on to the data value. DRL also has an environment declaration statement in which the user can indicate specific peripheral devices by unit number for files. The rest of the language consists of an operation repertory of input-output functions and other data manipulations.
DRL is implemented as a preprocessor to FORTRAN V on the UNIVAC 1108, under EXEC II Operating system. Key words act as triggers and are replaced by blocks of FORTRAN code.
The purpose of this project is to investigate the design of an information retrieval language to handle a generalized data base. The DRL system consists of a set of primitives utilizing both compile-time macros and runtime subroutines. These primitives are embedded in a high-level procedure-oriented programming language—the "host language"—FORTRAN in this case. These primitives form a base upon which a class of languages can be defined.

Franklin, A. D., Marzullo, S., **9.—EPR study of point-defect equilibria in CaF_2 containing GdF_3,** *Proc. No. 19 British Ceramic Society, "Role of Point Defects in Solid State Mass", Mass Transport Proc. Non-Metallic Solids, London, England, Dec. 17–18, 1969, pp. 135–150 (British Ceramic Society, Stoke-on-Trent, England, 1971).*

Key words: Calcium fluoride; defect equilibria; electron paramagnetic resonance; point defects.

Room temperature measurements have been made of EPR spectra at 9.5 GHz arising from tetragonal and cubic centers in CaF_2 containing GdF_3. The concentrations ranged from 0.01 to 0.45 mol %. The crystals were annealed in a 30:1 He-HF atmosphere at temperatures ranging from 500 to 1100 °C and then rapidly cooled to room temperature. The annealing times were long enough to achieve steady-state EPR data, and the cooling rapid enough so that a considerably slower cooling gave essentially the same result. It was found that the ratio of the concentration of tetragonal centers to that of cubic centers diminished as the total GdF_3 concentration increased. At a given GdF_3 concentration, this ratio passed over a maximum as the annealing temperature increased. This behavior is inconsistent with a model including only anion interstitials and vacancies. If cation vacancies are included, and if they are assumed to be immobile while the anions can move during cooling, the qualitative features of the data can be produced by the model. Direct experimental confirmation of these assumptions and of the presence of cation vacancies has not been obtained.

Geist, J. C., Richmond, J. C., **On the absorptance of cavity-type receivers,** *Nat. Bur. Stand. (U.S.), Tech. Note 575, 38 pages (July 1971) 45 cents, SD Catalog No. C13.46:575.*

Key words: Absorptance; black coatings; cavity absorptance; cavity reflectance; laser-source reflectometer; Parsons black; retro-reflectance.

The directional-hemispherical reflectance of a number of flat samples that had been coated with Parsons Optical Black Lacquer procured from Thos. Parsons and Sons and The Eppley Laboratory, respectively, was measured at 0.6328 and 1.15 μm with a laser-source integrating sphere reflectometer. The reflectance varied significantly with method of application, and was significantly higher for the Eppley lacquer than for the Parsons lacquer. The reflectance of two cavity receivers, one coated with each lacquer, was also measured. At 0.6328 μm the reflectance of the Parsons cavity was higher, but at 1.15 μm it was lower. The measured reflectance of the Parsons cavity was appreciably higher than that computed from the measured reflectance of the lacquer and the geometry of the cavity, assuming the coating to be a perfectly diffuse reflector. Retro-reflectance measurements revealed that both lacquers reflected more radiant energy back into directions near the direction of incidence than would a perfect diffuser of the same directional-hemispherical reflectance, but the Parsons lacquer was by far the more pronounced retro-reflector. The principal conclusion is that the diffuse assumption can lead to significant errors in computing the absorptance of cavity-type receivers, when the cavity coating is in fact not diffuse.

Geller, S. B., **Standard reference materials: Calibration of NBS secondary standard magnetic tape (computer amplitude reference) SRM 3200 using the reference tape amplitude measurement "Process A" Model II,** *Nat. Bur. Stand. (U.S.), Spec. Publ. 260–29, 57 pages (June 1971) 60 cents, SD Catalog No. C13.10:260–29.*

Key words: Average signal peak level; computer amplitude reference; magnetic tape; master standard; saturation curves; secondary standard; signal level calibration; standard reference materials; unrecorded reference.

This publication describes the design, operation and calibration of the NBS signal amplitude measuring system (Process A—Model II) that is used for calibrating unrecorded Secondary Standard Magnetic Tapes (Computer Amplitude Reference) SRM 3200. This system supercedes the measurement system that was described in the NBS Special Publication 260–18 (November 1969). The signal level calibration is made with respect to a reference signal level derived from the NBS Master Standard Magnetic Tape (Computer Amplitude Reference) that is kept in repository at NBS. The techniques for measuring and recording the data that accompany each Secondary Standard Magnetic Tape in the form of strip chart recordings and saturation curves are described.

Godfrey, J. T., Vidal, C. R., Smith, E. W., Cooper, J., **Effect of time ordering in the unified theory,** *Phys. Rev. A.* **3,** *No. 5, 1543–1546 (May 1971).*

Key words: Lyman-α; Stark-broadening; time-ordering; unified theory.

Using a previously developed unified theory of spectral line broadening, the effects of time-ordering over the complete line profile are investigated. The results of calculations for the Lyman-alpha line are presented.

443-082 OL - 71 - 6

Godfrey, J. T., Vidal, C. R., Smith, E. W., Cooper, J., **The effect of time ordering on the Lyman α profile,** *Nat. Bur. Stand. (U.S.), Monogr. 121, 14 pages (June 1971) 30 cents, SD Catalog No. C13.44:121.*

Key words: Lyman-α; Stark-broadening; time-ordering; unified theory.

Using a unified theory of spectral line broadening previously developed, the effects of time-ordering over the complete line profile are investigated. The behavior of the time-ordered thermal average and un-time-ordered thermal average is obtained analytically. Calculations for the line profile of the Lyman-α line of hydrogen are presented and are representative in that the full thermal average is replaced by the thermal average with the electron velocity distribution approximated by $f(v)=\delta(v-v_{av})$ where v_{av} is the thermal velocity for the plasma in question.

Haller, W., Simmons, J. H., Napolitano, A., **Viscosity-drift technique for determination of critical liquid-liquid immiscibility temperature of glasses,** *J. Am. Ceram. Soc.* **54,** *No. 6, 299–302 (1971).*

Key words: Glass, viscosity; immiscibility; phase-separation; viscosity-drift.

The time dependence of the low-temperature viscosity was used to determine the occurrence of phase separation in glass systems and to measure the critical immiscibility temperature. The technique is fast and easily performed and can be applied to materials with very low immiscibility gaps. Immiscibility temperatures for several technically important glass compositions are given.

Haller, W., Winogradoff, N. N., **Explosive vapor release as cause of laser-induced surface damage of glass,** *J. Am. Ceram. Soc.* **54,** *No. 6, 314–315 (1971).*

Key words: Glass; laser; laser-energy; laser-damage.

Exposure of polished glass surfaces to focused gigawatt laser pulses causes roughening of the illuminated area and emission of small glass fragments (sputtering). Since the formation of the lesion obviously relates to the amount of energy absorbed, glass targets with various degrees of optical absorption for the laser light were studied. Three optical filter glasses of known absorption were exposed to single, nominal 30-J pulses of a 30-ns Q-switched Nd glass laser. The filter glasses were BG 18, KG3, and NG 1; the BG 18 has the strongest absorption for the laser wavelength.

Hatos, S. L., **U.S. Metric Study Interim Report. Commerical weights and measures,** *Nat. Bur. Stand. (U.S.), Spec. Publ. 345–3, 116 pages, (July 1971) $1.00, SD Catalog No. C13.10:345–3.*

Key words: Commercial weights and measures, International System of Units; metric conversion; metric system; metric usage; metrication; metrication, attitudes toward; metrication, costs and benefits of; metrication, impact of; SI; U.S. Metric Study.

This publication, one of a series prepared pursuant to the U.S. Metric Study Act, explores the impacts metrication would have on commercial weights and measures activities. More specifically, the report, concerns: (1) the cost of adapting or changing commercial weighing and measuring devices to record and/or indicate in metric units, and (2) the effects of metrication on state and local weights and measures jurisdictions.

Haupt, G. W., **Glass limit standards deposited at NBS for railway, highway and airways traffic signal colors—history, permanence and colorimetric properties,** *Nat. Bur. Stand. (U.S.), Tech. Note 564, 121 pages (June 1971) $1.00, SD Catalog No. C13.46:564.*

Key words: Aircraft signals; color standards; filter permanence; limit filters; railroad signals; signal colors; signal standards; spectral transmittance of glass filters; traffic signals.

Signal glass limit standards for railway, highway, and aviation colors, selected by user-organizations, are on deposit at the National Bureau of Standards. Many duplicates of these standards have been issued by NBS.

The first standards were selected in 1931 for railway use. Highway standards were adopted in 1940, and selection of aviation standards began in 1942. At the present time the NBS is custodian of 63 standards for these signal colors.

Permanence of the filters is examined, based on colorimetric conversions for CIE standard illuminant A derived from spectrophotometric measurements made on different instruments over periods of years.

Spectral transmittance data and the resulting colorimetric data are given for 9 illuminants ranging in distribution temperature from 1500 to 3250 kelvins and for CIE standard illuminants B and C. Figures show, for several filters of each color, the shifts occurring both in chromaticity (x, y) and in redness and brightness index (u, W*) with changes in illuminant.

Hoeve, C. A. J., **On the general theory of polymer absorption at a surface.** *J. Polymer Sci. Symposia, Part C, No. 30, 361–367 (1970).*

Key words: Configurations; excluded volume effect; loops; polymer adsorption; surface layer; Θ point; trains.

Previous theoretical work dealt with polymer absorption in which the adsorbed segments (trains) interact in the surface layer only. In this work the treatment is extended to include also interaction between the loops dangling in solution. Fortunately, the excluded volume effects for adsorbed polymer chains are found to be small. Therefore an approximate treatment is possible that leads to equations that govern polymer chains under a wide variety of conditions.

Hudson, R. D., Kieffer, L. J., **Compilation of atomic ultraviolet photoabsorption cross sections for wavelengths between 3000 and 10 Å,** *Atomic Data* **2,** *No. 3, 205–262 (May 1971).*

Key words: Atoms; compilation; cross section data; photoabsorption; photoionization; photon.

Graphical displays of selected experimental data on atomic photoabsorption cross sections as functions of wavelength are presented for 24 atoms. Criteria used in the data selection are discussed. References for all data chosen and an author index are included. The literature has been covered through October 1969.

Hummer, D. G., Rybicki, G. B., **Radiative transfer in spherically symmetric systems. The conservative grey case,** *Monthly Notices Roy Astron. Soc.* **152,** *No. 1, 1–19 (1971).*

Key words: Eddington factor; model atmospheres; spherical radiative transfer.

A practical computational method is presented for the solution of radiative transfer problems in spherically symmetric systems. This procedure involves iteration on the "Eddington factor" $f=K/J$ and is designed to handle the forward peaking of the radiation field in extended spherical systems. Extensive numerical results are obtained and discussed for systems in which $\kappa\rho=r^{-n}$, $0<r\leq R$, for $n=3/2$, 2 and 3.

Jacox, M. E., Milligan, D. E., **Matrix-isolation study of the vacuum-ultraviolet photolysis of chloroform. Infrared spectra of the CCl_3^+, $HCCl_2^+$, and HCl_2^- molecular ions,** *J. Chem. Phys.* **54,** *No. 9, 3935–3950 (May 1, 1971).*

Key words: CCl_3^+; chloroform; electron attachment; $HCCl_2^+$; HCl_2^-; $HCCl_3^-$; infrared spectrum; matrix isolation; photoionization; vacuum ultraviolet photolysis.

Photolysis of samples of $HCCl_3$ isolated in an argon matrix at 14 K using 1216-Å radiation leads not only to the isolation of a high yield of CCl_3, but also to the photoionization of CCl_3, resulting in the stabilization of a sufficient concentration of CCl_3^+ for direct infrared spectroscopic identification. The assignment of still other infrared

absorptions which appear in this system to negatively charged species has been confirmed by experiments in which a small concentration of an alkali metal atom is also present in the matrix, providing a photoelectron source. When matrix-isolated $HCCl_3$ is subjected to photolysis by 1067-Å argon resonance radiation, very little CCl_3 is produced, but $HCCl_2$, $HCCl_2^-$, and the same negatively charged species are stabilized in significant concentration. Studies of chloroform samples enriched in carbon-13 and of $DCCl_3$ samples have provided support for these identifications and have yielded data necessary for obtaining several of the force constants of these species. The infrared spectrum of the negatively charged species can most satisfactorily be explained by postulating that dissociative electron attachment to chloroform occurs, resulting in the stabilization of $HCCl_2^-$ in the matrix environment.

Jennings, D. A., Baldwin, D. L., **Construction of a flashlamp-pumped dye laser and an acousto-optic modulator for mode-locking,** *Nat. Bur. Stand. (U.S.), Tech. Note 603, 33 pages (July 1971) $1.00, SD Catalog No. C13.46:603.*

Key words: Acousto-optic modulator; flashlamp-pumped dye laser; mode-locking; subnanosecond pulses.

In this paper is presented the design of a flashlamp-pumped dye laser capable of emitting light pulses 500 ns wide (FWHM) with a risetime of 300 ns. The energy output in the visible region of light is 1 to 10mJ with an energy conversion efficiency of about 0.01% at a repetition rate of 30 pps. The design of an acousto-optic modulator used to mode-lock the dye laser by intracavity loss modulation is presented. The laser output for a given cavity length depends on the frequency and voltage applied to the modulator; a 10%–100% modulated output can be obtained with 1 V rms–20 V rms, whereas a train of light pulses narrower than 0.8 ns (FWHM) can be obtained with 80 V rms.

Klein, M., **Practical treatment of coupled gas equilibrium,** *Chapter in Physical Chemistry, Vol.* **1,** *Thermodynamics, Chapter 7, 489–544 (Academic Press, Inc., New York, N.Y., 1971).*

Key words: Chemical equilibrium; chemical reactions; equilibrium; gases; mass action; non-linear search.

Equations are derived for the species concentrations in coupled chemical equilibria in the gas phase. This is done both for the method of the direct minimization of the free energy as well as for the equilibrium constant method. The relations developed are such as to allow for the inclusion of detailed real gas effects. The emphasis is on practical problems encountered in the actual calculation of the species and the thermodynamic properties. Expressions are derived for the direct calculation of the concentration derivatives with respect to temperature and density required for the calculation of the derived properties (i.e. specific heats, sound velocities, etc.). Considerable space is given to discussions of the non-linear numerical methods available for the solution of the non-linear equations for the species concentrations.

Klose, J. Z., **Mean lives and absolute *f*-values in neutral iron,** *Astrophys. J.* **165,** *No. 3, 637–642 (May 1, 1971).*

Key words: atomic lifetimes; atomic spectra; *f*-values, iron

Mean lives of three levels in Fe I have been determined by using electronic excitation and a method of delayed coincidence. By the use of known relative *f*-values, absolute *f*-values were derived from the lifetime results for the transitions used in the lifetime measurements. The experimental results are summarized in the following table.

Level	(Å)	Mean Life (nsec)	*f*-Value
$z^5F_5^\circ$	3719.9	61.5±0.4	0.0410±0.0003
$z^5F_4^\circ$	3737.1	67.1±1.1	0.034
$y^5F_5^\circ$	3734.9	11.5±1.5	0.14

The error given with each quantity is the standard deviation as determined from the dispersion of the individual measurements. In addition, the experimental results are estimated to contain systematic errors of up to 2 percent. Both the lifetimes and the *f*-values are presented in comparison with experimental results of other workers.

Kurylo, M. J., Peterson, N. C., Braun, W., **Temperature and pressure effects in the addition of H atoms to propylene,** *J. Chem. Phys.* **54,** *No. 11, 4662–4666 (June 1, 1971).*

Key words: Absolute rate constant; activation energy; fluorescence; H atom; propylene; reaction kinetics.

The effect of He pressure on the rate of addition of hydrogen atoms to propylene was measured at 298 K. H atom signal was recorded by the method of resonance of Lyman α radiation at 121.6 nm. The results are consistent with the $1/p_{\frac{1}{2}}^2$ dependence of k_{b1} recently observed in the H atom-ethylene system. The limiting high pressure rate constant obtained in this work is

$$H + C_3H_6 \rightarrow C_3H_7 k_1 = 1.61 \pm 0.04 \times 10^{-12}\ cm^3 molec^{-1} s^{-1}.$$

The temperature dependence of the H atom addition was investigated at 50 torr total pressure over the temperature range 177–473 K. Analysis of the data below room temperature gives the following Arrhenius parameters for addition to the terminal olefinic position:

$$k_{b1}^{\infty} = (10.18 \pm 0.26) \times 10^{12} \exp\ [-(1211 \pm 11)/1.98T] cm^3 molec^{-1} s^{-1}$$

Deviations from this dependence above 298 K can be assigned to non-terminal addition. H atom abstraction, and increased decomposition of the excited propyl radicals.

Linsky, J. L., **Can the Ion H_3^+ account for missing opacity in the solar ultraviolet?** *Solar Physics* **11,** *No. 2, 198–207 (February 1970).*

Key words: H_3^+; opacity, continuous; solar photosphere; solar ultraviolet spectrum.

Limb darkening and specific intensity data imply more continuous opacity in the solar photosphere between 2000 Å and 3500 Å than has been predicted theoretically. The temperature dependence and wavelength dependence of this missing opacity are in qualitative agreement with those deduced for the ion H_3^+, but it is unlikely that H_3^+ is sufficiently abundant to account for this opacity.

Linsky, J. L., **On the relative residual intensities of the calcium H and K lines,** *Solid Physics* **11,** *No. 3, 355–373 (March 1970).*

Key words: Non-LTE radiative transfer; resonance lines, Ca II; solar chromosphere, physical properties; solar chromosphere, structure; spectral line formation; spectroscopic diagnostics.

We have observed the solar Ca II H and K lines to obtain well-calibrated ratios of their core residual intensities. From three independent calibrations, one using a standard lamp, we conclude that the residual intensity ratio $r(K_3)/r(H_3)$ is 1.048±0.03 in the quiet chromosphere and 1.20±0.03 in a plage region. These ratios correspond closely to those observed in stars with quiet and active chromospheres, respectively. For a chromospheric model suggested by the calcium lines and a four-level Ca II ion, we compute H and K line profiles varying the direct collisional coupling and indirect radiative and collisional coupling via the 3 ^{2}D level. We conclude that enhanced chromospheric activity in the sun and late-type stars results more from a steepening of the chromospheric thermal gradient than from a change in density.

Linsky, J. L., Teske, R. G., Wilkinson, C. W., **Observations of the infrared triplet of singly ionized calcium,** *Solar Physics* **11,** *No. 3, 374–383 (March 1970).*

Key words: Non-LTE radiative transfer; resonance lines, Ca II; solar chromosphere, physical properties; spectral line formation; spectroscopic diagnostics.

Observations are presented of the Ca II infrared triplet (8498 Å, 8542 Å, and 8662 Å) at three positions on the solar disk to make possible direct analyses of the line and comparisons with theoretical

computations. The source functions for the two strongest lines (8542 Å and 8662 Å) are equal at those heights corresponding to the wings of the lines ($|\Delta\lambda| > 0.4$ Å) but not to those of the cores. We suggest that the apparent source function inequality in the cores is due to limb darkening caused by inhomogeneities in the chromosphere.

Loebenstein, W. V., **The exchange of ^{45}Ca and ^{32}P with hydroxyapatite as interpreted by adsorption from solution,** *J. Colloid Interface Sci.* **36,** *No. 2, 234–246 (June 1971).*

Key words: Adsorption from solution; calcium phosphate; composite; isotopic exchange; kinetics of adsorption; mechanism of adsorption; solution adsorption.

A theory has been developed based on Langmuir kinetics for the adsorption of a component from solution by a reversible and an irreversible process, simultaneously. The theory has been applied to the removal of traces of ^{45}Ca and ^{32}P from saturated solutions of their nonradioactive counterparts as calcium and phosphate ions by isotopic exchange at the surface of hydroxyapatite. In testing the theory, a computer-programmed nonlinear least-square fit was used to evaluate the physically significant characteristic parameters. This has been accomplished for a number of similar experiments, each of which had a different pH, slurry density, and tagged ion concentration. The results of this study confirm that the approach is feasible and that the assumed model is reasonable. Not only does the theory fit the data, but the magnitude of the derived quantities is internally consistent. No change in calcium to phosphate ratio of the respective surface sites was evident from one experiment to another.

Myklebust, R. L., Heinrich, K. F. J., **Rapid quantitative electron probe microanalysis with a nondiffractive detector system,** *Am. Soc. Testing Mater. Spec. Tech. Publ.* **485,** *pp. 232–424 (1971).*

Key words: Electron diffraction; electron probes; evaluation; gas flow; lithium; microanalysis; multichannel analyzer; proportional counters; quantitative analysis; silicon; solid state counters; tests; x-ray spectra; x-ray spectrometers.

Nondiffractive detector systems on electron probe microanalyzers have decreased the time required for a qualitative analysis from 30 or 40 min to 1 or 2 min. The nondiffractive technique may be extended to the quantitative determination of an element by comparing either the peak height or the area beneath the peak of the signal from the specimen with that from the pure chemical element or a standard of known composition run under identical conditions. Results are given for quantitative analyses of several materials with a lithium-drifted silicon detector, used for x-ray lines above 1 keV, and a gas flow proportional detector, for x-ray lines from 0.16 to 1.5 keV. Quantitative analyses can be accomplished only when the experimental conditions are carefully selected and maintained throughout the measurement. They are then sufficiently precise to warrant the use of a "matrix" correction procedure to obtain concentrations. An analog curve analyzer is useful for resolving overlapping peaks and for integrating the areas beneath the peaks.

Nuttall, R. L., Laufer, A. H., Kilday, M. V., **The enthalpy of formation of ketene,** *J. Chem. Thermodynamics No. 3, 167–174 (1971).*

Key words: Bond energy; enthalpy of formation; heat of formation; ketene; methylene.

The enthalpy of reaction of ketene gas with aqueous sodium hydroxide was measured in an adiabatic solution calorimeter. For the reaction

$$CH_2CO(g) + NaOH(aq, 500H_2O) = CH_3CO_2Na(aq, NaOH\ soln),$$

$\Delta H(298\ K) = -(208.2 \pm 1.6)$ kJ mol^{-1} $= -(49.75 \pm 0.38)$ kcal mol^{-1}. The uncertainties indicated include estimated systematic errors and a 95 per cent confidence interval of ± 1.34 kJ mol^{-1}. This value of ΔH was combined with published values for the enthalpy of formation of aqueous sodium hydroxide and of aqueous sodium acetate to calculate the enthalpy of formation of ketent gas:

$\Delta H_f^\circ(298\ K) = -(47.7 \pm 1.6)$ kJ mol^{-1} $= -(11.4 \pm 0.4)$ kcal mol^{-1}

Odom, J. V., Editor, **U.S. Metric Study Interim Report. Testimony of nationally representative groups,** *Nat. Bur. Stand. (U.S.), Spec. Publ. 345–12, 180 pages (July 1971) $1.50, SD Catalog No. C13.10:345–12.*

Key words: International System of Units; metric conversion; metric system; metric usage; metrication; metrication, attitudes toward; metrication, costs and benefits of; metrication, impact of; National Metric Study Conferences; SI; U.S. Metric Study.

This publication, a part of the U.S. Metric Study series, summarizes the inputs received from the more than 700 associations, societies, unions and other groups which were invited to submit their opinions and viewpoints on the issues raised by the U.S. Metric Study Act. Most of these submissions were publicly presented at hearings held during the course of the Study.

Osinsky, V. I., Winogradoff, N. N., **Excitation and temperature dependence of band-edge photoluminescence in gallium arsenide,** *Phys. Rev. B.* **3,** *No. 10, 3341–3346 (May 15, 1971).*

Key words: Gallium arsenide lasers; impurity effects; intensity dependence; radiative recombination.

Photoluminescent spectra of *n*-type GaAs were studied as a function of the excitation intensity, temperature, and doping level. The spectra consisted of two major bands representing radiative band-to-band recombination and radiative transitions through impurity centers, respectively. The intensity of the peak of the former went through a minimum and a maximum as the temperature was increased from 175 to 500 K. The temperature corresponding to the above maximum increased as the excitation intensity was decreased or the doping level increased. These results suggest that the temperature dependence of the peak intensity in band-to-band transitions is primarily due to the thermal distribution of the carriers over the available energy states. The peak intensity would therefore normally be expected to decrease monotonically with an increase in temperature, while the above maxima and minima represent perturbations imposed by the presence of temperature dependent transitions through radiative or nonradiative impurity recombination centers.

Peterson, N. C., Kurylo, M. J., Braun, W., Bass, A. M., Keller, R. A., **Enhancement of absorption spectra by dye-laser quenching,** *J. Opt. Soc. Am.* **61,** *No. 6, 746–750 (June 1971).*

Key words: Detection of trace impurities; dye laser; iodine; laser; sodium.

A new technique has been developed to enhance the detection of absorption spectra of weak absorbers. Preliminary experiments which illustrate the technique are described. An organic dye laser normally emits a continuum over a 2 to 10 nm wide band. The effect of placing an absorbing gas sample inside a dye laser cavity results in laser quenching at those wavelengths where the sample absorption exceeds a minimum threshold absorption. The threshold for absorption quenching appears to be very low; absorption of the order of 0.5% can cause spoiling of laser action at the absorbing wavelengths and displacement of laser emission to wavelengths where absorption is below the critical switching level. Detection limits for atoms and molecules by means of absorption spectroscopy inside a laser cavity can be more than two orders of magnitude lower than those attainable through conventional absorption spectroscopy. Experiments with I_2 and sodium both inside and outside the cavity of a rhodamine 6-G laser are described. A qualitative consideration of the proposed mechanism indicates that the technique can be significantly improved with further development.

Phucas, C. B., Technical Standards Coordinator, **Package quantities of toothpaste,** *Nat. Bur. Stand. (U.S.), Prod. Stand. 50–71, 8 pages (July 1971) 25 cents, SD Catalog No. C13.20/2:50–71.*

Key words: Package quantities of toothpaste; toothpaste, package quantities.

This Voluntary Product Standard covers the net weights of the pack-

age quantities recommended for toothpaste having specific gravities within the range of 1.45 to 1.75. This standard also provides for the package quantities of toothpaste having specific gravities below 1.45 and above 1.75.

Risley, A. S., **The physical basis of atomic frequency standards,** *Nat. Bur. Stand. (U.S.) Tech. Note 399, 54 pages (April 1971) 60 cents, SD Catalog No. C13.46:399.*

Key words: Atomic frequency standards; cesium beam; energy levels; hydrogen maser; hyperfine interaction; rubidium gas cell; transition probability.

A tutorial discussion of the physical basis of atomic frequency standards is given. These principles are then related to the conditions under which an atom can be used as the working substance of a stable and accurate frequency standard. The three primary examples of atomic frequency standards—the hydrogen maser, the cesium beam, and the rubidium gas cell—are then discussed in terms of these principles and conditions. The functions of the fundamental parts of each device become apparent through this development.

Robinson, B. D., **U.S. Metric Study Interim Report. Education,** *Nat. Bur. Stand. (U.S.), Spec. Publ. 345–6, 216 pages (July 1971) $1.75, SD Catalog No. C13.10:345–6.*

Key words: Education; International System of Units; metric conversion; metric system; metric usage; metrication; metrication, attitudes toward; metrication, costs and benefits of; metrication, impact of; SI; U.S. Metric Study.

This publication concerns the effects of increasing worldwide use of the metric system on education in the United States. The study was carried out and the report prepared for the U.S. Metric Study by the Education Development Center in Newton, Massachusetts. The aims of this education study were fourfold: (1) to assess the educational advantages and disadvantages of both the metric and the customary systems of units, (2) to determine the current usage of metric measures in U.S. schools and trends in that usage, (3) to find the ways in which education would have to change as the U.S. accommodates to increased worldwide use of the metric system, under a laissez faire or a planned approach, and estimate the costs of the changes, and (4) to make recommendations of ways in which to take best advantage of said changes. The report also discusses and suggests ways of achieving curriculum changes needed in view of increasing metric usage. The publication includes the program of the Education Conference, held in October, 1970, as one of a series of National Metric Study Conferences, and the texts of the key papers presented at that conference by the National Education Association and the National Science Teachers Association.

Robinson, D. C., **Determination of dynamic loads in a high-frequency direct-stress fatigue machine,** *Nat. Bur. Stand. (U.S.), Tech. Note 578, 24 pages (June 1971) 35 cents, SD Catalog No. C13.46:578.*

Key words: Dynamic loads; dynamometer; fatigue machine.

A refined test procedure is given for accurately recording the dynamic signals from instrumented test bars used to measure loads during simulated fatigue tests. Loads indicated by the load transducer of a direct-stress fatigue machine are compared with those determined from these instrumented test bar specimens which have been calibrated under static conditions. An application of this procedure is described for a resonant, electromagnetic, direct-stress fatigue machine having an optical dynamometer for indicating programmed loads. The variables investigated were the operating frequency, cyclic load and specimen stiffness. In addition, the influence of test fixture mass on the load measurements was determined at one test frequency. The mean loads indicated by the instrumented test bars are compared with those indicated by the dynamometer to determine the errors in load measurements under various test conditions.

Rothrock, B. D., Editor, **U.S. Metric Study Interim Report. The consumer,** *Nat. Bur. Stand. (U.S.), Spec. Publ. 345–7, 152 pages (July 1971) $1.25, SD Catalog No. C13.10:345–7.*

Key words: Consumers; International System of Units; metric conversion; metric system; metric usage; metrication; metrication, attitudes toward; metrication, costs and benefits of; metrication, impact of; National Metric Study Conferences; SI; U.S. Metric Study.

This report, one of a series prepared pursuant to the U.S. Metric Study Act, presents information on U.S. consumers' knowledge of the metric system and attitudes and opinions regarding metrication in the U.S., and discusses the effects of increasing worldwide metric usage on selected areas of consumer concern. This study is based on (1) an extensive survey conducted by the Survey Research Center of the University of Michigan and (2) prepared expert papers on selected areas of consumer interest. The survey data permitted an analysis of the receptivity of consumers to metrication, and of the need and possible effectiveness of a program to educate citizens should planned metrication be undertaken.

Rupp, N. W., Paffenbarger, G. C., **Significance to health of mercury used in dental practice: A review,** *J. Am. Dental Assoc.* **82,** *1401–1407 (June 1971).*

Key words: Contamination; dental amalgam; environment; hazards; hygiene; mercury; vapor.

In view of widespread interest and concern over possible mercury poisoning and mercury pollution of rivers and lakes. this review of the literature was undertaken for the members of the profession to determine in what way, if any, dentistry is implicated. The review evaluates the exposure of the patient to mercury and the long-term exposure of dental personnel, suggests ways for minimizing any possible mercury hazards to the patient and dental personnel, and restates methods of disposing of mercury residue and waste amalgam to avoid any possible contamination of the environment through dental procedures. This review does not indicate any significant hazard to the patient. There is no contamination of the environment if proper office procedures are followed and if scrap amalgam is collected and salvaged. Further, the review concludes that proper mercury hygiene minimizes any possible danger to dental personnel. The report, however, re-emphasizes the importance of the evaluation from time to time by the profession of its procedures as new information becomes available on the physiological significance of the increased exposure to mercury from all sources.

Schramm, R. E., **Corrections and calculations on a x-ray diffraction line profile: A computer program,** *Nat. Bur. Stand. (U.S.), Tech. Note 600, 34 pages (June 1971) 40 cents, SD Catalog No. C13.46:600.*

Key words: Computer programs; Fourier analysis; nickel steels; x-ray analysis; x-ray diffraction; statistics.

This computer program was written to perform corrections and make calculations on an x-ray diffraction profile before Fourier analysis. The corrections are for background and for variations of intensity with the Bragg angle. Also calculated are the separation of the $K\alpha_1 - K\alpha_2$ doublet and the centroid and position of peak maximum with their standard deviations. There is also an option to smooth the profile.

Simmons, J. A., deWit, R., Bullough, R., Editors, **Fundamental aspects of dislocation theory,** *Proceedings of a Conference held at the National Bureau of Standards, Gaithersburg, Maryland, April 21–25, 1969, Nat. Bur. Stand. (U.S.), Spec. Publ. 317, Vol.* **1,** *752 pages and Vol.* **2,** *624 pages (Dec. 1970). Price $8.25 per set of 2 volumes, sold in sets only, SD Catalog No. C13.10:317.*

Key words: Conference; continuum mechanics; crystal physics; disclinations; dislocations; elasticity; electron-dislocation interactions; lattice defects; phonon-dislocation interactions; solid-state; theoretical physics; thermally activated processes; twinning.

These Proceedings contain research papers, discussions thereon, and panel discussions for the conference on "Fundamental Aspects of Dislocation Theory," held under the auspices of the Institute for Materials Research, April 21–25, 1969, at the laboratories of the

National Bureau of Standards, Gaithersburg, Maryland. Approximately 75 contributed papers and two panel discussions are included. Topics covered are Discrete Dislocations in Continuum Elasticity, Lattice Theories, Dislocation-Phonon Interactions, Applications of the Geometry of Dislocations, Intrinsic Properties of Dislocations, Dislocation Field Theories, Thermally Activated Processes and Statistical Theories, Dislocation-Electron Interactions, and Future Directions for Dislocation Theory.

Smith, C. E., Milligan, D. E., Jacox, M. E., **Matrix-isolation study of the vacuum-ultraviolet photolysis of chlorofluoromethane. The infrared and ultraviolet spectra of the free radical ClCF,** *J. Chem. Phys.* **54,** *No. 7, 2780–2793 (April 1, 1971).*

Key words: ClCF, chlorofluoromethane; chlorofluoromethane-d_2; fluorescence spectrum; free radical; infrared spectrum; matrix isolation; photolysis; ultraviolet spectrum.

The vacuum-ultraviolet photolysis of CH_2ClF and of CD_2ClF isolated in an argon matrix at 14 K leads to the appearance of prominent absorptions at 742 and at 1146 cm^{-1} which have been assigned to the two stretching fundamentals of ClCF. A weak absorption band system between 3900 and 3490 Å, with a 376 ± 10 cm^{-1} average band spacing, may be tentatively attributed to ClCF, as may be an emission band system which appears between 4000 and 4900 Å when the sample is excited by 3650-Å radiation. The 379 ± 10 cm^{-1} average band spacing associated with this emission band system has been tentatively attributed to the bending mode of ground-state ClCF, permitting a normal coordinate analysis for this molecule. The bending and the C-Cl stretching modes are appreciably mixed. Several other groups of absorptions also have been observed in these experiments, but the species responsible for them have not been definitively identified.

Spiegel, V., Jr., Murphey, W. M., **Computer code for the calculation of thermal neutron absorption in spherical and cylindrical neutron sources,** *Nat. Bur. Stand. (U.S.), Tech. Note 576, 25 pages (May 1971) 35 cents, SD Catalog No. C13.46:576.*

Key words: Manganous sulfate bath calibration of neutron sources; neutron; neutron standards.

A computer code has been written in FORTRAN IV for the calculation of thermal neutron absorption in spherical and cylindrical neutron sources. The formalism of the calculation, the structure of the computer code, a listing of the code, and some sample results are presented. The comparison of the results of this calculation to experiment appears elsewhere (1).

Stiehler, R. D., **U.S. Metric Study Interim Report. Engineering standards,** *Nat. Bur. Stand. (U.S.), Spec. Publ. 345–11, 264 pages (July 1971) $2.00, SD Catalog No. C13.10:345–11.*

Key words: Engineering standards; international standards: International System of Units; metric conversion; metric system; metrication; metrication and engineering standards; SI; standards; U.S. Metric Study.

This report, one of a series prepared pursuant to the U.S. Metric Study Act, is concerned with (1) the relationship between measurement language and engineering standards, and (2) the compatibility of U.S. Standards with corresponding international standards. Incompatibilities between corresponding standards result from differences of engineering practice. Measurement units contribute to the incompatibilities among many dimensional specifications which comprise about 25% of engineering standards. In the remaining standards, measurement units are either not involved or serve merely as a language. The study compares U.S. standards with other national and international standards.

Sugar, J., **New energy levels of triply ionized praseodymium,** *J. Opt. Soc. Am.* **61,** *No. 6, 727–732 (June 1971).*

Key words: Praseodymium; spectra; wavelengths.

Measurements of the spectrum of triply ionized praseodymium produced by a 500-A sliding-spark discharge revealed new high-lying energy levels of both even and odd parity. Nearly all levels of the $4f5f$ configuration were found as well as portions of $4f6d$, $4f7s$, and $5d6p$. Radial parameters were fitted to $4f5f$ and $4f6d$. A value for the ionization limit of $314\,200 \pm 200$ cm^{-1} was deduced from the $4f6s$, $7s$ series.

Swartzendruber, L. J., **Localized moments on Fe impurities in Nb-Mo alloys: Mössbauer-effect absorber study,** *J. Appl. Phys.* **42,** *No. 4, 1 (March 15, 1971).*

Key words: Alloys; iron; magnetism; Mo; Mössbauer effect; Nb.

Mössbauer-effect spectra for absorbers of Mo and $Mo_{0.8}Nb_{0.2}$ alloys containing ^{57}Fe impurities have been obtained in an external field as a function of temperature. The spectra for the Mo-Fe alloys are in close agreement with the results of Kitchens et al. for (^{57}Co) Mo sources. The $Mo_{0.8}Nb_{0.2}$ spectra show directly the presence of two distinct moment values for the Fe impurities, one with a moment of 1.9 μ_B and one with a moment of less than 0.6 μ_B, with the two moments present in roughly equal proportions. This result gives support for a discontinuous formation model of the type proposed by Jaccarino and Walker. The saturation hyperfine field of 115 kG for Fe in Mo is apparently reduced to 90 kG for moment bearing Fe in $Mo_{0.8}Nb_{0.2}$. There appears to be no quenching of the Fe moment for Fe-Fe pairs such as that observed for Co-Co pairs in Mo-Nb alloys.

Taylor, B. N., **Report on the International Conference on Precision Measurement and Fundamental Constants,** *held at the National Bureau of Standards, Gaithersburg, Md., Aug. 3–7, 1970, Metrologia* **7,** *No. 1, 39–42 (Jan. 1971).*

Key words: Fundamental constants; least squares adjustments; precision measurements.

This is a report of the International Conference on Precision Measurement and Fundamental Constants held at the National Bureau of Standards, Gaithersburg, Maryland, August 3–7, 1970. It includes a brief discussion of the purpose and significance of the Conference as well as some of the organizational details as they pertain to the Conference sponsors, topics covered, publication of the Conference Proceedings, etc. The bulk of the report is devoted to a summary by topic of the Conference highlights and conclusions.

Utton, D. B., **Temperature dependence of ^{35}Cl NQR in sodium chlorate,** *J. Chem. Phys.* **54,** *No. 12, 5441–5442 (June 15, 1971).*

Key words: $^{35}Chlorine$; nuclear quadrupole resonance; sodium chlorate; temperature dependence 14 K–90 K.

The temperature dependence of the ^{35}Cl NQR in sodium chlorate has been measured in the temperature range 14–90 K. It is shown that the Bayer-Kushida theory satisfactorily explains the data if two distinct lattice vibrations are active. The results are compared with the Raman spectrum and the crystal structure.

Vidal, C. R., Cooper, J., Smith, E. W., **Unified theory calculations of stark broadened hydrogen lines including lower state interactions, (Short Version),** *J. Quant. Spectry. Radiative Transfer* **11,** *263–281 (1970).*

Key words: Classical path; hydrogen line; line wings; stark broadening; unified theory.

Recently published calculations of hydrogen Stark broadening on the basis of the unified classical path theory have been extended to include lower state interactions in the final line profile. A detailed comparison with experiments in the density range 10^{13}–10^{17} cm^{-3} is given.

Viezbicke, P. P., Editor, **NBS frequency and time broadcast services. Radio stations WWV, WWVH, WWVB, and WWVL,**

Nat. Bur. Stand. (U.S.), Spec. Publ. 236, 15 pages (July 1971) 25 cents, SD Catalog No. C13.11:236. Supersedes NBS Special Publication 236, 1970 and Previous Editions.

Key words: Broadcast of standard frequencies; high frequency; low frequency; standard frequencies; time signals; very low frequency.

Detailed descriptions are given of the technical services provided by the National Bureau of Standards radio stations WWV, WWVH, WWVB, and WWVL. These services are: 1. Standard radio frequencies; 2. Standard audio frequencies; 3. Standard musical pitch; 4. Standard time intervals; 5. Time signals; 6. UT corrections; and 7. Official announcements. In order to provide users with the best possible services, occasional changes in broadcasting schedules are required. This publication shows the schedules in effect on July 1, 1971. Annual revisions will be made. Current data relating to standard frequencies and time signals are available monthly in the Time and Frequency Services Bulletin. Advance notices of changes occurring between revisions will be sent to users of NBS broadcast services who request such notice on the basis of need.[1]

Waxler, R. M., **Laser glass composition and the possibility of eliminating electrostrictive effects,** *IEEE, J. Quantum Electron.* **QE-7,** *No. 4, 166–167 (April 1971).*

Key words: Electrostriction; glass; lasers; photoelasticity.

Many authors have stated that electrostrictive self-trapping of the light beam initiates laser damage in solid transparent dielectrics. By systematically varying composition, it may be possible to find a glass in which electrostrictive effects are eliminated.

Weiss, M. J., Kuyatt, C. E., Mielczarek, S., **Inelastic electron scattering from formaldehyde,** *J. Chem. Phys.* **54,** *No. 10, 4147–4150 (May 15, 1971).*

Key words: Formaldehyde; inelastic electron scattering; ultraviolet absorption.

The electron scattering spectrum of H_2CO has been determined in the energy loss range between 0 and 16.0 eV. Three Rydberg series in the region 7–11 eV can be identified with the *s*, *p*, and *d* series reported in the literature by ultraviolet absorption studies. Oscillator strengths are determined for some of the Rydberg states and comparison is made with recent ultraviolet absorption work employing photoelectric methods of detection. A serious disagreement exists between the *f* values obtained by the two methods for the $3s_a$ Rydberg. Another Rydberg series, probably converging to the third ionization potential of H_2CO, is observed in the electron scattering spectrum in the region 12.4–14.0-eV energy loss. Erratic behavior of the quantum defects of the first Rydberg series as well as failure to detect the $II \rightarrow II^*$ transition in H_2CO is discussed in the light of recent theories involving valence states which can seriously perturb members of a Rydberg series.

Weiss, M. J., Mielczarek, S. R., Kuyatt, C. E., **Inelastic electron scattering from nitrous oxide between 5.0 and 20.0 eV energy loss,** *J. Chem. Phys.* **54,** *No. 3, 1412–1414 (Feb. 1, 1971).*

Key words: Far uv absorption: inelastic electron scattering; nitrous oxide; oscillator strengths.

The electron impact spectrum of N_2O is reported between 5.0 and 20.0 eV energy loss. A number of Rydberg series, converging to the second and fourth ionization potentials of N_2O, are observed in the spectra above the first *i.p.* Relative *f*-values, determined for some of the transitions in the 13–17 eV region, are in excellent agreement with those derived from recent vacuum ultraviolet absorption measurements.

West, E. D., **Data analysis for isoperibol laser calorimetry,** *Nat. Bur. Stand. (U.S.), Tech. Note 396, 34 pages (Feb. 1971) 40 cents, SD Catalog No. C13.46:396.*

Key words: Calorimetry; laser; laser calorimetry; laser energy; laser power.

Isoperibol calorimeters (those operating in a constant-temperature environment) are used to measure the power and energy in laser beams relative to electrical standards. The derivation of the basic formula is reviewed. Two methods are presented for analyzing the data taken at equal time intervals: (1) An approximate manual method with criteria for avoiding significant errors of approximation and (2) A least squares method for use with automatic digital computers.

Wiese, W. L., Kelleher, D. E., **On the cause of the redshifts in white-dwarf spectra,** *Astrophys. J.* **166,** *L59–L63 (June 1, 1971).*

Key words: Hydrogen lines; redshifts; Stark shift; white-dwarf.

Detailed laboratory measurements of the profiles of some Stark-broadened Balmer lines reveal systematic slight shifts of these lines to the red, which are linear functions of the electron density. It appears that the Stark-induced redshift accounts for a portion of the observed redshift in white dwarfs which has previously been attributed entirely to gravitation.

Yates, J. T., Jr., Madey, T. E., **Interactions between chemisorbed species: H_2 and CO on (100) tungsten,** *J. Chem. Phys.* **54,** *No. 12, 4969–4978 (June 15, 1971).*

Key words: Carbon monoxide; chemisorption; co-adsorption; displacement reaction; hydrogen; single crystal; tungsten; work function.

The interaction of CO with chemisorbed β-hydrogen on the (100) plane of tungsten has been investigated using flash desorption and work function methods. CO efficiently displaces chemisorbed hydrogen from tungsten at temperatures near 300 K. This is a result of the CO-induced lowering of the activation energy for H_2 desorption, with the CO chemisorbing initially on sites other than those occupied by hydrogen. At ~ 100 K, little CO-induced displacement of chemisorbed hydrogen occurs, and the production of three weakly bound hydrogen states (designated ν-hydrogen) is observed. Each ν state exhibits a range of desorption energies. During the CO-induced surface conversion of β-hydrogen to ν-hydrogen, a decrease in work function is observed. All of this behavior is indicative of a major interaction between adsorbed CO and adsorbed hydrogen. A weakly-bound molecular H_2 state (ν-hydrogen) may be populated by adsorption of H_2 on top of partial CO layers on W(100) at ~ 100 K. The sites adsorbing this molecular state of hydrogen are related to the presence of β-CO species, and are probably the same sites which could adsorb α-CO at higher CO coverages. In thermal desorption, the liberation of two discrete hydrogen binding states (β_1 and β_2) from pure hydrogen layers on W(100) is probably a result of coverage-dependent interactions between identical adsorbed H-atom species. No chemical differences are observed in this work between hydrogen species responsible for the two β-hydrogen binding states. No catalytic production of H_2CO, HCO, CH_4, or C_2H_6 was observed in coadsorption of hydrogen and CO on W(100).

Barnes, J. A., Chi, A. R., Cutler, L. S., Healey, D. J., Leeson, D. B., McGunigal, T. E., Mullen, J. A., Jr., Smith, W. L., Sydnor, R. L., Vessot, R. F. C., Winkler, G. M. R., Characterization of frequency stability, IEEE Trans. Instr. Meas. **IM-20,** No. 2, 105–120 (May 1971).

Beatty, R. W., Fentress, G. H., A simple tuning circuit for waveguide and transmission line systems, IEEE Trans. Microwave Theory Tech. **MTT-19,** No. 3, 337–338 (March 1971).

Blair, B. E., Time and Frequency: A bibliography of NBS literature, published July 1955–December 1970, Nat. Bur. Stand. (U.S.). Spec. Publ. 350, 52 pages (June 1971) 55 cents, SD Catalog No. C13.10:350.

Bowman, R. R., Quantifying hazardous electromagnetic fields:

Practical considerations, Nat. Bur. Stand. (U.S.), Tech. Note 389, 15 pages (April 1970) 30 cents, COM-71-00681. (For further information concerning availability, write to National Technical Information Service, Springfield, Virginia 22151.)

Brennan, J. A., Dean, J. W., Mann, D. B., Kneebone, C. H., An evaluation of positive displacement cryogenic volumetric flowmeters, Nat. Bur. Stand. (U.S.), Tech. Note 605, 134 pages (July 1971) $1.25, SD Catalog No. C13.46:605.

Brenner, F. C., Kondo, A., Research for a uniform quality grading system for tires. IV. Tread wear, Rubber Chem. Technol. **44, No. 1,** 106-121 (March 1971).

Colwell, J. H., Mangum, B. W., Thornton, D. D., Low-temperature magnetic susceptibility and heat capacity of $GdAsO_4$, Phys. Rev. B. **3,** No. 11, 3855-3861 (June 1, 1971).

Davis, D. D., Frequency standard hides in every color TV set, Electronics pp. 96-98 (May 10, 1971).

Day, G. W., Linear and nonlinear optical properties of trigonal selenium, Appl. Phys. Letters **18,** No. 8, 347-349 (April 15, 1971).

Dove, R. B., Marshak, H., Shaft seal for mechanical pump, J. Vacuum Sci. Technol. **8,** No. 3, 519 (May-June 1971).

Edgerly, D. E., Weights and Measures Labeling Handbook, Nat. Bur. Stand. (U.S.), Handb. 108, 406 pages (May 1971) $3.25, SD Catalog No. C13.11:108.

Engen, G. F., Power equations: A new concept in the description and evaluation of microwave systems, IEEE Trans. Instr. Meas. **IM-20,** No. 1, 49-57 (Feb. 1971).

Evans, B. J., Swartzendruber, L. J., Mössbauer study of local molecular fields, cation distributions, and recoilless fractions in Sb-substituted lithium ferrite, J. Appl. Phys. **42,** No. 4, 1628-1630 (March 15, 1971).

Evenson, K. M., Wells, J. S., Matarrese, L. M., Jennings, D. A., Variable output-coupling far-infrared Michelson laser, J. Appl. Phys. **42,** No. 3, 1233-1234 (March 1, 1971).

Greenspan, M., Comment on "Response of ideal circuit elements to sinusoidal excitations", Am. J. Phys. **39,** No. 5, 586-587 (May 1971).

Karp, S. S., Matteson, T. T., The integrated team concept of simulation model development, Proc. 1971 Summer Computer Simulation Conf., Boston, Mass., July 19-21, 1971, pp. 1301-1307 (July 1971).

Keysar, B. C., Specifications and tolerances for reference standards and field standard weights and measures—3. Specifications and tolerances for metal volumetric field standards, Nat. Bur. Stand. (U.S.), Handb. 105-3, 8 pages (May 1971) 25 cents, SD Catalog No. C13.11:105-3.

Kushner, L. M., Welcoming address, Proc. Footwear Manufacturing Executive Conf. held at the King's Grant Motor Inn, Danvers, Mass., Dec. 1, 1970, pp. 7-11 (sponsored by the COMTECH, American Footwear Manufacturers Association, and the New England Footwear Association, December 1970).

Larson, W., Hunter, R. D., A broadband noncontacting sliding short, Nat. Bur. Stand. (U.S.), Tech. Note 602, 18 pages (June 1971) 30 cents, SD Catalog No. C13.46:602.

Lutz, G. J., Boreni, R. J., Maddock, R. S., Meinke, W. W., Editors. Activation analysis: A bibliography, Nat. Bur. Stand. (U.S.), Tech. Note 467, Part 1, 477 pages and Part 2, Appendices, 202 pages (May 1971). Supersedes publication issued September 1968 and December 1969. Price $5.25 per set of 2 volumes, sold in sets only. SD Stock No. 0303-0852.

Means, C. R., Rupp, N. W., Paffenbarger, G. C., Clinical evaluation of two types of resilient liners on dentures, J. Am. Dental Assoc. **82,** 1375-1380 (June 1971).

Merris, R., Pierce, S., A class of representations of the full linear group, J. Algebra **17,** No. 3, 346-351 (March 1971). Motz, J. W., Dick, C. E., Lucas, A. C., Placious, R. C., Sparrow, J. H., Production of high-intensity K x-ray beams, J. Appl. Phys. **42,** No. 5, 2131-2133 (April 1971).

Ogburn, F., Shives, T. R., Brady, C. H., Calibration of a filar micrometer, J. Mater. **6,** No. 1, 60-66 (March 1971).

Page, C. H., Comments on "Nonlinear resistors that generate subharmonics", Proc. IEEE Letters **59,** No. 2, 301 (Feb. 1971).

Parks, E. J., Thermal analysis of modified cellulose, Tappi **54,** No. 4, 537-544 (April 1971).

Selby, M. C., Translator, Standard reference materials; Standard samples issued in the USSR, by R. S. Gorozhanina, A. Y. Freedman, and A. B. Shaievitch, All-Union Scientific Research Institute of Metrology Sverdlovsk Branch, All-Union Scientific Research Center of the State Service for Standard Samples, USSR, Nat. Bur. Stand. (U.S.), Spec. Publ. 260-30, 86 pages (June 1971) $1.00, SD Catalog No. C13.10:260-30.

Sher, A. H., Carrier trapping in Ge(Li) detectors, IEEE Trans. Nucl. Sci. **NS-18,** No. 1, 175-183 (Feb. 1971).

Souders, T. M., A wide range current comparator system for calibrating current transformers, IEEE Trans. Power Appar. Syst. PAS-90, **1,** 318-324 (January/February 1971).

Vadelund, E. A., The role of the Department of Commerce under the fair packaging and labeling act (Proc. Conf. 11th Annual Meeting—Food Distribution Research Society, St. Louis, Mo., Oct. 25-28, 1970), J. Food Distribution Res. 2, No. 1, 103-106 (The Food Distribution Research Society, Inc., Hyattsville, Md., Feb. 1971).

Weissler, P. G., ANSI-1969 Standard reference threshold sound-pressure levels for Audiometers: Some comments, J. Acoust. Soc. Am. **49,** No. 4, Part 2, 1319-1320 (April 1971).

Wright, J. R., Editor, Industrialized building in the Soviet Union. A report of the U.S. delegation to the U.S.S.R., Nat. Bur. Stand. (U.S.), Spec. Publ. 334, 81 pages (Dec. 1970) 75 cents, SD Catalog No. C13.10:334.

Yokel, F. Y., Dikkers, R. D., Strength of load bearing masonry walls, J. Struct. Div. Am. Soc. Civil Engineers **97,** No. ST5, 1593-1609 (May 1971).

**Publications for which a price is indicated are available by purchase from the Superintendent of Documents, U.S. Government Printing Office, Washington, D.C. 20402 (foreign postage, one-fourth additional). The NBS non-periodical series are also available from the National Technical Information Service (NTIS), Springfield, Va. 22151, which was formerly the Clearinghouse. Reprints from outside journals and the NBS Journal of Research may often be obtained directly from the authors.*

JOURNAL OF RESEARCH of the National Bureau of Standards—A. Physics and Chemistry
Vol. 75A, No. 6, November–December 1971

INDEX TO VOLUME 75A

January to December 1971

A

Page

Abramowitz, S., Acquista, N., The infrared spectrum of matrix ioslated BaO_2 ... 23
Absolute determination of viscosity using a torsional pendulum... 541
Absolute determination of viscosity using channel flow ... 553
Absolute measurement ... 541, 553
Absolute measurement of viscosity ... 535
Absorbing center ... 261
Absorption coefficient ... 481
Absorption spectrum ... 455
Accuracy of viscosity measurement ... 535
Accuracy of viscosity measurements of liquids ... 535
Accurate analysis ... 429
Acquista, N., Abramowitz, S., The infrared spectrum of matrix isolated BaO_2 ... 23
Activation analysis ... 429
Alumina ... 155, 401
Alumina standard reference material for resonance frequency and dynamic elastic moduli measurement. I. For use at 25 °C... 155
Aluminum alloy ... 269
Aluminum oxide ... 401
Annealed and quenched glass ... 113
Antimony ... 247
Aragonite ... 197
Atomic spectra ... 109
Atomic theory ... 109
Atomic weight ... 561
Ausloos, P., Gorden, R., Jr., The solid phase photolysis and radiolysis of ethylene at 20 to 77 K ... 141
—, *Lias, S. G.*, Isomerization processes in ions of the empirical formula $C_4H_8^+$ ... 591
—, *Rebbert, R. E.*, Ionization quantum yields and absorption coefficients of selected compounds at 58.4 and 73.6–74.4 nm ... 481
—, —, *Lias, S. G.*, The photochemistry of propane at high photon energies (8.4–21.2 eV) ... 607
—, *Sieck, L. W., Searles, S. K.*, Kinetic mass spectrometric investigation of the ion-molecule reactions occurring in C_4 and C_5 alkanes following photoionization at 106.7 and 104.8 nm... 147

B

Barium ... 23
Barium calcium carbonate ... 197
Barium oxides ... 23
Beckett, C. W., Cezairliyan, A., McClure, J. L., High-speed (subsecond) measurement of heat capacity, electrical resistivity, and thermal radiation properties of tantalum in the range 1900 to 3200 K ... 1
Benedict, W. S., Dowling, J. A., Silverman, S., Quinn, J. W., A study of line shape of CO infrared emission lines ... 469
Bennet, H. S., Heat diffusion near absorbing centers in laser materials ... 261
—, Inclusions in laser materials ... 247
Bestul, A. B., Chang, S. S., Heat capacities of *cis*-1, 4-polyisoprene from 2 to 360 K ... 113
Bis (phenylhydrazone) ... 573
BKZ fluid ... 33
Boric acid ... 421
Bowen, J. S., Dickens, B., Refinement of the crystal structure of the aragonite phase of $CaCO_3$ ... 27
—, —, The crystal structure of $BaCa(CO_3)_2$ (barytocalcite) ... 197
Boyd, M. E., Quantum corrections to the second virial coefficient for the Lennard-Jones (m-6) potential ... 57
Brown, W. E., Dickens, B., Hyman, A., Crystal structure of $Ca_2Na_2(CO_3)_3$ (shortite) ... 129
Bulk modulus ... 121
Butene ... 591

C

Calcium carbonate ... 197
Calcium carbonates ... 27
Calcium crystal structure ... 197
Calcium sodium carbonate ... 129
Calculated continuous emission of a hydrogen plasma ... 291
Calibration ... 541, 553
Calibration of viscometers ... 535
Calorimetry ... 113
Carbon monoxide ... 469
Carbonates ... 27
Cezairliyan, A., High-speed (subsecond) measurement of heat capacity, electrical resistivity, and thermal radiation properties of niobium in the range 1500 to 2700 K ... 565
—, *McClure, J. L., Beckett, C. W.*, High-speed (subsecond) measurement of heat capacity, electrical resistivity, and thermal radiation properties of tantalum in the range 1900 to 3200 K ... 1
—, —, High-speed (subsecond) measurement of heat capacity, electrical resistivity, and thermal radiation properties of tungsten in the range 2000 to 3600 K ... 283
Champion, C. E., Marinenko, G., High precision coulometric titrations of boric acid ... 421
Chang, S. S., Bestul, A. B., Heat capacities of *cis*-1,4-polyisoprene from 2 to 360 K ... 113
Chemical composition ... 163
Chromates ... 435
Cis-1,4-polyisoprene ... 113
Clausius Clapeyron equation ... 213
Cleek, G. W., Waxler, R. M., Refractive indices of fused silica at low temperatures ... 279
—, —, *Malitson, I. H., Dodge, M. J., Hahn, T. A.*, Optical and mechanical properties of some neodymium-doped laser glasses ... 163
CO ... 455
CODATA ... 97
Collision parameters ... 469
Combined low-pressure and high-pressure measurements of density and bulk modulus of aviation instrument oil and 2-methylbutane and their mixtures ... 121
Complementary error function ... 261

Page

Compressibility ... 121
Cooper, M. J., Expanded formulation of thermodynamic scaling in the critical region ... 103
Corundum ... 401
Corundum spin hamiltonian ... 493
Coulometric titration ... 421
Coulometry ... 561
Critical point theories ... 175
Critical region ... 103
Cryogenics ... 269
Crystal structure ... 27, 129
Crystal structure of $BaCa(CO_3)_2$ (barytocalcite) ... 197
Crystal structure of $Ca_2Na_2(CO_3)_3$ (shortite) ... 129
Crystallography of some double sulfates and chromates ... 435
Curve fitting ... 441
Cyclic inter-intramolecular mechanism ... 41
Cyclobutane ... 591

D

Data analysis ... 441
deGroot, J., McMurdie, H. F., Morris, M. C., Swanson, H. E., Crystallography of some double sulfates and chromates ... 435
Density ... 121, 163
Determination of the atomic weight of zinc ... 561
Determination of trace elements in ruby laser crystals by neutron activation analysis ... 429
Dickens, B., Bowen, J. S., Refinement of the crystal structure of the aragonite phase of $CaCO_3$ ... 27
—, —, The crystal structure of $BaCa(CO_3)_2$ (barytocalcite) ... 197
—, *Hyman, A., Brown, W. E.*, Crystal structure of $Ca_2Na_2(CO_3)_3$ (shortite) ... 129
Dickson, R. W., Wachtman, J. B., Jr., An alumina standard reference material for resonance frequency and dynamic elastic moduli measurement. I. For use at 25 °C ... 155
Diene polymerization ... 41
Dilatometric measurements ... 121
Dipole ... 337
Discrimination between equations of state ... 441
Dissociation ... 185
Ditmars, D. A., Douglas, T. B., Measurement of the relative enthalpy of pure α-Al_2O_3 (NBS heat capacity and enthalpy standards reference material No. 720) from 273 to 1173 K ... 401
Dodge, M. J., Waxler, R. M., Cleek, G. W., Malitson, I. H., Hahn, T. A., Optical and mechanical properties of some neodymium-doped laser glasses ... 163
Douglas, T. B., Ditmars, D. A., Measurement of the relative enthalpy of pure α-Al_2O_3 (NBS heat capacity and enthalpy standard reference material No. 720) from 273 to 1173 K ... 401
Dowling, J. A., Silverman, S., Benedict, W. S., Quinn, J. W., A study of line shape of CO infrared emission lines ... 469
Drop calorimetry ... 401

E

Effect of environment of viscous flow in inorganic oxide glasses ... 175
Elastic modulus ... 155
Electrical resistivity ... 1, 269, 283, 565
Electronic transitions ... 455
Emission coefficient ... 291
Emittance ... 1, 283, 565
Energy levels ... 335
Energy levels of Gd^{+++} in Al_2O_3 ... 493
Energy levels, wave functions, dipole and quadrupole transitions of trivalent gadolinium ions in sapphire ... 493
Enthalpy ... 401
Equation of state ... 103
Equations of state ... 441
Equilibrium ... 185
Equivalent width ... 469
E.S.R. ... 573

Page

Ethylene ... 141
Expanded formulation of thermodynamic scaling in the critical region ... 103

F

Fatiadi, A. J., Stable radical-anions derived from glyoxal *bis*(phenylhydrazones) ... 573
Fearn, J. E., Synthesis of fluorodienes ... 41
Flame spectra ... 469
Fluorodienes ... 41
Foley, R. T., Marinenko, G., A determination of the atomic weight of zinc ... 561
Free radical reactions ... 141
Fused silica ... 279

G

Gallagher, J. S., Klein, M., Tables of second virial coefficients and their first and second derivatives for the Stockmayer (m, 6, 3) potential function ... 337
Gamma rays ... 579
Gas ... 337
Gas phase ... 147
Glasses ... 113
Glass transformation ... 163, 279
Glyoxal ... 573
Goodwin, R. D., Thermophysical properties of methane: orthobaric densities and some thermal properties ... 15
Gorden, R., Jr., Ausloos, P., The solid phase photolysis and radiolysis of ethylene at 20 to 77 K ... 141
Greenspan, L., Wexler, A., Vapor pressure equation for water in the range 0 to 100 °C ... 213

H

Hahn, T. A., Waxler, R. M., Cleek, G. W., Malitson, I. H., Dodge, M. J., Optical and mechanical properties of some neodymium-doped laser glasses ... 163
Hardness ... 163
Heat capacities of *cis*-1,4-polyisoprene from 2 to 360 K ... 113
Heat capacity ... 1, 113, 283, 565
Heat capacity standard ... 401
Heat conduction ... 247
Heat diffusion ... 261
Heat diffusion near absorbing centers in laser materials ... 261
Heats of vaporization ... 15
Helium resonance radiation ... 481
Hellner, L., Sieck, L. W., Kinetic mass spectrometric investigation of the reactions of t-$C_4H_9^+$ ions with some simple polar molecules at thermal energies ... 487
Heydemann, P. L. M., Houck, J. C., Combined low-pressure and high-pressure measurements of density and bulk modulus of aviation instrument oil and 2-methylbutane and their mixtures ... 121
High-precision acidimetry ... 421
High-precision coulometric titrations of boric acid ... 421
High-precision coulometry ... 421
High pressure ... 121
High-speed measurements ... 1, 283, 565
High-speed (subsecond) measurement of heat capacity, electrical resistivity, and thermal radiation properties of niobium in the range 1500 to 2700 K ... 565
High-speed (subsecond) measurement of heat capacity, electrical resistivity, and thermal radiation properties of tantalum in the range 1900 to 3200 K ... 1
High-speed (subsecond) measurement of heat capacity, electrical resistivity, and thermal radiation properties of tungsten in the range 2000 to 2600 K ... 283
High temperature ... 1, 23, 283, 565
Houck, J. C., Heydemann, P. L. M., Combined low-pressure

Page

and high-pressure measurements of density and bulk modulus of aviation instrument oil and 2-methylbutane and their mixtures ... 121
Hust, J. G., Weitzel, D. H., Powell, R. L., Thermal conductivity electrical resistivity, and thermopower of aerospace alloys from 4 to 300 K ... 269
Hydrocarbons ... 147, 481
Hydrofluoric acid ... 205
Hydrogen ... 291
Hydrogen continuum ... 291
Hyman, A., Dickens, B., Brown, W. E., Crystal structure of $Ca_2Na_2(CO_3)_3$ (shortite) ... 129

I

Immiscibility ... 175
Inclusions in laser materials ... 247
Infrared ... 23
Infrared spectrum of matrix isolated BaO_2 ... 23
Inorganic molecules ... 481
Interfering reactions ... 429
Interferometry ... 279
Intermediates ... 41
(*m*-6) Intermolecular potential ... 57
Intermolecular potential function ... 337
Ionization constant ... 205
Ionization efficiency ... 481
Ionization of hydrofluoric acid at 25 °C ... 205
Ionization potential ... 335
Ionization quantum yield ... 481
Ionization quantum yields and absorption coefficients of selected compounds at 58.4 and 73.7–74.4 nm ... 481
Ion-molecule reaction ... 607
Ion-molecule reactions ... 141, 147, 487
Ion structure ... 591
Isomerization ... 591
Isomerization processes in ions of the empirical formula $C_4H_8^+$ ... 591

K

Kearsley, E. A., Penn, R. W., An absolute determination of viscosity using channel flow ... 553
—, *White, H. S.*, An absolute determination of viscosity using a torsional pendulum ... 561
Key values ... 97
Kinetic mass spectrometric investigation of the ion-molecule reactions occurring in C_4 and C_5 alkanes following photoionization at 106.7 and 104.8 nm ... 147
Kinetic mass spectrometric investigation of the reactions of *t*-$C_4H_9^+$ ions with some simple polar molecules at thermal energies ... 487
Klein, M., Gallagher, J. S., Tables of second virial coefficients and their first and second derivatives for the Stockmayer (*m*, 6, 3) potential function ... 337

L

Langbeinites ... 435
Lanthanum fluoride electrode ... 205
Laser ... 163, 429
Laser host ... 261
Laser materials ... 247
Lattice constants ... 435
Least-squares procedure ... 205
Lennard-Jones gas ... 57
Lias, S. G., Ausloos, P., Isomerization processes in ions of the empirical formula $C_4H_8^+$ ... 591
—, *Rebbert, R. E., Ausloos, P.*, The photochemistry of propane at high photon energies (8.4–21.2 eV) ... 607
Lewiner, J., Meijer, P. H. E., Energy levels, wave functions, dipole and quadrupole transitions of trivalent gadolinium ions in sapphire ... 493
Line shapes ... 469
Liquid-gas transition ... 103
Liquids ... 121
Lorenz ratio ... 269
LTE ... 291

M

Macdonald, J. R., Powell, D. R., Discrimination between equations of state ... 441
Macedo, P. B., Simmons, J. H., Effect of environment of viscous flow in inorganic oxide glasses ... 175
Malitson, I. H., Waxler, R. M., Cleek, G. W., Dodge, M. J., Hahn, T. A., Optical and mechanical properties of some neodymium-doped laser glasses ... 163
Marinenko, G., Champion, C. E., High-precision coulometric titrations of boric acid ... 421
—, *Foley, R. T.*, A determination of the atomic weight of zinc ... 561
Martin, W. C., Table of spin-orbit energies for *p*-electrons in neutral atomic (core) *np* configurations ... 109
Marvin, R. S., The accuracy of viscosity measurements of liquids ... 535
Mass spectrometry ... 147, 487
Matrix isolations ... 23
McClure, J. L., Cezairliyan, A., High-speed (subsecond) measurement of heat capacity, electrical resistivity, and thermal radiation properties of tungsten in the range 2000 to 3600 K ... 283
—, —, *Beckett, C. W.*, High-speed (subsecond) measurement of heat capacity, electrical resistivity, and thermal radiation properties of tantalum in the range 1900 to 3200 K ... 1
McDaniel, C. L., Schneider, S. J., Phase relations in the SrO-IrO-Ir system in air ... 175
McMurdie, H. F., Morris, M. C., deGroot, J., Swanson, H. E., Crystallography of some double sulfates and chromates ... 435
Measurement of the relative enthalpy of pure α-Al_2O_3 (NBS heat capacity and enthalpy standard reference material No. 720) from 273 to 1173 K ... 401
Meijer, P. H. E., Lewiner, J., Energy levels, wave functions, dipole and quadrupole transitions of trivalent gadolinium ions in sapphire ... 493
Methane ... 15
2-Methylbutane ... 121
Methylcyclopropane ... 591
Methyl sulfoxide ... 573
Miller, E. C., Thompson, B. A., Determination of trace elements in ruby laser crystals by neutron activation analysis ... 429
Model discrimination ... 441
Mohr, R. K., Scharf, K., Temperature dependence of photocurrents produced by x and gamma rays in silicon radiation detectors ... 579
Moreno, E. C., Patel, P. R., Patel, J. M., Ionization of hydrofluoric acid at 25 °C ... 205
Morris, M. C., McMurdie, H. F., deGroot, J., Swanson, H. E., Crystallography of some double sulfates and chromates ... 435

N

Natural rubber ... 113
Nd-doped glass ... 247
Neon resonance radiation ... 481
Neopentane ... 487
New absorption bands and isotopic studies of known transitions in CO ... 455
Nickel ... 335
Nickel alloys ... 269
Niobium ... 565
Nondestructive analysis ... 429
Nonlinear behavior ... 33
Normal and supercooled liquid ... 113

O

Page

Optical and mechanical properties of some neodymium-doped laser glasses ... 163
Optical homogeneity ... 163
Optics ... 279
Orthobaric densities ... 15
Oxygen ... 573

P

Patel, J. M., Patel, P. R., Moreno, E. C., Ionization of hydrofluoric acid at 25 °C ... 205
Patel, P. R., Moreno, E. C., Patel, J. M., Ionization of hydrofluoric acid at 25 °C ... 205
Penn, R. W., Kearsley, E. A., An absolute determination of viscosity using channel flow ... 553
Phase boundary ... 103
Phase relations ... 185
Phase relations in the SrO-IrO_2-Ir systems in air ... 185
Phase transition ... 103
Phase transitions ... 175
Phillips, J. C., Zapas, L. J., Simple shearing flows in polyisobutylene solutions ... 33
Photochemistry of propane at high photon energies (8.4–21.2 eV) ... 607
Photocurrents ... 579
Photoelasticity ... 163
Photoionization ... 147, 487, 591, 607
Photolysis ... 141, 591
Platinum ... 247
Poiseuille flow ... 553
Polar ... 337
Polyisobutylene ... 33
Polymerization ... 41, 141
Potentiometric measurements ... 205
Powell, D. R., Macdonald, J. R., Discrimination between equations of state ... 441
Powell, R. L., Hust, J. G., Weitzel, D. H., Thermal conductivity, electrical resistivity, and thermopower of aerospace alloys from 4 to 300 K ... 269
Propane ... 605
Proton affinity ... 487
Purity ... 41

Q

Quadrupole transitions ... 493
Quantum corrections ... 57
Quantum corrections to the second virial coefficient for the Lennard-Jones (*m*-6) potential ... 57
Quantum yields ... 607
Quinn, J. W., Dowling, J. A., Silverman, S., Benedict, W. S., A study of line shape of CO infrared emission lines ... 469

R

Radiation ... 579
Radiation detector ... 579
Radiation dosimetry ... 579
Radical anion ... 573
Radiolysis ... 141, 591
Rare-gas resonance radiation ... 607
Rate constants ... 147, 487
Rebbert, R. E., Ausloos, P., Ionization quantum yields and absorption coefficients of selected compounds at 58.4 and 73.6–74.4 nm ... 481
—, *Lias, S. G., Ausloos, P.*, The photochemistry of propane at high proton energies (8.4–21.2 eV) ... 607
Refinement of the crystal structure of the aragonite phase of $CaCO_3$ ... 27
Refractive index ... 163, 279
Refractive indices of fused silica at low temperatures ... 279
Resonance frequency ... 155
Roberts, J. R., Voigt, P. A., The calculated continuous emission of a hydrogen plasma ... 291
Rotational analysis ... 455
Rubber, natural ... 113
Ruby ... 429

S

Saturation vapor pressure over water ... 213
Scharf, K., Mohr, R. K., Temperature dependence of photocurrents produced by x and gamma rays in silicon radiation detectors ... 579
Schneider, S. J., McDaniel, C. L., Phase relations in the SrO-IrO_2-Ir system in air ... 185
Searles, S. K., Sieck, L. W., Ausloos, P., Kinetic mass spectrometric investigation of the ion-molecule reactions occurring in C_4 and C_5 alkanes following photoionization at 106.7 and 104.8 nm ... 147
Second spectrum of nickel (Ni II) (addenda and errata) ... 335
Second virial coefficient ... 57, 337
Seebeck effect ... 269
Shear modulus ... 155
Shenstone, A. G., The second spectrum of nickel (Ni II) (addenda and errata) ... 335
Shortite ... 129
Sieck, L. W., Hellner, L., Kinetic mass spectrometric investigation of the reactions of $t\text{-}C_4H_9^+$ ions with some simple polar molecules at thermal energies ... 487
—, *Searles, S. K., Ausloos, P.*, Kinetic mass spectrometric investigation of the ion-molecule reactions occurring in C_4 and C_5 alkanes following photoionization at 106.7 and 104.8 nm ... 147
Silicon radiation detector ... 579
Silverman, S., Dowling, J. A., Benedict, W. S., Quinn, J. W., A study of line shape of CO infrared emission lines ... 469
Simmons, J. D., Tilford, S. D., New absorption bands and isotopic studies of known transitions in CO ... 455
Simmons, J. H., Macedo, P. B., Effect of environment of viscous flow in inorganic oxide glasses ... 175
Simple shearing flows in polyisobutylene solutions ... 33
Single crystal x-ray diffraction ... 27, 129
Single x-ray diffraction ... 197
Solid phase photolysis and radiolysis of ethylene at 20 to 77 K ... 141
Special radiance standard ... 291
Specific heat ... 401
Specific heats of the saturated liquid ... 15
Spectral series ... 335
Spectroscopy ... 335
Spin-orbit interaction ... 109
SrO:IrO_2 compounds ... 185
SrO:IrO_2-Ir system ... 185
Stable radical-anions derived from glyoxal *bis*(phenylhydrazones) ... 573
Standard ... 541, 553
Standard reference material ... 155, 401
Stark-broadening ... 291
Statistical mechanics ... 57
Steam ... 213
Stockmayer ... 337
Stress components ... 247
Stress relaxation ... 33
Structural relaxation ... 175
Sulfates ... 435
Sunner, S., Tentative set of key values for thermodynamics—part I. Report of the ICSU–CODATA Task Group on Key Values for Thermodynamics, October 1970 ... 97
Surface fitting ... 441
Swanson, H. E., McMurdie, H. F., Morris, M. C., deGroot, J., Crystallography of some double sulfates and chromates ... 435
Synthesis ... 41
Synthesis of fluorodienes ... 41
Synthetic sapphire ... 401

T

Table of spin-orbit energies for *p*-electrons in neutral atomic (core) *np* configurations ... 109
Tables of second virial coefficients and their first and second derivatives for the Stockmayer (*m*, 6, 3) potential function ... 337

Page

Tantalum 1
Telomerization 41
Temperature dependence 579
Temperature dependence of photocurrents produced by x and gamma rays in silicon radiation detectors 579
Tentative set of key values for thermodynamics—Part I. Report of the ICSU–CODATA Task Group on Key Values for Thermodynamics, October 1970 97
Thermal conductivity 163, 269
Thermal conductivity, electrical resistivity, and thermopower of aerospace alloys from 4 to 300 K 269
Thermal diffusivity 113
Thermal radiation properties 1, 283, 565
Thermal transmittance 163
Thermodynamic functions 401
Thermodynamic properties 113
Thermodynamic scaling 103
Thermodynamics 1, 57, 97, 283, 565
Thermoelastic theory 247
Thermofunctions for ideal gas states 15
Thermo-optic properties 163
Thermophysical properties 15
Thermophysical properties of methane: orthobaric densities and some thermal properties 15
Thompson, B. A., Miller, E. C., Determination of trace elements in ruby laser crystals by neutron activation analysis 429
Tilford, S. D., Simmons, J. D., New absorption bands and isotopic studies of known transitions in CO 455
Titanium alloy 269
Torsional pendulum 541
Trace elements 429
Transition probabilities 493
Transport phenomena 175
Transport properties 269
Tungsten 283
Tutton salts 435

U

Ultrasonic (paramagnetic) resonance 493
Ultrasonics 121
Ultrasonic transition probabilities 493
Uncertainty of viscosity measurements 535
Unimolecular dissociation 607

V

Vapor pressure 213
Vapor pressure equation for water in the range 0 to 100 °C 213
Vapor pressure of water 213
Vibrational analysis 455
Vibrational and rotational constants 455
Virial coefficients 213
Viscosity 33, 535, 541, 553
Viscous flow 175, 553
Voigt, P. A., Roberts, J. R., The calculated continuous emission of a hydrogen plasma 291

W

Wachtman, J. B., Dickson, R. W., An alumina standard reference material for resonance frequency and dynamic elastic moduli measurement. I. For use at 25 °C 155
Water vapor 213
Wave functions of Gd^{+++} 493
Wavelength 335
Waxler, R. M., Cleek, G. W., Refractive indices of fused silica at low temperatures 279
—, —, *Malitson, I. H., Dodge, M. J., Hahn, T. A.*, Optical and mechanical properties of some neodymium-doped laser glasses 163
Weitzel, D. H., Hust, J. G., Powell, R. L., Thermal conductivity, electrical resistivity, and thermopower of aerospace alloys from 4 to 300 K 269
Wexler, A., Greenspan, L., Vapor pressure equation for water in the range 0 to 100 °C 213
White, H. S., Kearsley, E. A., An absolute determination of viscosity using a torsional pendulum 561

X

X rays 579

Y

Young's modulus 155

Z

Zapas, L. J., Phillips, J. C., Simple shearing flows in polyisobutylene solutions 33
Zinc, atomic weight 561

U. S. GOVERNMENT PRINTING OFFICE : 1971 OL - 443-082

UNITED STATES
GOVERNMENT PRINTING OFFICE
PUBLIC DOCUMENTS DEPARTMENT
WASHINGTON, D.C. 20402

OFFICIAL BUSINESS

PENALTY FOR PRIVATE USE, $300

POSTAGE AND FEES PAID
U.S. GOVERNMENT PRINTING OFFICE

U.S.MAIL

JOURNAL OF RESEARCH of the National Bureau of Standards
A. Physics and Chemistry

Vol. 75A, No. 6 November–December 1971

Contents

Page

The accuracy of measurements of viscosity of liquids. Robert S. Marvin. 535

An absolute determination of viscosity using a torsional pendulum. Hobart S. White and Elliot A. Kearsley. 541

An absolute determination of viscosity using channel flow. Robert W. Penn and Elliot A. Kearsley. 553

A new determination of the atomic weight of zinc. George Marinenko and Robert T. Foley. 561

High-speed (subsecond) measurement of heat capacity, electrical resistivity, and thermal radiation properties of niobium in the range 1500 to 2700 K. Ared Cezairliyan. 565

Stable radical-anions derived from glyoxal bis(phenylhydrazones). Alexander J. Fatiadi. 573

Temperature dependence of photocurrents produced by x and gamma rays in silicon radiation detectors. Karl Scharf and Robert K. Mohr. 579

Isomerization processes in ions of the empirical formula $C_4H_8^+$. S. G. Lias and P. Ausloos. 591

The photochemistry of propane at high photon energies (8.4–21.2 eV). R. E. Rebbert, S. G. Lias, and P. Ausloos. 607

Publications of the National Bureau of Standards. 613

Index to Volume 75A, January to December 1971. 623

MIAMI UNIVERSITY LIBRARY

Library of Congress Catalog Card Number: 62–37059

For sale by the Superintendent of Documents, U.S. Government Printing Office, Washington, D.C. 20402. (Order by SD Catalog No. C 13.22/sec.A:74/5). Single copy price varies. This issue $1.75. Subscription price $9.50 a year; $2.25 additional for foreign mailing.

UNITED STATES GOVERNMENT PRINTING OFFICE, WASHINGTON : 1971